Syntheses, Structures, and Catalytic Evaluation of Cationic Ru(II)-NHC Pincer Complexes

Ph.D. Thesis

By

RAHUL KUMAR SINGH

DEPARTMENT OF CHEMISTRY
INDIAN INSTITUTE OF TECHNOLOGY INDORE
DECEMBER 2024

Syntheses, Structures, and Catalytic Evaluation of Cationic Ru(II)-NHC Pincer Complexes

A THESIS

Submitted in partial fulfillment of the requirements for the award of the degree

of

DOCTOR OF PHILOSOPHY

by

RAHUL KUMAR SINGH

(Roll No.: 1801231004)

DEPARTMENT OF CHEMISTRY
INDIAN INSTITUTE OF TECHNOLOGY INDORE
DECEMBER 2024

INDIAN INSTITUTE OF TECHNOLOGY INDORE

CANDIDATE'S DECLARATION

I hereby certify that the work which is being presented in the thesis entitled **"Syntheses, Structures, and Catalytic Evaluation of Cationic Ru(II)-NHC Pincer Complexes"** in the partial fulfillment of the requirements for the award of the degree of **DOCTOR OF PHILOSOPHY** and submitted in the **DEPARTMENT OF CHEMISTRY, INDIAN INSTITUTE OF TECHNOLOGY INDORE**, is an authentic record of my own work carried out during the time period from **December 2018** to **December 2024** under the supervision of **Dr. Amrendra K. Singh**, **Associate Professor**, **Department of Chemistry**, **Indian Institute of Technology Indore**.

The matter presented in this thesis has not been submitted by me for the award of any other degree of this or any other institute.

Rahul Kumar Singh
26/12/2024
Signature of the Student with date
(RAHUL KUMAR SINGH)

This is to certify that the above statement made by the candidate is correct to the best of my knowledge.

26/12/2024
Signature of Thesis Supervisor with date
(Dr. AMRENDRA K. SINGH)

RAHUL KUMAR SINGH has successfully given his Ph.D. Oral Examination held on **June 30, 2025**.

30/06/2025
Signature of Thesis Supervisor with date
(Dr. AMRENDRA K. SINGH)

ACKNOWLEDGEMENTS

This Thesis is

Dedicated

to

My Beloved

Grandparents

Parents

&

My Respected

Thesis Supervisor

Rahul Kumar Singh

SYNOPSIS

The thesis entitled "Syntheses, Structures, and Catalytic Evaluation of Cationic Ru(II)-NHC Pincer Complexes" includes seven chapters that contain the synthesis and characterization of cationic Ru(II)-NHC pincer complexes, the reactivity of multiple carbene complexes, and their photophysical and electrochemical properties. All the synthesized ruthenium complexes were investigated for various catalytic reactions. The first chapter briefly introduces the pincer ligand system with varying types of donor ligands and their coordination geometries. Further, the ruthenium complexes with NHC-based pincer ligands and their applications in catalysis were discussed. Chapter two discusses the syntheses and characterization of Ru(II)-CNC pincer complexes with various ancillary ligands. The catalytic reactivity of these Ru(II)-CNC pincer complexes was investigated for transfer hydrogenation of cyclohexanone and acceptorless dehydrogenation of benzyl alcohol. Chapter three describes the catalytic activity of the ADC (Acceptorless Dehydrogenative Coupling) reaction with *N*-methyl, *N*-isopropyl, and *N*-cyclohexyl wingtip complexes with various ancillary ligands. In ADC catalysis, a reversal in catalytic activity was observed, which can be explained in terms of the *trans*-effect. Complexes with PPh$_3$ and DMSO show better reactivity than their other derivatized complexes. In the ADC reaction mechanism, *ortho*-C–H activation is observed with the benzaldehyde molecule, confirming the reaction pathways. The aldehyde group has traditionally been employed as a directing group for C–H activation; this work presents the first report of *ortho*-C–H activation facilitating the nucleophilic attack on the aldehyde group. The fourth chapter describes the synthesis and characterization of Ru(II)-CNC pincer complexes with multiple NHC carbene donor ligands. Observing two sets of signals in NMR spectra and their justification through less nucleophilic, non-coordinating solvent acetone-d$_6$, confirmed that only one species is present in solution. Further, chapter five discusses the catalytic evaluation for nitrile

hydration from Ru(II)-CNC pincer complexes. This catalysis was reported in mild reaction conditions, i.e., low catalyst loading, low base loading, lower temperature, and less reaction time in an aqueous medium. A plausible reaction mechanism was reported for the hydration of nitrile, initiated by a highly reactive intermediate i.e., Ru-OH species, facilitated by the hemilability of a pyridine ligand. Chapter six describes the reactivity of Ru(II)-CNC pincer complexes with CH_3CN and PPh_3 ligands. A comparative study was reported for the hydration of nitriles from these derivatized complexes. The final chapter describes the concluding points of this thesis and briefly discusses their future scopes.

Chapter 1. Introduction and Background

Pincer ligands are tridentate chelating ligands that bind with the metal centre through three adjacent coplanar sites with a meridional geometry [1]. Moulton and Shaw first reported it in 1976 [2]. Pincer ligands have been classified in literature in two categories, i.e., (a) Symmetry and charge (neutral or ionic) of the binding motif, and (b) Donor atoms and coordination modes [1, 3, 4]. Pincer complexes are formed by combining two fused metallacycles, with two side arms that stabilize the complexes and significantly impact their electronic properties [1]. Synthesis of Ru(II)-NHC pincer complexes is the most challenging process in synthetic chemistry [5, 6]. Pincer ligands coordinate with the ruthenium centre to form stable complexes that govern the reactivity and behaviour of the catalyst. Ruthenium centres easily display superior stability in different oxidation states, and coordination geometries make them suitable for various applications [7]. Ruthenium is less expensive than other transition metals (Pd, Pt, Rh, and Ir), and has made it more convenient for various catalytic reactions. Ruthenium complexes show superior biocompatibility to many other metallodrugs, enhancing their pharmaceutical usage. Ru(II)-NHC pincer complexes showcase enhanced efficiency,

selectivity, and notable tolerance towards various functional groups in contrast to the traditional ruthenium catalysts. Previously, several methodologies have been documented for the synthesis of ruthenium complexes featuring CNC pincer ligands [8–12]. However, complexes featuring CNC-pincer ligands have been relatively less investigated in diverse catalytic reactions. Ruthenium catalysis offers a versatile and efficient means to carry out a wide range of chemical transformations, significantly advancing synthetic chemistry. Our research endeavours to fill this gap in synthetic chemistry by synthesizing CNC pincer complexes and exploring their potential applications. The primary objective of this thesis is to design and synthesize highly efficient cationic Ru(II)-CNC pincer complexes and explore their catalytic utility in various organic transformations.

❖ To synthesize cationic Ru(II)-CNC pincer complexes with various ancillary ligands and study their chemical behaviour.

❖ To examine the catalytic efficiency of cationic Ru(II)-CNC pincer complexes and explore the impact of ancillary ligands on the selectivity of the reaction.

❖ Incorporation of multiple NHC donor ligands in the Ru(II)-CNC pincer-type complexes.

❖ To evaluate the reactivity of cationic Ru(II)-CNC pincer complexes with multiple NHC donor ligands.

Chapter 2. Syntheses, Characterization, and Catalytic Activity of Cationic Ru(II)-CNC Pincer Complexes

This chapter describes the synthesis and characterization of new cationic Ru(II)-CNC pincer complexes [Ru(CNC^{Cy})(CO)(PPh$_3$)Cl]PF$_6$ (**1c**), [Ru(CNC^{Cy})(CO)(PPh$_3$)H]PF$_6$ (**2c**), [Ru(CNC^{Cy})(PPh$_3$)$_2$Cl]PF$_6$

(**3c**), [Ru(CNC^{Cy})(PPh$_3$)$_2$H]PF$_6$ (**4c**), and [Ru(CNC^{Cy})(DMSO)$_2$Cl]PF$_6$ (**5c**) with various ancillary ligands (Figure **1**). The imidazolium ligand precursor (CNC^{Cy}·2HCl) was treated with Ag$_2$O in methanol, affording the silver-carbene complex, which gives Ru–CNC (CNC = Pyridine dicarbene ligand) complexes through in situ transmetallation with different Ru-precursors. All the newly synthesized complexes have been fully characterized by different spectroscopic techniques. The catalytic activity of these new complexes was investigated for transfer hydrogenation of cyclohexanone and acceptorless dehydrogenation of benzyl alcohol, and found in line with the previously observed trend based on the *trans* effect of ancillary ligands. The effect of ancillary ligands (CO, PPh$_3$, and DMSO) has been demonstrated during catalysis. Complexes with more π-acid ligands, CO perform better compared with those with PPh$_3$ and DMSO ligands. A plausible reaction mechanism for TH and AAD is reported with the involvement of a reactive intermediate [Ru(CNC^{Cy})(CO)(PPh$_3$)H]PF$_6$ (**2c**), supporting the previous investigations with smaller *N*-alkyl wing tips in terms of *trans* effect [13–15].
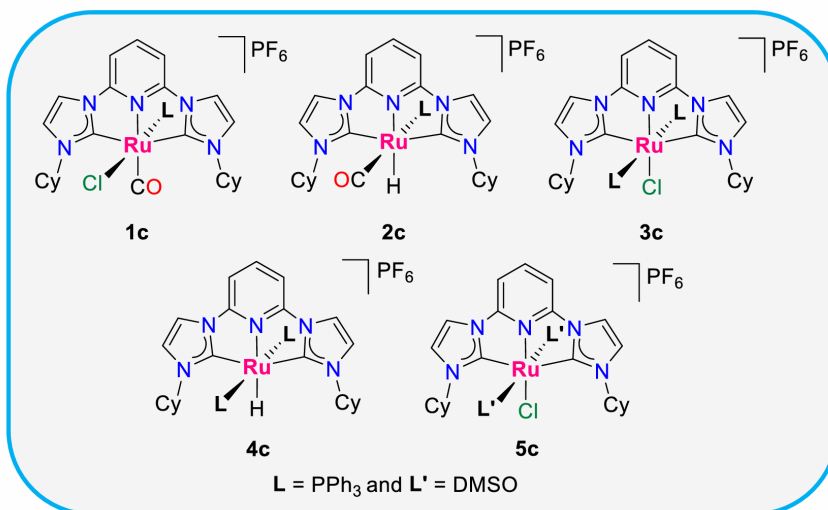
Figure 1. Schematic representation of newly synthesized cationic Ru(II)-CNC pincer complexes with various ancillary ligands.

Chapter 3. Role of Ancillary Ligands in Selectivity Towards Acceptorless Dehydrogenative Coupling of Alcohols and Amines Catalyzed by Cationic Ru(II)-CNC Pincer Complexes

This chapter describes the effect of ancillary ligands on catalytic performance, and a comparison of the four ligands (CO, COD, DMSO, PPh$_3$) has been investigated, which can be explained in terms of the *trans* effect of ligands. The CNC pincer ligand platform provides a unique ligand framework with no metal-ligand cooperativity, allowing this comparison between ancillary ligands. An unexpected reversal in catalytic activity for acceptorless dehydrogenative coupling was observed, where complexes containing PPh$_3$ ligands performed better than complexes containing CO ligands (Figure **2**). Previously, no such studies on selectivity among ADC catalysis have been reported for the impact of ancillary ligands. Further, all complexes have been utilized as catalysts in the dehydrogenative coupling reaction of benzyl alcohol with amines. For acceptorless dehydrogenative coupling reaction, complexes with PPh$_3$ and DMSO ligands performed better than complexes containing CO and COD ligands. NMR and mass investigation of the mixture of catalytic reactions indicated a C-N coupling step at the metal-bound aldehyde. Although the aldehyde group has long been utilized as a directing group for C-H activation, we report, for the first time, *ortho*-C-H activation playing a supportive role in the nucleophilic attack on the aldehyde group. Further, substrate scope for the dehydrogenative coupling reaction of benzyl alcohol with a wide range of amines has been explored, including synthesizing some pharmaceutically important imines.
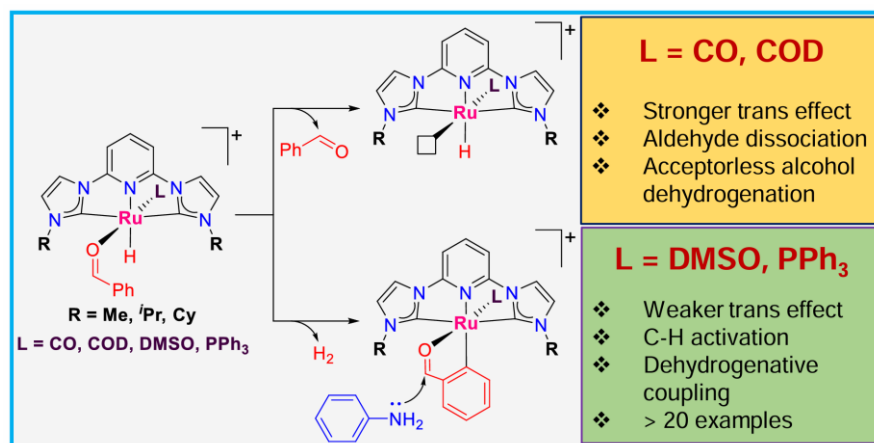
Figure 2. Schematic representation of the role of ancillary ligands in selectivity towards acceptorless dehydrogenative coupling of alcohols and amines.

Chapter 4. Syntheses and Characterization of Cationic Ru(II)-CNC Pincer Complexes with Multiple NHC Donor Ligands

This chapter describes the synthesis of new electron-rich, phosphine-free complexes [Ru(CNC^{Me})(CN^{Me})I]PF$_6$ (**7a**), [Ru(CNC$^{i\text{-}Pr}$)(CN^{Me})I]PF$_6$ (**7b**), [Ru(CNC^{Cy})(CN^{Me})I]PF$_6$ (**7c**), [Ru(CNC$^{t\text{-}Bu}$)(CN^{Me})I]PF$_6$ (**7d**), [Ru(CNC^{Me})(CN$^{i\text{-}Pr}$)I]PF$_6$ (**8a**), [Ru(CNC$^{i\text{-}Pr}$)(CN$^{i\text{-}Pr}$)I]PF$_6$ (**8b**), [Ru(CNC^{Cy})(CN$^{i\text{-}Pr}$)I]PF$_6$ (**8c**), [Ru(CNC$^{t\text{-}Bu}$)(CN$^{i\text{-}Pr}$)I]PF$_6$ (**8d**), [Ru(CNC^{Me})(Py-Bim^{Me})I]PF$_6$ (**9a**), and [Ru(CNC^{Me})(3MePy-Im^{Me})I]PF$_6$ (**10a**) have fully characterized by multinuclear NMR spectroscopy and high-resolution mass spectrometry (HRMS) (Figure **3**). These complexes contained the multiple *N*-heterocyclic carbene (NHC) ligands, with CNC (2,6-bis(alkylimidazol-2-ylidene)-pyridine) and CN [(2-(3-alkylimidazol-2-ylidene)-pyridine), (2-(3-methylbenzaimidazol-2-ylidene)-pyridine) and (2-(3-methylimidazol-2-ylidene)-3-methyl-pyridine)] as key ligand precursors. These complexes were synthesized by the reaction of bidentate ruthenium precursors with pincer ligand precursors in ethylene glycol under

reflux conditions, followed by ion exchange with the saturated solution of KPF$_6$, which afforded these multiple carbene complexes. The molecular structures of complexes [Ru(CNC^{Me})(CN^{Me})I]PF$_6$ (**7a**), [Ru(CNC$^{i\text{-}Pr}$)(CN^{Me})I]PF$_6$ (**7b**) and [Ru(CNC^{Cy})(CN^{Me})I]PF$_6$ (**7c**) have been confirmed by single-crystal X-ray diffraction technique. The existence of only one isomer (*trans*-isomer) was confirmed by the spectral studies of complexes in DMSO-d$_6$, i.e., [Ru(CNC^{Me})(CN^{Me})I]PF$_6$ (**7a**) and [Ru(CNC^{Me})(CN^{Me})CH$_3$CN]PF$_6$ (**11a**, vide infra), and further confirmed by the ^{1}H NMR spectrum of complex **7a**, which was recorded in less nucleophilic, non-coordinating solvent acetone-d$_6$, which shows only one species in solution.
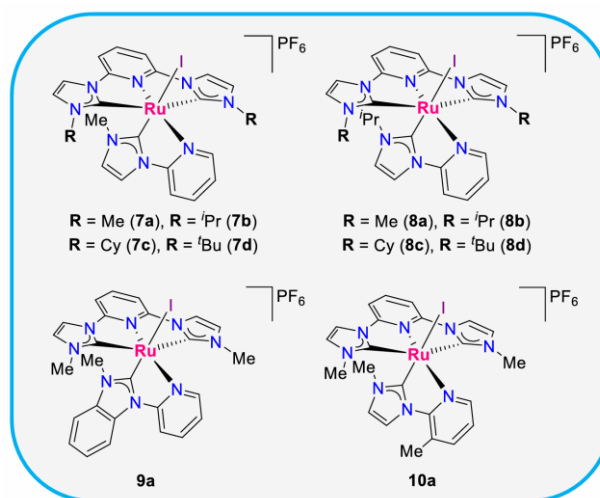
Figure 3. Schematic representation of newly synthesized cationic Ru(II)-CNC pincer complexes.

Chapter 5. Cationic Ru(II)-CNC Pincer Complexes as Phosphine-free Catalysts for Nitrile Hydration to Amides in Aqueous Medium

This chapter contains the catalytic activity of all the synthesized Ru(II)-CNC pincer complexes for the hydration of nitriles in an aqueous medium under mild reaction conditions. All the synthesized Ru(II)-NHC pincer complexes reveal good reactivity with excellent

selectivity in the hydration of nitriles. The catalytic activity of these Ru(II)-CNC pincer complexes has been explored for nitrile hydration to amide in an aqueous medium. Particularly, complex [Ru(CNC$^{i\text{-}Pr}$)(CN^{Me})I]PF$_6$ (**7b**) exhibited better reactivity among all the complexes (Figure **4**). Mechanistic investigations revealed a catalytic pathway initiated by a [Ru-OH] species, facilitated by the hemilability of a pyridine ligand. This catalysis was reported in mild reaction conditions, i.e., low catalyst loading, low base loading, lower temperature, and shorter reaction time in an aqueous medium. The versatility of these Ru(II)-CNC pincer complexes as catalysts for nitrile hydration has been demonstrated through successful conversions of a diverse range of nitriles, encompassing electron-releasing, electron-withdrawing, and heterocyclic nitriles into the corresponding amides with high reactivity and good to excellent yields. The present study contributes to the advancement of nitrile hydration as an efficient, versatile, and sustainable approach for amide synthesis. Additionally, the effective conversion of a wide range of nitriles highlights the potential of these catalysts for producing valuable amide derivatives in various chemical and pharmaceutical applications.
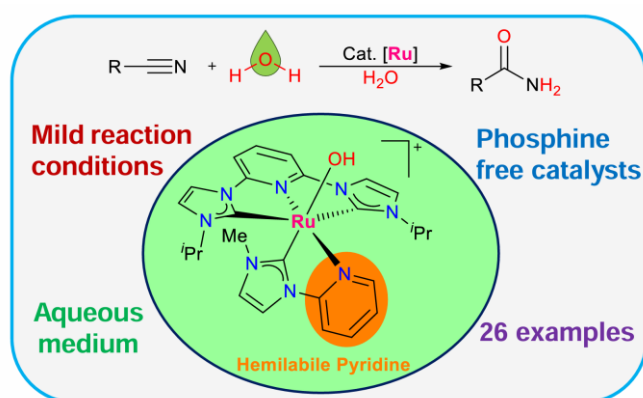
Figure 4. Cationic Ru(II)-CNC pincer catalyzed nitrile hydration to amides in an aqueous medium.

Chapter 6. Syntheses, Characterization, and Catalytic Activity of Dicationic Ru(II)-CNC Pincer Complexes with CH$_3$CN and PPh$_3$ Ligands

The reactivity of cationic Ru(II)-CNC pincer complexes [Ru(CNC^{Me})(CN^{Me})I]PF$_6$ (**7a**), [Ru(CNC$^{i\text{-}Pr}$)(CN^{Me})I]PF$_6$ (**7b**) and [Ru(CNC^{Cy})(CN^{Me})I]PF$_6$ (**7c**) with CH$_3$CN and PPh$_3$ ligands has been examined and afforded dicationic Ru(II)-CNC pincer complexes namely, [Ru(CNC^{Me})(CN^{Me})CH$_3$CN]2PF$_6$ (**11a**), [Ru(CNC$^{i\text{-}Pr}$)(CN^{Me})CH$_3$CN]2PF$_6$ (**11b**), [Ru(CNC^{Cy})(CN^{Me})CH$_3$CN]2PF$_6$ (**11c**), [Ru(CNC^{Me})(CN^{Me})PPh$_3$]2PF$_6$ (**12a**), [Ru(CNC$^{i\text{-}Pr}$)(CN^{Me})PPh$_3$]2PF$_6$ (**12b**), and [Ru(CNC^{Cy})(CN^{Me})PPh$_3$]2PF$_6$ (**12c**) (Figure **5**). Complexes (**11a–c**) were synthesized in CH$_3$CN at 40 °C, while complexes (**12a–c**) were synthesized in methanol at reflux conditions. All the newly synthesized complexes were fully characterized spectroscopically by multinuclear NMR and HRMS, and complexes **11a, 11c, 12a,** and **12b** were characterized by solid-state single-crystal X-ray diffraction techniques. The UV-Vis spectra of these complexes exhibited the hypsochromic shift by exchanging the anionic I$^-$ ligand to neutral PPh$_3$ and CH$_3$CN ligands. Electrochemical studies of these complexes show peaks of different heights within the accessible potential gap. Compare the catalytic activity for nitrile hydration with all the complexes with the I$^-$, CH$_3$CN, and PPh$_3$ ligands and find that the I$^-$ based catalysts are more active than CH$_3$CN-based catalysts and the poor catalytic activity with PPh$_3$ containing ligands. In the catalytic reaction mechanism, a Ru-OH species was generated and initiated the reaction with the coordination of benzonitrile.
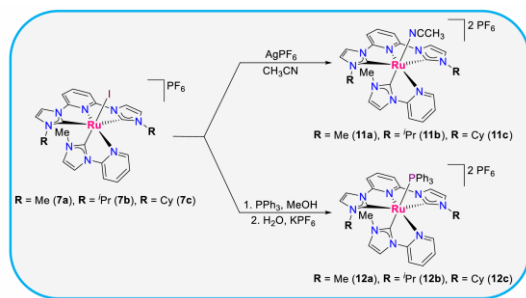
Figure 5. Syntheses of dicationic Ru(II)-CNC pincer complexes with CH₃CN and PPh₃ ligands.

Chapter 7. Conclusion and Future Scope

In summary, we have reported the syntheses and characterization of cationic Ru(II)-CNC pincer complexes with various ancillary ligands. These complexes have been utilized in TH, AAD, and ADC catalysis and found satisfactory results. In ADC catalysis, we investigated the effects of ancillary ligands (CO, COD, DMSO, and PPh₃) and the steric effects at N-wingtip (Me, ^{i}Pr, and Cy) of pincer ligands in catalysis to facilitate the removal of the catalytic products. Catalyst [Ru(CNC$^{i\text{-Pr}}$)(PPh₃)₂Cl]PF₆ (**3b**) shows excellent reactivity for ADC catalysis among all the catalysts. Furthermore, it was found that PPh₃ and DMSO-containing complexes performed better reactivity than complexes with CO and COD ligands. Continuing this study, we have investigated the syntheses of Ru(II)-CNC pincer complexes with multiple NHC carbene donor ligands. These complexes are fully characterized, and the catalytic activity for nitrile hydration in aqueous conditions is investigated. Catalyst [Ru(CNC$^{i\text{-Pr}}$)(CN^{Me})I]PF₆ (**7b**) exhibits better reactivity among all the synthesized ruthenium complexes. These complexes are highly reactive with CH₃CN and PPh₃ ligands and easily show ligand substitution under normal conditions. In comparing catalytic activities for nitrile hydration, I⁻ based catalysts were more active than those based on CH₃CN, whereas catalysts with PPh₃ ligands demonstrated low catalytic efficiency. These complexes will be explored shortly for water oxidation, carbon

dioxide reduction, small molecule activation, and various organic transformations.

References

1. Peris E., Crabtree R. H. (2018), Key factors in pincer ligand design, Chem. Soc. Rev., 47(6), 1959–1968 (DOI: 10.1039/C7CS00693D).

2. Moulton C. J., Shaw B. L. (1976), Transition metal-carbon bonds. Part XLII. Complexes of nickel, palladium, platinum, rhodium and iridium with the tridentate ligand 2,6-bis[(di-*t*-butylphosphino)methyl]phenyl, J. Chem. Soc., Dalton Trans., (11), 1020–1024 (DOI: 10.1039/DT9760001020).

3. Lawrence M. A. W., Green K.-A., Nelson P. N., Lorraine S. C. (2018), Review: Pincer ligands-Tunable, versatile and applicable, Polyhedron, 143, 11–27, (DOI: 10.1016/j.poly.2017.08.017).

4. Andrew R. E., González-Sebastián L., Chaplin A. B. (2016), NHC-based pincer ligands: carbenes with a bite, Dalton Trans., 45(4), 1299–1305 (DOI: 10.1039/C5DT04429D).

5. Hopkinson M. N., Richter C., Schedler M., Glorius F. (2014), An overview of *N*-heterocyclic carbenes, Nature, 510(7506), 485–496 (DOI: 10.1038/nature13384).

6. Crudden C. M., Allen D. P. (2004), Stability and reactivity of *N*-heterocyclic carbene complexes, Coord. Chem. Rev., 248(21), 2247–2273 (DOI: 10.1016/j.ccr.2004.05.013).

7. Gunanathan C., Milstein D. (2014), Bond Activation and Catalysis by Ruthenium Pincer Complexes. Chem. Rev., 114(24), 12024–12087 (DOI: 10.1021/cr5002782).

8. Poyatos M., Mata J. A., Falomir E., Crabtree R. H., Peris E. (2003), New Ruthenium(II) CNC-Pincer Bis(carbene) Complexes: Synthesis and Catalytic Activity, Organometallics, 22(5), 1110–1114 (DOI: 10.1021/om020817w).

9. Danopoulos A. A., Braunstein P., Saßmannshausen J., Pugh D., Wright J. A. (2020), "Pincer" Pyridine–Dicarbene–Iridium and -

Ruthenium Complexes and Derivatives Thereof, Eur. J. Inorg. Chem., 2020(35), 3359–3369, (DOI: 10.1002/ejic.202000429).

10. Vaquer L., Miró P., Sala X., Bozoglian F., Masllorens E., Benet-Buchholz J., Fontrodona X., Parella T., Romero I., Roglans A., Rodríguez M., Bo C., Llobet, A. (2013), Understanding Electronic Ligand Perturbation over Successive Metal-Based Redox Potentials in Mononuclear Ruthenium-Aqua Complexes, ChemPlusChem, 78(3), 235–243 (DOI: 10.1002/cplu.201200268).

11. Arikawa Y., Nakamura T., Ogushi S., Eguchi K., Umakoshi K. (2015), Fixation of atmospheric carbon dioxide by ruthenium complexes bearing an NHC-based pincer ligand: formation of a methyl carbonate complex and its methylation, Dalton Trans., 44(12), 5303–5305 (DOI: 10.1039/C5DT00476D).

12. Boudreaux C. M., Liyanage N. P., Shirley H., Siek S., Gerlach D. L., Qu F., Delcamp J. H., Papish E. T. (2017), Ruthenium(II) complexes of pyridinol and *N*-heterocyclic carbene derived pincers as robust catalysts for selective carbon dioxide reduction, Chem. Commun., 53(81), 11217–11220 (DOI: 10.1039/C7CC05706G).

13. Yadav D., Misra S., Kumar D., Singh S., Singh A. K. (2021), Cationic ruthenium(II)–NHC pincer complexes: Synthesis, characterisation and catalytic activity for transfer hydrogenation of ketones, Appl. Organomet. Chem., 35(8), e6287 (DOI: 10.1002/aoc.6287).

14. Yadav D., Singh R. K., Singh S., Shirage P. M., Singh A. K. (2021), Cationic ruthenium(II)-NHC pincer complexes with hemilabile COD: Solid-state structural characterization and theoretical study of an η2-(E,Z)-COD ligand, J. Organomet. Chem., 953, 122061 (DOI: 10.1016/j.jorganchem.2021.122061).

15. Yadav D., Singh R. K., Misra S., Singh A. K. (2022), Ancillary ligand effects and microwave-assisted enhancement on the catalytic performance of cationic ruthenium(II)-CNC pincer complexes for acceptorless alcohol dehydrogenation, Appl. Organomet. Chem., e6756 (DOI: 10.1002/aoc.6756).

LIST OF PUBLICATIONS

1. **R. K. Singh**, D. Yadav, S. Misra and A. K. Singh, Role of Ancillary Ligands in Selectivity Towards Acceptorless Dehydrogenation versus Dehydrogenative Coupling of Alcohols and Amines Catalyzed by Cationic Ruthenium(II)-CNC Pincer Complexes, *Dalton Trans.,* 2023, 52(43), 15878-15895 (DOI: 10.1039/d3dt03149g). Impact Factor: 3.3.

2. **R. K. Singh**, D. Yadav and A. K. Singh, Cationic Ruthenium(II)-CNC Pincer Complexes as Phosphine-free Catalysts for Nitrile Hydration to Amides in Aqueous Medium, *Mol. Catal.,* 2023, 549, 113523 (DOI: 10.1016/j.mcat.2023.113523). Impact Factor: 4.9.

3. **R. K. Singh**, D. Yadav, A. Singh, S. Misra and A. K. Singh, Nitrile Hydration via Outer-Sphere Electrophilic Attack of Nitrile on Ru-OH: A Combined Experimental and DFT Investigation with Cationic Ru(II)-CNC Pincer Complexes (Under Review).

4. N. Shahid, **R. K. Singh**, N. Srivastava and A. K. Singh, Base-Free Synthesis of Benchtop Stable Ru(III)-NHC Complexes from $RuCl_3 \cdot 3H_2O$ and Their Use as Precursors for Ru(II)-NHC Complexes, *Dalton Trans.,* 2023, 52(13), 4176-4185 (DOI: 10.1039/d3dt00243h). Impact Factor: 3.3.

5. D. Yadav, **R. K. Singh**, S. Misra and A. K. Singh, Ancillary Ligand Effects and Microwave-Assisted Enhancement on the Catalytic Performance of Cationic Ruthenium(II)-CNC Pincer Complexes for Acceptorless Alcohol Dehydrogenation, *Appl. Organomet. Chem.,* 2022, e6756 (DOI: 10.1002/aoc.6756). Impact Factor: 3.7.

6. **R. K. Singh**, S. Misra and A. K. Singh, Tripodal Ligands as Powerful Platforms for Designing New Catalysts, In *A Closer Look at Coordination Complexes*, S. Kaur-Ghumaan (ed.), Nova Science Publishers, Inc., 2021, 1-55, ISBN: 978-1-68507-199-8 (DOI: 10.52305/ENZL4915).

7. **R. K. Singh**, T. K. Khan, S. Misra and A. K. Singh, CAACs as Efficient Ancillary Ligands for the Synthesis of Robust Catalysts, *J. Organomet. Chem.,* 2021, 956, 122133 (DOI: 10.1016/j.jorganchem.2021.122133). Impact Factor: 2.4.

8. D. Yadav, **R. K. Singh**, S. Singh, P. M. Shirage and A. K. Singh, Cationic Ruthenium(II)-NHC Pincer Complexes with Hemilabile COD: Solid-state Structural Characterisation and Theoretical Study of an η^2-(*E,Z*)-COD Ligand, *J. Organomet. Chem.,* 2021, 953, 122061 (DOI: 10.1016/j.jorganchem.2021.122061). Impact Factor: 2.4.

CONFERENCE AND WORKSHOP

1. Attended Workshop on "Electrochemical Energy Storage Devices" organized by the Department of Metallurgical Engineering and Materials Science, Indian Institute of Technology (IIT), Indore, India (December 2024).

2. Attended Symposium on "Material Sciences Towards New Horizon-2023" jointly organized by the Royal Society of Chemistry and Department of Chemistry, Indian Institute of Technology (IIT), Indore, India (January 2023).

3. Poster presentation in 30th Chemical Research Society of India, National Symposium in Chemistry (30th CRSI-NSC & 16th CRSI-RSC Symposium Series in Chemistry) jointly organized by the Special Centre for Molecular Medicine (SCMM) and School of Physical Sciences (SPS), Jawaharlal Nehru University (JNU), New Delhi, India (February 2023); R. K. Singh, D. Yadav, and A. K. Singh, Cationic Ruthenium(II)-CNC Pincer Complexes with Multiple NHC Ligands: Catalytic Application in Hydration of Nitriles under mild Condition.

4. Poster presentation in International Conference Modern Trends in Inorganic Chemistry, (MTIC-XIX, 2022) organized by the Department of Chemistry, Institute of Science, Banaras Hindu University (BHU), Varanasi, India (December 2022); R. K. Singh, D. Yadav, S. Misra, and A. K. Singh, Tuning Stereoelectronic Properties Towards Selectivity in Catalysis by Cationic Ruthenium(II)-CNC Pincer Complexes.

5. Oral presentation in CHEM-2022 organized by the Department of Chemistry, Indian Institute of Technology (IIT), Indore, India (March 2022); R. K. Singh, and A. K. Singh, Ruthenium

Complexes with Multiple NHC Donor Ligands: Synthesis, Structure and Reactivity.

6. Attended Workshop on "Computationally Designing of Materials for Materials Genome" organized by the Department of Chemistry, Indian Institute of Technology (IIT), Indore, India (March 2021).

7. Poster presentation in Frontiers in Organometallics and Catalysis (FOMC-2021) organized by the Department of Chemistry, Malaviya National Institute of Technology (MNIT), Jaipur, India (January 2021); R. K. Singh, and A. K. Singh, Ruthenium Complexes with Multiple NHC Donor Ligands: Synthesis, Structure, and Reactivity.

8. Attended conference on "1st Virtual International Symposium on C-H Activation" organized by the Georg-August-Universität Göttingen, Germany (July 2020).

9. Attended "Author Workshop" jointly organized by Springer Nature and Indian Institute of Technology (IIT), Indore, India (September 2019).

10. Attended international conference on "Emerging Trends in Chemistry" organized by the Department of Chemistry, Indian Institute of Technology (IIT), Indore, India (July 2019).

TABLE OF CONTENTS

LIST OF FIGURES

Chapter 1: Introduction and Background

Chapter 2: Syntheses, Characterization, and Catalytic Activity of Cationic Ru(II)-CNC Pincer Complexes

Chapter 3: Role of Ancillary Ligands in Selectivity Towards Acceptorless Dehydrogenative Coupling of Alcohols and Amines Catalyzed by Cationic Ru(II)-CNC Pincer Complexes

Chapter 6: Syntheses, Characterization, and Catalytic Activity of Dicationic Ru(II)-CNC Pincer Complexes with CH₃CN and PPh₃ Ligands

LIST OF SCHEMES

LIST OF TABLES

NOMENCLATURE

α	Alpha
β	Beta
γ	Gamma
δ	Delta
σ	Sigma
π	Pi
θ	Theta
%	Percentage
λ	Wavelength
Å	Angstrom
J	Coupling constant
Hz	Hertz
MHz	Megahertz
K	Kelvin
D	Density
V	Volume
°	Degree
˚C	Degree centigrade
cm	Centimetre
cm^3	Cubic centimetre
g	Gram
mg	Milligram
ppm	Parts per million
nm	Nanometre
mL	Millilitre
μL	Microlitre
mmol	Millimole
mM	Millimolar
μM	Micromolar
μA	Microampere
a.u.	Arbitrary Unit

ACRONYMS

DFT	Density Functional Theory
NMR	Nuclear Magnetic Resonance
UV-vis	Ultraviolet-visible Spectroscopy
CV	Cyclic Voltammetry
DPV	Differential Pulse Voltammetry
ESI-MS	Electrospray Ionization-Mass Spectrometry
GC-MS	Gas Chromatography-Mass Spectrometry
HOMO	Highest Occupied Molecular Orbital
LUMO	Lowest Unoccupied Molecular Orbital
TH	Transfer Hydrogenation
AAD	Acceptorless Alcohol Dehydrogenation
ADC	Acceptorless Dehydrogenative Coupling
TLC	Thin Layer Chromatography
ρcalc	Density Calculated
SCXRD	Single Crystal X-ray Diffraction
GOF	Goodness of Fit
TEP	Tolman Electronic Parameter
$CDCl_3$	Chloroform-*d*
DMSO-d_6	Dimethylsulphoxide-*d_6*
NHC	*N*-Heterocyclic Carbene
IAd	1,3-Bis(adamantyl)imidazol-2-ylidene
Bpy	Bipyridine
Im	Imidazole
Bim	Benzimidazole
KHMDS	Potassium hexamethyldisilazane
Ag_2O	Silver oxide
NEt_3	Triethylamine
Cs_2CO_3	Cesium carbonate
$Pd(OAc)_2$	Palladium diacetate

BEMP	2-*tert*-Butylimino-2-diethylamino-1,3-dimethylperhydro-1,3,2-diazaphosphorine
NaOH	Sodium hydroxide
KOH	Potassium hydroxide
Na_2CO_3	Sodium carbonate
$NaHCO_3$	Sodium bicarbonate
NaO^iPr	Sodium isopropoxide
^tBuOK	Potassium *tert*-butoxide
LiBr	Lithium bromide
PCy_3	Tricyclohexylphosphine
PPh_3	Triphenylphosphine
COE	Cyclooctene
COD	1,4-Cyclooctadiene
CO	Carbon Monoxide
DMSO	Dimethyl Sulphoxide
NBD	2,5-Norbornadiene
NH_4PF_6	Ammonium hexafluorophosphate
KPF_6	Potassium hexafluorophosphate
$TBAPF_6$	Tetrabutylammonium hexafluorophosphate
MS	Molecular Sieves
o	Ortho
m	Meta
p	Para
Li	Lithium
Na	Sodium
K	Potassium
Fe	Iron
Ru	Ruthenium
Os	Osmium
Co	Cobalt
Rh	Rhodium

Ir	Iridium
Ni	Nickel
Pd	Palladium
Pt	Platinum
Kr	Krypton
TON	Turnover number
TOF	Turnover frequency
Min	Minute
Temp	Temperature
Equiv	Equivalent
Cat	Catalyst
Calc	Calculated
Me	Methyl
^{i}Pr	*iso*-propyl
Cy	Cyclohexyl
^{t}Bu	*tert*-butyl
^{n}Bu	*n*-butyl
Ph	Phenyl
Mes	Mesityl
Dipp	2,6-Diisopropylphenyl
p-Cym	*p*-Cymene
MeOH	Methanol
EtOH	Ethanol
i-PrOH	Isopropanol
CHCl$_3$	Chloroform
DCM	Dichloromethane
CH$_3$CN	Acetonitrile
Et$_2$O	Diethyl ether
THF	Tetrahydrofuran
DME	Dimethyl ether

Chapter 1

Introduction and Background

1.1. Introduction

Ligand design is a critical aspect of coordination chemistry that involves tailoring molecules to bind selectively and effectively to metal centres, inducing the properties and reactivity of resulting complexes. In coordination chemistry, a ligand is an organic or main-group molecule, and ions bind to the metal centre and generate coordination complexes. Metal-ligand bonding interactions are crucial steps for the synthesis and stability of coordination compounds, which are important in various fields, including chemistry, biochemistry, and materials science [1, 2]. In these complexes, metals act as Lewis acids, readily accepting electron pairs from ligands, which function as Lewis bases. The nature of the metal-ligand bond is highly dependent on the metal's electronic configuration and the ligand's coordinating properties. Coordination bonds can range from ionic to highly covalent, influencing the overall structure and reactivity of the complex. Ligand plays an important role in inorganic and organometallic chemistry as well as metal-catalyzed homogeneous reactions, and it also affects the structure and reactivity of metal complexes and has allowed for the discovery of new and enhanced metal-catalyzed reactions.

The study of organometallic chemistry, especially homogeneous catalysis, has greatly profited from the unfolding of a wide variety of ligands with amazing influence on the reactivity of metal complexes. Pincer ligands are tridentate chelating ligands that bind with the metal centre through three adjacent coplanar sites with a meridional geometry (Figure **1.1**). It was first reported by Moulton and Shaw in 1976 [3]. Pincer ligands get more attention due to their

1

versatility and afford a highly promising group of catalysts that offer numerous possibilities and potential catalytic applications. Pincer ligands form two stable cyclometallated rings upon coordination with the metal centre, which can be five, six, or both five and six-membered or one five and one six-membered rings. In 1989, Van Koten described for the first time pincer tridentate ligands with two flanking binding units and a central anionic carbon that impose meridional geometry around the metal centre [4, 5]. The first organometallic complex with tridentate ligands was reported in the late 1970s with a meridional geometry [5]. Pincer ligands prefer a meridional geometry; however, in some circumstances, the facial form may be adopted. This definition states that tripodal ligands are not pincer-type ligands because they exhibit a definite preference for the facial coordination mode. Two fused metallacycles are combined to form pincer complexes, having two side arms that stabilize the complexes and significantly impact their electronic properties. Pincer complexes are explored for their remarkable thermal stability, which is especially valued in homogeneous catalysis since it allows for high-temperature reactions. Over the last two decades, there has been considerable interest in pincer ligands for their crucial role in coordinating various compounds. Researchers have particularly focused on understanding their coordination mechanisms within a wide range of chemical structures.
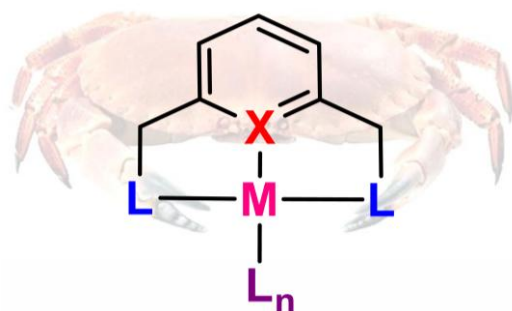
Figure 1.1. Schematic representation of a typical pincer ligand appended metal complex with two flanking donor arms and their binding sites like a crab.

The modular characteristics of pincer ligands allow for facile fine-tuning of their steric and electronic properties while maintaining the integrity of the coordination geometry. Pincer ligands, featuring centrally disubstituted aromatic rings with two flanking arms, exhibit significant alterations in steric crowding around the metal centre by varying the nature of these flanking arms, with minimal electronic impact. The introduction of a bulky **R** group directly influences steric hindrance around the metal centre. The reactivity of pincer complexes can be diversified by manipulating the bite angle, a parameter highly dependent on the ring size and alterable through linker arm size. Electronic property modifications, with limited influence on the ligand series, can be achieved by controlling the nature of **Z**, a central aromatic ring substituent. The central donor atom (**X**, usually C or N) can exert a significant electronic influence, particularly through changes in the *trans*-effect [6]. Moreover, incorporating chirality with chiral **Y/LR_n** groups introduces a substantial modification to pincer ligands (Figure **1.2**) [7]. This modification is particularly relevant for applications in asymmetric catalysis, where the chiral environment near the metal centre plays a crucial role in determining the enantioselectivity of catalytic reactions. Overall, the ability to make precise modifications in pincer ligands offers a wide range of possibilities for tailoring their properties to specific applications, ranging from catalysis to materials science. The modular approach you described allows researchers to explore various combinations and optimize ligand structures for desired outcomes.
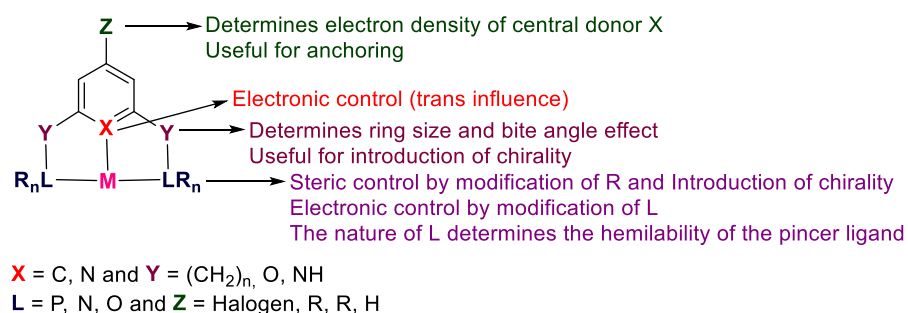
Figure 1.2. Steric and electronic control of pincer ligands.

3

1.2. Classification of the pincer ligand system

The literature classifies pincer ligands in two different ways: (**1.2.1**) the symmetry and charge (neutral or ionic) of the binding motif and (**1.2.2**) donor atoms and coordination modes.

1.2.1. Peris and Crabtree classified the pincer ligands based on the symmetry and charge (neutral or ionic) of the binding motif [2].

1.2.1.1. Palindromic type pincer - The six-electron donor L3 ligands feature identical donor atoms at both terminals, as illustrated by configurations like NCN, CNC, PCP, and analogous structures, all of which constitute palindromic pincers [2].

L = flanking neutral donor = PR_2, NR_2, OR, SR, C (from NHC)
$L'R_2$ = central neutral donor = Py, PR_3, NR_3, C (from NHC)
X = flanking anionic donor = O, NR, C (from phenyl)
X' = central anionic donor = C (from phenyl), SiR, N (imide)
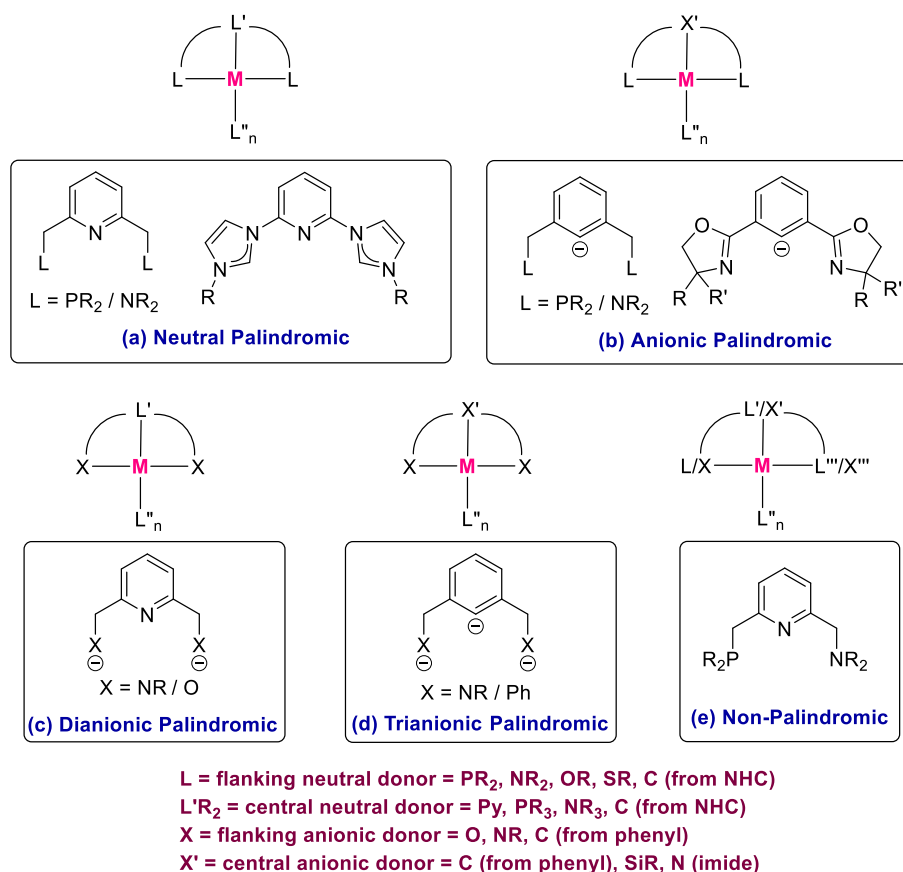
Figure 1.3. Classification of pincer ligands.

(a) Neutral palindromic - All the donor atoms are neutral, serving as six-electron donors of L3 ligands (Figure **1.3a**).

(b) Monoanionic palindromic pincer - The monoanionic palindromic pincers, typically featuring a central aryl ring and two adjacent neutral donors of either P or N, are the most common among all types of pincers and the first to be reported (Figure **1.3b**).

(c) Dianionic palindromic pincer - Dianionic palindromic pincer ligands are less common, in which the central donor is neutral at the binding position and the anionic donor units are positioned in the ligand flanking arms (Figure **1.3c**).

(d) Trianionic palindromic pincer - They have high charge and are suitable for establishing stable complexes with high-valent metal species (Figure **1.3d**).

1.2.1.2. Non-palindromic type pincer - These are the ligands with various donor atoms at the side arms, such as NNP, NNC, etc. Ligands with such structures can indeed offer diverse coordination possibilities and are valuable in coordination chemistry (Figure **1.3e**). The asymmetry introduced by non-palindromic ligands allows for more flexibility in adjusting the characteristics of metal complexes. However, non-palindromic type pincers have been less studied [2].
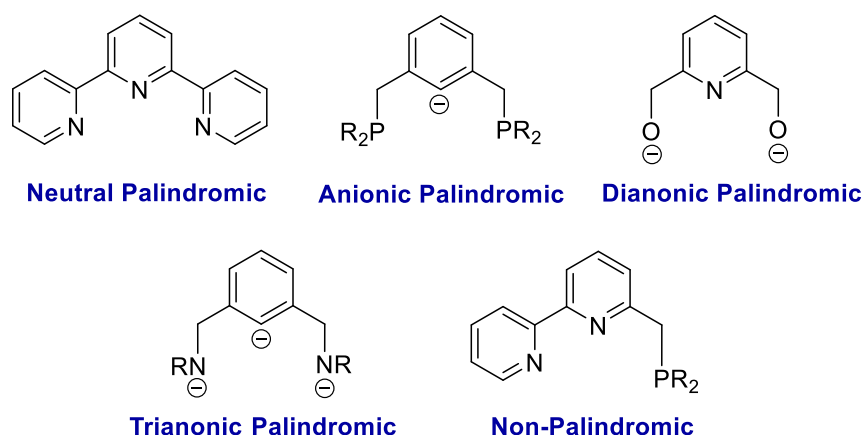
Figure 1.4. Some examples of palindromic and non-palindromic types of pincer ligands.

Palindromic ligands have been more extensively studied, and non-palindromic ligands are gaining attention for their potential to

bring variations in coordination environments and reactivity. Researchers are likely exploring the synthesis and coordination chemistry of these ligands to understand their unique properties and applications in catalysis, sensing, or other areas of interest. Some selected examples of palindromic and non-palindromic pincer ligands have been listed in Figure **1.4**.

1.2.2. In literature, pincer ligands have been categorized into two groups based on their donor atoms and coordination modes [8].

1.2.2.1. ECE (E = N, P) and ENE (E = C, S, Se, P) donor pincer ligands

ECE-type pincer ligands are monoanionic, with two side arms of the pincer bearing donor groups ''E'' (E = N or P) and a central aryl anionic carbon donor group. The ENE pincer system possesses a central nitrogen donor, with two side arms of the pincer bearing donor groups ''E'' (E = C, S, Se, or P). Symmetrical pincer ligands are simpler to synthesize than their non-symmetrical counterparts. In general, the two ligand sites are instantly modified to initiate the reaction with a symmetrical ligand. This involves incorporating donor groups into the two side arms of the pincer, facilitating the synthesis of symmetrical pincer ligands. The synthesis of symmetrical pincer ligands is generally easier than synthesizing non-symmetrical counterparts.

(a) CNC and NCN donor pincer ligands

CNC and NCN are the most popular pincer ligands in organometallic chemistry, and these ligands vary significantly in architecture and composition (Figure **1.5**) [8, 9]. These pincer systems are favoured for their ease of synthesis of metal complexes over other alternative pincer ligands. It is possible to impose steric necessities determined by the mechanism of ligand coordination and induce chirality when substituents are present around coordination sites. The NCN pincer has

one metal-carbon σ bond, whereas the tridentate mode in CNC pincer ligands has two metal-carbon σ bonds. In homogeneous catalysis, the metal-carbon bonds reduce metal leaching and increase the stability of the complexes. Depending upon the oxidation state of the metal centre in specific circumstances, the NCN pincers occasionally display fluxional behaviour in their binding modes, such as the tridentate meridional, the NC bidentate, and bridging modes.
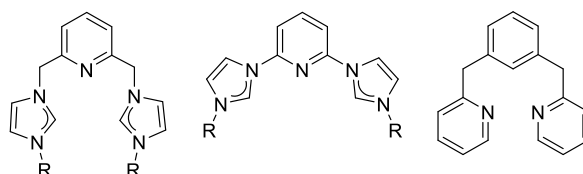
Figure 1.5. CNC and NCN donor pincer ligands.

(b) PCP and PNP donor pincer ligands

Phosphorus displays notable nucleophilic and reducing properties when in low oxidation states, but to maintain stability in the air, it often requires bulky groups. PCP and PNP-type pincers having phosphorous as coordination sites have found numerous applications in catalysis (Figure **1.6**) [10]. The metal centres were stabilized by phosphorous in both high and low oxidation states.
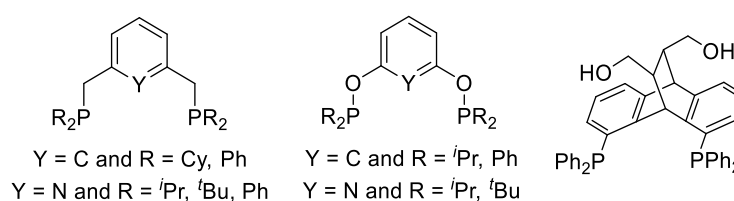
Figure 1.6. PCP and PNP donor pincer ligands.

Phosphines and phosphites as donor groups are the most extensively studied class of pincer ligands. A small change in PCP and PNP pincer ligands has a more dramatic impact on their reactivity. In the PCP pincer ligand, the metal-carbon σ bond increased the complex stability in comparison to the PNP complexes. Synthesis techniques for pincer ligands may vary depending on the spacer between the

phosphines and the central aromatic ring. Treatment with lithium phosphides can convert 2,6-bis(bromomethyl)pyridine or 1,3-bis(bromomethyl)benzene into PNP and PCP ligands, respectively, featuring methylene group spacers [8, 10]. Resorcinol and chlorophosphines are used to make PCP pincer, also known as POCOP pincer [10–12]. A more effective chiral pocket was formed with more traditional techniques by using the distinctive topology of the dibenzobarrelene-based PCsp^{3}P pincer to develop chiral-at-frame pincer ligands [13].

(c) SNS and SeNSe donor pincer ligands

Sulphur atoms are commonly used as donor atoms to modify the electronic characteristics of various metal centres. These metal centres can act as σ-donor, π-acceptor, and even π-donor ligands, capable of accommodating both soft and hard auxiliary ligands. Chalcogen-centred pincer ligands represent emerging classes of ligand systems. One notable example of pincer ligands containing sulphur donor atoms is derived from a 2,6-bis-thioamido-pyridine backbone [14]. Although selenium exhibits some chemical similarities with sulphur, compounds incorporating selenium have been documented to a lesser extent compared to their sulphur counterparts (Figure **1.7**) [15].
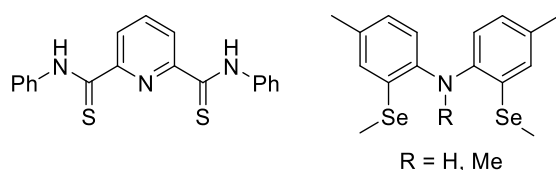
Figure 1.7. SNS and SeNSe donor pincer ligands.

(d) NNN donor pincer ligands

NNN-type pincer ligands have received more attention in coordination chemistry, homogeneous catalysis, and organic synthesis due to the robust reactivity exhibited by metal complexes featuring nitrogen donor ligands (Figure **1.8**). A wide range of NNN donor pincer ligands

has been extensively studied, including bis(imino)pyridines, bis(pyridylimino)isoindoles, 2,6-bis-amido-pyridine, and 2,6-bis(5-tert-butyl-1H-pyrazol-3-yl) pyridine. An illustrative instance of an NNN-type pincer ligand is 2,6-bis(3,5-dimethylpyrazole-1-yl) pyridine (Me$_4$BPPy), as reported by Wu et al. in 2005, in association with Ru(II) complexes [16]. Furthermore, Zhengkun investigated the NNN-type unsymmetrical pincer metal complex with Ru(II) bearing a pyridyl-based benzimidazolyl-benzotriazolyl ligand [17]. Pyridine-2,6-dicarboxylic acid bisphenylamide is an amide-containing pincer ligand that was first synthesized in the 1970s, and these amide-based pincer ligands offer an attractive scaffold owing to their facile synthesis and modifiability [18, 19].
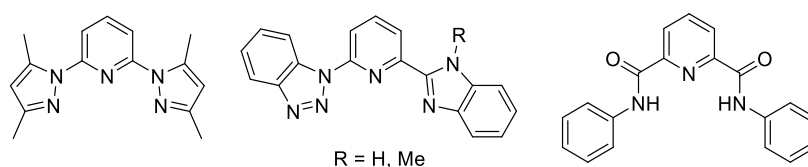
Figure 1.8. NNN donor pincer ligands.

(e) LX$_2$ type NHC core pincer ligands (NCN and OCO donor pincer ligands)

The LX$_2$ type pincer ligand is a symmetrical donor ligand with NHC occupying the central position and the *N*-substituents by two lateral arms carrying anionic coordinating atoms, which are relatively little explored as compared to others (Figure **1.9**) [20]. The interaction of NHCs with anionic donors indeed allows for the stabilization as well as modulation of the reactivity of different metal complexes throughout the periodic table [21, 22].
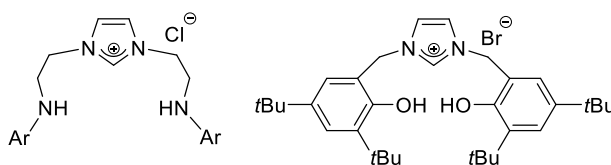
Figure 1.9. NCN and OCO donor pincer ligands.

9

1.2.2.2. PCN and YNX (Y = C, N or O; X = N, O or S) donor pincer ligands

PCN and YNX type pincer systems, obtained through the modification in the pincer "arm" significantly impact the catalytic activity of the resulting complexes. Substituting a weaker donor group for one of the donor groups can promote ligand dissociation from the metal centre, potentially increasing the hemilability of the pincer complexes and thus enhancing their catalytic performance. Consequently, there has been a focus on developing mixed or hybrid pincer systems based on pyridine as a core for ruthenium complexes. These systems aim to enhance the possibility of potential "hemilability" within the newly synthesized ligand. The synthesis of unsymmetrical pincer ligands involves a multi-step approach, often posing significant challenges. This strategy involves initiating with a symmetrical ligand precursor and subsequently modifying it in separate steps to introduce two distinct donor sites.

(a) PCN, PNN, and CNN donor pincer ligands

Unsymmetrical donor-containing pincer ligands represent a growing category within the realm of pincer ligands (Figure **1.10**) [23, 24]. PCN pincers mainly employ backbones such as aminophosphine-imidazoline, pyrazolyl aminophosphine, and (oxazolinyl)phenyl phosphinite [25]. These pincer systems have the potential to offer a greater range of catalytic properties; however, their inherent asymmetry demands more intricate synthetic approaches compared to the ECE and ENE classes of pincer ligand.
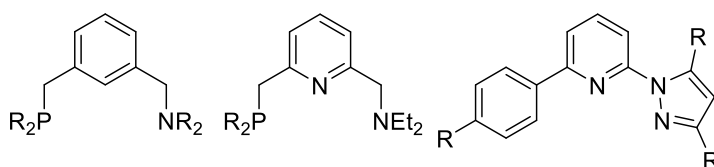
Figure 1.10. PCN, PNN, and CNN donor pincer ligands.

(b) ONS and PNS donor pincer ligands

The pincer ligands with mixed donor atoms [ONS] and [PNS] provide asymmetric metal complexes (Figure **1.11**) [26–28]. ONS-type pincer systems exhibit relatively less incidence compared to other ones, and their chemistry needs more investigation. ONS pincers coordinate with different approaches via the κ^3-ONS mode [26]. This type of system was first reported by Crabtree in the 1990s, featuring a ligand derived from a thiosemicarbazone backbone (2-hydroxy-5-methylacetophenone N, N-dimethylthiosemicarbazonato) [29].
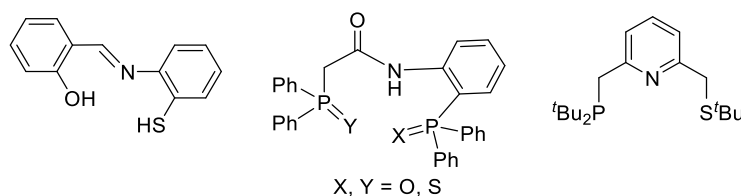
Figure 1.11. ONS and PNS donor pincer ligands.

(c) YNX (Y = N or C and X = O or S) donor pincer ligands

Pincer ligands incorporating mixed donor atoms offer flexibility in selecting metal precursors, yielding pincers with κ^3-YNX coordination modes (Figure **1.12**). Their metal complexes exhibit remarkable optical sensitivity to various substrates, including organic molecules [30–32].
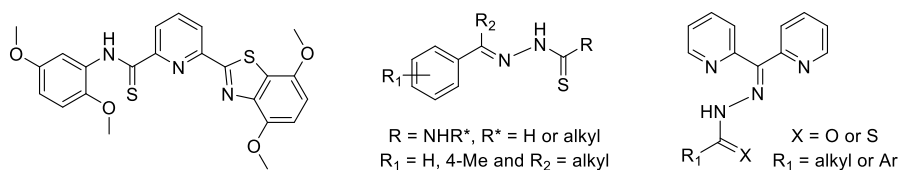
Figure 1.12. YNX (Y = N or C and X = O or S) donor pincer ligands.

1.3. Advantages of pincer ligands

Pincer-type ligand systems offer several distinct advantages over other chelating ligands. These ligands enable precise coordination around the metal centre. Pincer ligands have the unique ability to provide their

metal complexes with remarkable thermal stability, which is particularly useful for homogeneous catalysis. These rigid pincer ligands, when equipped with appropriate substituents, effectively produced metal complexes for asymmetric catalysis. Pincer ligands stabilized the metal complexes exhibiting unusual oxidation states. If donor groups are neutral exhibit hemilability. Metal complexes can be easily fine-tuned through stereoelectronic tunability. These advantages collectively enhance the potential of this ligand class in developing superior catalytic systems when coordinated with a metal centre.

1.4. Introduction of carbenes

Carbenes serve as highly efficient auxiliary ligands for synthesizing transition metal complexes, extensively investigated for their adjustable stereoelectronic properties. Their applications across various chemistry domains have been demonstrated extensively. Metal carbene complexes encompass a range of donor carbenes, including NHCs [33], CAACs [34], protic [35], abnormal [36], and mesoionic carbenes [37]. Carbene-containing metal complexes have found considerable interest in organic, inorganic, organometallic, medicinal, and materials chemistry. Carbenes (: CH_2) have six electrons in the valence shell and are electronically neutral species with a divalent carbon atom [33, 38, 39]. Carbenes are highly reactive due to their incomplete octet and coordinative unsaturation. Carbenes exhibit high reactivity resulting from their coordinative unsaturation and incomplete octet. Carbenes and their derivatives are chemical species in which either two univalent groups or a divalent group are covalently bonded to a carbon atom that possesses a pair of nonbonding electrons. Before the isolation of stable free carbenes, they were primarily considered highly unstable intermediates produced during organic transformations like cyclopropanation processes [40]. Carbenes were first described in organic chemistry by Doering in 1954 [41] and in organometallic chemistry by Fischer in 1964 [42]. Since then, carbenes have become

12

the most popular ligands of high synthetic interest. Furthermore, two distinct types of carbenes can be differentiated by their spin multiplicity [43].

1.4.1. Triplet carbene - The non-bonding electrons are in two distinct orbitals that have parallel spins. They have an electronic configuration like $\sigma^1 p_\pi^1$ ($^3B_1$) (Figure **1.13a**).

1.4.2. Singlet carbene - The two non-bonding electrons are in the same σ or p_π orbital with opposite spins, and their electronic configurations are either σ^2 or p_π^2 ($^1A_1$) (Figure **1.13b**, **1.13c**). The more stable electronic configuration of singlet carbene is σ^2 with bent geometry. The electronic configuration $\sigma^1 p_\pi^1$ ($^1B_1$) is an excited state of singlet carbene that is more energetic than the $^1A_1$ state (Figure **1.13d**).
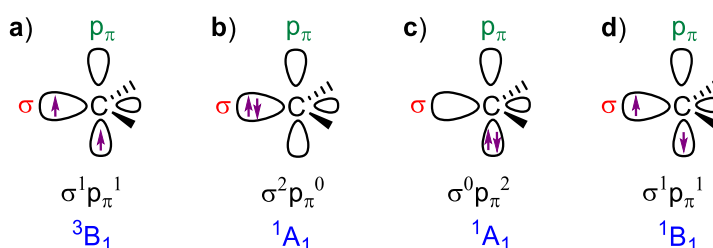
Figure 1.13. Orbital representation of the possible electronic arrangements of carbenes.

1.5. Electronic properties of carbenes

The geometry around the carbenic carbon can vary depending on the degree of hybridization. When a carbene centre possesses two non-bonding degenerate orbitals (p_x and p_y), it signifies a sp-hybridized carbene centre with linear geometry. However, most carbenes exhibit a bent geometry, where the molecule deviates from the linear arrangement of orbitals. In such cases, the degeneracy is lost, leading to the rehybridization of the p_x-orbital to sp^2, depicted as a σ-orbital, while the p_y-orbital, also represented as a $p\pi$ orbital, remains

unchanged (Figure **1.14**). It should be noted that we rarely see linear geometry, as most of the carbenes are of bent geometry [40, 44].

$\theta_{X-C-X} = 120°$ $\theta_{X-C-X} = 180°$
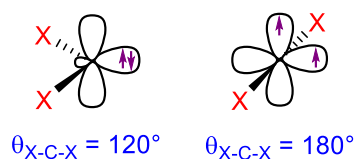
Figure 1.14. The sp^2 and sp-hybridized orbitals of the carbene carbon atom.

The spin multiplicity of carbenes is the primary factor that determines their reactivity. The singlet carbene has an ambiphilic nature due to the presence of both an empty and a filled orbital, while the triplet carbene is diradical because it has two partially occupied orbitals.
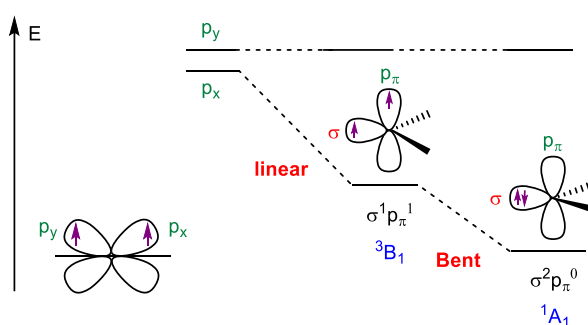
Figure 1.15. Relationship between the bond angle at the carbene centre and the nature of the frontier orbitals.

The ground state multiplicity of carbenes is dictated by the energy difference between the σ and pπ orbitals. According to Hoffmann, approximately 2.0 eV above this energy level, a $^1B_1$ state with bent geometry emerges, while a singlet ground state $^1A_1$ lies approximately 1.5 eV higher (Figure **1.15**) [45].

According to Hund's rule of maximum spin multiplicity, which is applicable to degenerate px and py orbitals, only the $p_x{}^1p_y{}^1$ electronic configuration is possible for the linear geometry. The spin multiplicity = 3 is the result of both unpaired electrons being "spin up" (*ms* = ½).

14

This produces a total spin of $S = 1$. As a result, linear carbenes are generally triplet in nature and have the electronic configuration $\sigma^1 p_\pi^1$ ($^3B_1$). Tomika described the synthesis and characterization of the triplet carbene, and it was stable in solution at room temperature [44].

1.6. Classification of carbenes

Carbenes can be broadly classified according to their electro-/nucleophilicity, substituents, and spin multiplicity. These can be categorized as (**1**) Fischer carbene, (**2**) Schrock carbene, and (**3**) *N*-Heterocyclic carbene (NHC).

1.6.1. Fischer carbene - Methoxy/methyl substituted methylene carbene coordinated Tungsten(0) pentacarbonyl was the first organometallic metal-carbene compound reported by Dr. Ernst Otto Fischer in 1964, when carbenes were starting to find trending applications in organic chemistry [42]. Fischer carbene is electrophilic and singlet in nature. Fischer carbene typically forms complexes with middle or late transition metals in a low oxidation state (0, +1) (Figure **1.16a**). The carbene carbon is attached to π-donor groups like alkoxy and alkylated amino groups, while the metal possesses π-acceptor ligands. The M-C bond is donor-acceptor in nature, resulting from the σ-donation of the carbene to the metal and the π-back donation of the metal to the carbene [46].

(**a**) Singlet Fischer Carbene   (**b**) Triplet Schrock Carbene

Fischer carbene complex   **Schrock carbene complex**
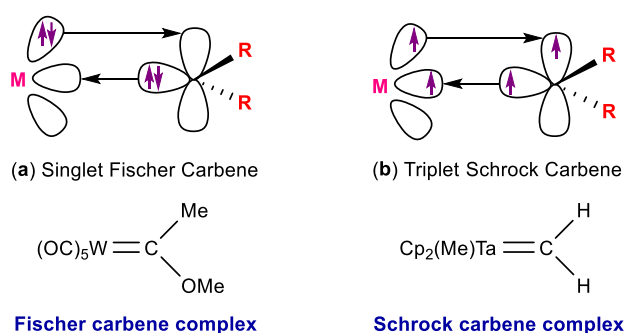
Figure 1.16. Schematic illustrations of (**a**) donor-acceptor type bonding in Fischer carbene complexes and (**b**) the covalent bonding in Schrock carbene complexes.

1.6.2. Schrock carbene - Schrock carbene was reported by Richard R. Schrock in 1975 [47]. The carbene carbon is nucleophilic and triplet in nature. Schrock carbene complexes are typically formed through the interaction of a triplet carbene with a metal fragment, as illustrated in Figure **1.16b**. The M-C bond is covalent; upon the polarization of the bond between metal and carbene, the carbene centre is nucleophilic. Schrock carbene generally forms complexes with the early transition metals (Ti/Ta) in a high oxidation state (+4, +5), coordinated with π-donor ligands [48]. A well-known example of Schrock carbene is generated from Tebbe's reagent via deprotonation of the alkyl group, which is a titanium-based complex.

1.6.3. *N*-heterocyclic carbenes - *N*-heterocyclic carbenes (NHCs) have emerged as highly versatile neutral ligands capable of donating two electrons. They exhibit significantly greater σ-donation compared to traditional divalent carbon donor ligands like carbon monoxide and isocyanides, which have been known for over a century [49]. Initially, carbenes were observed only with stabilized metal complexes [50–52]. In 1960, Wanzlick investigated the synthesis of an imidazolidin-2-ylidene by α-elimination of chloroform from 1,3-diphenyl-2-trichloromethylimidazolidine but was unable to isolate the free carbene [53]. They suggested that this carbene and its dimer, a derivative of tetraaminoethylene, are constantly in equilibrium [53]. Reasonable progress in the field of carbene chemistry was delayed before 1960 by the belief that carbenes were too reactive to be isolated. The discovery and thorough investigation of uncoordinated carbenes proved to be a challenge until innovative research emerged in the late 1980s and early 1990s, despite several attempts to synthesize carbenes from as early as 1835. In 1988, the Bertrand group achieved a milestone by successfully synthesizing a stable carbene, [bis-(diisopropylamino)phosphino](trimethylsilyl)carbene, which was stabilized through beneficial interactions with neighbouring phosphorus and silicon substituents [54]. Three years later, in 1991,

Arduengo and co-workers made a significant breakthrough by isolating and characterizing 1,3-bis(adamantyl)imidazol-2-ylidene (IAd), marking the first instance of a free and stable "bottle-able" *N*-heterocyclic carbene (Figure **1.18a**) [55]. Since then, intensive research has been devoted to carbene chemistry, particularly focusing on these compounds and their metal complexes. Initially, *N*-heterocyclic carbenes (NHCs) were supposed merely as imitators of phosphine-based ligands due to their similar coordination properties [56]. However, despite this resemblance, there are notable differences between these two prevalent classes of ancillary ligands. NHC-based metal complexes exhibit greater bond dissociation energy and shorter bond lengths between the metal and carbenic carbon, rendering the metal-carbene bond thermodynamically stronger [49]. Even in comparison to most Lewis basic phosphine (PCy_3) based metal complexes, the bond dissociation energy of NHC-derived metal complexes remains higher [56]. Consequently, the resulting less labile M-NHC bond contributes to the formation of thermally and oxidatively stable complexes [57]. With these salient features, NHCs have replaced phosphines as efficient ancillary ligands in organometallic chemistry. A famous example is the second-generation Grubb's catalyst, which was synthesized by the replacement of the phosphine in the first-generation Grubb's catalyst with the IMes ligand, and it enhanced the thermal stability and performance of the catalyst significantly (Figure **1.17**) [58, 59].

Grubb's first generation

Grubb's second generation
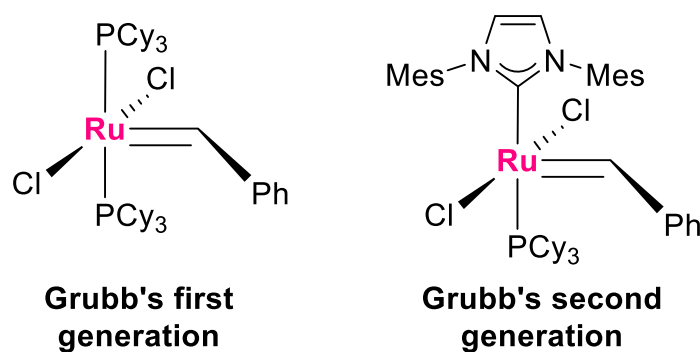
Figure 1.17. Grubb's first and second-generation metathesis catalysts.

NHCs have been the most versatile ligand system over the last couple of decades in organometallic chemistry, due to their unique steric and electronic properties [60]. NHCs find diverse applications, serving as spectator ligands in catalytically active complexes [61–65], acting as organocatalysts [66–68], and contributing to stabilizing unconventional complexes and miscellaneous other areas [69, 70].

1.7. Structural features of NHCs

NHCs typically constitute heterocyclic compounds featuring nitrogen atoms integrated within the ring and a carbenic carbon. The resulting carbene compounds can exhibit diverse characteristics, such as varying substituents, ring sizes, and degrees of heteroatom stabilization. The following structural features collectively influence the stabilization of NHCs, though their impact can differ between compounds (Figure **1.18a**) [40, 71].

(a) Nitrogen atoms - The nitrogen atoms play a crucial role in electronically stabilizing the carbene centre. The stable ground state of NHC is singlet in nature, and the nonbonding electron pair resides in a sp^2-hybridized orbital which is HOMO (Highest Occupied Molecular Orbital), while the π-orbital on the C2 carbon atom is LUMO (Lowest Unoccupied Molecular Orbital), remains unoccupied. The nitrogen atoms stabilize the carbenes by employing inductive as well as mesomeric effects. The inductive effect involves pulling σ-electrons from the adjacent carbene centre which lowers the energy of occupied σ-orbital (HOMO) whereas, the mesomeric effect entails the donation of π-electron in the empty $p\pi$-orbital (LUMO) of carbene hence, raises its energy (Figure **1.18b**) [49].

(b) Ring size - The cyclic structure of NHCs favours a singlet ground state, enforcing a bent-like sp^2 arrangement of the carbene carbon. The ring size affects the sterics and electronic stability of carbene [40].

(c) Backbone - The properties of NHCs are predominantly influenced by the heterocycle class, while the substitution pattern of the ring backbone also holds significant importance. Furthermore, electronic stabilization can also be achieved *via* the induction of aromaticity at the backbone substituents [72].

(d) *N*-substituents - The bulky substituents on the nitrogen atoms inhibit the Wanzlick equilibrium by sterically preventing carbene dimerization into the corresponding alkene [73]. The steric hindrance of *N*-substituents kinetically stabilizes the carbene. It also affects the electronic influence on carbene and has the potential for asymmetric induction.
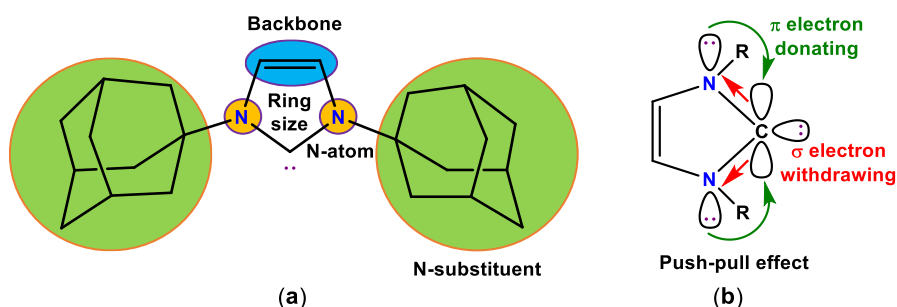
Figure 1.18. (**a**) Structural features of IAd, and (**b**) the singlet carbene structure is stabilized through the nitrogen heteroatoms by σ-withdrawing and π-donating effects.

1.8. Steric and electronic properties of *N*-heterocyclic carbenes

(a) Stability of carbenes - The stability of carbene is governed by the following two factors: the influence of nitrogen atoms and the *N*-substituents on the carbene skeleton.

(b) Push-pull effect - The nitrogen atom enhances the stability of the carbene through both negative inductive (-I) and positive mesomeric (+M) effects. The -I effect stabilizes the carbene σ orbital by withdrawing (i.e., "pull") electron density from the carbene centre due

to the higher electronegativity of nitrogen. In contrast, the +M effect, originating from the lone pair on nitrogen, donates (i.e. "push") electron density to the vacant pπ-orbital of the carbene carbon, thereby increasing its electron density and reducing its energy. As a result, the energy difference between the two frontier orbitals increases, leading to the stabilization of the singlet ground state. These two effects combined simultaneously are described as a "push-pull effect". In classical NHCs, two nitrogen atoms are attached to the carbene carbon and stabilized through the "push-pull effect", which increases the stability of NHCs [49].
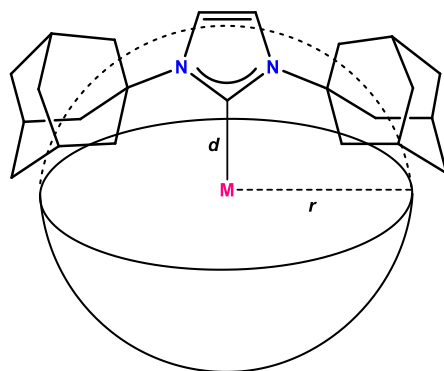
Figure 1.19. Sphere dimensions are utilized to determine the steric parameter ($\%V_{Bur}$) of NHC ligands.

(c) Steric effects - The extent of steric effects exhibited by *N*-heterocyclic carbenes (NHCs) can be assessed by calculating the *$\%V_{bur}$* value. This value represents the percentage of space within a defined radius "r" that is filled or "buried" by the ligand when it coordinates with a metal positioned at the sphere centre. It was first observed by Nolan in 2003 [74]. *$\%V_{bur}$* value can be obtained either through analysis of crystallographic data or by conducting theoretical calculations by utilizing free NHC ligands. For a clear understanding of the bulkiness of the NHCs ligand, the metal-carbene bond distance (d) remains fixed at 2 Å, while the sphere radius (r) is set at either 3 Å or 3.5 Å, as depicted in Figure **1.19**. These parameters are utilized for geometry analysis, where a higher *$\%V_{bur}$* value signifies a stronger

steric influence of the ligand on the metal centre. The presence of bulky substituents at nitrogen atoms contributes to the kinetic stabilization of the carbene by structurally hindering the formation of dimers in favour of the corresponding olefin [74].

(d) Electronic effect - The Tolman electronic parameter (TEP) is frequently employed to characterize the electronic properties of NHCs. This property was initially designed for phosphines, TEP determines the electron-donating capacity by analyzing the infrared-stretching frequencies of carbonyl ligands in simplified transition metal carbonyl complexes. A higher TEP value signifies a more potent electron-donating ligand, resulting in a more electron-rich metal centre [75, 76]. This enhances π-back bonding into carbonyl ligands, reducing their bond order and the frequency of the A1 vibration of the complex. For determining the TEP value of NHCs containing complex [Ni(CO)$_3$(IMe)] (where, IMe = 1,3-dimethylimidazolin-2-ylidene), the A$_1$ stretching frequency of carbonyl was found to be 2055 cm^{-1} in hexane. This observation leads to the inference that IMe exhibits superior strength compared to the most effective phosphine ligand in Tolman's investigation, namely P^{t}Bu$_3$ (A$_1$ = 2056 cm^{-1}, CH$_2$Cl$_2$) [77, 78].

1.9. Bonding of *N*-heterocyclic carbenes to metal centres

NHC plays a crucial role as ligands with transition metal and main group chemistry, showing remarkable diversity in metal complex formation. A wide range of metal complexes involving various oxidation states and a diverse variety of NHC ligands have been identified. NHCs exhibit a unique ability to bind the majority of metals across the periodic table, including alkali/alkaline metals, rare earth elements, and main group elements, as well as transition metals [49]. The σ-donating ability of NHCs, facilitated by their sp^2 hybridized lone pair of electrons, plays a crucial role in their compatibility as

ligand systems for synthesizing metal-NHC complexes. This strong electron-donating ability contributes to the formation of stable metal-NHC complexes [79, 80]. Additionally, the π-back donation from the metal to an empty *p*-orbital of the carbene is also very important. Frneking *et al.* demonstrated that π-contributions can be found in up to 20% of the total bond energy in complexes involving group 11 metals and imidazolin-2-ylidene/imidazolidin-2-ylidene donors [81]. Notably, they proposed that the metal-carbene bond behaves as a single bond rather than a double bond. This interpretation is supported by the observed single bond rotation around the M-C2 bond, which suggests the difference between the conventional Fischer/Schrock carbenes and NHCs.

1.10. NHC-based transition metal complexes with CEC (E = CH or N) pincer ligands

The synthesis of NHC-containing transition metal complexes is the most challenging process (Scheme **1.1**). The singlet carbene species coordinated with metals via deprotonation of the imidazolium pro-ligand with a strong base is the most straightforward approach [9]. The inherent reactivity of these species frequently poses challenges to their isolation. To avoid such issues, mild bases such as Et_3N, Cs_2CO_3, or coordinated bases ([M]OAc, [M]NR$_2$) can be employed to manage the reactivity of these highly reactive intermediates [82]. Transmetallation is another prominent method in which the use of silver transfer agents is produced by the reaction of the corresponding pro-ligands with Ag_2O [83]. Coordination of CCC-type pincer ligands with metals usually proceeds via cyclometalation of the backbone in the C-H or C-Br bonds. However, employing zirconium transfer agents produced by reaction with $Zr(NMe_2)_4$ or preparing anionic free-carbenes in situ has also been shown to be beneficial substitutes [84]. Transition metal complexes with pincer ligands have been extensively synthesized and utilized in various catalytic reactions [85–90].
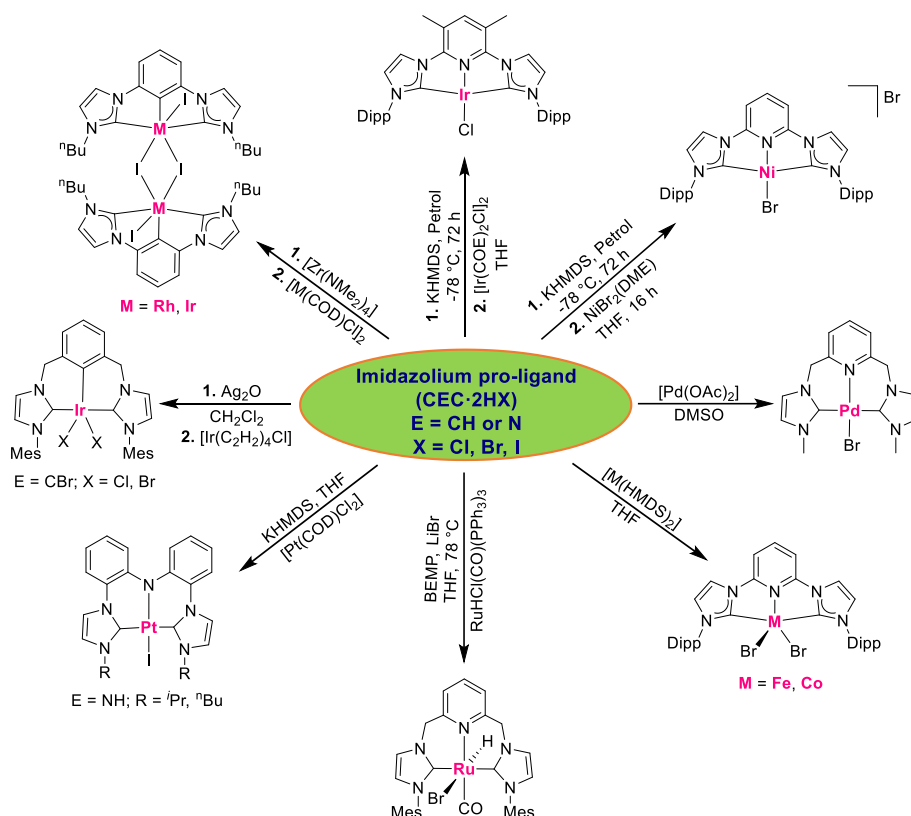
Scheme 1.1. Syntheses of NHC-based transition metal complexes with pincer ligands.

1.11. NHC containing ruthenium complexes with CNC pincer ligands

Ruthenium, a transition metal having atomic number 44 with electronic configuration [Kr] $4d^7 5s^1$, exhibits versatile reactivity, and the choice of ligands can fine-tune its properties for specific catalytic transformations. Jedrzej Sniadecki in 1808, examining platinum ores from South America, claimed to have discovered a novel metal, which he named vestium. However, subsequent attempts by French chemists to replicate his findings proved unsuccessful, leading Sniadecki to retract his assertion due to doubts about its accuracy. Gottfried Osann, in 1825 from the Dorpat University (now Tartu) in the Baltic region, examined platinum sourced from the Ural Mountains and reported the discovery of three new elements, i.e., pluranium, polinium, and ruthenium. It was not until 1840 that Karl Karlovich Klaus, from the

Kazan University, successfully isolated and confirmed the existence of ruthenium as a distinct metal. Klaus opted to retain Osann's proposed name of ruthenium, though the validity of pluranium and polinium could never be verified [91].
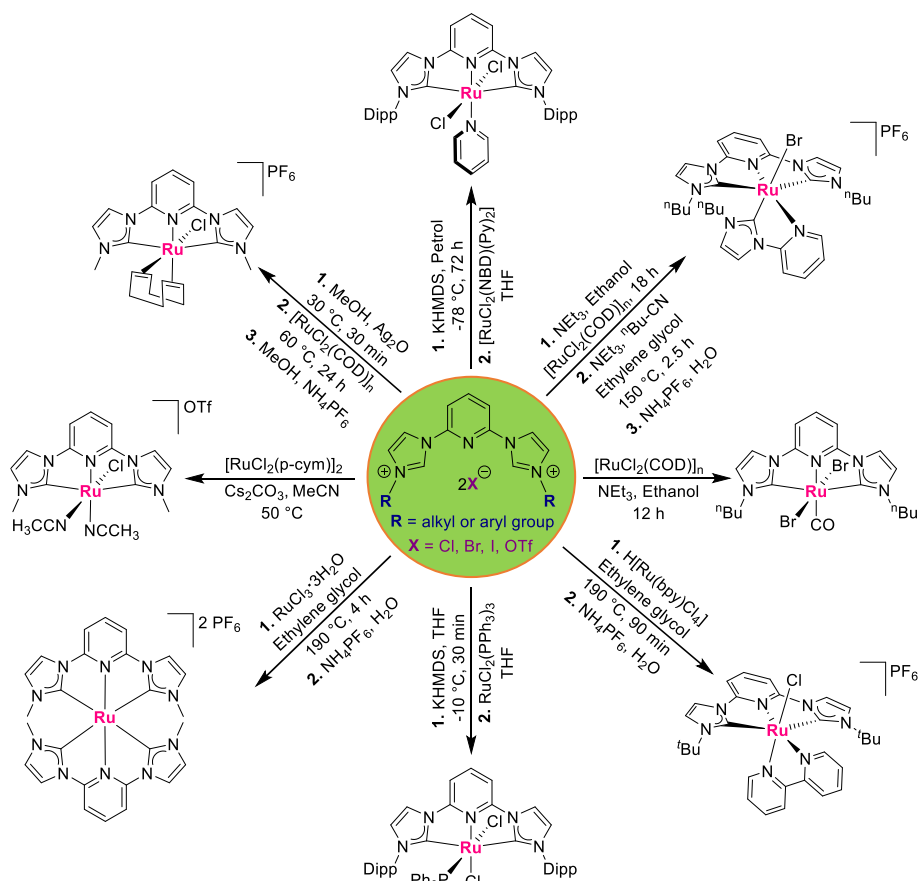
Scheme 1.2. Various methods for the synthesis of NHC-based ruthenium complexes with CNC pincer ligand.

The coordination of ligands to ruthenium centres forms stable complexes that govern the reactivity and behaviour of the catalyst. The flexibility of the Ru centre, which displays superior stability in different oxidation states and coordination geometries, makes it suitable for various applications. Previously, many ruthenium complexes have been reported for catalytic drug production due to their low toxicity and potential uses in catalysis. Ruthenium is less expensive than other transition metals (Pd, Pt, Rh, and Ir), and has made it more convenient for many catalytic reactions. Ruthenium

complexes have superior biocompatibility to many other metallodrugs, which increases their usage as pharmaceuticals.

NHC-based ruthenium pincer complexes showcase enhanced efficiency, selectivity, and notable tolerance towards various functional groups in contrast to traditional ruthenium catalysts. Previously, several methodologies have been documented for the synthesis of ruthenium complexes featuring CNC pincer ligands (Scheme **1.2**) [92–99]. These pincer complexes were produced by treating an imidazolium salt with a base to generate carbenes through transmetallation or by activating C-H bonds to obtain the desired ruthenium complexes. Ancillary ligands play a crucial role in determining the catalytic activity and stability of organometallic complexes. In the literature, various types of co-ligands (CO, PPh_3, CH_3CN, DMSO, halides, etc.) are extensively reported to have ruthenium-CNC pincer complexes. These co-ligands can modulate the electronic and steric properties at the ruthenium metal centre, leading to exciting coordination chemistry. A key structural aspect of CNC pincer complexes involves the variation of substituents located at the wing tip on the NHCs, which significantly influences the steric environment around the metal centre.

1.12. Application of NHC-based ruthenium complexes in different organic transformations

NHC-based transition metal catalysts exhibit better reactivity than phosphines, and these complexes have taken superiority over their corresponding phosphine complexes in terms of synthesis and application [56, 100–103]. In 1995, Hermann first demonstrated the use of NHCs for the synthesis of homogeneous catalysts [104]. Ruthenium complexes incorporating NHC ligands have found significant attention due to their enormous investigation and their applications in a variety of organic conversions like hydrogenation [105], dehydrogenation [106], olefin metathesis [107], hydrosilylation

25

[108], water oxidation [109], carbon dioxide reduction [110], asymmetric transformations [111], and many other transformations. Some selected active NHC-containing ruthenium catalysts for different catalytic reactions are listed below (Figure **1.20**). Ruthenium pincer complexes emerge as highly potent catalysts for crucial organic transformations, potentially attributed to their stability, accessibility in various stable oxidation states, and diverse coordination geometries [10, 112].
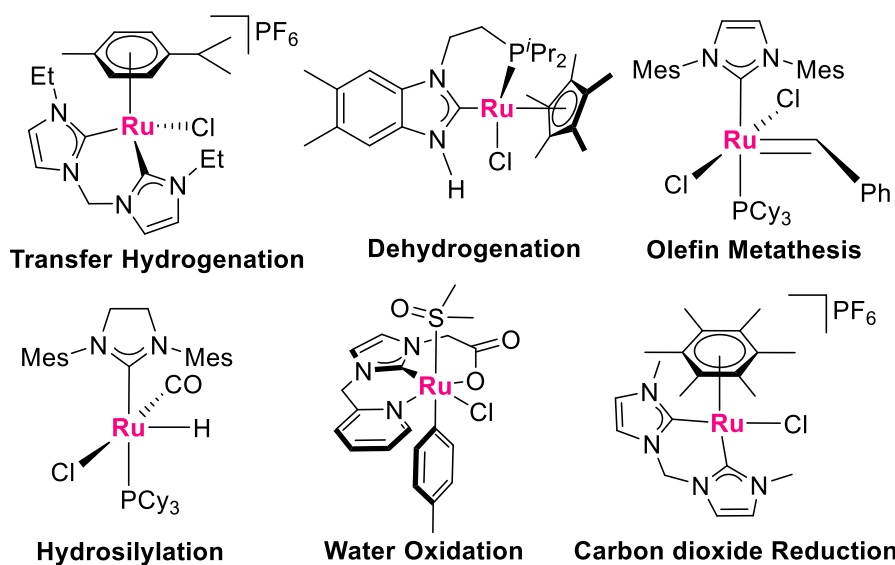
Figure 1.20. Some selected ruthenium catalysts for different catalytic reactions.

1.12.1. Application of ruthenium complexes in transfer hydrogenation reactions

Hydrogenation is one of the most fundamental chemical reactions in organic synthesis. They have many industrial uses, ranging from compound synthesis for fine chemicals to therapeutic applications [113]. Hydrogenation requires hydrogen source for the conversion of organic unsaturated molecules, either from H_2 gas or any organic molecule (isopropanol or formic acid) that supplies hydrogen through transfer hydrogenation [114].

Scheme 1.3. Ruthenium catalyzed transfer hydrogenation of ketone.

The metal-catalyzed reactions that are usually utilized in this process are stable and easily accessible, making it a much safer and more atom-efficient method than the traditional hydrogenation reactions, which need highly combustible dihydrogen molecules. Ruthenium complexes show effective precatalysts for TH reactions (Scheme **1.3**) [115].

Reduction of the carbonyl functional group in ketones to alcohols is an important organic transformation in both laboratories and industries. Researchers are actively pursuing environmentally friendly organic transformations, recognizing the significance of alcohols and the eco-friendly nature of transfer hydrogenation (TH). Transition metal-based NHC complexes have been employed as catalysts for the transfer hydrogenation of ketones, utilizing 2-propanol as the hydrogen source [114]. This approach eliminates the need for traditional reducing agents such as LiAlH4, NaBH4, hazardous molecular hydrogen, and high-pressure equipment. Peris [94] and Danopoulos [93] reported Ru(II)-NHC complexes with 2,6-bis(1-alkylimidazolium-3-yl) pyridine salts as a CNC source of tridentate bis-carbenes ligand to coordinate with the Ru centre, giving new pincer complexes that show excellent reactivity for TH reactions. Later, Baratta [116] and Yu [117] reported Ru(II) complexes with NHC containing l,3,4-triphenyl-4,5-dihydro-1H-l,2,4-triazol-5-ylidene with the complex [Ru-2-(aminomethyl)-pyridine] and pyridyl-based pincer (pyrazol-3-yl)-*N*-heterocyclic carbene ligand, respectively, with excellent reactivity for TH reactions. Recently, Rit [118] and Gupta [119] described the ruthenium-catalyzed TH reaction under mild reaction conditions with bidentate NHC ligand and coumarin-amide-

based ligand. Selection of some active ruthenium catalysts for the transfer hydrogenation of ketones (Figure **1.21**). Ru(II)-NHC complexes with alterations in substituents on both the wingtip and backbone, influencing their steric and electronic properties. Systematic investigations were conducted on Ru(II)-NHC complexes in the transfer hydrogenation of ketones, employing 2-propanol as the environmentally friendly hydrogen source. A metal hydride intermediate is involved in the transfer hydrogenation of ketones to accomplish this catalysis. This innovative approach not only demonstrates the versatility of transition metal-based NHC complexes but also aligns with the ongoing efforts to develop sustainable and green organic synthetic methodologies.
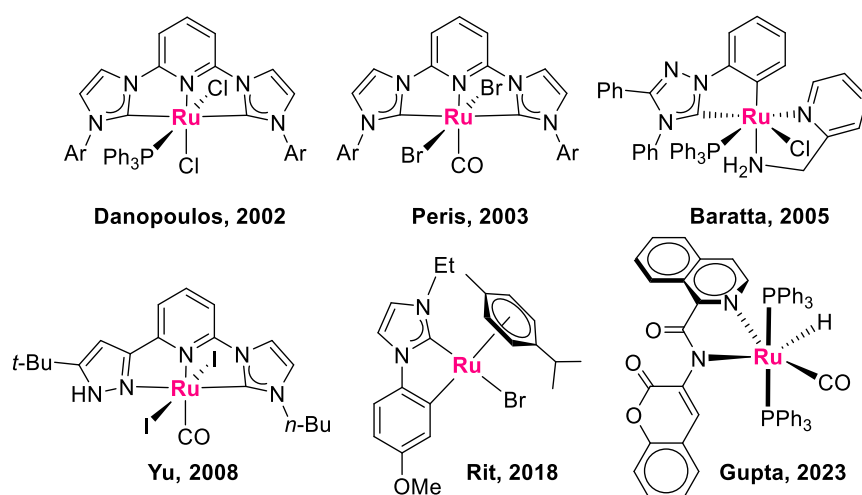
Figure 1.21. Previously reported ruthenium catalysts for the transfer hydrogenation of ketones.

1.12.2. Application of ruthenium complexes in acceptorless dehydrogenation of alcohols

Dehydrogenation refers to the removal of hydrogen from an organic compound, leading to the formation of a new compound, typically transitioning from saturated to unsaturated compounds [120]. Alcohol undergoes acceptorless dehydrogenation to give aldehydes or ketones. Developing an environment-friendly chemical process that provides

28

higher yields with excellent selectivity is the most challenging task in modern chemistry [121]. Traditional synthetic procedures for dehydrogenative reactions use inorganic oxidants to afford the intended products, and many toxic byproducts. Modern chemistry favours transition metal-catalyzed dehydrogenation reactions due to their numerous advantages over outdated methods [121]. These reactions provide an array of applications in organic synthesis that are considerably greener approach than conventional or sacrificial methods. In acceptorless alcohol dehydrogenation (AAD) reactions, the elimination of one molecule of dihydrogen from the comparatively less reactive alcohols produces the carbonyls as useful synthons (Scheme **1.4**).
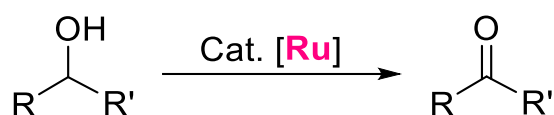
Scheme 1.4. Ruthenium catalyzed acceptorless dehydrogenation of alcohol.
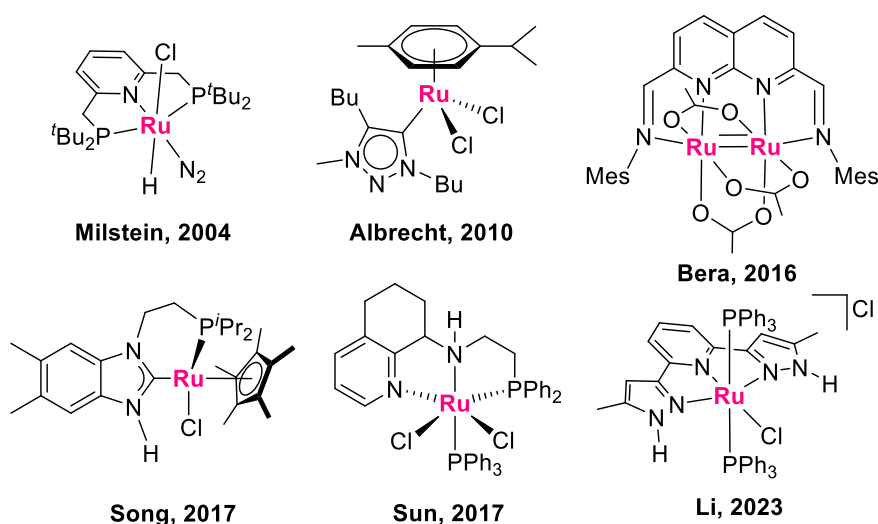
Figure 1.22. Some selected active ruthenium catalysts for acceptorless dehydrogenation of alcohol.

Transition metal-catalyzed AAD reaction proves to be an active and reliable method for synthesizing valuable compounds compared to

conventional synthetic approaches [120]. The AAD reaction is indeed of particular interest for energy production because it allows for the synthesis of H_2 from alcohols derived from renewable biomass [120]. The AAD reaction plays a crucial role in producing alkylated ketones or alcohols by coupling primary and secondary alcohols through dehydrogenation. More significantly, M-NHC complexes have effectively converted the organic compounds into the intended products by an acceptorless dehydrogenation reaction without any toxic byproducts [122]. Milstein [123], Sun [124], and Li [125] reported the PNP, NNP, and NNN-based ruthenium pincer complexes for AAD under mild reaction conditions. Bera described the naphthyridine-diimine and three acetates bridged containing diruthenium complex for AAD reaction [126]. Albrecht [127] and Song [106] reported the NHC-based ruthenium complexes for the AAD reaction. In the AAD reaction mechanism, a metal hydride intermediate was actively involved in this catalytic transformation [120]. Selected examples of well-defined ruthenium catalysts for AAD reaction are listed in Figure **1.22**.

1.12.3. Application of ruthenium complexes in acceptorless dehydrogenative coupling reaction

The dehydrogenative coupling reaction is a highly desirable and extensively researched organic transformation. Acceptorless dehydrogenative coupling (ADC) emerges as a leading technique in organic synthesis, facilitating the coupling of alcohols and amines to yield imines, amides, and alkylated amines via hydrogen borrowing methodology [128]. Imines are pivotal compounds in organic and medicinal chemistry, having widespread applications in laboratory and industrial synthetic processes [129]. Notably, imines showcase diverse biological activities, including lipoxygenase inhibition, anti-inflammatory, anti-cancer, antibacterial, and antifungal properties [128]. Traditionally, imines were synthesized using ketones or

30

aldehydes with amines in the presence of an acid catalyst. Furthermore, imines were obtained either through the self-condensation of amines upon oxidation or via the oxidation of secondary amines. Metal-catalyzed *N*-alkylation of amines with alcohols proceeds through an imine intermediate, followed by further hydrogenation to afford the desired product (Scheme **1.5**) [128]. ADC is a more effective, eco-friendly technique for directly synthesizing imines through the interaction of amines and alcohols, liberating H$_2$ gas and water in the process.
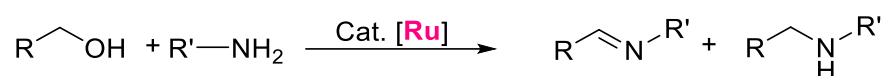
Scheme 1.5. Ruthenium catalyzed acceptorless dehydrogenation coupling reaction.

Although many synthetic procedures have been reported for imine synthesis, it is still quite difficult to synthesize imines from alcohols and amines. Tremendous progress has been made by several groups for imine synthesis through the use of different transition metal complexes [128]. Milstein reported a PNP-based ruthenium pincer complex for imine synthesis with excellent reactivity with low catalyst loading [130]. Zhu reported 2,6-bis(imidazo[1,2-α]pyridin-2-yl) pyridine-based NNN-type ruthenium pincer complex for C-N bond formation through hydrogen borrowing methodology [131]. Gelman [13], and Nishibayashi [132] described dibenzobarrelene and NHC, phosphine-based PCP-type ruthenium pincer complexes for ADC reaction. Recently, Kumar [133] and Ghosh [134] reported the NNN-type ruthenium pincer complex for *N*-alkylation of amines with low catalyst loading. Selected examples of active ruthenium catalysts for ADC reaction of alcohols and amines are shown below (Figure **1.23**). In the ADC reaction mechanism, initially, dehydrogenation of alcohol gives rise to the ruthenium hydride complex, and aldehyde or ketone undergoes condensation followed by dehydration to afford the

31

corresponding imine [135]. After that, imine was hydrogenated to give the *N*-alkylated product and regenerate the dehydrogenative catalyst.
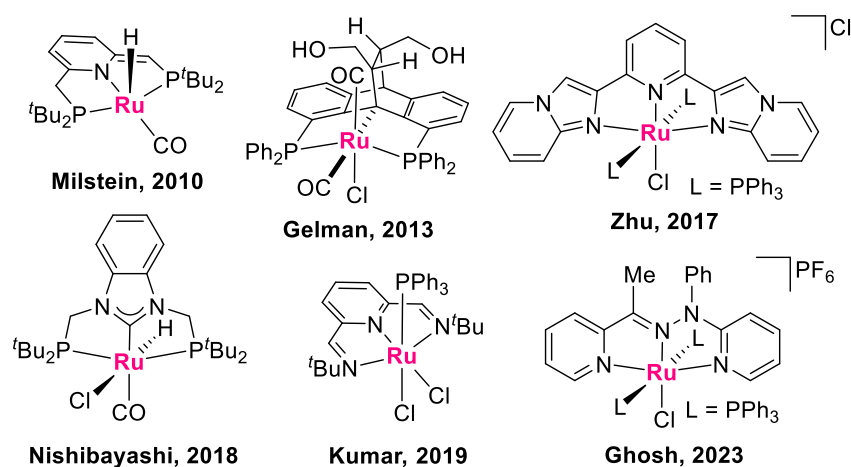
Figure 1.23. Previously reported active ruthenium catalysts for acceptorless dehydrogenative coupling reaction.

1.12.4. Application of ruthenium complexes in the hydration of nitriles

Hydration of nitriles involves the addition of water to the carbon-nitrogen triple bond, resulting in the formation of an amide [136]. This reaction can be carried out under acidic or basic conditions, such as the use of a strong acid like sulfuric acid, while basic conditions involve the use of a hydroxide ion source, such as sodium hydroxide [137]. In acidic conditions, the nitrile is protonated by the acid and increases its susceptibility to nucleophilic attack by water, while in basic conditions, hydroxide ions attack the nitrile and afford the desired compounds [138]. The ruthenium complexes show excellent reactivity for the hydration of nitriles (Scheme **1.6**).
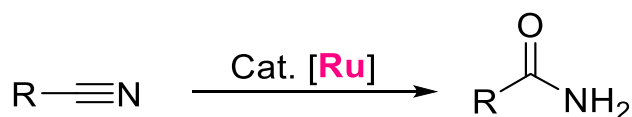
Scheme 1.6. Ruthenium catalyzed hydration of nitrile.
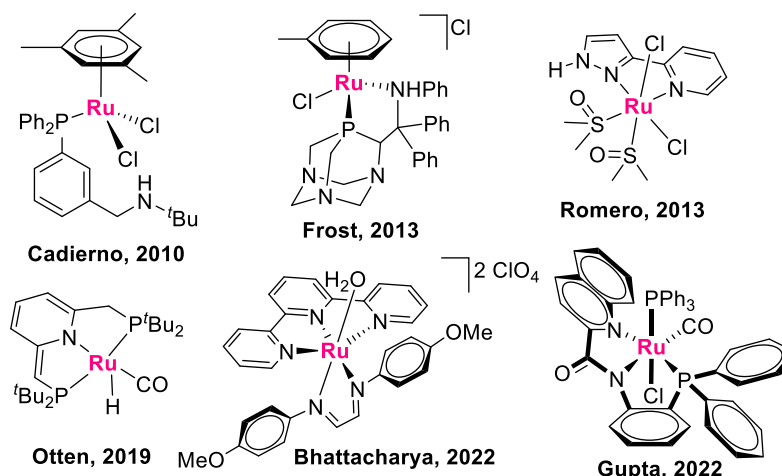
Figure 1.24. Previously reported active ruthenium catalysts for the hydration of nitriles.

The metal-catalyzed hydration of nitriles is a particular type of reaction where a metal catalyst facilitates the addition of water to the carbon-nitrogen triple bond, affording amides or carboxylic acids [139]. Ruthenium complexes have shown the ability as efficient catalysts for the hydration of nitriles at mild reaction conditions, providing enhanced selectivity and efficiency [140]. Previously, a variety of ruthenium catalysts have been documented for the hydration of nitriles in mild reaction conditions [141, 142]. Cadierno [143] and Frost [144] initially described the hydration of nitriles with ruthenium catalysts. Romero stated Ru-dmso complex contains the ligands 2-(3-pyrazolyl) pyridine for the same catalysis under mild conditions [145]. Recently, Otten [140], Bhattacharya [146], and Gupta [147] reported ruthenium catalysts with pincer and tridentate ligands for the hydration of nitriles. Some listed active ruthenium catalysts for nitrile hydration to amide in mild reaction conditions (Figure **1.24**). Other transition metal complexes, with or without additives under mild reaction conditions are also described for the hydration of nitriles [148–152]. The mechanism involves the coordination of the nitrile to the metal centre, followed by the nucleophilic attack of the water molecule after subsequent protonation or other steps leading to the formation of the amides [153–155]. The use of metal catalysts in this reaction can

improve the efficiency of this transformation, allowing for milder reaction conditions and improved selectivity. Furthermore, organic synthesis frequently uses metal-catalyzed reactions to achieve selective and efficient transformations.

1.13. Mechanistic aspects of the catalytic reactions

The mechanistic aspects of catalytic reactions are a powerful technique for understanding the reaction pathways. Homogeneous catalysis is effective for carrying out chemical changes under mild conditions. It also gives exact information about the reaction mechanism and its catalytic pathway. Recent studies on the kinetics and mechanisms of homogeneous catalysis shed light on the significance of transition metal complexes in catalysis. The quantitative details of the chemical processes occurring at the atomic level are exhibited in the mechanisms of transition metal-catalyzed reactions. Such chemical reaction mechanistic data is crucial for producing novel transition metal homogeneous catalysts. Mechanistic investigations provide a better understanding of the catalytic pathway, addressing issues such as catalyst efficiency and eventually enhancing catalytic activity and selectivity. In literature, various reports emphasize the study of reaction pathways through a variety of instrumental techniques. In situ, generated catalytically active intermediate species were characterized by NMR, GC-MS, and mass spectrometric analysis. UV spectroscopic studies highlight interactions between the complex and solvent by revealing differences in absorption bands compared to the starting substrate. One of the most important tools to trap the highly unstable intermediate species through NMR and mass experiments in different time intervals provides significant information about the active species, which directly facilitates the reaction pathways. DFT study is a modern technique for mechanistic investigations that provides insights into the fate and stability of various active intermediate species through energy-related calculations.

1.14. Objectives of the thesis

Ruthenium catalysis encompasses a broad spectrum of reactions owing to the exceptional properties of ruthenium complexes. However, complexes featuring CNC-pincer ligands have been relatively less investigated in diverse catalytic reactions. Ruthenium catalysis offers a versatile and efficient means to carry out various chemical transformations, significantly advancing synthetic chemistry. Our research endeavors to fill this gap in synthetic chemistry by exploring CNC pincer complexes and their potential applications. The primary objective of this thesis is to design and synthesize exceptionally effective cationic Ru(II)-CNC pincer complexes and examine their catalytic utility across various organic transformations.

❖ To synthesize cationic Ru(II)-CNC pincer complexes with various ancillary ligands and study their chemical behaviour.

❖ To examine the catalytic efficiency of cationic Ru(II)-CNC pincer complexes and explore the impact of ancillary ligands on the selectivity of the reaction.

❖ Incorporation of multiple NHC donor ligands in the Ru(II)-CNC pincer type complexes.

❖ To evaluate the reactivity of cationic Ru(II)-CNC pincer complexes with multiple NHC donor ligands.

1.15. Organization of thesis

The present thesis work describes the syntheses, characterization, and catalytic activities of cationic Ru(II)-CNC pincer complexes incorporating various co-ligands.

Chapter 1 provides an overview of different types of pincer ligands and their classifications, encompassing NHC-based pincer ligands and their metal complexes, and explores their significance in various catalytic reactions.

Chapter 2 discusses the syntheses, characterization, and catalytic performance of cationic Ru(II)-CNC pincer complexes incorporating various co-ligands.

Chapter 3 discusses the catalytic activity of cationic Ru(II)-CNC pincer complexes and their selectivity for acceptorless dehydrogenative coupling of alcohols and amines concerning different ancillary ligands.

Chapter 4 discusses the syntheses and characterization of cationic Ru(II)-CNC pincer complexes from bidentate ruthenium precursors featuring multiple NHC donor ligands.

Chapter 5 discusses the catalytic activity of cationic Ru(II)-CNC pincer complexes for the hydration of nitriles to amides under mild reaction conditions in an aqueous medium.

Chapter 6 discusses the syntheses and characterization of dicationic Ru(II)-CNC pincer complexes with CH_3CN and PPh_3 ligands and studies their catalytic and photophysical properties.

Chapter 7 discusses the summary and future scope of the present thesis work.

1.16. References

1. Elsevier C. J., Reedijk J., Walton P. H., Ward M. D. (2003), Ligand design in coordination chemistry: approaches to new catalysts, new materials, and a more sustainable environment, Dalton Trans., (10), 1869-1880 (DOI: 10.1039/B303975G).

2. Peris E., Crabtree R. H. (2018), Key factors in pincer ligand design, Chem. Soc. Rev., 47(6), 1959-1968 (DOI: 10.1039/C7CS00693D).

3. Moulton C. J., Shaw B. L. (1976), Transition metal-carbon bonds. Part XLII. Complexes of nickel, palladium, platinum, rhodium and iridium with the tridentate ligand 2,6-bis[(di-t-butylphosphino)methyl]phenyl, J. Chem. Soc., Dalton Trans., (11), 1020-1024 (DOI: 10.1039/DT9760001020).

4. Koten G. van (1989), Tuning the reactivity of metals held in a rigid ligand environment, Pure Appl. Chem., 61(10), 1681-1694 (DOI: 10.1351/pac198961101681).

5. Koten G. van, Timmer K., Noltes J. G., Spek A. L. (1978), A novel type of Pt–C interaction and a model for the final stage in reductive elimination processes involving C–C coupling at Pt; synthesis and molecular geometry of [1,N,N′-η-2,6-bis{(dimethylamino)methyl}-toluene]iodoplatinum(II) tetra fluoroborate, J. Chem. Soc., Chem. Commun., (6), 250-252 (DOI: 10.1039/C39780000250).

6. Choi J., MacArthur A. H. R., Brookhart M., Goldman A. S. (2011), Dehydrogenation and Related Reactions Catalyzed by Iridium Pincer Complexes, Chem. Rev., 111(3), 1761-1779 (DOI: 10.1021/cr1003503).

7. Deng Q.-H., Melen R. L., Gade L. H. (2014), Anionic Chiral Tridentate *N*-Donor Pincer Ligands in Asymmetric Catalysis, Acc. Chem. Res., 47(10), 3162-3173 (DOI: 10.1021/ar5002457).

8. Lawrence M. A. W., Green K.-A., Nelson P. N., Lorraine S. C. (2018), Review: Pincer ligands-Tunable, versatile and applicable, Polyhedron, 143, 11-27 (DOI: 10.1016/j.poly.2017.08.017).

9. Andrew R. E., González-Sebastián L., Chaplin A. B. (2016), NHC-based pincer ligands: carbenes with a bite, Dalton Trans., 45(4), 1299-1305 (DOI: 10.1039/C5DT04429D).

10. Gunanathan C., Milstein D. (2014), Bond Activation and Catalysis by Ruthenium Pincer Complexes, Chem. Rev., 114(24), 12024-12087 (DOI: 10.1021/cr5002782).

11. Selander N., Szabó K. J. (2011), Catalysis by Palladium Pincer Complexes, Chem. Rev., 111(3), 2048-2076 (DOI: 10.1021/cr1002112).

12. Valdés H., Rufino-Felipe E., van Koten G., Morales-Morales D. (2020), Hybrid POCZP Aryl Pincer Metal Complexes and their Catalytic Applications, Eur. J. Inorg. Chem., 2020(47), 4418-4424 (DOI: 10.1002/ejic.202000817).

13. Musa S., Fronton S., Vaccaro L., Gelman D. (2013), Bifunctional Ruthenium(II) PCP Pincer Complexes and Their Catalytic Activity in Acceptorless Dehydrogenative Reactions, Organometallics, 32(10), 3069-3073 (DOI: 10.1021/om400285r).

14. Teratani T., Koizumi T., Yamamoto T., Tanaka K., Kanbara T. (2011), Deprotonation/protonation of coordinated secondary thioamide units of pincer ruthenium complexes: Modulation of voltammetric and spectroscopic characterization of the pincer complexes, Dalton Trans., 40(35), 8879-8886 (DOI: 10.1039/C0DT01283A).

15. Charette B. J., Ritch J. S. (2016), A Selenium-Containing Diarylamido Pincer Ligand: Synthesis and Coordination Chemistry with Group 10 Metals, Inorg. Chem., 55(12), 6344-6350 (DOI: 10.1021/acs.inorgchem.6b01203).

16. Deng, Yu, Dong, Wu (2005), 2,6-Bis(3,5-dimethylpyrazol-1-yl)pyridine: A Useful Pseudo-N_3 Ligand in Efficient

Ruthenium(II)-Catalyzed Transfer Hydrogenation of Ketones, Organometallics, 24(17), 4110-4112 (DOI: 10.1021/om050467o).

17. Du W., Wu P., Wang Q., Yu Z. (2013), Ruthenium(II) Complex Catalysts Bearing a Pyridyl-Based Benzimidazolyl-Benzotriazolyl Ligand for Transfer Hydrogenation of Ketones, Organometallics, 32(10), 3083-3090 (DOI: 10.1021/om400298c).

18. Banihashemi A., Eghbali M. (1976), Polycondensation of pyridine-2,6-dicarboxylic acid with some di- and tetraamino compounds, J. Polym. Sci., Polym. Chem. Ed., 14(11), 2659-2664 (DOI: 10.1002/pol.1976.170141107).

19. Patra A. K., Mukherjee R. (1999), Bivalent, Trivalent, and Tetravalent Nickel Complexes with a Common Tridentate Deprotonated Pyridine Bis-Amide Ligand. Molecular Structures of Nickel(II) and Nickel(IV) and Redox Activity, Inorg. Chem., 38(7), 1388-1393 (DOI: 10.1021/ic980672e).

20. Taakili R., Canac Y. (2020), NHC Core Pincer Ligands Exhibiting Two Anionic Coordinating Extremities, Molecules, 25(9), 2231 (DOI: 10.3390/molecules25092231).

21. Zhang D., Aihara H., Watanabe T., Matsuo T., Kawaguchi H. (2007), Zirconium complexes of the tridentate bis(aryloxide)-*N*-heterocyclic-carbene ligand: Chloride and alkyl functionalized derivatives, J. Organomet. Chem., 692(1), 234-242 (DOI: 10.1016/j.jorganchem.2006.03.044).

22. Spencer L. P., Winston S., Fryzuk M. D. (2004), Tridentate Amido Carbene Ligands in Early-Transition-Metal Coordination Chemistry, Organometallics, 23(14), 3372-3374 (DOI: 10.1021/om0498089).

23. Kohl S. W., Weiner L., Schwartsburd L., Konstantinovski L., Shimon L. J. W., Ben-David Y., Iron M. A., Milstein D. (2009), Consecutive Thermal H_2 and Light-Induced O_2 Evolution from Water Promoted by a Metal Complex, Science, 324(5923), 74-77 (DOI: 10.1126/science.1168600).

24. Du W., Wang L., Wu P., Yu Z. (2012), A Versatile Ruthenium(II)-NNC Complex Catalyst for Transfer Hydrogenation of Ketones and Oppenauer-Type Oxidation of Alcohols, Chem. Eur. J., 18(37), 11550-11554 (DOI: 10.1002/chem.201201938).

25. Fleckhaus A., Mousa A. H., Lawal N. S., Kazemifar N. K., Wendt O. F. (2015), Aromatic PCN Palladium Pincer Complexes. Probing the Hemilability through Reactions with Nucleophiles, Organometallics, 34(9), 1627-1634 (DOI: 10.1021/om501231k).

26. Fandos R., Otero A., Rodríguez A. M., Suizo S. (2014), Monocyclopentadienyl titanium complexes supported by functionalized Shiff Base ligands, J. Organomet. Chem., 759, 74-82 (DOI: 10.1016/j.jorganchem.2014.02.023).

27. Aleksenko V. Yu., Sharova E. V., Artyushin O. I., Aleksanyan D. V., Klemenkova Z. S., Nelyubina Yu. V., Petrovskii P. V., Kozlov V. A., Odinets I. L. (2013), Coordination of P(X)-modified (X = O, S) *N*-aryl-carbamoylmethylphosphine oxides and sulfides with Pd(II) and Re(I) ions: Facile formation of 6,6-membered pincer complexes featuring atropisomerism, Polyhedron, 51, 168-179 (DOI: 10.1016/j.poly.2012.12.025).

28. Gargir M., Ben-David Y., Leitus G., Diskin-Posner Y., Shimon L. J. W., Milstein D. (2012), PNS-Type Ruthenium Pincer Complexes, Organometallics, 31(17), 6207-6214 (DOI: /10.1021/om300516j).

29. Lu Z., White C., Rheingold A. L., Crabtree R. H. (1993), Deprotonated thioamides as thiolate S-donor ligands with a high tendency to avoid M-S-M bridge formation: crystal and molecular structure of bis(2-hydroxy-5-methylacetophenone N,N-dimethylthiosemicarbazonato)dinickel, Inorg. Chem., 32(19), 3991-3994 (DOI: 10.1021/ic00071a006).

30. Vila J. M., Pereira M. T., Ortigueira J. M., Graña M., Lata D., Suárez A., Fernández J. J., Fernández A., López-Torres M., Adams H. (1999), Formation, characterization, and structural

studies of novel thiosemicarbazone palladium(II) complexes. Crystal structures of [{Pd[C$_6$H$_4$C(Et)NNC(S)NH$_2$]}$_4$], [Pd{C$_6$H$_4$C(Et)NN   C(S)NH$_2$}(PMePh$_2$)] and [{Pd[C$_6$H$_4$C(Et)NNC(S)NH$_2$]}$_2$(μ-Ph$_2$PCH$_2$PPh$_2$)], J. Chem. Soc., Dalton Trans., (23), 4193-4201 (DOI: 10.1039/A906276I).

31. Bakir M., Lawrence M. A. W., McBean S. (2015), Spectroscopic and electrochemical properties of group 12 acetates of di-2-pyridylketone thiophene-2-carboxylic acid hydrazone (dpktch-H) complexes. The structure of [Cd(η3-N,N,O-dpktch-H)$_2$], Spectrochim. Acta A, 146, 323-330 (DOI: 10.1016/j.saa.2015.03.079).

32. Lawrence M. A. W., Jackson Y. A., Mulder W. H., Björemark P. M., Håkansson M. (2014), Synthesis and Structure of a Novel Substituted Benzothiazolyl-N-phenyl-2-pyridinecarbothioamide; Kinetics of Formation and Electrochemistry of Two of its Palladium Pincer Complexes, Aust. J. Chem., 68(5), 731-741 (DOI: 10.1071/CH14380).

33. Hopkinson M. N., Richter C., Schedler M., Glorius F. (2014), An overview of *N*-heterocyclic carbenes, Nature, 510(7506), 485-496 (DOI: 10.1038/nature13384).

34. Singh R. K., Khan T. K., Misra S., Singh A. K. (2021), CAACs as efficient ancillary ligands for the synthesis of robust catalysts, J. Organomet. Chem., 956, 122133 (DOI: 10.1016/j.jorganchem.2021.122133).

35. Kuwata S., Hahn F. E. (2018), Complexes Bearing Protic *N*-Heterocyclic Carbene Ligands, Chem. Rev., 118(19), 9642-9677 (DOI: 10.1021/acs.chemrev.8b00176).

36. Gründemann S., Kovacevic A., Albrecht M., Robert J. W. F., Crabtree H. (2001), Abnormal binding in a carbene complex formed from an imidazolium salt and a metal hydride complex, Chem. Commun., (21), 2274-2275 (DOI: 10.1039/B107881J).

37. Lee W.-T., Dickie D. A., Metta-Magaña A. J., Smith J. M. (2013), A Tripodal Ligand Constructed from Mesoionic Carbene

Donors, Inorg. Chem., 52(21), 12842-12846 (DOI: 10.1021/ic402311c).

38. Crabtree R. H. (2013), Abnormal, mesoionic and remote *N*-heterocyclic carbene complexes, Coord. Chem. Rev., 257(3), 755-766 (DOI: 10.1016/j.ccr.2012.09.006).

39. Jalal M., Hammouti B., Touzani R., Aouniti A., Ozdemir I. (2020), Metal-NHC heterocycle complexes in catalysis and biological applications: Systematic review, Mater. Today Proc., 31, S122-S129 (DOI: 10.1016/j.matpr.2020.06.398).

40. Bourissou D., Guerret O., Gabbaï F. P., Bertrand G. (2000), Stable Carbenes, Chem. Rev., 100(1), 39-92 (DOI: 10.1021/cr940472u).

41. Doering W. von E., Hoffmann A. K. (1954), The Addition of Dichlorocarbene to Olefins, J. Am. Chem. Soc., 76, 23, 6162-6165 (DOI: 10.1021/ja01652a087).

42. Fischer E. O., Maasböl A. (1964), Zur Frage eines Wolfram-Carbonyl-Carben-Komplexes, Angew. Chem., 76(14), 645-645 (DOI: 10.1002/ange.19640761405).

43. Tomioka H. (1997), Persistent Triplet Carbenes, Acc. Chem. Res., 30(8), 315-321 (DOI: 10.1021/ar9602157).

44. Tomioka H., Iwamoto E., Itakura H., Hirai K. (2001), Generation and characterization of a fairly stable triplet carbene, Nature, 412(6847), 626-628 (DOI: 10.1038/35088038).

45. Hoffmann R., Zeiss G. D., Van Dine G. W. (1968), The electronic structure of methylenes, J. Am. Chem. Soc., 90(6), 1485-1499 (DOI: 10.1021/ja01008a017).

46. Dötz K. H., Stendel J. Jr. (2009), Fischer Carbene Complexes in Organic Synthesis: Metal-Assisted and Metal-Templated Reactions, Chem. Rev., 109(8), 3227-3274 (DOI: 10.1021/cr900034e).

47. Schrock R. R. (1975), First isolable transition metal methylene complex and analogs. Characterization, mode of decomposition,

and some simple reactions, J. Am. Chem. Soc., 97(22), 6577-6578 (DOI: 10.1021/ja00855a048).

48. Tebbe F. N., Parshall G. W., Reddy G. S. (1978), Olefin homologation with titanium methylene compounds, J. Am. Chem. Soc., 100(11), 3611-3613 (DOI: 10.1021/ja00479a061).

49. Nesterov V., Reiter D., Bag P., Frisch P., Holzner R., Porzelt A., Inoue S. (2018), NHCs in Main Group Chemistry, Chem. Rev., 118(19), 9678-9842 (DOI: 10.1021/acs.chemrev.8b00079).

50. Wanzlick H.-W., Schönherr H.-J. (1968), Direct Synthesis of a Mercury Salt-Carbene Complex, Angew. Chem. Int. Ed., 7(2), 141-142 (DOI: 10.1002/anie.196801412).

51. Öfele K. (1968), 1,3-Dimethyl-4-imidazolinyliden-(2)-pentacarbonylchrom ein neuer übergangsmetall-carben-komplex, J. Organomet. Chem., 12(3), P42-P43 (DOI: 10.1016/S0022-328X(00)88691-X).

52. Cardin D. J., Cetinkaya B., Lappert M. F., Manojlović-Muir L., Muir K. W. (1971), An electron-rich olefin as a source of co-ordinated carbene; synthesis of *trans*-PtCl$_2$[C(NPhCH$_2$)$_2$]PEt$_3$, J. Chem. Soc. D, (8), 400-401 (DOI: 10.1039/C29710000400).

53. Wanzlick H.-W., Schikora E. (1960), Ein neuer Zugang zur Carben-Chemie, Angew. Chem., 72(14), 494-494 (DOI: 10.1002/ange.19600721409).

54. Igau A., Grutzmacher H., Baceiredo A., Bertrand G. (1988), Analogous α, α'-bis-carbenoid triply bonded species: synthesis of a stable λ^3-phosphino carbene-λ^5-phosphaacetylene, J. Am. Chem. Soc., 110(19), 6463-6466 (DOI: 10.1021/ja00227a028).

55. Arduengo III A. J., Harlow R. L., Kline M. (1991), A stable crystalline carbene, J. Am. Chem. Soc., 113(1), 361-363 (DOI: 10.1021/ja00001a054).

56. Crabtree R. H. (2005), NHC ligands versus cyclopentadienyls and phosphines as spectator ligands in organometallic catalysis, J. Organomet. Chem., 690(24), 5451-5457 (DOI: 10.1016/j.jorganchem.2005.07.099).

57. Crudden C. M., Allen D. P. (2004), Stability and reactivity of *N*-heterocyclic carbene complexes, Coord. Chem. Rev., 248(21), 2247-2273 (DOI: 10.1016/j.ccr.2004.05.013).

58. Scholl M., Ding S., Lee C. W., Grubbs R. H. (1999), Synthesis and Activity of a New Generation of Ruthenium-Based Olefin Metathesis Catalysts Coordinated with 1,3-Dimesityl-4,5-dihydroimidazol-2-ylidene Ligands, Org. Lett., 1(6), 953-956 (DOI: 10.1021/ol990909q).

59. Vougioukalakis G. C., Grubbs R. H. (2010), Ruthenium-Based Heterocyclic Carbene-Coordinated Olefin Metathesis Catalysts, Chem. Rev., 110(3), 1746-1787 (DOI: 10.1021/cr9002424).

60. Schuster O., Yang L., Raubenheimer H. G., Albrecht M. (2009), Beyond Conventional *N*-Heterocyclic Carbenes: Abnormal, Remote, and Other Classes of NHC Ligands with Reduced Heteroatom Stabilization, Chem. Rev., 109(8), 3445-3478 (DOI: 10.1021/cr8005087).

61. Díez-González S., Marion N., Nolan S. P. (2009), *N*-Heterocyclic Carbenes in Late Transition Metal Catalysis, Chem. Rev., 109(8), 3612-3676 (DOI: 10.1021/cr900074m).

62. Poyatos M., Mata J. A., Peris E. (2009), Complexes with Poly(*N*-heterocyclic carbene) Ligands: Structural Features and Catalytic Applications, Chem. Rev., 109(8), 3677-3707 (DOI: 10.1021/cr800501s).

63. Corberán R., Mas-Marzá E., Peris E. (2009), Mono-, Bi- and Tridentate *N*-Heterocyclic Carbene Ligands for the Preparation of Transition-Metal-Based Homogeneous Catalysts, Eur. J. Inorg. Chem., 2009(13), 1700-1716 (DOI: 10.1002/ejic.200801095).

64. Würtz S., Glorius F. (2008), Surveying Sterically Demanding *N*-Heterocyclic Carbene Ligands with Restricted Flexibility for Palladium-catalyzed Cross-Coupling Reactions, Acc. Chem. Res., 41(11), 1523-1533 (DOI: 10.1021/ar8000876).

65. Trnka T. M., Grubbs R. H. (2001), The Development of L_2X_2RuCHR Olefin Metathesis Catalysts: An Organometallic

Success Story, Acc. Chem. Res., 34(1), 18-29 (DOI: 10.1021/ar000114f).

66. Enders D., Niemeier O., Henseler A. (2007), Organocatalysis by *N*-Heterocyclic Carbenes, Chem. Rev., 107(12), 5606-5655 (DOI: 10.1021/cr068372z).

67. Marion N., Díez-González S., Nolan S. P. (2007), *N*-Heterocyclic Carbenes as Organocatalysts, Angew. Chem. Int. Ed., 46(17), 2988-3000 (DOI: 10.1002/anie.200603380).

68. Grossmann A., Enders D. (2012), *N*-Heterocyclic Carbene Catalyzed Domino Reactions, Angew. Chem. Int. Ed., 51(2), 314-325 (DOI: 10.1002/anie.201105415).

69. Radloff C., Weigand J. J., Hahn F. E. (2009), A tetranuclear molecular rectangle from four gold(I) atoms linked by dicarbene and diphosphine ligands, Dalton Trans., (43), 9392-9394 (DOI: 10.1039/B916651C).

70. Conrady F. M., Fröhlich R., to Brinke C. S., Pape T., Hahn F. E. (2011), Stepwise Formation of a Molecular Square with Bridging NH,O-Substituted Dicarbene Building Blocks, J. Am. Chem. Soc., 133(30), 11496-11499 (DOI: 10.1021/ja205021p).

71. de Frémont P., Marion N., Nolan S. P. (2009), Carbenes: Synthesis, properties, and organometallic chemistry, Coord. Chem. Rev., 253(7), 862-892 (DOI: 10.1016/j.ccr.2008.05.018).

72. Herrmann W. A., Köcher C. (1997), *N*-Heterocyclic Carbenes, Angew. Chem., Int. Ed. Engl., 36(20), 2162-2187 (DOI: 10.1002/anie.199721621).

73. Wanzlick H. W. (1962), Aspects of Nucleophilic Carbene Chemistry, Angew. Chem., Int. Ed. Engl., 1(2), 75-80 (DOI: 10.1002/anie.196200751).

74. Hillier A. C., Sommer W. J., Yong B. S., Petersen J. L., Cavallo L., Nolan S. P. (2003), A Combined Experimental and Theoretical Study Examining the Binding of *N*-Heterocyclic Carbenes (NHC) to the Cp*RuCl (Cp* = η^5-C$_5$Me$_5$) Moiety: Insight into Stereoelectronic Differences between Unsaturated

and Saturated NHC Ligands, Organometallics, 22(21), 4322-4326 (DOI: 10.1021/om034016k).

75. Tolman C. A. (1970), Electron donor-acceptor properties of phosphorus ligands. Substituent additivity, J. Am. Chem. Soc., 92(10), 2953-2956 (DOI: 10.1021/ja00713a006).

76. Tolman C. A. (1977), Steric effects of phosphorus ligands in organometallic chemistry and homogeneous catalysis, Chem. Rev., 77(3), 313-348 (DOI: 10.1021/cr60307a002).

77. Dorta R., Stevens E. D., Scott N. M., Costabile C., Cavallo L., Hoff C. D., Nolan S. P. (2005), Steric and Electronic Properties of *N*-Heterocyclic Carbenes (NHC): A Detailed Study on Their Interaction with Ni(CO)$_4$, J. Am. Chem. Soc., 127(8), 2485-2495 (DOI: 10.1021/ja0438821).

78. Dorta R., Stevens E. D., Hoff C. D., Nolan S. P. (2003), Stable, Three-Coordinate Ni(CO)$_2$(NHC) (NHC = *N*-Heterocyclic Carbene) Complexes Enabling the Determination of Ni−NHC Bond Energies, J. Am. Chem. Soc., 125(35), 10490-10491 (DOI: 10.1021/ja0362151).

79. Díez-González S., Nolan S. P. (2007), Stereoelectronic parameters associated with *N*-heterocyclic carbene (NHC) ligands: A quest for understanding, Coord. Chem. Rev., 251(5), 874-883 (DOI: 10.1016/j.ccr.2006.10.004).

80. Jacobsen H., Correa A., Poater A., Costabile C., Cavallo L. (2009), Understanding the M(NHC) (NHC = *N*-heterocyclic carbene) bond, Coord. Chem. Rev., 253(5), 687-703 (DOI: 10.1016/j.ccr.2008.06.006).

81. Nemcsok D., Wichmann K., Frenking G. (2004), The Significance of π Interactions in Group 11 Complexes with *N*-Heterocyclic Carbenes, Organometallics, 23(15), 3640-3646 (DOI: 10.1021/om049802j).

82. Gründemann S., Albrecht M., Loch J. A., Faller J. W., Crabtree R. H. (2001), Tridentate Carbene CCC and CNC Pincer Palladium(II) Complexes: Structure, Fluxionality, and Catalytic

Activity, Organometallics, 20(25), 5485-5488 (DOI: 10.1021/om010631h).

83. Schultz K. M., Goldberg K. I., Gusev D. G., Heinekey D. M. (2011), Synthesis, Structure, and Reactivity of Iridium NHC Pincer Complexes, Organometallics, 30(6), 1429-1437 (DOI: 10.1021/om101024x).

84. Bauer E. B., Andavan G. T. S., Hollis T. K., Rubio R. J., Cho J., Kuchenbeiser G. R., Helgert T. R., Letko C. S., Tham F. S. (2008), Air- and Water-Stable Catalysts for Hydroamination/Cyclization. Synthesis and Application of CCC−NHC Pincer Complexes of Rh and Ir, Org. Lett., 10(6), 1175-1178 (DOI: 10.1021/ol8000766).

85. Danopoulos A. A., Pugh D., Wright J. A. (2008), "Pincer" Pyridine–Dicarbene–Iridium Complexes: Facile C-H Activation and Unexpected η2-Imidazol-2-ylidene Coordination, Angew. Chem. Int. Ed., 47(50), 9765-9767 (DOI: 10.1002/anie.200804573).

86. Cross W. B., Daly C. G., Ackerman R. L., George I. R., Singh K. (2010), N-heterocyclic carbene tethered amido complexes of palladium and platinum, Dalton Trans., 40(2), 495-505 (DOI: 10.1039/C0DT01149E).

87. Danopoulos A. A., Wright J. A., Motherwell W. B., Ellwood S. (2004), N-Heterocyclic "Pincer" Dicarbene Complexes of Cobalt(I), Cobalt(II), and Cobalt(III), Organometallics, 23(21), 4807-4810 (DOI: 10.1021/om049489l).

88. Danopoulos A. A., Tsoureas N., Wright J. A., Light M. E. (2004), N-Heterocyclic Pincer Dicarbene Complexes of Iron(II): C-2 and C-5 Metalated Carbenes on the Same Metal Center, Organometallics, 23(2), 166-168 (DOI: 10.1021/om0341911).

89. Filonenko G. A., Cosimi E., Lefort L., Conley M. P., Copéret C., Lutz M., Hensen E. J. M., Pidko E. A. (2014), Lutidine-Derived Ru-CNC Hydrogenation Pincer Catalysts with Versatile

Coordination Properties, ACS Catal., 4(8), 2667-2671 (DOI: 10.1021/cs500720y).

90. Pugh D., Boyle A., Danopoulos A. A. (2008), 'Pincer' pyridine dicarbene complexes of nickel and their derivatives, Unusual ring opening of a coordinated imidazol-2-ylidene, Dalton Trans., (8), 1087-1094 (DOI: 10.1039/B715769J).

91. Seddon E. A., Seddon K. R. (1984), The Chemistry of Ruthenium (Vol. 19), Elsevier (ISBN: 0-444-42375-3).

92. Yadav D., Singh R. K., Singh S., Shirage P. M., Singh A. K. (2021), Cationic ruthenium(II)-NHC pincer complexes with hemilabile COD: Solid-state structural characterization and theoretical study of an η^2-(E,Z)-COD ligand, J. Organomet. Chem., 953, 122061 (DOI: 10.1016/j.jorganchem.2021.122061).

93. Danopoulos A. A., Winston S., Motherwell W. B. (2002), Stable N-functionalised 'pincer' bis carbene ligands and their ruthenium complexes; synthesis and catalytic studies, Chem. Commun., (13), 1376-1377 (DOI: 10.1039/B202814J).

94. Poyatos M., Mata J. A., Falomir E., Crabtree R. H., Peris E. (2003), New Ruthenium(II) CNC-Pincer Bis(carbene) Complexes: Synthesis and Catalytic Activity, Organometallics, 22(5), 1110-1114 (DOI: 10.1021/om020817w).

95. Son S. U., Park K. H., Lee Y.-S., Kim B. Y., Choi C. H., Lah M. S., Jang Y. H., Jang D.-J., Chung Y. K. (2004), Synthesis of Ru(II) Complexes of N-Heterocyclic Carbenes and Their Promising Photoluminescence Properties in Water, Inorg. Chem., 43(22), 6896-6898 (DOI: 10.1021/ic049514f).

96. Danopoulos A. A., Braunstein P., Saßmannshausen J., Pugh D., Wright J. A. (2020), "Pincer" Pyridine-Dicarbene-Iridium and -Ruthenium Complexes and Derivatives Thereof, Eur. J. Inorg. Chem., 2020(35), 3359-3369 (DOI: 10.1002/ejic.202000429).

97. Vaquer L., Miró P., Sala X., Bozoglian F., Masllorens E., Benet-Buchholz J., Fontrodona X., Parella T., Romero I., Roglans A., Rodríguez M., Bo C., Llobet A. (2013), Understanding Electronic

Ligand Perturbation over Successive Metal-Based Redox Potentials in Mononuclear Ruthenium-Aqua Complexes, ChemPlusChem, 78(3), 235-243 (DOI: 10.1002/cplu.201200268).

98. Boudreaux C. M., Liyanage N. P., Shirley H., Siek S., Gerlach D. L., Qu F., Delcamp J. H., Papish E. T. (2017), Ruthenium(II) complexes of pyridinol and *N*-heterocyclic carbene derived pincers as robust catalysts for selective carbon dioxide reduction, Chem. Commun., 53(81), 11217-11220 (DOI: 10.1039/C7CC05706G).

99. Arikawa Y., Nakamura T., Ogushi S., Eguchi K., Umakoshi K. (2015), Fixation of atmospheric carbon dioxide by ruthenium complexes bearing an NHC-based pincer ligand: formation of a methylcarbonato complex and its methylation, Dalton Trans., 44(12), 5303-5305 (DOI: 10.1039/C5DT00476D).

100. Gaillard S., Renaud J.-L. (2013), When phosphorus and NHC (*N*-heterocyclic carbene) meet each other, Dalton Trans., 42(20), 7255-7270 (DOI: 10.1039/C2DT32789A).

101. Nelson D. J., Nolan S. P. (2013), Quantifying and understanding the electronic properties of *N*-heterocyclic carbenes, Chem. Soc. Rev., 42(16), 6723-6753 (DOI: 10.1039/C3CS60146C).

102. Tao W., Akita S., Nakano R., Ito S., Hoshimoto Y., Ogoshi S., Nozaki K. (2017), Copolymerisation of ethylene with polar monomers by using palladium catalysts bearing an *N*-heterocyclic carbene-phosphine oxide bidentate ligand, Chem. Commun., 53(17), 2630-2633 (DOI: 10.1039/C7CC00002B).

103. Xu Q., Duan W.-L., Lei Z.-Y., Zhu Z.-B., Shi M. (2005), A novel cis-chelated Pd(II)–NHC complex for catalyzing Suzuki and Heck-type cross-coupling reactions, Tetrahedron, 61(47), 11225-11229 (DOI: 10.1016/j.tet.2005.09.010).

104. Herrmann W. A., Elison M., Fischer J., Köcher C., Artus G. R. J. (1995), Metal Complexes of *N*-Heterocyclic Carbenes-A New Structural Principle for Catalysts in Homogeneous Catalysis,

Angew. Chem. Int. Ed. Engl., 34(21), 2371-2374 (DOI: 10.1002/anie.199523711).

105. DePasquale J., Kumar M., Zeller M., Papish E. T. (2013), Variations on an NHC Theme: Which Features Enhance Catalytic Transfer Hydrogenation with Ruthenium Complexes?, Organometallics, 32(4), 966-979 (DOI: 10.1021/om300547f).

106. Chang W., Gong X., Wang S., Xiao L.-P., Song G. (2017), Acceptorless dehydrogenation and dehydrogenative coupling of alcohols catalysed by protic NHC ruthenium complexes, Org. Biomol. Chem., 15(16), 3466-3471 (DOI: 10.1039/C7OB00542C).

107. Urbina-Blanco C. A., Leitgeb A., Slugovc C., Bantreil X., Clavier H., Slawin A. M. Z., Nolan S. P. (2011), Olefin Metathesis Featuring Ruthenium Indenylidene Complexes with a Sterically Demanding NHC Ligand, Chem. Eur. J., 17(18), 5045-5053 (DOI: 10.1002/chem.201003082).

108. Mutoh Y., Mohara Y., Saito S. (2017), (Z)-Selective Hydrosilylation of Terminal Alkynes with $HSiMe(OSiMe_3)_2$ Catalyzed by a Ruthenium Complex Containing an *N*-Heterocyclic Carbene, Org. Lett., 19(19), 5204-5207 (DOI: 10.1021/acs.orglett.7b02477).

109. Su W., Younus H. A., Zhou K., Khattak Z. A. K., Chaemcheun S., Chen C., Verpoort F. (2017), Chemical and photochemical water oxidation catalyzed by novel ruthenium complexes comprising a negatively charged NCNHCO ligand, Catal. Sci. Technol., 7(2), 387-395 (DOI: 10.1039/C6CY02333A).

110. Sanz S., Azua A., Peris E. (2010), '(η^6-arene)Ru(bis-NHC)' complexes for the reduction of CO_2 to formate with hydrogen and by transfer hydrogenation with ^{i}PrOH, Dalton Trans., 39(27), 6339-6343 (DOI: 10.1039/C003220D).

111. Janssen-Müller D., Schlepphorst C., Glorius F. (2017), Privileged chiral *N*-heterocyclic carbene ligands for asymmetric transition-

metal catalysis, Chem. Soc. Rev., 46(16), 4845-4854 (DOI: 10.1039/C7CS00200A).

112. Younus H. A., Ahmad N., Su W., Verpoort F. (2014), Ruthenium pincer complexes: Ligand design and complex synthesis, Coord. Chem. Rev., 276, 112-152 (DOI: 10.1016/j.ccr.2014.06.016).

113. Ito J., Nishiyama H. (2014), Recent topics of transfer hydrogenation, Tetrahedron Lett., 55(20), 3133-3146 (DOI: 10.1016/j.tetlet.2014.03.140).

114. Wang D., Astruc D. (2015), The Golden Age of Transfer Hydrogenation, Chem. Rev., 115(13), 6621-6686 (DOI: 10.1021/acs.chemrev.5b00203).

115. Yadav D., Misra S., Kumar D., Singh S., Singh A. K. (2021), Cationic ruthenium(II)-NHC pincer complexes: Synthesis, characterisation and catalytic activity for transfer hydrogenation of ketones, Appl. Organomet. Chem., 35(8), e6287 (DOI: 10.1002/aoc.6287).

116. Baratta W., Schütz J., Herdtweck E., Herrmann W. A., Rigo P. (2005), Fast transfer hydrogenation using a highly active orthometalated heterocyclic carbene ruthenium catalyst, J. Organomet. Chem., 690(24), 5570-5575 (DOI: 10.1016/j.jorganchem.2005.07.001).

117. Zeng F., Yu Z. (2008), Ruthenium(II) Complexes Bearing a Pyridyl-Supported Pyrazolyl-*N*-Heterocyclic Carbene (NNC) Ligand and Their Catalytic Activity in the Transfer Hydrogenation of Ketones, Organometallics, 27(22), 6025-6028 (DOI: 10.1021/om8006213).

118. Bauri S., Donthireddy S. N. R., Illam P. M., Rit A. (2018), Effect of Ancillary Ligand in Cyclometalated Ru(II)-NHC-Catalyzed Transfer Hydrogenation of Unsaturated Compounds, Inorg. Chem., 57(23), 14582-14593 (DOI: 10.1021/acs.inorgchem.8b02246).

119. Yadav S., Gupta R. (2023), Base-Free Transfer Hydrogenation Catalyzed by Ruthenium Hydride Complexes of Coumarin-

Amide Ligands, ACS Sustain. Chem. Eng., 11(23), 8533-8543 (DOI: 10.1021/acssuschemeng.3c01104).

120. Pandey P., Dutta I., Bera J. K. (2016), Acceptorless Alcohol Dehydrogenation: A Mechanistic Perspective, Proc. Nat. Acad. Sci., India Sect. A: Phys. Sci., 86(4), 561-579 (DOI: 10.1007/s40010-016-0296-7).

121. Crabtree R. H. (2017), Homogeneous Transition Metal Catalysis of Acceptorless Dehydrogenative Alcohol Oxidation: Applications in Hydrogen Storage and to Heterocycle Synthesis, Chem. Rev., 117(13), 9228-9246 (DOI: 10.1021/acs.chemrev.6b00556).

122. Yadav D., Singh R. K., Misra S., Singh A. K. (2022), Ancillary ligand effects and microwave-assisted enhancement on the catalytic performance of cationic ruthenium(II)-CNC pincer complexes for acceptorless alcohol dehydrogenation, Appl. Organomet. Chem., e6756 (DOI: 10.1002/aoc.6756).

123. Zhang J., Gandelman M., Shimon L. J. W., Rozenberg H., Milstein D. (2004), Electron-Rich, Bulky Ruthenium PNP-Type Complexes. Acceptorless Catalytic Alcohol Dehydrogenation, Organometallics, 23(17), 4026-4033 (DOI: 10.1021/om049716j).

124. Wang Z., Pan B., Liu Q., Yue E., Solan G. A., Ma Y., Sun W.-H. (2017), Efficient acceptorless dehydrogenation of secondary alcohols to ketones mediated by a PNN-Ru(II) catalyst, Catal. Sci. Technol., 7(8), 1654-1661 (DOI: 10.1039/C7CY00342K).

125. Chen Y., Cui T., Chen H., Zheng X. li, Fu H., Li R. (2023), Pyrazole-pyridine-pyrazole (NNN) ruthenium(II) complex catalyzed acceptorless dehydrogenation of alcohols to aldehydes, Dalton Trans., 52(35), 12368-12377 (DOI: 10.1039/D3DT01430D).

126. Dutta I., Sarbajna A., Pandey P., Rahaman S. M. W., Singh K., Bera J. K. (2016), Acceptorless Dehydrogenation of Alcohols on a Diruthenium(II,II) Platform, Organometallics, 35(10), 1505-1513 (DOI: 10.1021/acs.organomet.6b00085).

127. Prades A., Peris E., Albrecht M. (2011), Oxidations and Oxidative Couplings Catalyzed by Triazolylidene Ruthenium Complexes, Organometallics, 30(5), 1162-1167 (DOI: 10.1021/om101145y).

128. Patil R. D., Adimurthy S. (2013), Catalytic Methods for Imine Synthesis, Asian J. Org. Chem., 2(9), 726-744 (DOI: 10.1002/ajoc.201300012).

129. Belowich M. E., Stoddart J. F. (2012), Dynamic imine chemistry, Chem. Soc. Rev., 41(6), 2003-2024 (DOI: 10.1039/C2CS15305J).

130. Gnanaprakasam B., Zhang J., Milstein D. (2010), Direct Synthesis of Imines from Alcohols and Amines with Liberation of H_2, Angew. Chem. Int. Ed., 49(8), 1468-1471 (DOI: 10.1002/anie.200907018).

131. Yang F.-L., Wang Y.-H., Ni Y.-F., Gao X., Song B., Zhu X., Hao X.-Q. (2017), An Efficient Homogenized Ruthenium(II) Pincer Complex for N-Monoalkylation of Amines with Alcohols, Eur. J. Org. Chem., 2017(24), 3481-3486 (DOI: 10.1002/ejoc.201700486).

132. Eizawa A., Nishimura S., Arashiba K., Nakajima K., Nishibayashi Y. (2018), Synthesis of Ruthenium Complexes Bearing PCP-Type Pincer Ligands and Their Application to Direct Synthesis of Imines from Amines and Benzyl Alcohol, Organometallics, 37(18), 3086-3092 (DOI: 10.1021/acs.organomet.8b00465).

133. Das K., Nandi P. G., Islam K., Srivastava H. K., Kumar A. (2019), N-Alkylation of Amines Catalyzed by a Ruthenium-Pincer Complex in the Presence of in situ Generated Sodium Alkoxide, Eur. J. Org. Chem., 2019(40), 6855-6866 (DOI: 10.1002/ejoc.201901310).

134. Singh S., Choudhury A. R., Ghosh K. (2023), Facile synthesis of quinolines and N-alkylation reactions catalyzed by ruthenium(II) pincer type complexes: Reaction mechanism and evidences for

ruthenium hydride intermediate, Mol. Catal., 549, 113424 (DOI: 10.1016/j.mcat.2023.113424).

135. Yu X., Li Y., Fu H., Zheng X., Chen H., Li R. (2018), Mechanistic investigation of imine formation in ruthenium-catalyzed *N*-alkylation of amines with alcohols, Appl. Organomet. Chem., 32(4), e4277 (DOI: 10.1002/aoc.4277).

136. Gao P., Szostak M. (2023), Hydration reactions catalyzed by transition metal-NHC (NHC = *N*-heterocyclic carbene) complexes, Coord. Chem. Rev., 485, 215110 (DOI: 10.1016/j.ccr.2023.215110).

137. Edward J. T., Meacock S. C. R. (1957) 383. Hydrolysis of amides and related compounds. Part I. Some benzamides in strong aqueous acid, J. Chem. Soc., 2000-2007 (DOI: 10.1039/JR9570002000).

138. O'Connor C. (1970), Acidic and basic amide hydrolysis, Q. Rev. Chem. Soc., 24(4), 553-564 (DOI: 10.1039/QR9702400553).

139. Tu T., Wang Z., Liu Z., Feng X., Wang Q. (2012), Efficient and practical transition metal-free catalytic hydration of organonitriles to amides, Green Chem., 14(4), 921-924 (DOI: 10.1039/C2GC16637B).

140. Guo B., Vries J. G. de, Otten E. (2019), Hydration of nitriles using a metal-ligand cooperative ruthenium pincer catalyst, Chem. Sci., 10(45), 10647-10652 (DOI: 10.1039/C9SC04624K).

141. Tomás-Mendivil E., Suárez F. J., Díez J., Cadierno V. (2014), An efficient ruthenium(IV) catalyst for the selective hydration of nitriles to amides in water under mild conditions, Chem. Commun., 50(68), 9661-9664 (DOI: 10.1039/C4CC04058A.

142. Chouhan K. K., Chowdhury D., Mukherjee A. (2023), Cyclotrimetaphosphate-assisted ruthenium catalyst for the hydration of nitriles and oxidation of primary amines to amides under aerobic conditions in water, Org. Biomol. Chem., 21(11), 2429-2439 (DOI: 10.1039/D3OB00062A).

143. García-Álvarez R., Díez J., Crochet P., Cadierno V. (2010), Arene-Ruthenium(II) Complexes Containing Amino-Phosphine Ligands as Catalysts for Nitrile Hydration Reactions, Organometallics, 29(17), 3955-3965 (DOI: 10.1021/om1006227).

144. Lee W.-C., Sears J. M., Enow R. A., Eads K., Krogstad D. A., Frost B. J. (2013), Hemilabile β-Aminophosphine Ligands Derived from 1,3,5-Triaza-7-phosphaadamantane: Application in Aqueous Ruthenium Catalyzed Nitrile Hydration, Inorg. Chem., 52(4), 1737-1746 (DOI: 10.1021/ic301160x).

145. Ferrer Í., Rich J., Fontrodona X., Rodríguez M., Romero I. (2013), Ru(II) complexes containing dmso and pyrazolyl ligands as catalysts for nitrile hydration in environmentally friendly media, Dalton Trans., 42(37), 13461-13469 (DOI: 10.1039/C3DT51580J.

146. Saha R., Mukherjee A., Bhattacharya S. (2022), Development of a ruthenium-aquo complex for utilization in synthesis and catalysis for selective hydration of nitriles and alkynes, New J. Chem., 46(19), 9098-9110 (DOI: 10.1039/D1NJ04736A).

147. Yadav S., Gupta R. (2022), Hydration of Nitriles Catalyzed by Ruthenium Complexes: Role of Dihydrogen Bonding Interactions in Promoting Base-Free Catalysis, Inorg. Chem., 61(39), 15463-15474 (DOI: 10.1021/acs.inorgchem.2c02058).

148. Tomás-Mendivil E., García-Álvarez R., Vidal C., Crochet P., Cadierno V. (2014), Exploring Rhodium(I) Complexes [RhCl(COD)(PR$_3$)] (COD = 1,5-Cyclooctadiene) as Catalysts for Nitrile Hydration Reactions in Water: The Aminophosphines Make the Difference, ACS Catal., 4(6), 1901-1910 (DOI: 10.1021/cs500241p).

149. Fan X.-N., Deng W., Liu Z.-J., Yao Z.-J. (2020), Half-Sandwich Iridium Complexes for the One-Pot Synthesis of Amides: Preparation, Structure, and Diverse Catalytic Activity, Inorg. Chem., 59(22), 16582-16590 (DOI: 10.1021/acs.inorgchem.0c02497).

150. Buil M. L., Cadierno V., Esteruelas M. A., Gimeno J., Herrero J., Izquierdo S., Oñate E. (2012) Selective Hydration of Nitriles to Amides Promoted by an Os-NHC Catalyst: Formation and X-ray Characterization of κ^2-Amidate Intermediates, Organometallics, 31(19), 6861-6867 (DOI: 10.1021/om3006799).

151. Ramón R. S., Marion N., Nolan S. P. (2009), Gold Activation of Nitriles: Catalytic Hydration to Amides, Chem. Eur. J., 15(35), 8695-8697 (DOI: 10.1002/chem.200901231).

152. Xing X., Xu C., Chen B., Li C., Virgil S. C., Grubbs R. H. (2018), Highly Active Platinum Catalysts for Nitrile and Cyanohydrin Hydration: Catalyst Design and Ligand Screening via High-Throughput Techniques, J. Am. Chem. Soc., 140(50), 17782-17789 (DOI: 10.1021/jacs.8b11667).

153. Ahmed T. J., Knapp S. M. M., Tyler D. R. (2011), Frontiers in catalytic nitrile hydration: Nitrile and cyanohydrin hydration catalyzed by homogeneous organometallic complexes, Coord. Chem. Rev., 255(7), 949-974 (DOI: 10.1016/j.ccr.2010.08.018).

154. Allen C. L., Williams J. M. J. (2011), Metal-catalysed approaches to amide bond formation, Chem. Soc. Rev., 40(7), 3405-3415 (DOI: 10.1039/C0CS00196A).

155. de Figueiredo R. M., Suppo J.-S., Campagne J.-M. (2016), Nonclassical Routes for Amide Bond Formation, Chem. Rev., 116(19), 12029-12122 (DOI: 10.1021/acs.chemrev.6b00237).

Chapter 2

Syntheses, Characterization, and Catalytic Activity of Cationic Ru(II)-CNC Pincer Complexes

2.1. Introduction

Pincer complexes have found significant attention due to their enormous properties and extensive applications in organic transformations [1, 2]. These complexes are known for their high thermal stability, robust nature, and variable oxidation states, making them essential catalysts for high-temperature and pressure reactions without decomposition [3, 4]. Pincer complexes are widely utilized in small molecule activation, CO_2 reduction, and H_2O oxidation catalysis [5–7]. In catalytic reactions, the pincer ligands provide chemical and thermal stability, which helps to reduce the metal leaching during the catalytic cycle [8].

   NHCs-based metal complexes have been found to be privileged over other metal complexes [9, 10]. NHCs containing pincer complexes have been extensively utilized in homogeneous catalysis, offering excellent thermal stability and facilitating a wide variety of metal-based reactivity [3, 4, 11]. NHCs are readily available as stable salts with diverse *N*-substituents, central ring sizes, and functionalization, making them versatile ligands for numerous reactions [12, 13]. NHCs and pyridine-derived CNC pincer are the most popular ligands in the pincer family. CNC pincer complexes are becoming more popular as robust catalysts due to their ability to enhance the electron density at the coordinated metal centre [3]. Ruthenium pincer complexes with CNC backbone have found attention

as efficient catalysts with a wide range of catalytic applications [14–16].

Hydrogenation is one of the most essential processes in organic synthesis, and its applications for the production of fine chemicals and pharmaceuticals are well-known [17]. Hydrogenation is employed by direct hydrogenation with a pressure of H_2 gas or transfer hydrogenation reaction [17, 18]. Ruthenium-catalyzed hydrogenation/transfer hydrogenation of carbonyl compounds are widely accepted process to produce alcohols via H_2 or isopropanol rather than other reducing agents like $NaBH_4$ and $LiAlH_4$ [15, 19]. This approach provided higher control of selectivity and atom economy compared to classical methods. Ru(II) complexes with a pincer backbone are well explored in catalysis, but CNC-based Ru(II) complexes are less explored for the TH of ketones [2, 19].

Dehydrogenation is an essential step in organic synthesis, in which oxidation of alcohols to carbonyl compounds occurs with a stoichiometric amount of oxidants [20]. The metal-catalyzed acceptorless dehydrogenation is a more favourable oxidation method by releasing molecular hydrogen as the sole by-product [21, 22]. Acceptorless dehydrogenation is an atom-efficient and environment-friendly technique for the oxidation of alcohol [22, 23]. Ru(II)-CNC pincer complexes are less explored for the acceptorless dehydrogenation of alcohols. Ruthenium pincer complexes show high efficiency for acceptorless dehydrogenation of alcohols with excellent selectivity of products [24].

Previously, our group reported cationic Ru(II)-CNC pincer complexes featuring various ancillary ligands (CO, COD, DMSO, PPh$_3$) with smaller *N*-alkyl wingtips for TH and AAD catalytic reactions (Figure **2.1**) [25–27]. In TH and AAD catalysis, CO-containing complexes show superior reactivity as compared to their other analogous complexes. Based on our investigations and earlier

58

studies [24, 28], we reported a plausible catalytic cycle for both TH and AAD catalysis. In the mechanistic cycle, a CO hydride species was identified as actively participating in the catalysis. However, this species was not fully characterized, and attempts to isolate it were unsuccessful, leaving the proposed mechanism for TH and AAD catalysis less conclusive. Notably, in the AAD mechanism, the CO ligand exhibits a stronger *trans* effect than other ancillary ligands, increasing the lability of benzaldehyde and facilitating its dissociation from the ruthenium centre. This phenomenon likely accounts for the enhanced reactivity of CO-containing complexes. When the CO ligand is *trans* to benzaldehyde, it supports the idea that the CO hydride complex is involved in catalysis. The precise coordination of CO in the hydride species, whether *trans* or *cis*, to the pincer pyridine remains unclear, as this species has yet to be isolated or synthesized. To address this gap and provide stronger support for our proposed mechanism, we have decided to synthesize complexes with bulkier *N*-alkyl wingtips, to isolate the elusive CO hydride species and gain further insight into its role in catalysis.

L^1, L^2, L^3 = CO, PPh$_3$, COD, DMSO, Cl, H
R = Me, ^{i}Pr and X = Cl, PF$_6$
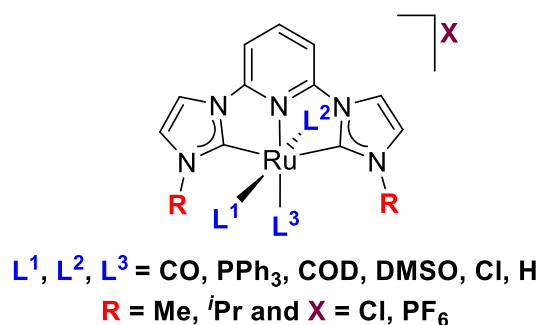
Figure 2.1. Previously reported cationic Ru(II)-CNC pincer complexes for TH and AAD reaction from our group.

N-wingtip substituents on the imidazole ring in CNC pincer ligands can modulate the steric environment around the ruthenium centre and control the reactivity of complexes [12]. Herein, we describe the synthesis, characterization, and catalytic activity of Ru(II)-CNC pincer complexes with bulky *N*-cyclohexyl wingtips, namely

[Ru(CNC^{Cy})(CO)(PPh$_3$)Cl]PF$_6$ **(1c)**, [Ru(CNC^{Cy})(CO)(PPh$_3$)H]PF$_6$ **(2c)**, [Ru(CNC^{Cy})(PPh$_3$)$_2$Cl]PF$_6$ **3c**, [Ru(CNC^{Cy})(PPh$_3$)$_2$H]PF$_6$ **(4c)** and [Ru(CNC^{Cy})(DMSO)$_2$Cl]PF$_6$ **(5c)**. The catalytic activity of complexes **(1c-5c)** was investigated for the transfer hydrogenation of cyclohexanone and acceptorless dehydrogenation of benzyl alcohol. The CO hydride complex **2c** was involved in the mechanistic pathway of both these transformations and formed during catalysis with the precatalyst **1c**.

2.2. Results and Discussion

2.2.1. Synthesis and characterization of cationic Ru(II)-CNC pincer complexes

The synthesis of imidazolium ligand precursors CNC^{Cy}·2HCl was achieved by a reported procedure and characterized by ^{1}H NMR spectrum [29]. Treatment of an imidazolium ligand precursor with Ag$_2$O in methanol affords the silver–carbene complex, which gives Ru–CNC complexes through in situ transmetallation with different Ru-precursors (Scheme **2.1**). The generation of carbene during complex formation in CNC^{Cy}·2HCl was confirmed by the disappearance of imidazolium protons, appearing as a singlet at 11.13 ppm.
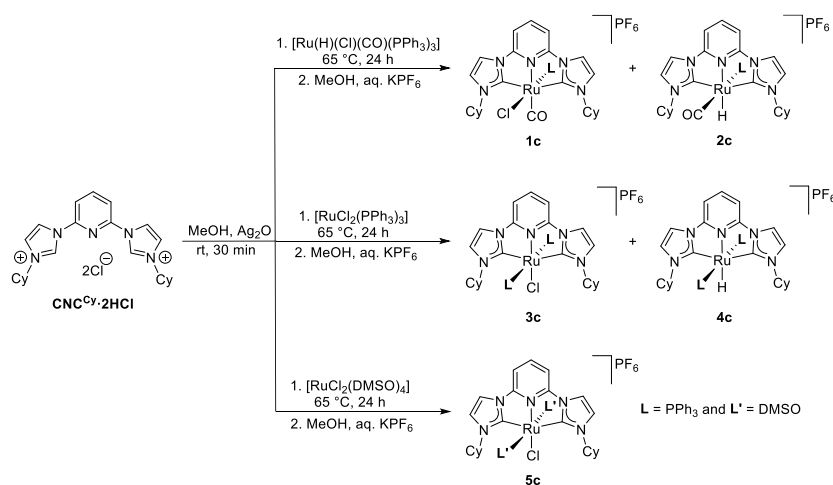
Scheme 2.1. Syntheses of cationic Ru(II)-CNC pincer complexes **1c-5c**.

The reaction of the *in-situ* generated silver-carbene complex with [RuHCl(CO)(PPh$_3$)$_3$] for 24 h in methanol, followed by the addition of aq. KPF$_6$ affords complex **1c**, characterized by the multinuclear NMR and mass analysis. The ESI$^+$ HRMS signal at *m/z* 802.2046 corresponds to species [**1c**-PF$_6$]$^+$. In the ^{1}H NMR spectrum of complex **1c**, the pyridine protons are represented by a doublet at 8.45 ppm and a triplet at 8.23 ppm, whereas for the imidazol-2-ylidene protons, two doublets at 7.81 and 7.71 ppm are observed. Complex **1c** displays a multiplet for two methine protons at 4.25–4.18 ppm, and the other protons of cyclohexyl appear in the aliphatic regions. In the ^{13}C NMR spectrum of complex **1c**, the CO signals appear as a doublet at 207.21 ppm ($^2J_{C-P}$ = 14.8 Hz). The carbene carbon signals of **1c** appear as a doublet at 188.78 ppm ($^2J_{C-P}$ = 11.5 Hz). The ^{31}P NMR spectrum of complex **1c** showed a peak at 48.23 ppm for PPh$_3$, which is slightly shifted from our previously reported *N*-Me analogue complex (43.27 ppm) [25] and a septate at -144.19 ppm for PF$_6^-$ counterion, and their splitting was due to the coupling with six ^{19}F nuclei. The C=O stretching frequency of complex **1c** found at 1953 cm^{-1}, comparable to the similar CNC complexes (1952-1954 cm^{-1}) [30], and our recently reported *N*-Me analogue complex (1954 cm^{-1}) [25] but higher than 1922 cm^{-1} of another Ru–CNC pincer complex [14].

During the synthesis of **1c**, complex **2c** is also obtained which could be separated by column chromatography. Complex **2c** exhibits ESI$^+$ HRMS signal at *m/z* 768.2425 corresponds to [**2c**-PF$_6$]$^+$. In ^{1}H NMR spectrum of **2c**, a doublet at 8.44 ppm and a triplet at 8.08 ppm for the pyridine protons, and two doublets at 7.73 ppm, 7.70 ppm are observed for the imidazol-2-ylidene protons. Similarly, the two methine protons of cyclohexyl, as well as the remainder of the protons for **2c**, disclose the ^{1}H resonance within the range observed for **1c** while the hydride signal appears as a doublet at -9.13 ppm ($^2J_{H-P}$ = 23.1 Hz). In ^{13}C NMR of **2c**, the CO signal was detected as a doublet at 198.63 ppm ($^2J_{C-P}$ = 81.9 Hz) with a high coupling constant, suggesting

that the CO ligand trans to PPh$_3$ ligand [31], and the carbene carbon signal as a doublet at 190.62 ppm ($^2J_{C-P}$ = 13.8 Hz). ^{31}P NMR of complex **2c** showed a peak at 41.98 ppm for the PPh$_3$ ligand and a septate at -144.19 ppm for PF$_6^-$ counterion and their splitting was due to the coupling with six ^{19}F nuclei. The C=O stretching frequency of complex **2c** found at 1950 cm^{-1}, is slightly lower than the chloride complex **1c**.

The synthesis of complex **3c** was accomplished similarly by using [RuCl$_2$(PPh$_3$)$_3$] as the ruthenium precursor. During the synthesis of complex **3c**, the hydride complex **4c** is also generated, similar to the *N*-methyl analogue complex reported earlier [25]. Complex **3c** was characterized by multinuclear NMR spectra and mass spectrometry. Complex **3c** exhibit ESI$^+$ HRMS signals at *m/z* 1036.3010, corresponding to [**3c**-PF$_6$]$^+$, while the other two signals are assigned to [**3c**-PF$_6$-Cl+H]$^+$ and [**3c**-PF$_6$-PPh$_3$]$^+$ at *m/z* 1002.3382, and 774.2072, respectively. In the ^{1}H NMR spectrum of **3c**, the aromatic protons for the pincer ligand appeared at 7.81, 7.68, 7.66, and 7.64 ppm. The two methine protons of cyclohexyl appeared as a multiplet at 5.04 – 4.97 ppm. In ^{13}C NMR, the carbene carbon signal of complex **3c** appears at 189.61 ppm. Furthermore, the ^{31}P NMR spectrum of complex **3c** shows two singlet peaks at 29.35, and 19.06 ppm for PPh$_3$ and another peak at -144.20 for PF$_6^-$ counterion, and their splitting as a septate due to coupling with six ^{19}F nuclei. These two singlets in the ^{31}P NMR of **3c** (without any signal for free PPh$_3$) are attributed to generating two species in solution due to the dissociation of chloride ligand. Mass analysis confirms this assumption as an ESI$^+$ HRMS signal at *m/z* 500.6667 is observed and assigned to [**3c**-PF$_6$-Cl]$^{2+}$.

Hydride complex **4c** can also be synthesized from complex **3c** on treatment with K$_2$CO$_3$ in isopropanol, as shown in Scheme **2.2**. Complex **4c** exhibits ESI$^+$ HRMS signal at *m/z* 1002.3385 for [**4c**-PF$_6$]$^+$. In the ^{1}H NMR spectrum of complex **4c**, the aromatic protons

for the pincer ligand appeared at 8.29, 7.78, 7.64, and 7.63 ppm. The cyclohexyl protons of complex **4c** are in the expected range, while the hydride signal appears as a triplet at -8.56 ppm ($^2J_{\text{H-P}}$ = 25.0 Hz). The ^{13}C NMR spectrum shows a triplet at 196.94 ppm ($^2J_{\text{C-P}}$ = 13.6 Hz) for the carbene carbon of the complex **4c**. Similarly, the ^{31}P NMR spectrum of complex **4c** exhibits a peak at 49.59 ppm for PPh$_3$, which is comparable with their *N*-methyl analogue reported earlier [25], and the other signal appeared at -144.19 ppm for PF$_6^-$ counterion, and its splitting is a septate due to coupling with six ^{19}F nuclei.
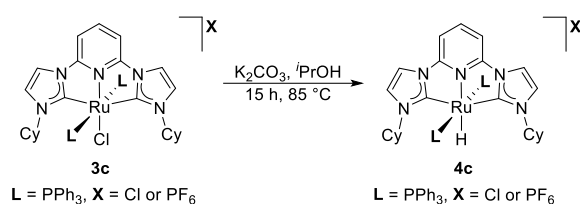
Scheme 2.2. Syntheses of ruthenium hydride complex.

Complex **5c** was synthesized from [RuCl$_2$(DMSO)$_4$] as the ruthenium source. Complex **5c** show ESI$^+$ HRMS signals at *m/z* 668.1456 and 590.1325 assigned to [**5c**-PF$_6$]$^+$, and [**5c**-PF$_6$-DMSO]$^+$ respectively. In the ^{1}H NMR spectrum of complex **5c**, the aromatic proton of pincer ligand appears at 8.60, 8.25, 8.01, and 7.96 ppm, while the methyl proton of DMSO appeared at 2.67 ppm and the cyclohexyl protons are in the expected range. In the ^{13}C NMR spectrum of **5c**, the carbene carbon signal appeared upfield shift at 183.94 ppm, compared to the phosphine complexes as discussed above. ^{31}P NMR spectrum shows peaks at -144.20 ppm for PF$_6^-$ counterion, and their splitting as a septate due to coupling with six ^{19}F nuclei.

2.2.2. Catalytic application in transfer hydrogenation of cyclohexanone

Ruthenium complexes have been investigated for the reduction of cyclohexanone via transfer hydrogenation (TH) with isopropanol in the

presence of a base. The optimized reaction conditions for TH catalysis were reported earlier by our group for similar analogue complexes [25]. We applied these optimized reaction conditions for the investigation of the newly synthesized ruthenium complexes. The NaO^{i}Pr base for the catalytic reaction is generated *in situ* by the addition of the required amount of sodium metal in the propan-2-ol solvent. This strategy provides simpler handling of moisture-sensitive NaO^{i}Pr base and has been utilized earlier, giving excellent results [32]. The reaction was monitored by gas chromatography with *n*-decane as an internal standard.

Table 2.1. Transfer hydrogenation of cyclohexanone with different catalysts.
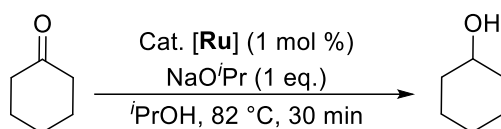
Entry[a]	Catalyst (mol%)	% Yield[b]	TON[c]/TOF[d](h^{-1})
1.	**1c** (1)	78	78/156
2.	**2c** (1)	69	69/138
3.	**3c** (1)	75	75/150
4.	**4c** (1)	74	74/148
5.	**5c** (1)	72	72/144

[a]Reaction conditions: Cyclohexanone (2.0 mmol), Catalyst (1 mol%), NaO^{i}Pr (1 eq.), ^{i}PrOH (5 mL), at 82 °C under a slow N$_2$ flow. [b]GC Yield determined by gas chromatography with *n*-decane as an internal standard. The product was characterized by GC-MS and NMR. [c]TON = (Number of moles of substrate converted)/(Number of moles of catalyst), at the end of the reaction. [d]TOF = [(TON)/ hour].

Using 2 mmol of cyclohexanone, 1 mol% of catalyst, and 1 equivalent of sodium *iso*-propoxide (NaO^{i}Pr) as the base with complex **1c** (78%, Table 2.1, entries 1) showed higher catalytic activity than other complexes viz, **3c**, and **5c** (75 and 72%) respectively (Table 2.1, entries 3 and 5). Additionally, hydride complexes **2c** and **4c** (69 and 74%, Table 2.2.1, entries 2 and 4) gave similar results as compared to their halide complexes (Table 2.1, entries 1 and 3). All reactions can

go to completion upon increasing reaction times; however, for comparison of catalyst reactivity, these reactions were stopped at 30 minutes. The ancillary ligand effects were similar to those of their analogue complexes, where CO-containing catalysts are the better catalysts for the TH reaction.

2.2.3. Catalytic application in acceptorless dehydrogenation of benzyl alcohol

An acceptorless dehydrogenation reaction was investigated for benzyl alcohol with newly synthesized ruthenium complexes, and better reactivity was found for this catalysis. The optimized reaction conditions for AAD catalysis were reported earlier by our group for similar analogue complexes [27]. We applied the previously reported optimized reaction conditions and explored the reactivity of these newly synthesized complexes.

Table 2.2. Acceptorless dehydrogenation of benzyl alcohol with different catalysts.
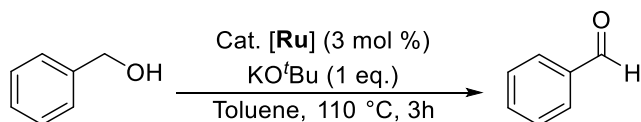
Entry[a]	Catalyst (mol%)	Conversion[b] (%)	TON[c]/TOF[d](h^{-1})
1.	**1c** (3)	53	18/6
2.	**2c** (3)	87	29/10
3.	**3c** (3)	36	12/4
4.	**4c** (3)	34	11/4
5.	**5c** (3)	39	13/4

[a]Reaction conditions: Benzyl alcohol (1 mmol), Catalyst (3 mol %), KO^{t}Bu (1 eq.), Toluene (5 mL) under a slow N_2 flow at 110 ºC for 3h. [b]Determined by gas chromatography without an internal standard. The product was characterized by GC-MS and NMR. [c]TON = [(Number of moles of substrate converted)/(Number of moles of catalyst)] at the end of the reaction. [d]TOF = [(TON)/hour].

Complexes **1c** and **5c** in toluene, in the presence of KO^{t}Bu at 110 °C for 3h, gave lower conversions, 53 and 39% (Table 2.2, entries

1 and 5), respectively. Further, complexes **3c** and **4c** gave much lower conversions, 36 and 34%, compared to others (Table 2.2, entries 3 and 4). Additionally, the hydride complex **2c** shows better conversion at 87% than its halide complex **1c** (Table 2.2, entry 2). The observed catalytic performance is similar to their analogue complexes [27]. The higher trans effect of CO gave better reactivity than other ancillary ligands.

2.2.4. Mechanism for the transfer hydrogenation reaction

A plausible reaction mechanism for transfer hydrogenation is proposed based on previous studies reported in the literature [28], and our investigations using complex **1c** as the catalyst precursor and **2c** as the Ru-hydride intermediate (Figure **2.2**). Our group previously reported the mechanistic investigation for the TH reaction using the *N*-methyl analogue complex [25]. The study with the *N*-cyclohexyl analogue containing CO as an ancillary ligand is presented below.

Figure 2.2. Plausible mechanism for the transfer hydrogenation reaction by complex **1c** with key intermediates **2c**.

The ruthenium alkoxide species **A** is produced when complex **1c** is treated with NaO^{i}Pr. The Ru-H intermediate **2c'** is formed from **A** via β-H elimination by releasing one molecule of acetone, or by dissociation of a PPh$_3$ ligand if starting from catalyst **2c**. The addition of cyclohexanone to the intermediate **2c'** produces another ruthenium alkoxide intermediate **B**, further hydride transfer to the electrophilic centre of the carbonyl group and generates intermediate **C**, which releases the hydrogenated product upon protonation from ^{i}PrOH, resulting in the formation of **A** again, and the catalytic cycle is completed.

2.2.5. Mechanism for acceptorless alcohol dehydrogenation

A plausible reaction mechanism for acceptorless alcohol dehydrogenation is proposed based on the earlier studies reported in the literature [24]. Our investigated mechanism was similar to our previously reported AAD mechanism with *N*-methyl analogue complex (Figure **2.3**) [27]. Although the involvement of Ru-H intermediate was confirmed in our earlier study with ^{1}H NMR and mass analysis [27], the exact stereochemistry around Ru is now confirmed with the ^{13}C NMR characterization of complex **2c**, having the hydride ligand *trans* to pyridine and CO ligand *trans* to PPh$_3$. The reaction starts with complex **1c** reacting with alcohol in the presence of KO^{t}Bu to produce the ruthenium alkoxide species **A'**, which isomerizes to **A** having a suitable vacant site at the *cis* position. The intermediate **B** is generated via β-H elimination resulting in the formation of the metal-bound aldehyde. The Ru-H intermediate **C** is formed by the release of the aldehyde molecule from **B**. If starting with the Ru-hydride complex **2c**, intermediate **B** can alternatively be formed after the dissociation of a PPh$_3$ ligand. Finally, in the AAD reaction, an intermediate **D** is formed by the coordination of an alcohol molecule to the intermediate **C**. Intermediate **D** liberates H$_2$ gas and regenerates the

ruthenium alkoxide species **A**, completing the acceptorless alcohol dehydrogenation step.
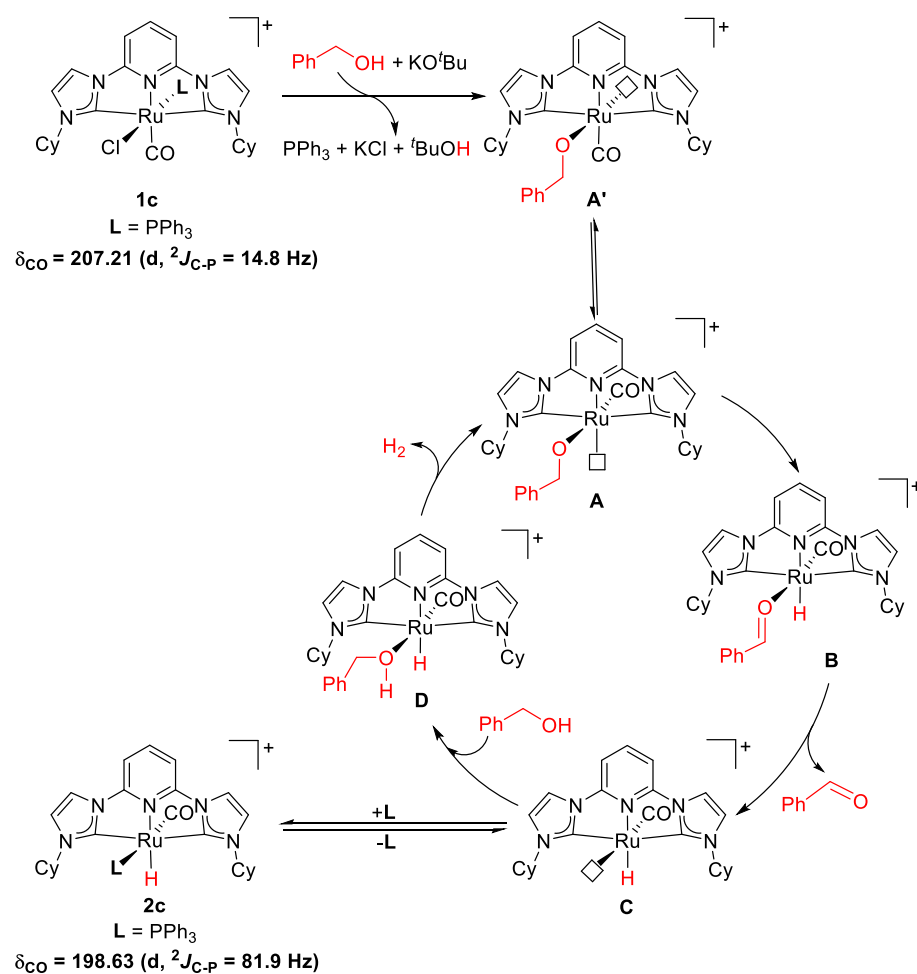
Figure 2.3. Plausible mechanism for acceptorless alcohol dehydrogenation by complex **1c** with key intermediates **2c**.

2.3. Conclusion

In summary, a series of new cationic Ru(II)-CNC pincer complexes [Ru(CNC^{Cy})(CO)(PPh$_3$)Cl]PF$_6$ (**1c**), [Ru(CNC^{Cy})(CO)(PPh$_3$)H]PF$_6$ (**2c**), [Ru(CNC^{Cy})(PPh$_3$)$_2$Cl]PF$_6$ (**3c**), [Ru(CNC^{Cy})(PPh$_3$)$_2$H]PF$_6$ (**4c**), and [Ru(CNC^{Cy})(DMSO)$_2$Cl]PF$_6$ (**5c**), have been synthesized. All the newly synthesized complexes have been characterized by different spectroscopic techniques. The catalytic activity of these new complexes was investigated for transfer hydrogenation of

cyclohexanone and acceptorless dehydrogenation of benzyl alcohol and found in line with the previously observed trend based on the *trans* effect of ancillary ligands. Catalyst **1c**, containing CO as ancillary ligands, shows better reactivity as compared to its PPh_3 and DMSO analogues. The CNC pincer ligand platform provides a unique ligand framework with no metal-ligand cooperativity, which allows this comparison between a set of ancillary ligands.

2.4. Experimental Section

2.4.1. General Considerations

All reactions were carried out under an inert atmosphere using the standard Schlenk technique. Solvents were purchased from S. D. Fine-Chem Limited and purified by distillation under an inert atmosphere. $[RuHCl(CO)(PPh_3)_3]$ [33], $[RuCl_2(PPh_3)_3]$ [34], and $[RuCl_2(DMSO)_4]$ [35], were prepared by the following literature procedure using $RuCl_3 \cdot 3H_2O$ and it was purchased from Sigma-Aldrich. Deuterated chloroform ($CDCl_3$) and deuterated dimethyl sulphoxide (DMSO-d_6) were purchased either from EURISOtop or Sigma-Aldrich. NMR spectra were recorded on Bruker Avance (III) spectrometer and Bruker Avance NEO spectrometer operating at 400 and 500 MHz for ^1H, 162 and 202 MHz for ^{31}P, and 101 and 126 MHz for ^{13}C NMR. NMR chemical shifts are reported in ppm and referenced to the solvent peaks for ^1H ($CDCl_3$ δ 7.26 and DMSO-d_6 δ 2.50 ppm) and ^{13}C (natural abundance of ^{13}C in $CDCl_3$ δ 77.16 and DMSO-d_6 δ 39.52 ppm) NMR. ^{31}P NMR chemical shifts are referenced to an external 85% H_3PO_4 standard as 0 ppm. Multiplicities are given as s (singlet), d (doublet), t (triplet), and m (multiplet), and the coupling constants *J* are given in hertz. The mass chromatograms were recorded on Bruker-Daltonics-MicroTOF-QII mass spectrometer in HPLC grade acetonitrile. Infrared spectra (IR) were recorded with a Bruker ALPHA II instrument. Elemental analysis was carried out on a Thermo Fischer

Scientific Flash 2000 (formerly the Flash EA1112) is the CHNS-O elemental analyzer. GC Samples were analyzed in Shimadzu QP2010 Ultra, with or without an internal standard.

2.4.2. General Procedure for the synthesis of metal complexes

A. An oven-dried Schlenk tube with the magnetic stirring bar was charged with the ligand precursor **CNC^{Cy}·2HCl** (0.224 g, 0.5 mmol) in 10 mL of bench-top methanol and degassed under N_2 atmosphere at reflux temperature for 30 minutes. After that, the Schlenk tube was cooled to room temperature under N_2 atmosphere, followed by the addition of Ag_2O (0.116 g, 0.5 mmol), and stirred at room temperature in the dark, covered with aluminium foil. After 30 min, a white precipitate was formed, and different ruthenium precursors were added to the reaction mixture and heated at 65 °C for 24 h. After that, the reaction mixture was filtered through celite, and the resulting filtrate was reduced in volume (2 mL), and addition of one equivalent of aqu. solution of KPF_6 (0.92 g, 0.5 mmol) gives the precipitation of the desired complexes, which was filtered and dried under vacuum.

B. An oven-dried Schlenk tube with the magnetic stirring bar was charged with the metal complex (1 eq.), followed by the addition of K_2CO_3 (2 eq.), and $^{i}PrOH$ (5 mL). The reaction mixture was refluxed at 85 °C for 15 h. The reaction mixture was filtered after the completion of the reaction, and the solvent was evaporated under a reduced vacuum to afford the desired complexes. The solid was washed with diethyl ether and dried under vacuum.

2.4.2.1. Synthesis of Complex (1c) [Ru(CNC^{Cy})(CO)(PPh$_3$)Cl]PF$_6$

Complex (**1c**) was prepared by general procedure **A**, using [RuHCl(CO)(PPh$_3$)$_3$] (0.476 g, 0.5 mmol) as a ruthenium precursor to give the desired complex. Further, the crude solid was purified by

column chromatography using neutral alumina with eluting solvent ((hexane/CH$_2$Cl$_2$)/CH$_3$OH) ((1:1):3) which gives **2c** as yellow solid and ((hexane/CH$_2$Cl$_2$)/CH$_3$OH) ((1:1):5) affords **1c** as light-yellow solids. Complex **1c**: Yield: 0.184 g (39 %). ^{1}H NMR (500 MHz, DMSO-d$_6$) δ 8.45 (d, *J* = 2.1 Hz, 2H), 8.23 (t, *J* = 8.2 Hz, 1H), 7.81 (d, *J* = 2.2 Hz, 2H), 7.71 (d, *J* = 8.2 Hz, 2H), 7.46 – 7.43 (m, 3H), 7.35 – 7.32 (m, 6H), 6.98 – 6.94 (m, 6H), 4.25 – 4.18 (m, 2H), 2.25 (dd, *J* = 8.9, 3.6 Hz, 2H), 1.92 – 1.86 (m, 4H), 1.73 – 1.69 (m, 2H), 1.51 – 1.42 (m, 6H), 1.41 – 1.38 (m, 2H), 1.37 – 1.33 (m, 2H), 1.24 – 1.23 (m, 2H). ^{13}C NMR (126 MHz, DMSO-d$_6$) δ 207.21 (d, *J* = 14.8 Hz), 188.78 (d, *J* = 11.5 Hz), 150.31, 144.69, 132.31, 131.92, 131.51 (d, *J* = 10.1 Hz), 128.83 (d, *J* = 9.9 Hz), 121.20, 119.11, 107.58, 61.39, 34.57, 30.21, 25.31, 25.20, 24.48. ^{31}P NMR (202 MHz, DMSO-d$_6$) δ 48.23, -144.19. IR (cm^{-1}): C=O (1953.47). HRMS for [M-PF$_6$]$^+$ [C$_{42}$H$_{44}$N$_5$OPRuCl]$^+$ calculated – 802.2018, found – 802.2046. Anal. Calcd. for [C$_{42}$H$_{44}$N$_5$OPRuCl]PF$_6$: C 53.25, H 4.68, N 7.39, found: C 53.37, H 4.71, N 7.55%. Complex **2c**: Yield: 0.072 g (16 %). ^{1}H NMR (500 MHz, DMSO-d$_6$) δ 8.44 (d, *J* = 1.9 Hz, 2H), 8.08 (t, *J* = 8.1 Hz, 1H), 7.73 (d, *J* = 2.1 Hz, 2H), 7.70 (d, *J* = 8.1 Hz, 2H), 7.35 – 7.32 (m, 4H), 7.23 – 7.20 (m, 6H), 6.87 – 6.83 (m, 5H), 4.32 – 4.26 (m, 2H), 1.86 – 1.80 (m, 4H), 1.63 (dd, *J* = 22.5, 11.0 Hz, 5H), 1.58 – 1.51 (m, 2H), 1.45 (dd, *J* = 15.1, 5.8 Hz, 3H), 1.19 (dd, *J* = 9.1, 4.3 Hz, 4H), 0.83 – 0.76 (m, 2H), -9.13 (d, *J* = 23.1 Hz, 1H). ^{13}C NMR (126 MHz, DMSO-d$_6$) δ 198.63 (d, *J* = 81.9 Hz), 190.62 (d, *J* = 13.8 Hz), 149.59, 140.51, 132.69, 132.38, 131.74 (d, *J* = 11.1 Hz), 129.73, 128.37 (d, *J* = 9.0 Hz), 120.54, 118.65, 106.19, 60.76, 33.51, 30.63, 25.12, 25.00, 24.51. ^{31}P NMR (202 MHz, DMSO-d$_6$) δ 41.98, -144.19. IR (cm^{-1}): C=O (1950.39). HRMS for [M-PF$_6$]$^+$ [C$_{42}$H$_{44}$N$_5$OPRuH]$^+$ calculated – 768.2411, found – 768.2425. Anal. Calcd. for [C$_{42}$H$_{44}$N$_5$OPRuH]PF$_6$: C 55.26, H 4.97, N 7.67, found: C 55.41, H 4.84, N 7.69%.

2.4.2.2. Synthesis of complex (3c) [Ru(CNC^{Cy})(PPh$_3$)$_2$Cl]PF$_6$

Complex (**3c**) was prepared by the general procedure **A**, using [RuCl$_2$(PPh$_3$)$_3$] (0.479 g, 0.5 mmol) as a ruthenium precursor to give the desired complex. Further, the crude solid was purified by column chromatography using neutral alumina with eluting solvent ((hexane/CH$_2$Cl$_2$)/CH$_3$OH) ((1:1):4) gives **4c** as yellow solid and ((hexane/CH$_2$Cl$_2$)/CH$_3$OH) ((1:1):6) affords **3c** as light-yellow solid. Complex **3c**: Yield: 0.180 g (30%). ^{1}H NMR (500 MHz, CDCl$_3$) δ 7.81 (d, J = 2.7 Hz, 2H), 7.68 (m, 1H), 7.66 (d, J = 1.9 Hz, 2H), 7.66 (m, 1H), 7.64 (d, J = 1.9 Hz, 1H), 7.55 (d, J = 1.9 Hz, 2H), 7.53 (d, J = 2.3 Hz, 2H), 7.48 (d, J = 3.1 Hz, 2H), 7.46 (d, J = 3.1 Hz, 3H), 7.20 – 7.18 (m, 6H), 7.05 (t, J = 7.6 Hz, 8H), 6.94 – 6.91 (m, 7H), 5.04 – 4.97 (m, 2H), 1.62 – 1.59 (m, 3H), 1.52 – 1.48 (m, 3H), 1.33 – 1.25 (m, 8H), 0.93 (d, J = 3.8 Hz, 1H), 0.91 (d, J = 3.8 Hz, 1H), 0.89 – 0.82 (m, 4H). ^{13}C NMR (126 MHz, CDCl$_3$) δ 189.61, 152.96, 134.55, 133.97, 133.33 (d, J = 4.9 Hz), 132.22 (d, J = 9.9 Hz), 132.09 (d, J = 2.8 Hz), 129.56, 128.64 (d, J = 12.2 Hz), 128.05 (t, J = 4.5 Hz), 127.82, 121.20, 117.99, 105.45, 58.56, 33.27, 25.84, 25.32. ^{31}P NMR (202 MHz, CDCl$_3$) δ 29.35, 19.06, -144.20. HRMS for [M-PF$_6$]$^+$ [C$_{59}$H$_{59}$ClN$_5$P$_2$Ru]$^+$ calculated – 1036.2985, found – 1036.3010. Anal. Calcd. for [C$_{59}$H$_{59}$ClN$_5$P$_2$Ru]PF$_6$: C 59.97, H 5.03, N 5.93, found: C 60.19, H 4.87, N 5.89%. Complex **4c**: Yield: 0.115 g (20%). ^{1}H NMR (500 MHz, DMSO-d$_6$) δ 8.29 (d, J = 2.3 Hz, 2H), 7.78 (t, J = 8.0 Hz, 1H), 7.64 (d, J = 1.7 Hz, 2H), 7.63 (d, J = 1.9 Hz, 2H), 7.62 – 7.61 (m, 2H), 7.60 (d, J = 2.3 Hz, 2H), 7.55 (d, J = 3.1 Hz, 2H), 7.54 – 7.53 (m, 2H), 7.26 (t, J = 7.3 Hz, 5H), 7.14 (t, J = 7.7 Hz, 8H), 6.78 – 6.74 (m, 9H), 3.88 – 3.81 (m, 2H), 1.38 – 1.35 (m, 3H), 1.23 – 1.20 (m, 5H), 0.88 – 0.81 (m, 5H), 0.77 – 0.69 (m, 4H), 0.23 – 0.21 (d, J = 8.6 Hz, 3H), -8.56 (t, J = 25.0 Hz, 1H). ^{13}C NMR (126 MHz, DMSO-d$_6$) δ 196.94 (t, J = 13.6 Hz), 149.84, 135.74 (t, J = 18.8 Hz), 133.12, 132.31, 132.03 (d, J = 2.8 Hz), 131.84 (t, J = 5.5 Hz), 131.48 (d, J = 10.1 Hz), 128.99, 128.74 (d, J = 12.0 Hz), 127.92, 120.46, 117.78, 104.50, 59.65, 31.15,

25.23, 24.39. ^{31}P NMR (202 MHz, DMSO-d$_6$) δ 49.59, -144.19. HRMS for [M-PF$_6$]$^+$ [C$_{59}$H$_{59}$N$_5$P$_2$RuH]$^+$ calculated – 1002.3378, found – 1002.3385. Anal. Calcd. for [C$_{59}$H$_{59}$N$_5$P$_2$RuH]PF$_6$: C 61.77, H 5.27, N 6.11, found: C 62.05, H 5.43, N 6.39%.

2.4.2.3. Synthesis of complex (4c) [Ru(CNC^{Cy})(PPh$_3$)$_2$H]X from (3c) [Ru(CNC^{Cy})(PPh$_3$)$_2$Cl]PF$_6$

Complex (4c) was prepared by general procedure **B**, by using complex [Ru(CNC^{Cy})(PPh$_3$)$_2$Cl]X (X = Cl, 0.181 g, 0.169 mmol or X = PF$_6$, 0.200 g, 0.169 mmol) and K$_2$CO$_3$ (0.047 g, 0.338 mmol) to give the desired complex. Yield: X = Cl, 0.132 g (75 %) and X = PF$_6$, 0.141 g (73 %).

2.4.2.4. Synthesis of complex (5c) [Ru(CNC^{Cy})(DMSO)$_2$Cl]PF$_6$

Complex (5c) was prepared by the general procedure **A**, using [RuCl$_2$(DMSO)$_4$] (0.242 g, 0.5 mmol) as a ruthenium precursor to give the desired complex. The pure complex was obtained by precipitation in acetonitrile and diethyl ether. Yield: 0.113 g (28 %). ^{1}H NMR (500 MHz, DMSO-d$_6$) δ 8.60 (d, J = 2.1 Hz, 2H), 8.25 (t, J = 8.2 Hz, 1H), 8.01 (d, J = 2.2 Hz, 2H), 7.96 (d, J = 8.2 Hz, 2H), 5.28 – 5.22 (m, 2H), 2.67 (s, 12H), 2.05 – 2.02 (m, 4H), 1.91 – 1.83 (m, 8H), 1.73 (d, J = 11.9 Hz, 2H), 1.40 – 1.34 (m, 4H), 1.28 (dd, J = 12.8, 3.5 Hz, 2H). ^{13}C NMR (126 MHz, DMSO-d$_6$) δ 183.94, 154.35, 141.03, 121.39, 119.34, 107.05, 58.29, 45.15, 32.63, 25.28, 24.70. ^{31}P NMR (202 MHz, DMSO-d$_6$) δ -144.20. HRMS for [M-PF$_6$]$^+$ [C$_{27}$H$_{41}$N$_5$RuO$_2$S$_2$Cl]$^+$ calculated – 668.1431, found – 668.1456. Anal. Calcd. for [C$_{27}$H$_{41}$N$_5$RuO$_2$S$_2$Cl]PF$_6$: C 39.88, H 5.08, N 8.61, found: C 39.99, H 4.95, N 8.87%.

2.4.3. General procedure for catalytic transfer hydrogen reaction

Cyclohexanone (0.207 mL, 2 mmol) and catalyst (1 mol%) were dissolved in ^{i}PrOH (5 mL), under an inert atmosphere in a Schlenk tube, followed by the addition of Na (23 mg, 1 eq., 2 mmol) to

generate NaO^{i}Pr, in situ. When the sodium metal was dissolved, the reaction mixture was quickly heated to reflux by lowering it into a preheated oil bath for 30 minutes. The yield of the corresponding product was determined by the relative peak area of the substrate and the product in GC with *n*-decane (0.195 mL, 1 mmol) as an internal standard (Table **2.1**). The product was purified by silica gel column chromatography using hexane and ethyl acetate as eluents. NMR data for the cyclohexanol product matched with the reported values. Cyclohexanol: ^{1}H NMR (500 MHz, DMSO-d$_6$) δ 4.43 (d, *J* = 4.3 Hz, 1H), 3.38 – 3.34 (m, 1H), 1.74 – 1.69 (m, 2H), 1.66 – 1.61 (m, 2H), 1.48 – 1.43 (m, 1H), 1.25 – 1.05 (m, 5H). ^{13}C NMR (126 MHz, DMSO-d$_6$) δ 68.29, 35.39, 25.41, 23.85.

2.4.4. General procedure for catalytic acceptorless dehydrogenation reaction

Typically, catalyst (3 mol%) was added to the solution of benzyl alcohol (0.104 mL, 1 mmol), KO^{t}Bu (0.112 g, 1 eq., 1 mmol) in toluene under an inert atmosphere in a Schlenk tube and heated at 110 °C for 3h by lowering it into a preheated oil bath. The conversion of the corresponding product was determined by the relative peak area of the substrate and the product in GC without an internal standard (Table **2.2**). After completion of the reaction, the product was extracted with chloroform and dried in a vacuum. The product was purified by silica gel column chromatography using hexane and ethyl acetate as eluents. NMR data for the benzaldehyde product matched with the reported values. Benzaldehyde: ^{1}H NMR (500 MHz, CDCl$_3$) δ 10.01 (s, 1H), 7.87 (d, *J* = 8.1 Hz, 2H), 7.62 (t, *J* = 7.4 Hz, 1H), 7.52 (t, *J* = 7.6 Hz, 2H). ^{13}C NMR (126 MHz, CDCl$_3$) δ 192.51, 136.47, 134.55, 129.82, 129.08.

2.4.5. Characterisation data of ligand and metal complexes
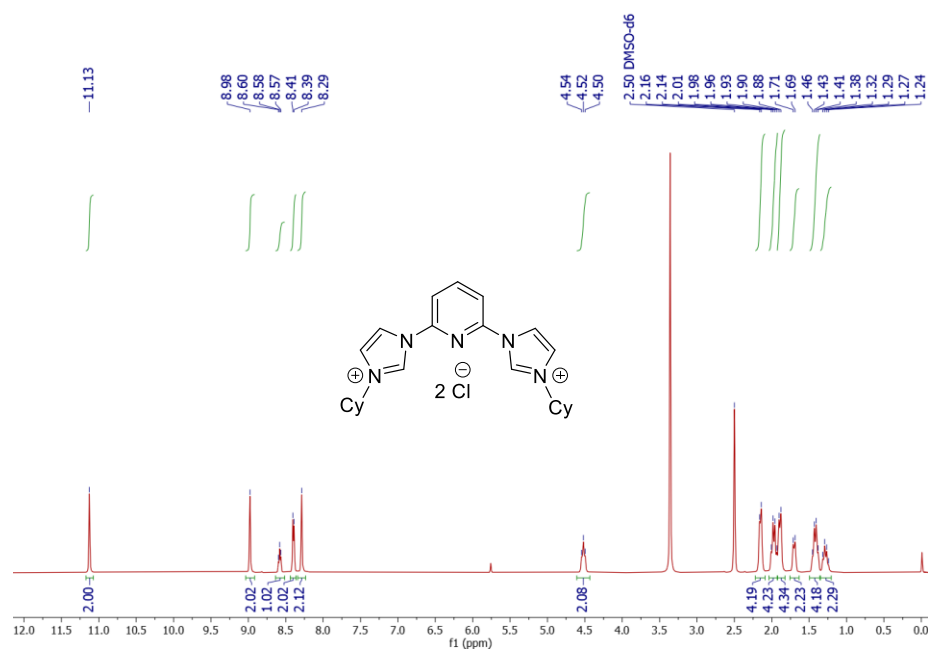
Figure 2.4. ^{1}H NMR spectrum of **CNC^{Cy}·2HCl**.
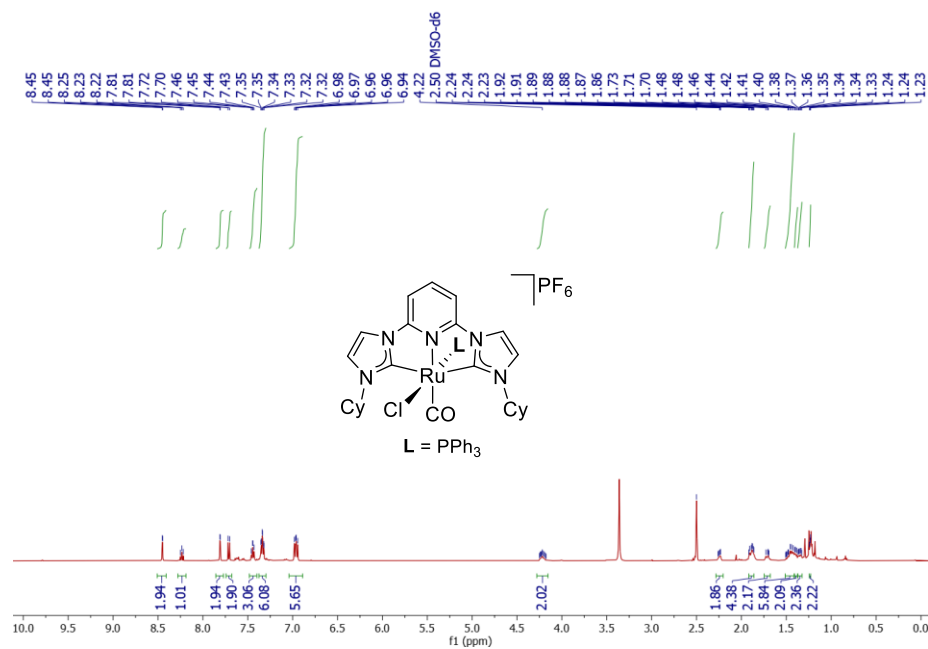
Figure 2.5. ^{1}H NMR spectrum of complex **1c**.
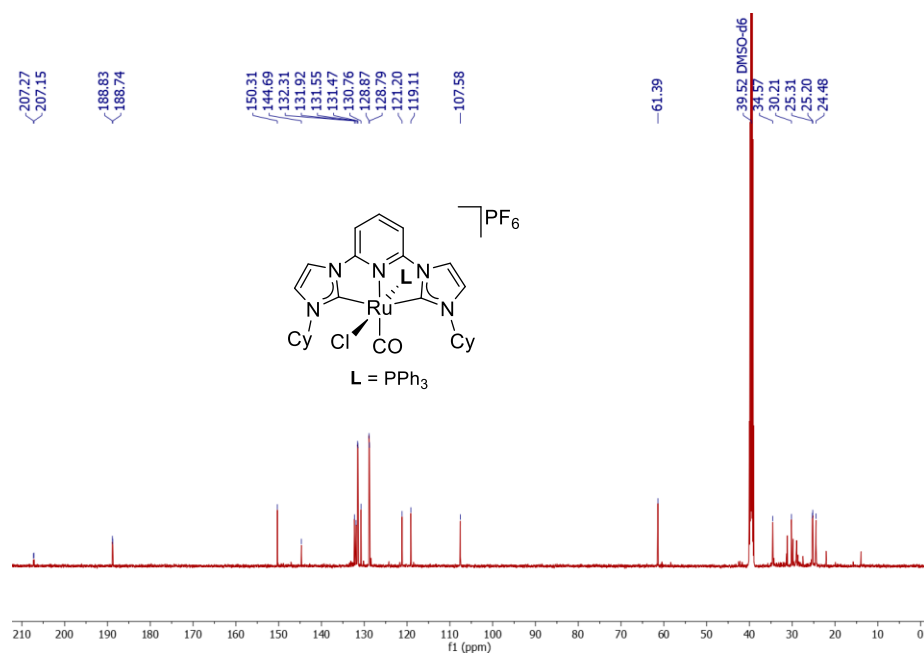
Figure 2.6. ^{13}C NMR spectrum of complex **1c**.
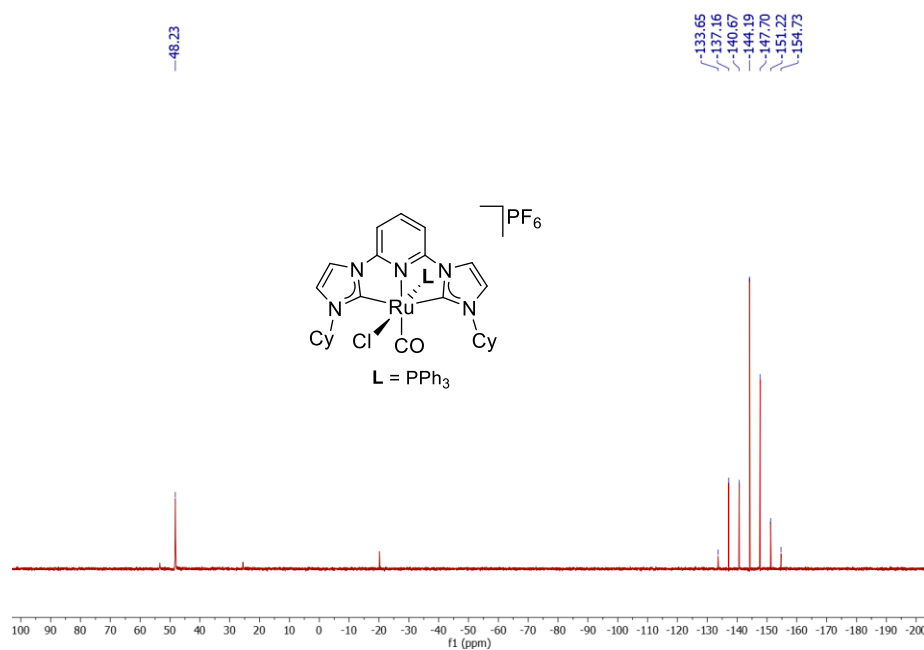
Figure 2.7. ^{31}P NMR spectrum of complex **1c**.
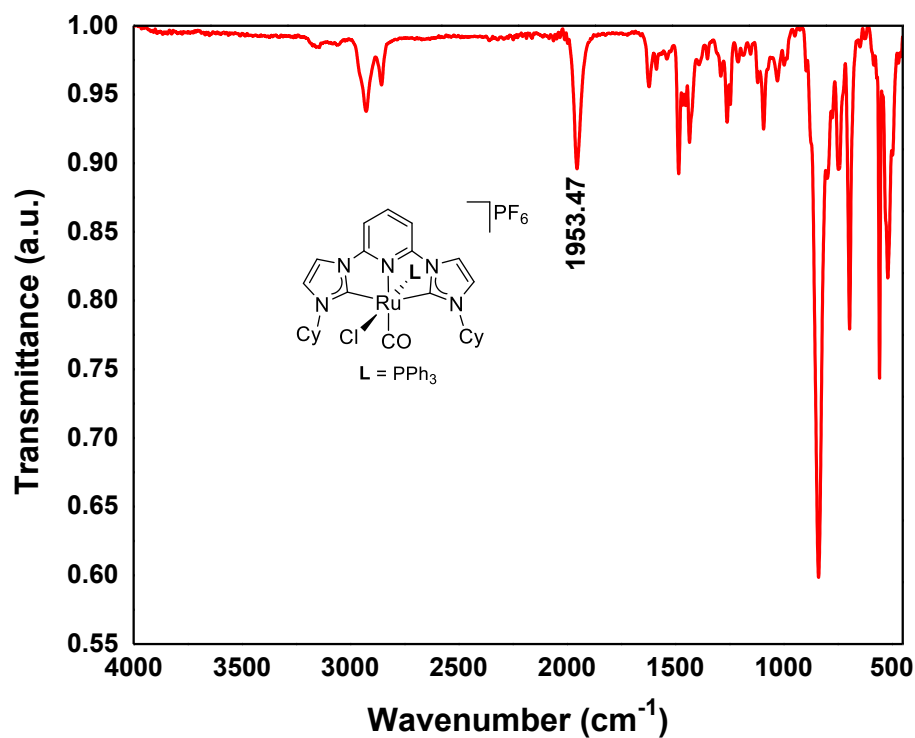
Figure 2.8. IR spectrum of complex **1c**.
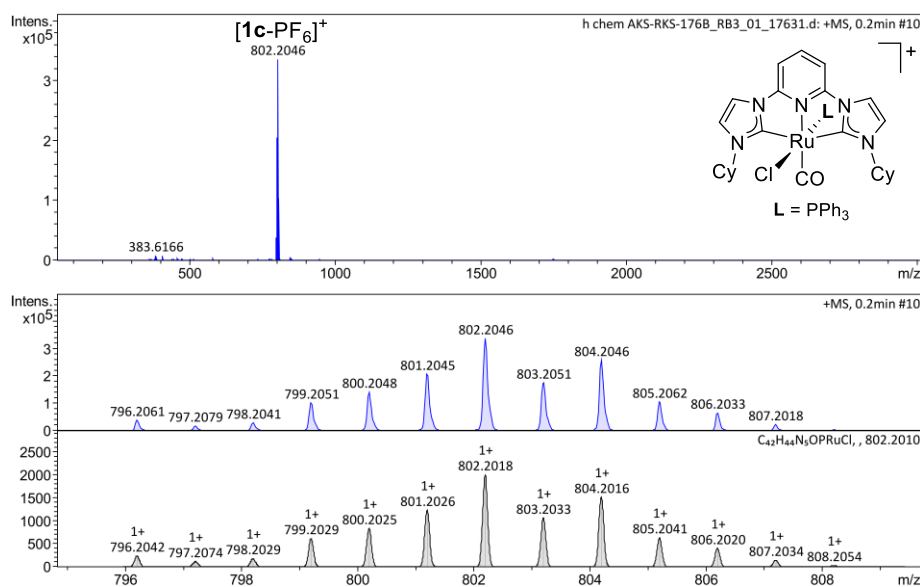
Figure 2.9. HRMS spectrum of complex **1c**.
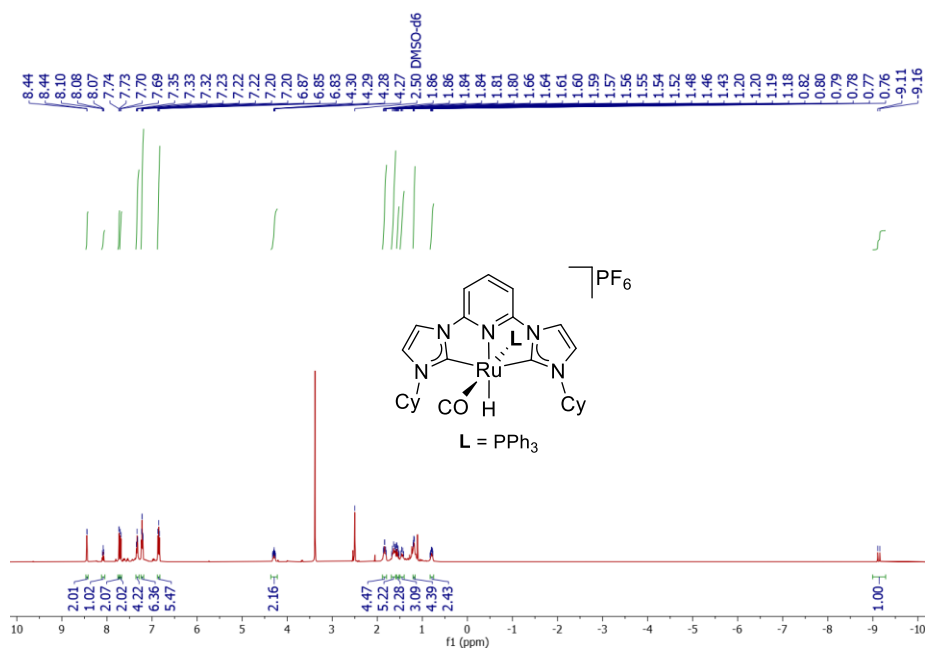
Figure 2.10. ^{1}H NMR spectrum of complex **2c**.
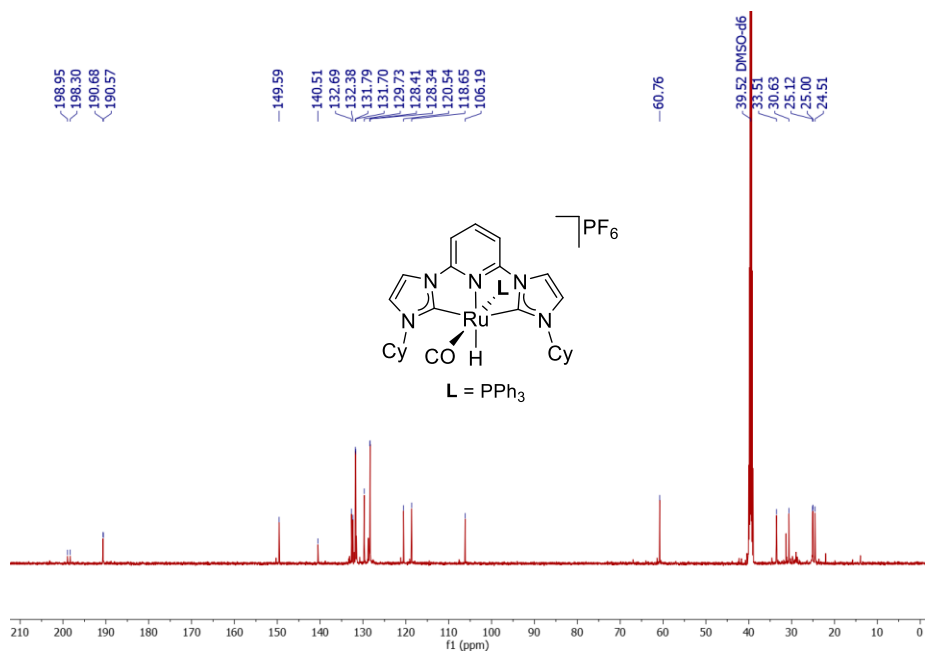
Figure 2.11. ^{13}C NMR spectrum of complex **2c**.
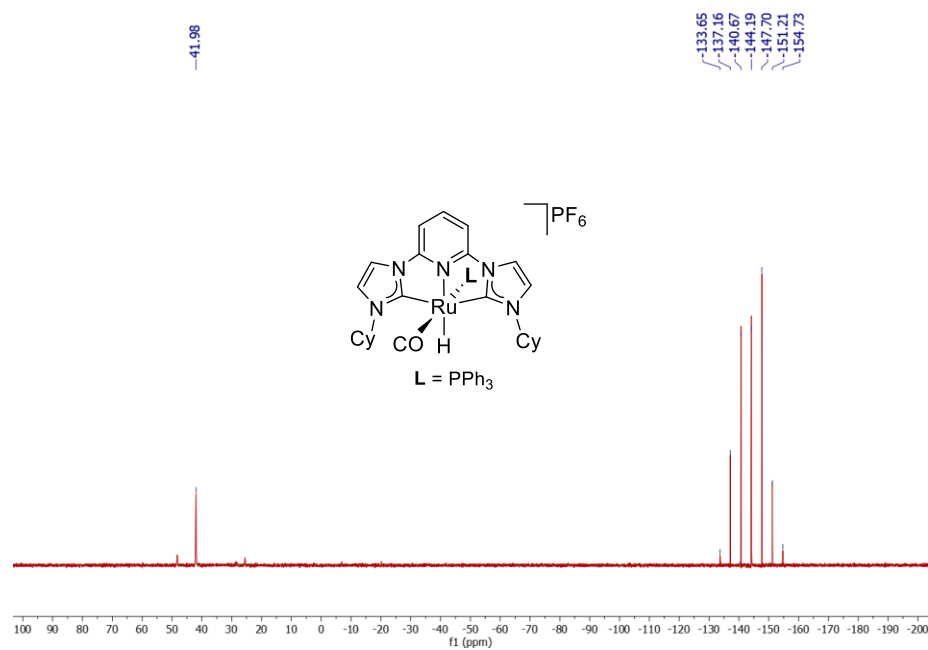
Figure 2.12. ^{31}P NMR spectrum of complex **2c**.
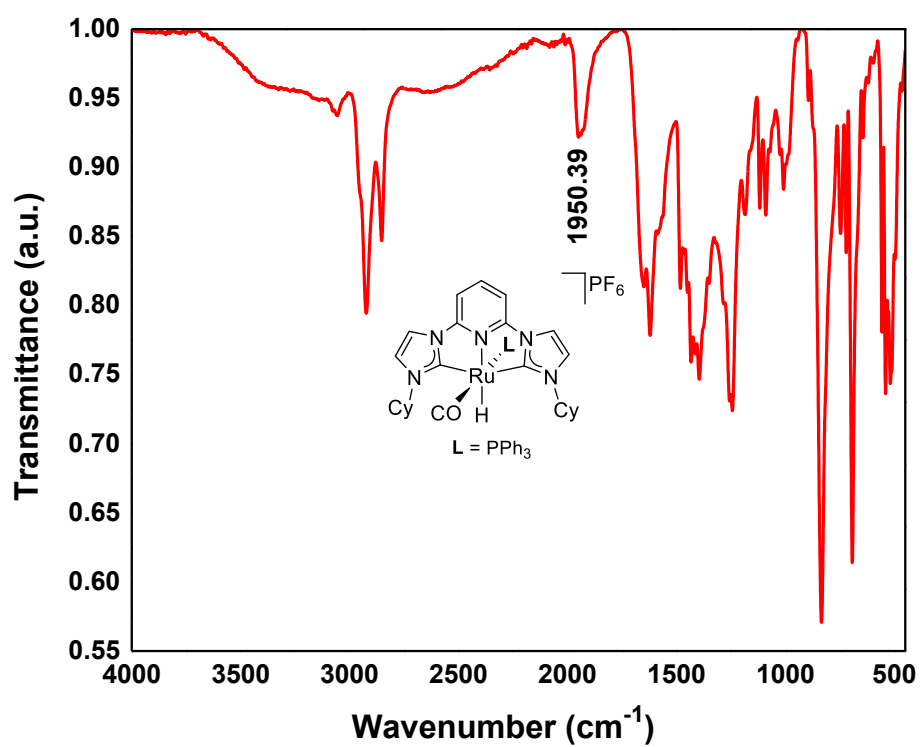
Figure 2.13. IR spectra of complex **2c**.
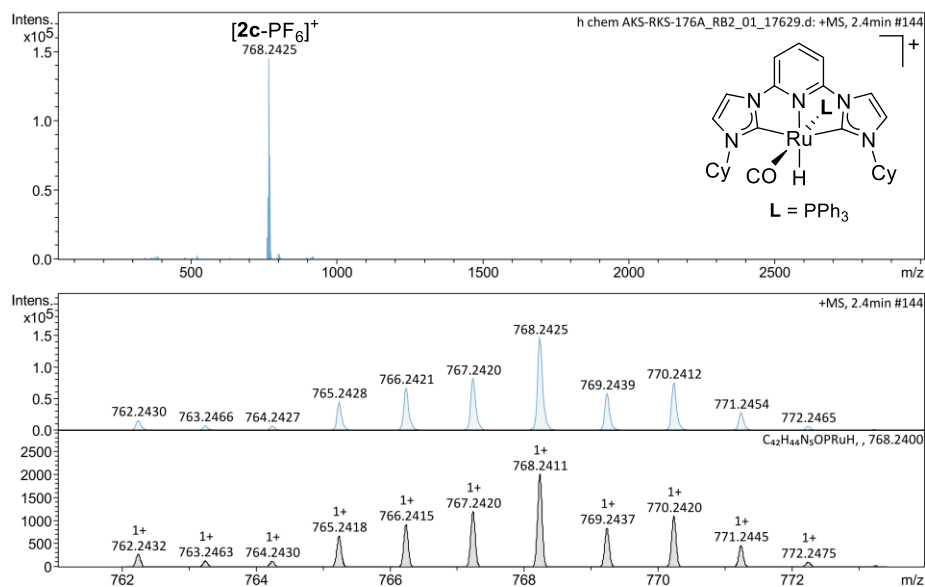
Figure 2.14. HRMS spectrum of complex **2c**.
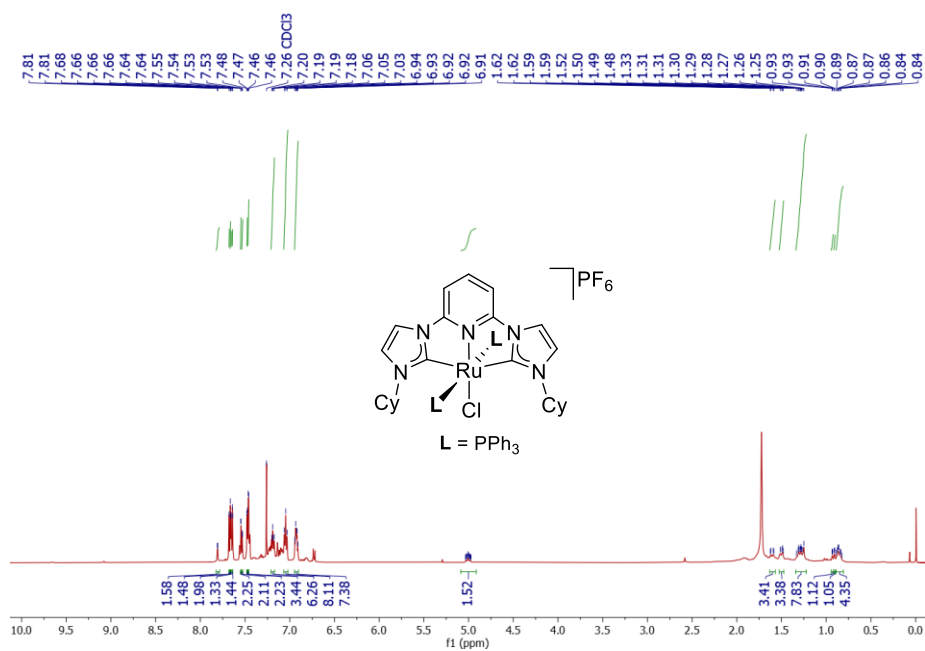
Figure 2.15. ^{1}H NMR spectrum of complex **3c**.
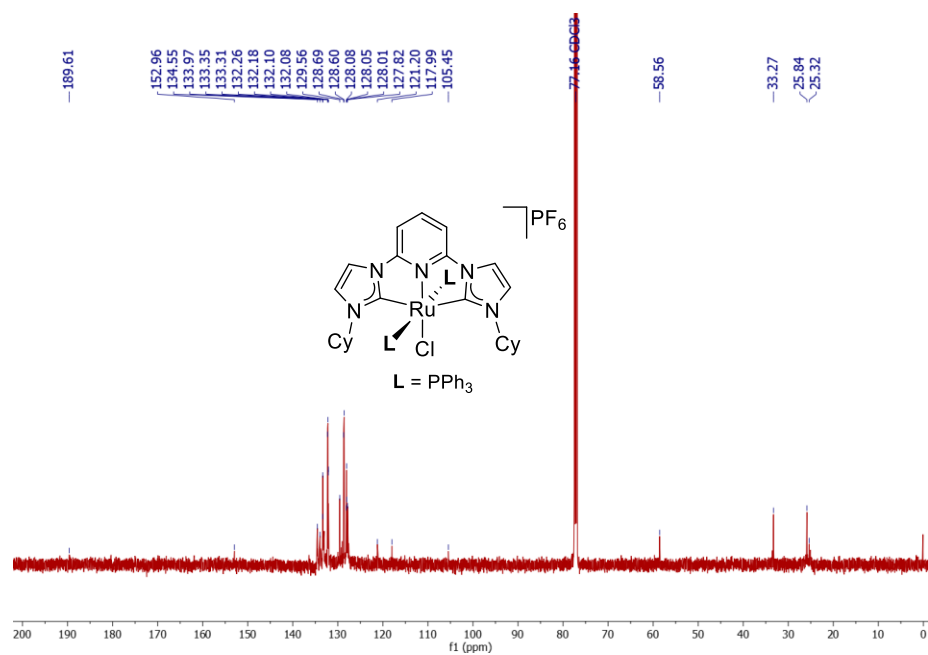
Figure 2.16. ^{13}C NMR spectrum of complex **3c**.
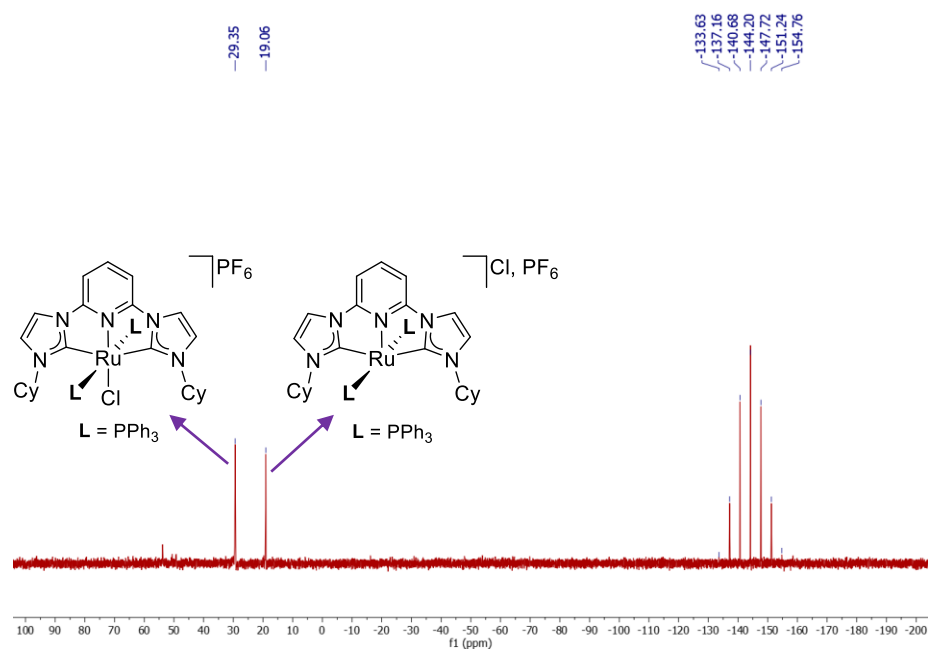
Figure 2.17. ^{31}P NMR spectrum of complex **3c**.

81
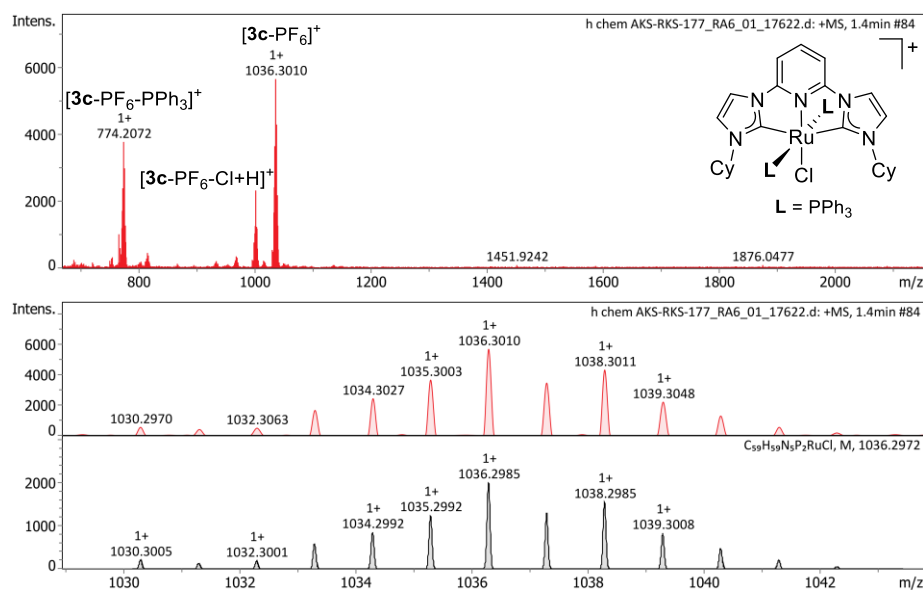
Figure 2.18. HRMS spectrogram of complex **3c**.
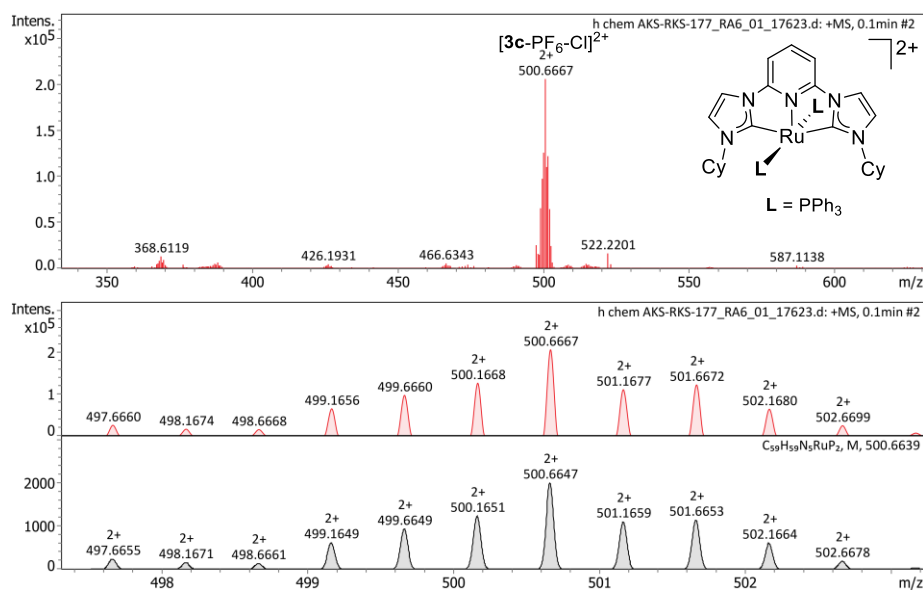
Figure 2.19. HRMS spectrogram of dicationic complex [**3c**-PF$_6$-Cl]$^{2+}$.
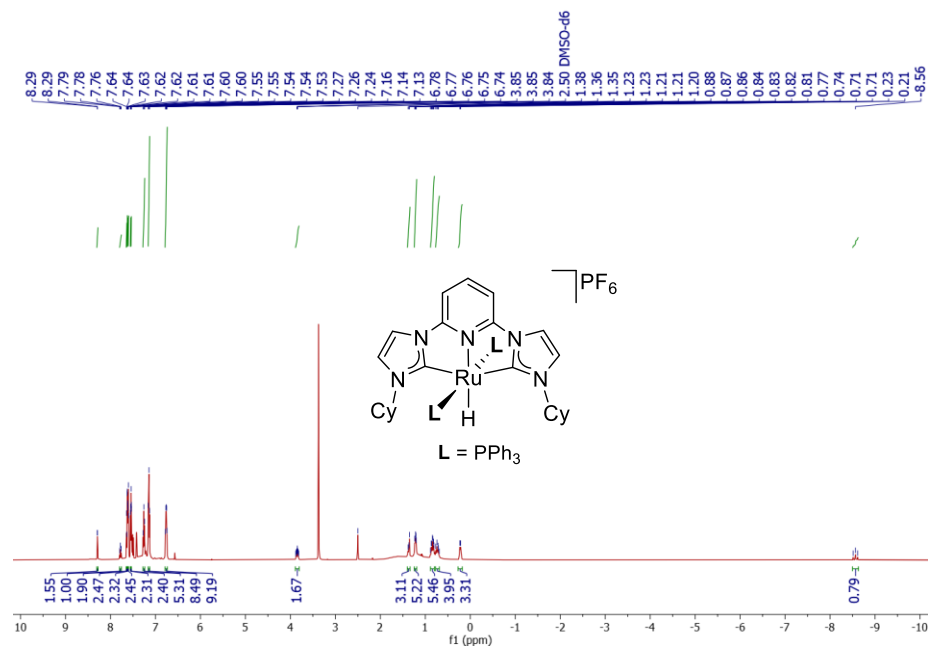
Figure 2.20. ^{1}H NMR spectrum of complex **4c**.
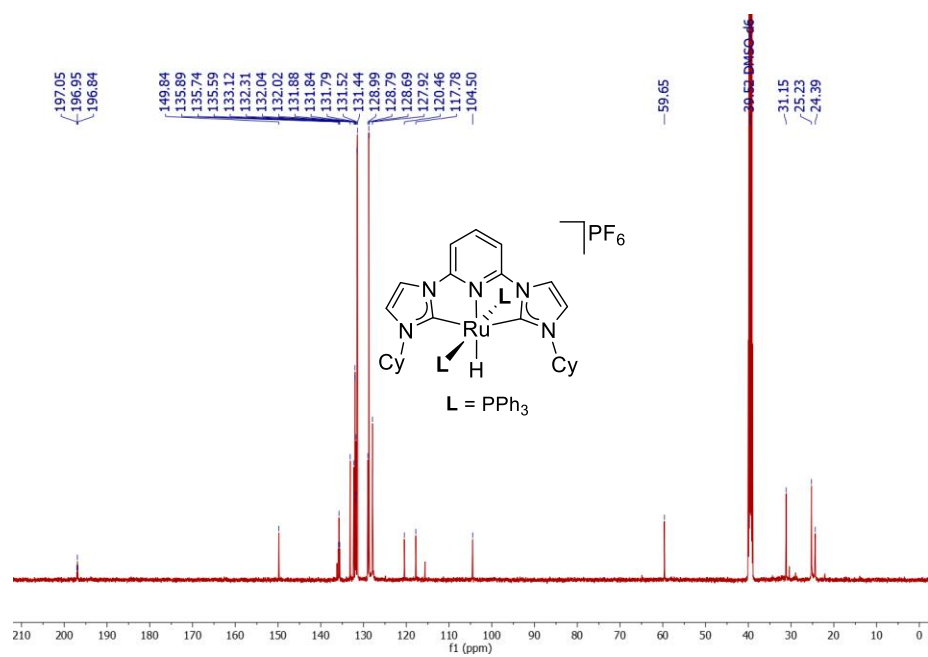
Figure 2.21. ^{13}C NMR spectrum of complex **4c**.
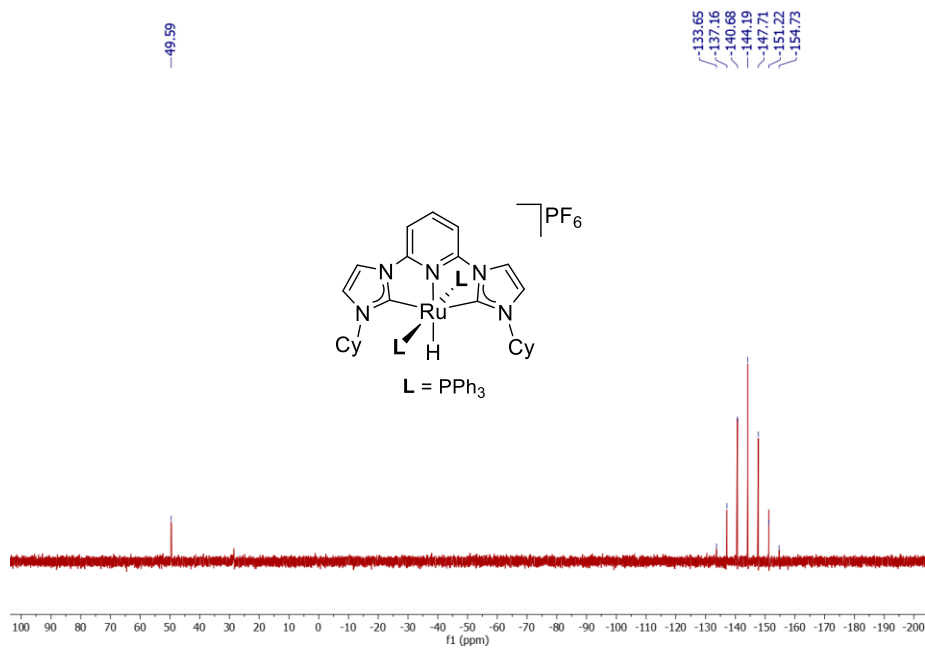
Figure 2.22. ^{31}P NMR spectrum of complex **4c**.
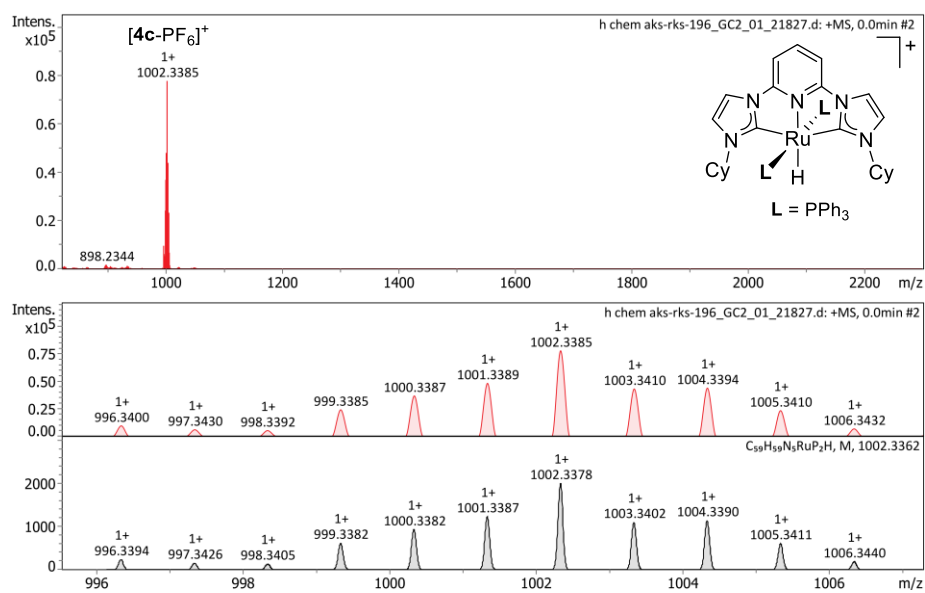
Figure 2.23. HRMS spectrogram of complex **4c**.

84
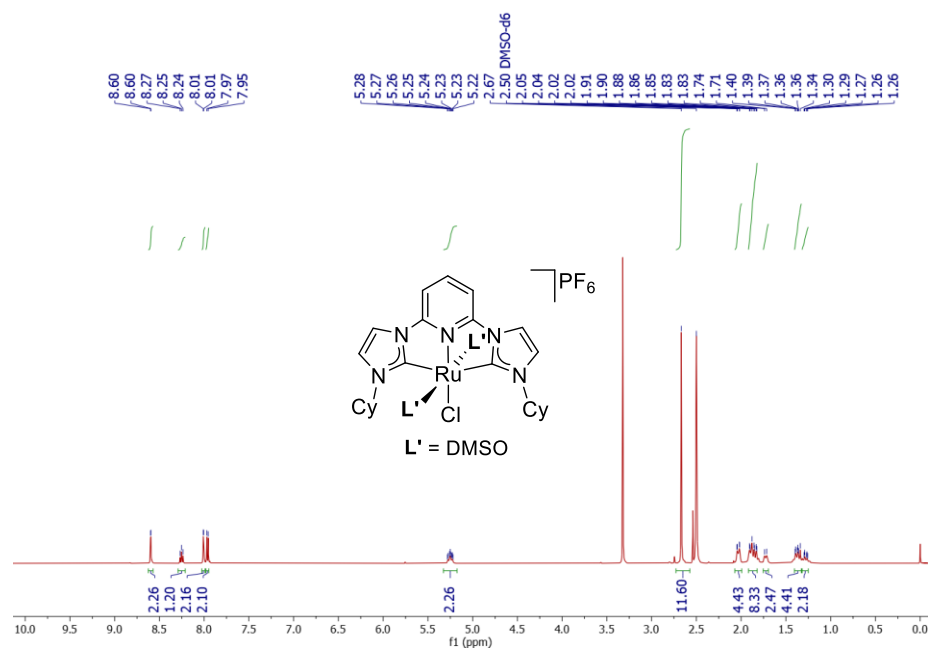
Figure 2.24. ^{1}H NMR spectrum of complex **5c**.
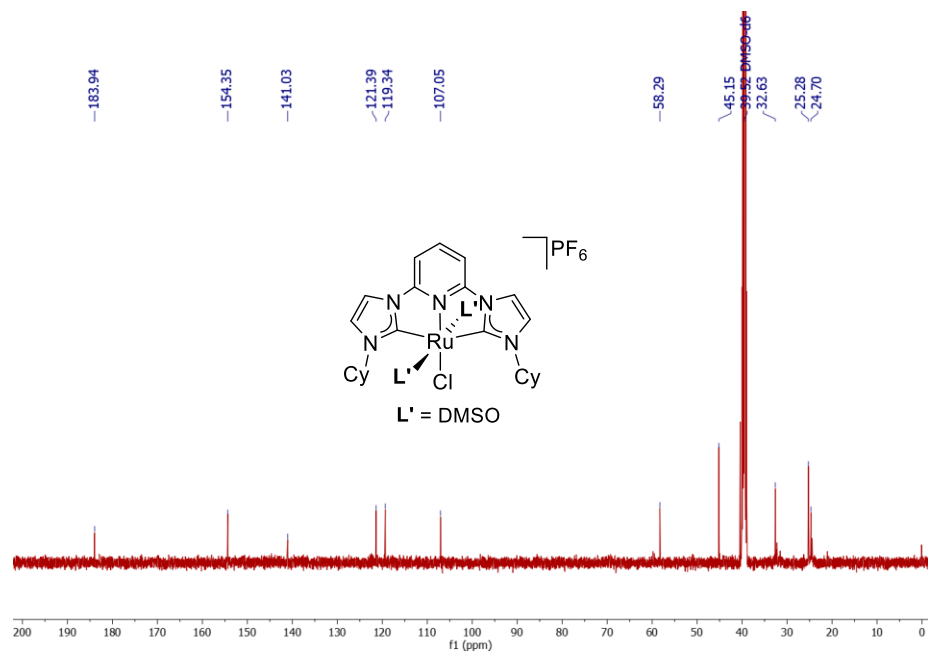
Figure 2.25. ^{13}C NMR spectrum of complex **5c**.

85
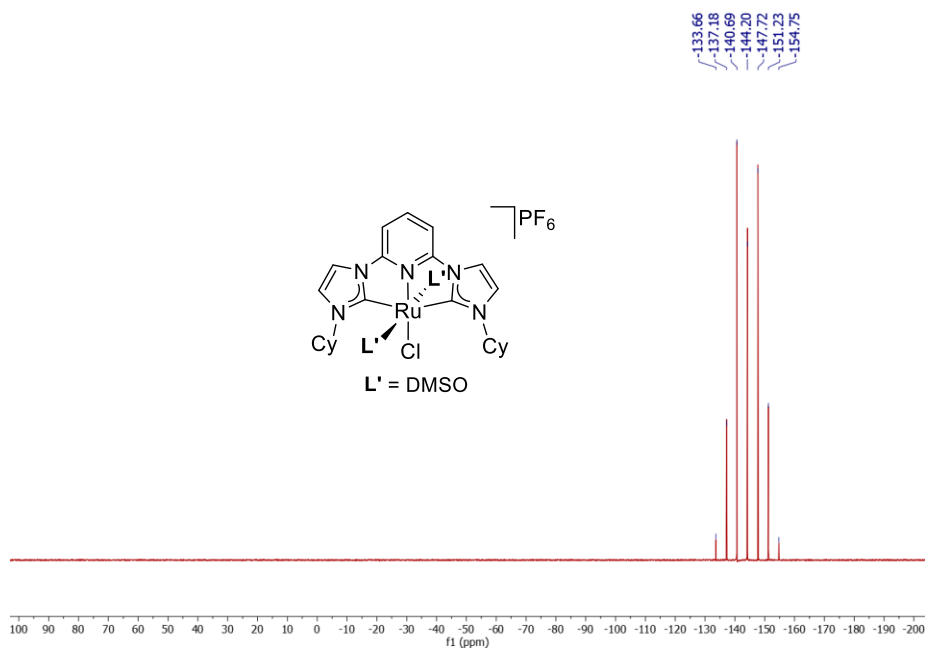
Figure 2.26. ^{31}P NMR spectrum of complex **5c**.
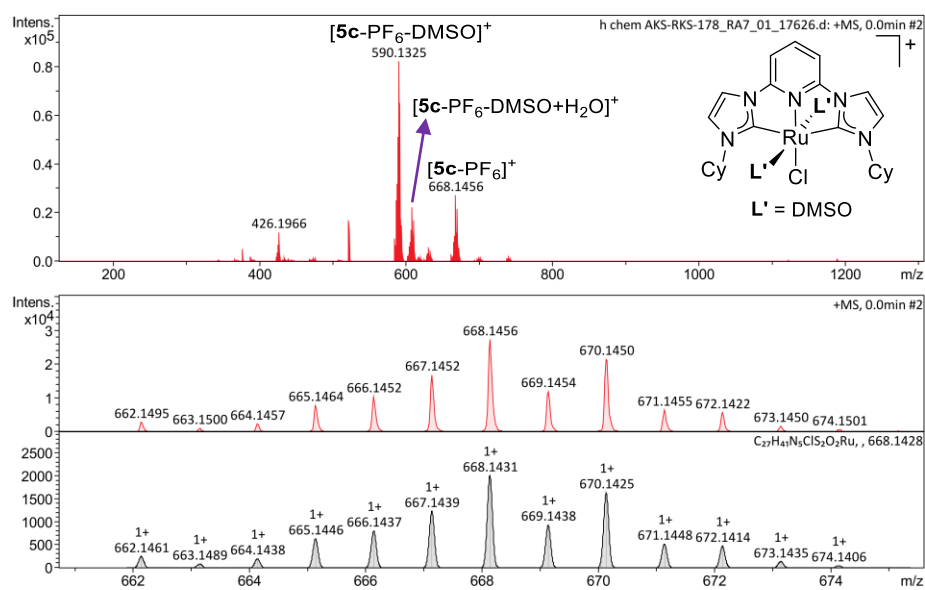
Figure 2.27. HRMS spectrum of complex **5c**.

2.5. References

1. Lawrence M. A. W., Green K.-A., Nelson P. N., Lorraine S. C. (2018), Review: Pincer Ligands-Tunable, versatile and applicable, Polyhedron, 143, 11-27 (DOI: 10.1016/j.poly.2017.08.017).

2. Gunanathan C., Milstein D. (2014), Bond Activation and Catalysis by Ruthenium Pincer Complexes, Chem. Rev., 114(24), 12024-12087 (DOI: 10.1021/cr5002782).

3. Andrew R. E., González-Sebastián L., Chaplin A. B. (2016), NHC-based pincer ligands: carbenes with a bite, Dalton Trans., 45(4), 1299-1305 (DOI: 10.1039/C5DT04429D).

4. Peris E., Crabtree R. H. (2018), Key factors in pincer ligand design, Chem. Soc. Rev., 47(6), 1959-1968 (DOI: 10.1039/C7CS00693D).

5. Boudreaux C. M., Liyanage N. P., Shirley H., Siek S., Gerlach D. L., Qu F., Delcamp J. H., Papish E. T (2017), Ruthenium(II) complexes of pyridinol and *N*-heterocyclic carbene derived pincers as robust catalysts for selective carbon dioxide reduction, Chem. Commun., 53(81), 11217-11220 (DOI: 10.1039/C7CC05706G).

6. Tseng H.-W., Zong R., Muckerman J. T., Thummel R. (2008), Mononuclear Ruthenium(II) Complexes That Catalyze Water Oxidation, Inorg. Chem., 47(24), 11763-11773 (DOI: 10.1021/ic8014817).

7. Zhao Q., Meng G., Nolan S. P., Szostak M. (2020), *N*-Heterocyclic Carbene Complexes in C–H Activation Reactions, Chem. Rev., 120(4), 1981-2048 (DOI: 10.1021/acs.chemrev.9b00634).

8. Piccirilli L., Lobo Justo Pinheiro D., Nielsen M. (2020), Recent Progress with Pincer Transition Metal Catalysts for Sustainability, Catalysts, 10(7), 773 (DOI: 10.3390/catal10070773).

9. Díez-González S., Marion N., Nolan S. P. (2009), N-Heterocyclic Carbenes in Late Transition Metal Catalysis, Chem. Rev., 109(8), 3612-3676 (DOI: 10.1021/cr900074m).

10. Nesterov V., Reiter D., Bag P., Frisch P., Holzner R., Porzelt A., Inoue S. (2018), NHCs in Main Group Chemistry, Chem. Rev., 118(19), 9678–9842 (DOI: 10.1021/acs.chemrev.8b00079).

11. Dragutan V., Dragutan I., Delaude L., Demonceau A. (2007), NHC-Ru complexes-Friendly catalytic tools for manifold chemical transformations, Coord. Chem. Rev., 251(5), 765-794 (DOI: 10.1016/j.ccr.2006.09.002).

12. Hopkinson M. N., Richter C., Schedler M., Glorius F. (2014), An overview of *N*-heterocyclic carbenes, Nature, 510(7506), 485-496 (DOI: 10.1038/nature13384).

13. Charra V., de Frémont P., Braunstein P. (2017), Multidentate *N*-heterocyclic carbene complexes of the 3d metals: Synthesis, structure, reactivity and catalysis, Coord. Chem. Rev., 341, 53-176 (DOI: 10.1016/j.ccr.2017.03.007).

14. Poyatos M., Mata J. A., Falomir E., Crabtree R. H., Peris E. (2003), New Ruthenium(II) CNC-Pincer Bis(carbene) Complexes: Synthesis and Catalytic Activity, Organometallics, 22(5), 1110-1114 (DOI: 10.1021/om020817w).

15. Danopoulos A. A., Winston S., Motherwell W. B. (2002), Stable *N*-functionalised 'pincer' bis carbene ligands and their ruthenium complexes; synthesis and catalytic studies, Chem. Commun., (13), 1376-1377 (DOI: 10.1039/B202814J).

16. Danopoulos A. A., Braunstein P., Saßmannshausen J., Pugh D., Wright J. A. (2020), "Pincer" Pyridine-Dicarbene-Iridium and Ruthenium Complexes and Derivatives Thereof, Eur. J. Inorg. Chem., 2020(35), 3359-3369 (DOI: 10.1002/ejic.202000429).

17. Wang D., Astruc D. (2015), The Golden Age of Transfer Hydrogenation, Chem. Rev., 115(13), 6621-6686 (DOI: 10.1021/acs.chemrev.5b00203).

18. Brieger G., Nestrick T. J. (1974), Catalytic transfer hydrogenation, Chem. Rev., 74(5), 567-580 (DOI: 10.1021/cr60291a003).

19. Enthaler S., Jackstell R., Hagemann B., Junge K., Erre G., Beller M. (2006), Efficient transfer hydrogenation of ketones in the presence of ruthenium *N*-heterocyclic carbene catalysts, J. Organomet. Chem., 691(22), 4652-4659 (DOI: 10.1016/j.jorganchem.2006.07.013).

20. Dobereiner G. E., Crabtree R. H. (2010), Dehydrogenation as a Substrate-Activating Strategy in Homogeneous Transition-Metal Catalysis, Chem. Rev., 110(2), 681-703 (DOI: 10.1021/cr900202j).

21. Choi J., MacArthur A. H. R., Brookhart M., Goldman A. S. (2011), Dehydrogenation and Related Reactions Catalyzed by Iridium Pincer Complexes, Chem. Rev., 111(3), 1761-1779 (DOI: 10.1021/cr1003503).

22. Wang Z., Pan B., Liu Q., Yue E., Solan G. A., Ma Y., Sun W.-H. (2017), Efficient acceptorless dehydrogenation of secondary alcohols to ketones mediated by a PNN-Ru(II) catalyst, Catal. Sci. Technol., 7(8), 1654-1661 (DOI: 10.1039/C7CY00342K).

23. Chang W., Gong X., Wang S., Xiao L.-P., Song G. (2017), Acceptorless dehydrogenation and dehydrogenative coupling of alcohols catalysed by protic NHC ruthenium complexes, Org. Biomol. Chem., 15(16), 3466–3471 (DOI: 10.1039/C7OB00542C).

24. Zhang J., Gandelman M., Shimon L. J. W., Rozenberg H., Milstein D. (2004), Electron-Rich, Bulky Ruthenium PNP-Type Complexes, Acceptorless Catalytic Alcohol Dehydrogenation, Organometallics, 23(17), 4026-4033 (DOI: 10.1021/om049716j).

25. Yadav D., Misra S., Kumar D., Singh S., Singh A. K. (2021), Cationic ruthenium(II)-NHC pincer complexes: Synthesis, characterisation and catalytic activity for transfer hydrogenation

of ketones, Appl. Organomet. Chem., 35(8), e6287 (DOI: 10.1002/aoc.6287).

26. Yadav D., Singh R. K., Singh S., Shirage P. M., Singh A. K. (2021), Cationic ruthenium(II)-NHC pincer complexes with hemilabile COD: Solid-state structural characterization and theoretical study of an η^2-(E,Z)-COD ligand, J. Organomet. Chem., 953, 122061 (DOI: 10.1016/j.jorganchem.2021.122061).

27. Yadav D., Singh R. K., Misra S., Singh A. K. (2022), Ancillary ligand effects and microwave-assisted enhancement on the catalytic performance of cationic ruthenium(II)-CNC pincer complexes for acceptorless alcohol dehydrogenation, Appl. Organomet. Chem., e6756 (DOI: 10.1002/aoc.6756).

28. Bauri S., Donthireddy S. N. R., Illam P. M., Rit A. (2018), Effect of Ancillary Ligand in Cyclometalated Ru(II)-NHC-Catalyzed Transfer Hydrogenation of Unsaturated Compounds, Inorg. Chem., 57(23), 14582-14593 (DOI: 10.1021/acs.inorgchem.8b02246).

29. Andrade G. A., DiMeglio J. L., Guardino E. T., Yap G. P. A., Rosenthal J. (2017), Synthesis and structure of palladium(II) complexes supported by bis-NHC pincer ligands for the electrochemical activation of CO_2, Polyhedron, 135, 134-143 (DOI: 10.1016/j.poly.2017.06.018).

30. Li X.-W., Chen F., Xu W.-F., Li Y.-Z., Chen X.-T., Xue Z.-L. (2011), Syntheses, structures and catalytic activities of ruthenium (II) carbonyl iodide complexes with CNC-pincer bis (carbene) ligand, Inorg. Chem. Commun., 14(10), 1673–1676 (DOI: 10.1016/j.inoche.2011.07.004).

31. Trnka T. M., Morgan J. P., Sanford M. S., Wilhelm T. E., Scholl M., Choi T.-L., Ding S., Day M. W., Grubbs R. H. (2003), Synthesis and Activity of Ruthenium Alkylidene Complexes Coordinated with Phosphine and N-Heterocyclic Carbene Ligands, J. Am. Chem. Soc., 125(9), 2546-2558 (DOI: 10.1021/ja021146w).

32. Das K., Nandi P. G., Islam K., Srivastava H. K., Kumar A. (2019), *N*-Alkylation of Amines Catalyzed by a Ruthenium–Pincer Complex in the Presence of in situ Generated Sodium Alkoxide, Eur. J. Org. Chem., 2019(40), 6855-6866 (DOI: 10.1002/ejoc.201901310).

33. Ahmad N., Lavison J. J., Robinson S. D., Uttley M. F. (1974), Triphenylphosphine complexes of transition metals, Inorganic Syntheses, 15, 48.

34. Hallman P. S., Stephenson T. A., Wilkinson G. (1970), Tetrakis(triphenylphosphine)dichlororuthenium(II) and Tris(triphenylphosphine)dichlororuthenium(II), Inorganic Syntheses (237-240), John Wiley and Sons, Ltd. (DOI: 10.1002/9780470132432.ch40).

35. Evans I. P., Spencer A., Wilkinson G. (1973), Dichlorotetrakis(dimethyl sulphoxide)ruthenium(II) and its use as a source material for some new ruthenium(II) complexes, J. Chem. Soc., Dalton Trans., (2), 204-209 (DOI: 10.1039/DT9730000204).

Chapter 3

Role of Ancillary Ligands in Selectivity Towards Acceptorless Dehydrogenative Coupling of Alcohols and Amines Catalyzed by Cationic Ru(II)-CNC Pincer Complexes

3.1. Introduction

Developing atom-efficient and environment-friendly strategies for constructing C-N bonds is a highly desirable and extensively studied area in chemistry [1–7]. Copper or palladium-catalyzed C–N bond-forming cross-coupling reactions remain among the most popular methods in organic synthesis [8, 9]. However, transition metal-catalyzed dehydrogenative coupling of alcohols and amines to produce imines, amides, and alkylated amines has emerged as one of the most atom-economic approaches for C–N bond formation [10–14]. Acceptorless dehydrogenative coupling (ADC) of alcohols with other alcohols or amines has found significant interest in recent times. ADC of alcohols and amines produces imines, which serve as versatile electrophilic reagents in several chemical reactions [1]. These chemical reactions include addition, cycloaddition, condensation, multi-component reactions, cross-dehydrogenative couplings, and asymmetric organocatalysis [1, 15–17]. Due to their high reactivity, imines find synthetic, medicinal, biological, and industrial applications as nitrogen sources [1, 15, 18]. Traditionally, imines are synthesized in the presence of an acid catalyst [15]. Despite the development of several techniques in recent years, synthesizing imines from alcohols and amines remains challenging. Researchers such as Milstein [19, 20], Beller [21, 22], Fujita [23, 24], Kempe [25], Williams [26], and Sun [27] have made tremendous contributions to ADC catalysis. Several

transition metal complexes have been developed to facilitate the key reaction step, i.e., the AAD reaction, as well as subsequent dehydrogenative coupling reactions [28, 29].
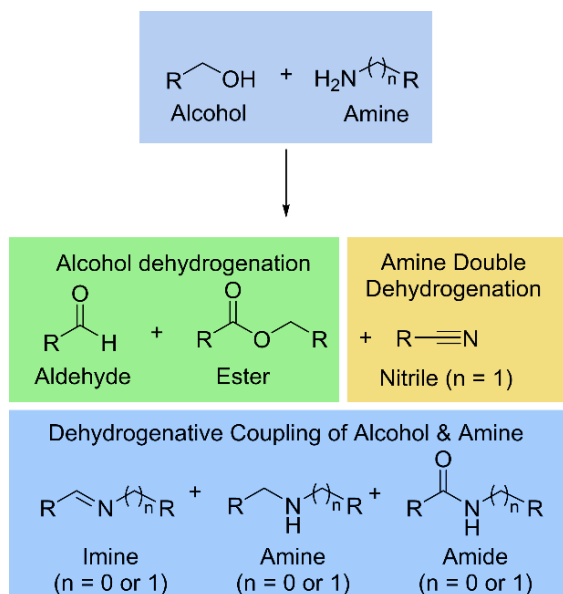
Scheme 3.1. Possible products from acceptorless alcohol dehydrogenation, amine double dehydrogenation, or acceptorless dehydrogenative coupling of alcohol and amines.

Metal-ligand cooperation (MLC) has been effectively utilized for a range of catalytic reactions, leading to the development of highly efficient catalysts that require only a small amount (0.01 mol%) to function [19, 20]. Although recent observations have shown more moderate reaction conditions, these reactions typically demand high temperatures, ranging from 100-140 ˚C, and extended reaction times of 24-72 hours [7, 8]. These high temperatures are generally detrimental to the selectivity of the reactions. For example, at higher temperatures, the selectivity between primary and secondary alcohol groups within the same molecule is often lost [30]. Additionally, there is a risk of forming undesired products, such as esters instead of aldehydes or amides instead of the desired imines (Scheme **3.1**) [31–33]. Several groups have made tremendous progress in imine or amine synthesis using different transition metal complexes. Milstein reported the

ruthenium pincer complex with low catalyst loading for selective amine synthesis with alcohol and ammonia [34]. Madsen described the dehydrogenative synthesis of imines through ruthenium NHC complexes [35]. Gelman [36] and Nishibayashi [37] reported the phosphine-based PCP-type ruthenium pincer complexes for ADC reaction. Kundu described the NNN-based ruthenium pincer catalyst for *N*-alkylation of amines with low catalyst loading [38]. Some selected active ruthenium catalysts for ADC reaction are shown below (Figure **3.1**). Alternative synthesis of imines and *N*-alkylation of amines by alcohols has been reported without the use of transition metal catalysts [39–41]. The vast applications of these related reactions in synthetic chemistry and new energy pathways highlight the need for new catalysts that are selective towards one type of reaction. Although the effects of the reaction temperature or steric effects due to ligands or substituents on the substrates are common, the electronic effects of spectator ligands in selectivity control have not been documented.
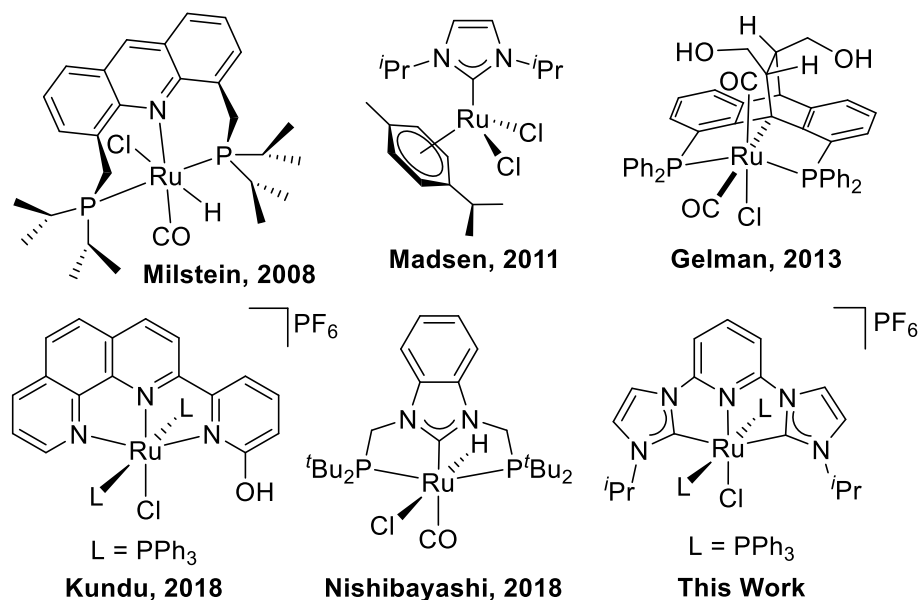
Figure 3.1. Some selected active ruthenium catalysts for acceptorless dehydrogenative coupling reaction.
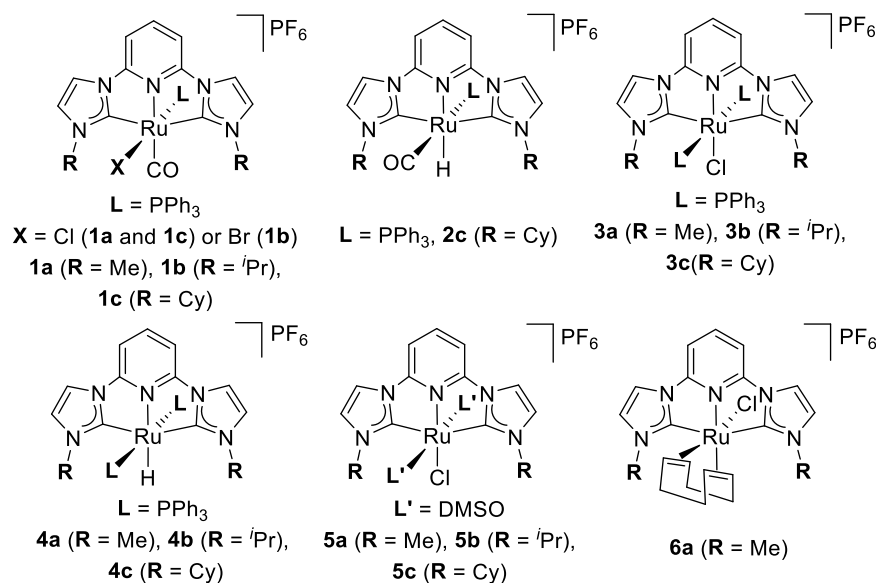
Figure 3.2. Cationic Ru(II)-CNC pincer complexes in this study.

Herein, we describe the catalytic activity of cationic Ru(II)-CNC pincer complexes for ADC reaction (Figure **3.2**). We have investigated the catalytic activity of all these complexes for acceptorless dehydrogenative coupling of benzyl alcohol and aniline. Additionally, we have examined the impact of ancillary ligands in ADC reactions. An interesting trend in catalytic activities was observed with these catalysts concerning different ancillary ligands. In the ADC reaction, complexes containing PPh$_3$ and DMSO ligands performed better reactivity than complexes containing CO and COD ligands.

3.2. Results and Discussion

3.2.1. Catalyst screening for Acceptorless dehydrogenative coupling (ADC) of benzyl alcohol and aniline

The acceptorless dehydrogenative coupling (ADC) of aniline with benzyl alcohol was examined as a model reaction, resulting in imine synthesis and *N*-alkylation of amines. Previously, our group reported

the optimized reaction conditions for AAD catalysis in toluene with KO^{t}Bu as the base with *N*-methyl analogue complexes [42]. By adding amines, we have incorporated these conditions in imine synthesis or *N*-alkylation of amines. The optimized reaction conditions for ADC (Ru-catalysts 3 mol% and base 1 eq. in toluene solvent heated at 110 ˚C for 3h) in a comparison of all the synthesized ruthenium complexes, it was observed that the Ru-complexes with *N*-isopropyl perform better than Ru-complexes with *N*-methyl and *N*-cyclohexyl wingtips for the ADC of alcohols and amines (Table **3.1**).

Table 3.1. Dehydrogenative coupling of benzyl alcohol and aniline with different catalysts.
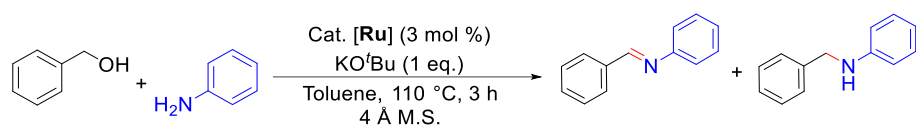
Entry[a]	Catalyst (L = Ancillary ligand, R = *N*-wingtip)	Yield[b] (%) (Imine:Amine)	TON[c]/ TOF[d]
1.	**1a** (L = CO, R = Me)	72 (75:25)	24/8
2.	**3a** (L = PPh$_3$, R = Me)	70 (100:0)	23/8
3.	**4a** (L = PPh$_3$, R = Me)	60 (13:86)	20/7
4.	**5a** (L = DMSO, R = Me)	96 (50:50)	32/11
5.	**6a** (L = COD, R = Me)	72 (100:0)	24/8
6.	**1b** (L = CO, R = ^{i}Pr)	89 (85:15)	30/10
7.	**3b** (L = PPh$_3$, R = ^{i}Pr)	98 (52:48)	33/11
8.	**4b** (L = PPh$_3$, R = ^{i}Pr)	62 (10:90)	21/7

9.	**5b** (L= DMSO, R = ^{i}Pr)	91 (70:30)	30/10
10.	**1c** (L = CO, R = Cy)	57 (13:87)	19/6
11.	**2c** (L = CO, R = Cy)	38 (7:93)	13/4
12.	**3c** (L = PPh$_3$, R = Cy)	81 (14:86)	27/9
13.	**4c** (L = PPh$_3$, R = Cy)	56 (21:79)	19/6
14.	**5c** (L = DMSO, R = Cy)	48 (19:81)	16/5
15.	-	14 (86:14)	-

[a]Reaction conditions: Aniline (1 mmol), Benzyl alcohol (1 mmol), Catalyst (3 mol %), KO^{t}Bu (1 eq.), Toluene (5 mL) under a slow N$_2$ flow at 110 °C for 3h. [b]Combined GC yield of imine and amine products determined by gas chromatography with *n*-decane as an internal standard. Imine and amine ratios in parentheses and products were characterized by GC-MS. [c]TON = [(Number of moles of substrate converted)/(Number of moles of catalyst)] at the end of the reaction. [d]TOF = [(TON)/hour].

For ADC, ruthenium complexes with PPh$_3$ (**3a-c**) and DMSO (**5a-c**) as a co-ligand show higher yields of 70, 98, 81, 96, 91, and 48% respectively (Table 3.1, entries 2, 7, 12, 4, 9, and 14) than the other analogous complexes with CO ligand (**1a-c**). Complexes with CO (**1a-c**) as a co-ligand gave 72, 89, and 57% yields (Table 3.1, entries 1, 6, and 10), while, the ruthenium hydride complexes (**4a-c** and **2c**) gave 60, 62, 56, and 38% which is poorer as compared to their chloride complexes (Table 3.1, entries 3, 8, 13, and 11) probably due to a longer induction period. Additionally, the COD complex (**6a**) gave 72% yield (Table 3.1, entry 5), similar to the analogues CO complex (**1a**) but poorer than the DMSO (**5a**) complex. Moreover, the reactivity was also investigated with no catalyst loading under optimized reaction conditions, showing only 14% yield (Table 3.1, entry 15). A remarkable trend in catalytic activity for ADC reaction was observed, indicating the involvement of the Ru-metal centre in the dehydrogenative coupling step in the catalytic cycle.
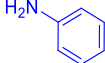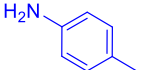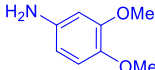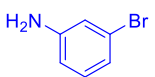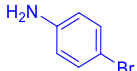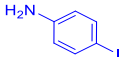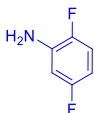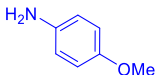
3.2.2. Substrate scope for dehydrogenative coupling of alcohol and amines
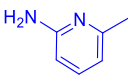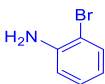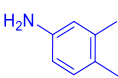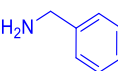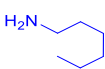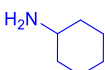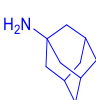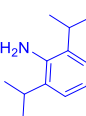
ADC of several amines, including benzylic, heterocyclic, cyclic, and acyclic aliphatic amines, were explored with benzyl alcohol to directly form C-N bond under the optimized reaction conditions (Table **3.2**). It was found that catalyst **3b** serves as an efficient pre-catalyst for a range of substrates and gives excellent yields in most cases. Several substrates containing electron-donating or electron-withdrawing groups in the aryl group of aniline reacted smoothly under optimal reaction conditions to give high yields of the desired ADC product. ADC of aniline gave an excellent yield of 98% in which the selectivity of the imine product is greater than the alkylated product (Table 3.2, entry 1). Similarly, 3-bromoaniline, 4-bromoaniline, and 4-iodoaniline gave both products, where alkylated products are in major yields, 89%, 90%, and 78%, respectively (Table 3.2, entries 4, 5, and 6). *p*-Toluidine and 3,4-dimethoxyaniline with benzyl alcohol have afforded good yields with more selectivity for the alkylated product 65% and 57%, respectively (Table 3.2, entries 2 and 3). However, reaction with 2,5-difluroaniline, *p*-Anisidine, and 2-Amino-6-methylpyridine gave only *N*-alkylated product with good yield (69%, 61%, and 74%) (Table 3.2, entries 7, 8 and 10), while 2-aminopyridine gives excellent yield with maximum selectivity for the alkylated product (95%) (Table 3.2, entry 9). In contrast, 2-bromoaniline, 3,4 dimethylaniline, and benzylamine gave only imine products with good to moderate yield (34%, 76%, and 43%) (Table 3.2, entries 11-13). Aliphatic amines were also tested under the optimized reaction conditions in which *n*-hexylamine, cyclohexylamine, and 1-adamantylamine give only the imine product with good to moderate yield (65%, 69%, and 29%) respectively, (Table 3.2, entries 14-16). In the case of 2,6-diisopropylaniline, no conversion was observed probably due to the steric bulkiness near the aniline group (Table 3.2, entry 17). While some of the aromatic amines give a mixture of imine and alkylated

amine, some give either imine or alkylated amine products. However, in the case of aliphatic amines, only imine products were obtained. At this point, the reason behind this contrast between aromatic and aliphatic amines is not certain.

Table 3.2. ADC of benzyl alcohol and various amines with catalyst **3b**.
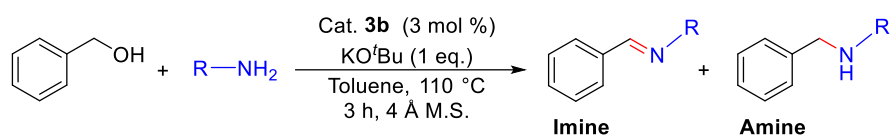
Entry[a]	Amine	Yield[b] (%)	Imine:Amine (%)	TON[c]/ TOF[d]
1.	H₂N–(phenyl)	98	52:48	33/11
2.	H₂N–(4-methylphenyl)	65	24:76	22/7
3.	H₂N–(3,4-dimethoxyphenyl)	57	38:62	19/6
4.	H₂N–(3-bromophenyl)	89	20:80	30/10
5.	H₂N–(4-bromophenyl)	90	5:95	30/10
6.	H₂N–(4-iodophenyl)	78	16:84	26/9
7.	H₂N–(2,5-difluorophenyl)	69	0:100	23/8
8.	H₂N–(4-methoxyphenyl)	61	0:100	20/7

9.		95	0:100	32/11
10.		74	0:100	25/8
11.		34	100:0	11/4
12.		76	100:0	25/8
13.		43	100:0	14/5
14.		65	100:0	22/7
15.		69	100:0	23/8
16.		29	100:0	10/3
17.		0	-	-
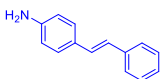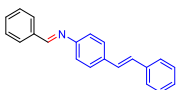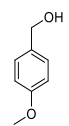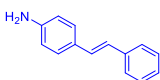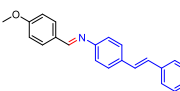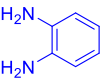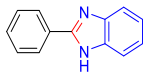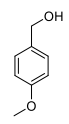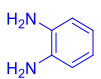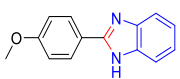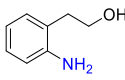
[a]Reaction conditions: Amine (1 mmol), Benzyl alcohol (1 mmol), Catalyst (3 mol %), KO^{t}Bu (1 eq.), Toluene (5 mL) under a slow N_2 flow at 110 °C for 3h. [b]GC yield was determined by gas chromatography with *n*-decane as an internal standard where combined imine and amine products (entries 1-6), amine products (entries 7-10), and imine products (entries 11-16). Products were characterized by GC-MS. [c]TON = [(Number of moles of substrate converted)/(Number of moles of catalyst)] at the end of the reaction. [d]TOF = [(TON)/hour].

3.2.3. Synthesis of biologically active compounds

To further evaluate the applicability of the reaction, different biologically active imine precursors were also synthesized under optimized reaction conditions (Table **3.3**). The reaction of 4-amino stilbene with benzyl alcohol and 4-methoxy benzyl alcohol under

101

similar reaction conditions gave 93% (with 55:45 ratios and 42% hydrogenated product) and 85% yields, respectively for Resveratrol precursors (Table 3.3, entries 1 and 2). Resveratrol-derived imines are active precursors for the resveratrol drugs which is used for Alzheimer's disease [43]. The reaction of 1,2-diaminobenzene with benzyl alcohol and 4-methoxy benzyl alcohol gave 2-phenyl benzimidazole and 2-(4-Methoxy-phenyl)-1H-benzoimidazole in 68% and 71% yield respectively (Table 3.3, entries 3 and 4). In addition, the synthesis of indole was also achieved with similar reaction conditions by treating 2-amino-phenylethanol (81% yield, Table 3.3, entry 5).

Table 3.3. Synthesis of some biologically active compounds with catalyst **3b**.

Entry[a]	Reactant (Alcohol)	Reactant (Amine)	Product	Yield[b] (%)	TON[c]/ TOF[d]
1.	benzyl alcohol	4-aminostilbene	imine product	51[e]	31/10
2.	4-methoxybenzyl alcohol	4-aminostilbene	methoxy imine product	85	28/9
3.	benzyl alcohol	1,2-diaminobenzene	2-phenylbenzimidazole	68	23/8
4.	4-methoxybenzyl alcohol	1,2-diaminobenzene	2-(4-methoxyphenyl)benzimidazole	71	24/8
5.	2-amino-phenylethanol	-	indole	81	27/9

[a]Reaction conditions: Amine (1 mmol), Alcohol (1 mmol), Catalyst (3 mol %), KO^{t}Bu (1 eq.), Toluene (5 mL) under a slow N_2 flow at 110 °C for 3h. [b]GC yield determined by gas chromatography with *n*-decane as an internal standard. Products were characterized by GC-MS. [c]TON = [(Number of moles of substrate converted)/(Number of moles of catalyst)] at the end of the reaction. [d]TOF = [(TON)/hour]. [e]Both the product form total yield of 93% with 55:45 ratios (42% hydrogenated product).

3.2.4. Mechanism for acceptorless dehydrogenative coupling of alcohols and amines

The mechanisms for ADC catalyzed by transition metal complexes have been studied by many other groups earlier [13, 35, 44–46]. The presence of ruthenium hydride complexes **4b** and **4b"** in the reaction mixture of ADC reactions starting from the precatalyst **3b** was confirmed through an NMR experiment with all the ingredients of the catalytic reaction heated in a J. Young NMR tube in DMSO-d_6 as solvent (Figure **3.6** and **3.7**). Further, the mass spectrometry of samples from the catalytic ADC reaction reveals the presence of intermediates **D**, with *ortho*-C-H activated, metal-bound aldehyde, and **E**, with the metal-bound aldimine product. Based on earlier studies reported in the literature and our investigation of the mechanism, a plausible mechanism starting from the most efficient precatalyst **3b** and involving the Ru-hydride complex **4b** as an intermediate is proposed in Figure **3.3**. The catalytic ADC reaction involves a preliminary AAD step, which begins with forming a ruthenium alkoxide species **A** by reacting complex **3b'** with alcohol in the presence of KO^{t}Bu. Further, the Ru-H intermediate **B** is formed via β-H elimination resulting in the generation of the metal-bound aldehyde. Release of the aldehyde molecule produces Ru-H intermediate **4b'** (Figure **3.5** for comparison of relative energy between **4b'** and **4b"**), which can also be formed by dissociation of a PPh$_3$ ligand, starting from the Ru-hydride complex **4b**. Finally, the addition of an alcohol molecule to the intermediate **4b'** produces another intermediate **C**, which liberates H$_2$ gas and regenerates the ruthenium alkoxide species **A**, completing the alcohol dehydrogenation step.

For the imine formation, the dehydrogenative coupling step can proceed via nucleophilic attack of an amine either on the free aldehyde or the metal-bound aldehyde. Metal-free base-catalyzed *N*-alkylation of amines has also been reported with alcohols [39–41]. However, the

catalytic activity of complexes containing PPh₃ ligands (**3a**, **3b**, and **3c**) indicates the role of these complexes during imine formation. Analysis of the mass spectrogram of the catalytic mixture provided proof of a metal-bound aldehyde, bound as a chelate after a Murai-type C-H activation of the phenyl ring [47–49]. The release of an H_2 molecule after the *ortho*-C-H activation of the phenyl ring in intermediate **B** generates intermediate **D**, which gives a peak at *m/z* 764.2116 (Figure **3.8**). Aldehyde, ketones, aldimines, and similar groups are known to act as directing groups for C-H activation and have been utilized for C-H functionalizations in aromatic compounds [47–50]. Further, a weaker *trans* effect of PPh₃ or DMSO ligands might be responsible for the aldehyde intermediate to remain metal-bound and facilitate this C-H activation step. To confirm this step, the *ortho*-C-H activation of benzaldehyde was checked with Ru-H complex **4b**, without any base. The ESI⁺ MS analysis of this test reaction confirms the presence of an intermediate containing Ru-bound benzoate, formed after the nucleophilic attack of a water molecule on the metal-bound benzaldehyde (Figure **3.9**).

The nucleophilic attack by incoming amine on the metal-bound, chelating aldehyde results in the C-N bond formation and generation of intermediate **E**. This nucleophilic attack should be facilitated on a metal-bound aldehyde due to decreased electron density at the carbon atom of a metal-bound carbonyl group. Proton transfer from the ammonium nitrogen to the oxygen atom then generates intermediate **F** with the coordinated hemiaminal species. Intermediate **F** with an *O*-bound hemiaminal species isomerizes to **F'** with an *N*-bound hemiaminal species, which can now lose a water molecule to generate intermediate **G**, with a metal-bound chelating aldimine. The existence of intermediate **G** was also confirmed in the mass spectrogram of the catalytic mixture (*m/z* 839.2545, Figure **3.8**). For the release of the aldimine product, intermediate **G** can go through hydrogenolysis with an H_2 molecule liberated during the *ortho*-C-H

activation of the phenyl ring to generate a Ru-H intermediate **H**, which gives intermediate **4b'** after the release of the imine product. Further, imine hydrogenation can take place at the intermediate **H**, generating intermediate **I**. Release of the hydrogenated product from **I** can again be achieved by hydrogenolysis, giving Ru-H intermediate **4b'**.
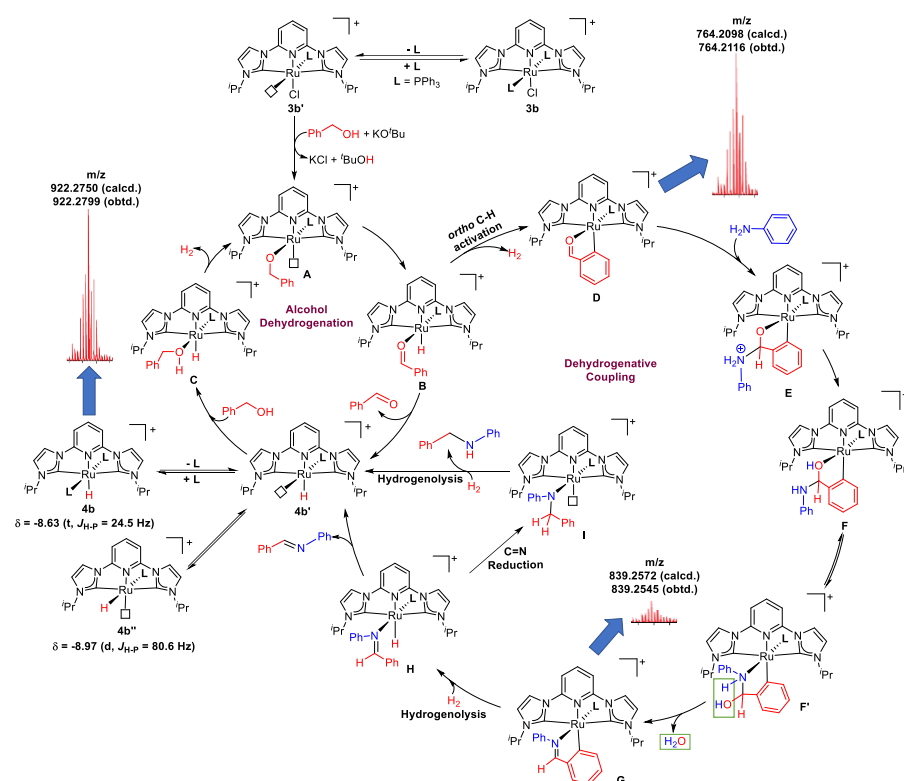
Figure 3.3. Plausible mechanism for acceptorless dehydrogenative coupling of aniline with benzyl alcohol by complex **3b**, with key intermediates **4b**, **D**, and **G** identified in the LCMS of the catalytic sample and intermediates **4b** and **4b''** identified through ^{1}H and ^{31}P NMR in the NMR scale catalytic reaction sample.

The observed trend in the catalytic activity during ADC catalysis by using complexes **1-6** indicates the potential role of ancillary ligands. The proposed mechanism can account for the trends observed in terms of the *trans*-effect of the ligands at the *trans* position to the aldehyde in the intermediate **B**. Ligands with more *trans*-effect (CO and COD) can facilitate the release of the aldehyde product and, therefore, precatalysts **1a-b**, and **5a** perform better at AAD (and TH)

105

reactions [42, 51, 52]. The relatively poorer performance of precatalysts **1c**, **3c**, and **5c** could be due to steric hindrance caused by the cyclohexyl groups in approaching the reactants. The trend with the *trans* effect is more distinct with the smaller *N*-alkyl group, i.e., methyl, with not much interference from the steric effect. Complexes with PPh₃ and DMSO ligands having comparatively weaker *trans*-effect undergo *ortho*-C-H activation of the metal-bound aldehyde product, followed by nucleophilic attack by an amine to give C-N coupling products. The *ortho*-C-H activation of the aldehydes on metal complexes is a well-known phenomenon where the aldehyde group is utilized as a directing group of C-H activation and further functionalizations [47–50].
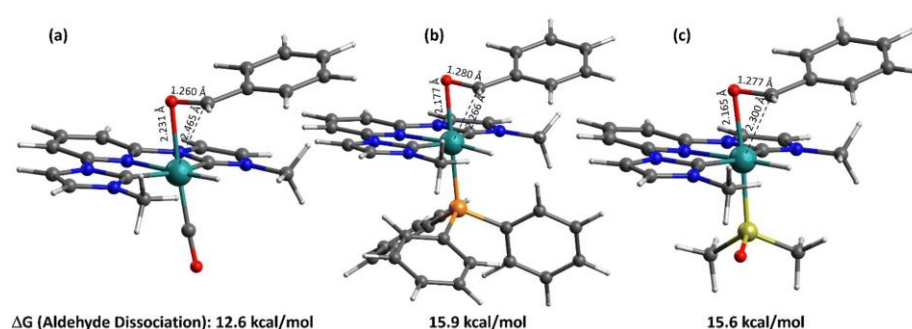
Figure 3.4. DFT-optimized geometries of analogous intermediates **B**^{L} (a) **L** = CO, (b) **L** = PPh₃ and (c) **L** = DMSO after β-hydride elimination from **A** for the AAD step are shown in Figure **3.3**.

DFT calculations were performed to validate the qualitative "*trans effect*" description in terms of quantifiable differences in the calculated structures for the intermediate **B** and its analogues with CO and DMSO ligands in place of the PPh₃ ligand. The structures of intermediates **B** and **4b'** were calculated along with their analogues with CO and DMSO ligands in place of PPh₃ (**B**^{L} and **[Ru-H]**^{L}; L = CO, PPh₃ and DMSO) using the ORCA 5.0.4 program [53–55]. The DFT-optimized structures of the analogous intermediate **B**^{L} are shown in Figure **3.4**, with relevant bond parameters for the metal-bound aldehyde product and the Gibbs free energy for the aldehyde

dissociation. The observed "*trans* influence" in the calculated structures of these intermediates supports the expected difference in catalytic activity. The Ru–O(C) bond parameters indicate a weaker interaction between the ruthenium centre and the carbonyl unit of the aldehyde in the intermediate $\mathbf{B^{CO}}$ with a CO ligand trans to the coordinated aldehyde. The shorter Ru-O and Ru-C bonds and a slightly longer C-O bond of the aldehyde unit in intermediate complex $\mathbf{B^{PPh_3}}$ and $\mathbf{B^{DMSO}}$ with PPh₃ or DMSO ligand trans to the aldehyde indicate a relatively tightly bound aldehyde.
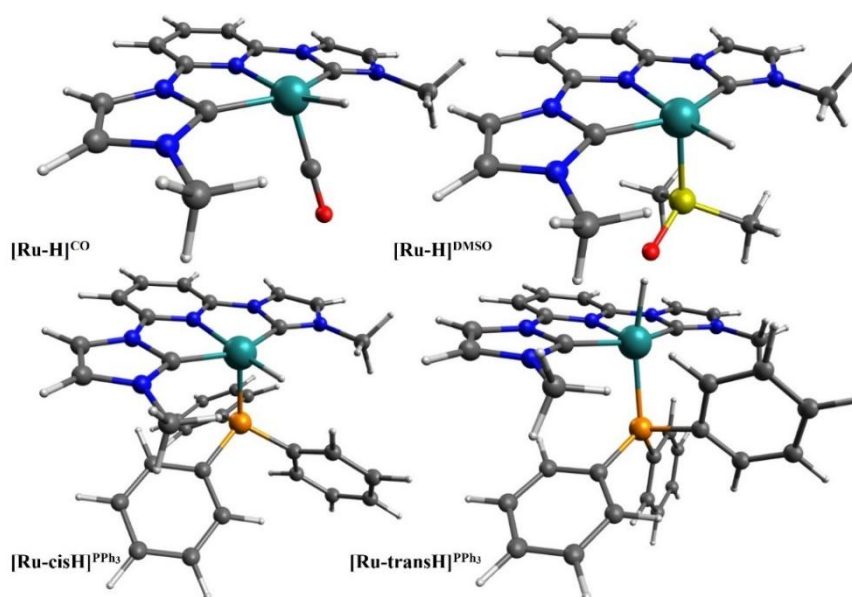
Figure 3.5. DFT optimized structures of $\mathbf{[Ru\text{-}H]^L}$ after aldehyde dissociation from $\mathbf{B^L}$ ($\mathbf{L}$ = CO, DMSO, and PPh₃). For $\mathbf{L}$ = PPh₃, two structures with hydride position w.r.t. PPh₃ ligand are calculated. The $\mathbf{[Ru\text{-}transH]}^{\mathbf{PPh_3}}$ (model for **4b''**, confirmed in ¹H NMR) is found -1.7 kcal/mol lower than $\mathbf{[Ru\text{-}cisH]}^{\mathbf{PPh_3}}$ (model for **4b'**) possibly due to an agostic interaction between Ru and a phenyl ring of PPh₃ ligand.

Gibbs free energies of aldehyde dissociation have been calculated by comparing the energies of DFT-optimized structures of $\mathbf{B^L}$ and $\mathbf{[Ru\text{-}H]^L}$ (Figure **3.5**). The calculated Gibbs free energies of aldehyde dissociations from $\mathbf{B^L}$ support the observation of complexes with CO ligands being better at catalyzing the AAD reactions since the

aldehyde product can easily dissociate and another alcohol dehydrogenation cycle is initiated. In the case of complexes with PPh$_3$ and DMSO ligands, the higher dissociation energies result in the retention of the aldehyde product, allowing the *ortho*-C-H activation and subsequent steps at the metal-bound aldehyde, thus making them better catalyst precursors for ADC reactions.

3.3. Conclusion

In summary, we described the effect of ancillary ligands on catalytic performance and a comparison of the four ligands (CO, COD, DMSO, PPh$_3$) can be explained in terms of the *trans* effect of these ligands on the release of the product of the catalytic reaction. No such studies for selectivity among ADC catalysis are reported with respect to the effect of ancillary ligands, perhaps because most of the pincer ligand-based complexes involve metal-ligand cooperativity. The CNC pincer ligand platform provides a unique ligand framework with no metal-ligand cooperativity, which allows this comparison between a set of ancillary ligands. Further, all these complexes have been utilized as catalysts in the dehydrogenative coupling reaction of benzyl alcohol with amines. An unexpected reversal in the catalytic activity was observed where complexes containing PPh$_3$ ligand performed better compared to complexes containing CO ligand. NMR and mass investigation of the catalytic reaction indicated C-N coupling step to occur at the metal-bound aldehyde. A plausible mechanism has been suggested to explain the difference in catalytic activity and its reversal during the dehydrogenative coupling reaction. Although the aldehyde group has long been utilized as a directing group for C-H activation, we report, for the first time, *ortho*-C-H activation playing a supportive role in the nucleophilic attack on the aldehyde group. Further, substrate scope for the dehydrogenative coupling reaction of benzyl alcohol with a wide range of amines has been explored for imine and amine synthesis including the formation of some biologically important imines.

3.4. Experimental Section

3.4.1. General Considerations

All reactions were carried out under an inert atmosphere using the standard Schlenk technique. All the used Ru(II) catalysts were synthesized by our previously reported procedures [51, 52, 56]. The synthesis of *N*-cyclohexyl Ru-complexes was discussed in Chapter 2. Solvents were purchased from S. D. Fine-Chem Limited and purified by distillation under an inert atmosphere. The mass chromatograms were recorded on Bruker-Daltonics-MicroTOF-QII mass spectrometer. GC Samples were analysed in Shimadzu QP2010 Ultra, with an internal standard.

3.4.2. General procedure for the catalytic dehydrogenative coupling reaction

Typically, catalyst (3 mol %) was added to the solution of alcohol (1 mmol), amine (1 mmol), KO′Bu (0.112 g, 1 eq., 1 mmol) in toluene under an inert atmosphere in a Schlenk tube and heated at 110 ˚C for 3 h by lowering into a preheated oil bath. The yield of the product with different catalysts was determined by the relative peak area of the benzyl alcohol and the product in GC with *n*-decane (0.195 mL, 1 mmol) as an internal standard based on the consumption of benzyl alcohol (Table **3.1**). In substrate scope analysis, the yield was determined by the relative peak area of their respective alcohol substrate and the product in GC with *n*-decane (0.195 mL, 1 mmol) as an internal standard (Tables **3.2** and **3.3**).

3.4.3. Experimental details for the identification of hydride intermediate

In a Glove Box, catalyst **3b** (0.033 g, 0.03 mmol) was added to a solution of benzyl alcohol (0.104 mL, 1 mmol), aniline (0.090 mL, 1

mmol), and KO^{t}Bu (0.112 g, 1 mmol) in DMSO-d$_6$ inside a J. Young NMR tube which was then closed, and taken outside of the glove box for recording ^{1}H NMR before and after heating at 110 ˚C for 30 minutes.

3.4.4. Experimental details for Mass analysis of the ADC reaction

In a Schlenk tube, catalyst **3b** (0.033 g, 0.03 mmol) was added to a solution of benzyl alcohol (0.104 ml, 1 mmol), aniline (0.090 ml, 1 mmol), and KO^{t}Bu (0.112 g, 1 mmol) in toluene under an inert atmosphere. The resulting reaction mixture was heated at 110 ˚C for 30 minutes and then LCMS analysis was performed.

3.4.5. Determination of % GC yield by gas chromatography

GC Samples were analyzed in Shimadzu QP2010 Ultra gas chromatograph. Yields of the product were determined using *n*-decane as an internal standard. Samples were prepared by filtering the reaction mixture through a celite pad with chloroform and further dilution with methanol solution. The reactants and products relative response factors (RF) were calculated using *n*-decane as the internal standard. *n*-Decane was added to the reaction mixture before the start of catalysis. The following equations are used to calculate the % GC yields [57].

Response factors were calculated using the following equation:

$$\text{RF} = \frac{\text{Area percentage of internal standard} \times \text{Moles of analyte}}{\text{Area percentage of analyte} \times \text{Moles of internal standard}}$$

Moles of remaining reactants and products were calculated using the following equation:

$$\text{Moles of analyte} = \frac{\text{RF} \times \text{Moles of internal standard} \times \text{Area percentage of analyte}}{\text{Area percentage of internal standard}}$$

The products of ADC catalysis experiments are analyzed with GC-MS only as the imine products are prone to hydrolysis during column chromatography.

3.4.6. Computational details

All DFT calculations were performed using the ORCA 5.0.4 program package developed by Neese and co-workers [53–55]. The geometry optimizations, along with frequency calculations, were carried out using r2Scan-3c composite functional, which is shown to produce excellent geometries for transition metal complexes. Stationary points were confirmed to have no imaginary frequency by performing analytical frequency calculations at the same level as the DFT method. Solvation energies in toluene were calculated on optimized geometries using the same DFT function as the SMD solvation model [58]. For final energies, single-point calculations were performed using range-separated hybrid meta-GGA functional ωB97M-V [59] developed by Martin Head-Gorden and coworkers which includes VV10 non-local correlation. Larger basis sets def2-QZVP with def2-ECP on Ru, and def2-TZVP on all other atoms were used for final single-point energy calculations. The energies obtained from single point calculations were converted to Gibbs free energies using the total corrections obtained for the thermochemical calculations following the frequency calculations at the r2Scan-3c level and the solvation energies. To account for the entropy penalty during the change in the number of components during a chemical change, the MHP scheme proposed by Martin, Hay, and Pratt was applied which has also been used in several systems to produce reasonable results [60]. According to this method, a correction of (n-m) $\times$ 4.3 kcal/mol is imposed whenever a reaction component changes from m components to n components. Gibbs free energies, ΔG are reported in Kcal/mols.

3.4.7. Characterisation data for reaction intermediates
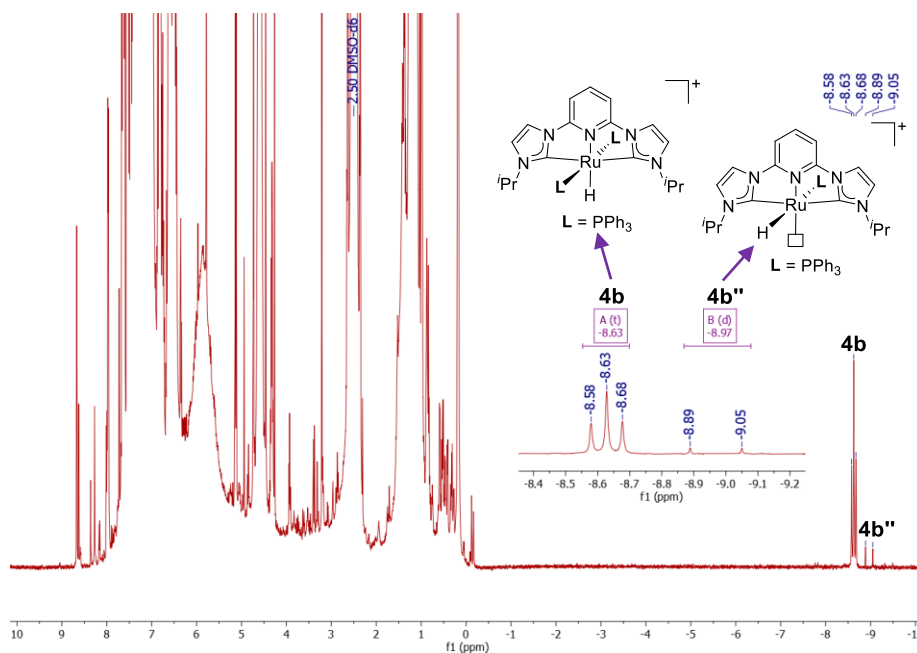
Figure 3.6. ^{1}H NMR experiment in DMSO-d$_6$ to observe the generation of ruthenium hydride intermediates **4b** and **4b''** from complex **3b** under catalytic reaction conditions.
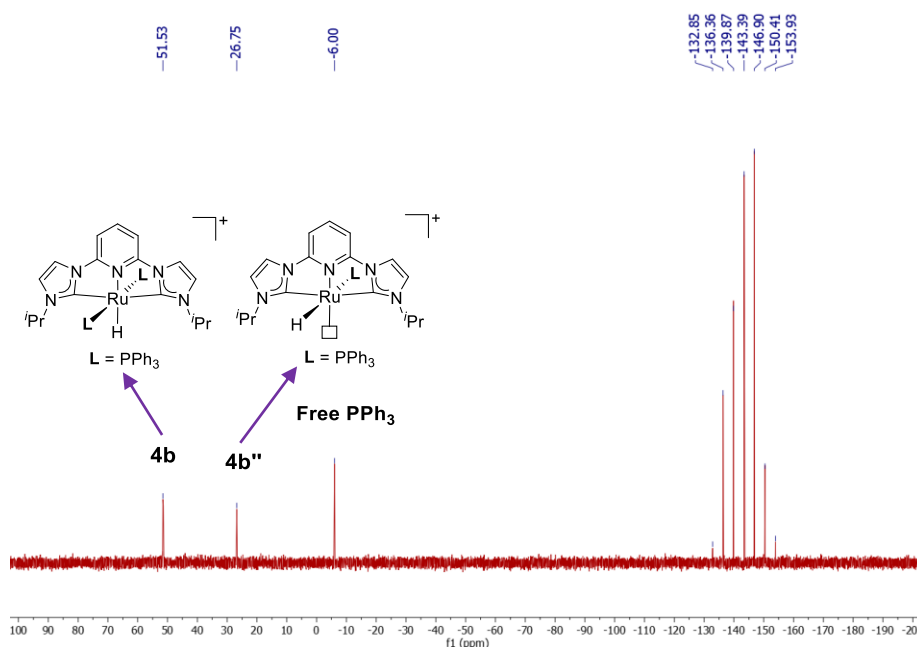
Figure 3.7. ^{31}P NMR experiment in DMSO-d$_6$ to observe the generation of ruthenium hydride intermediates **4b** and **4b''** from complex **3b** with free phosphine under catalytic reaction conditions.
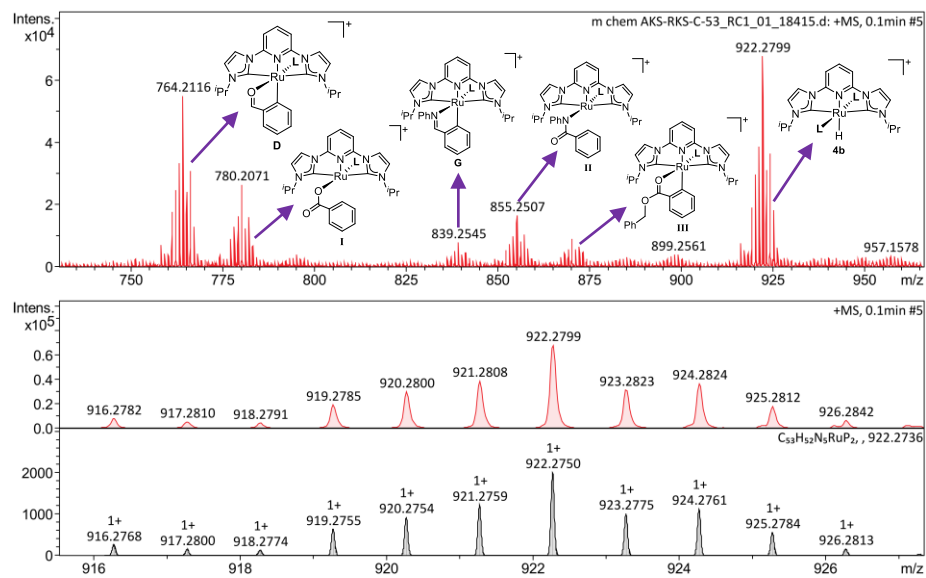
Figure 3.8. LCMS spectrogram of the catalytic reaction mixture after half an hour ($L = PPh_3$).
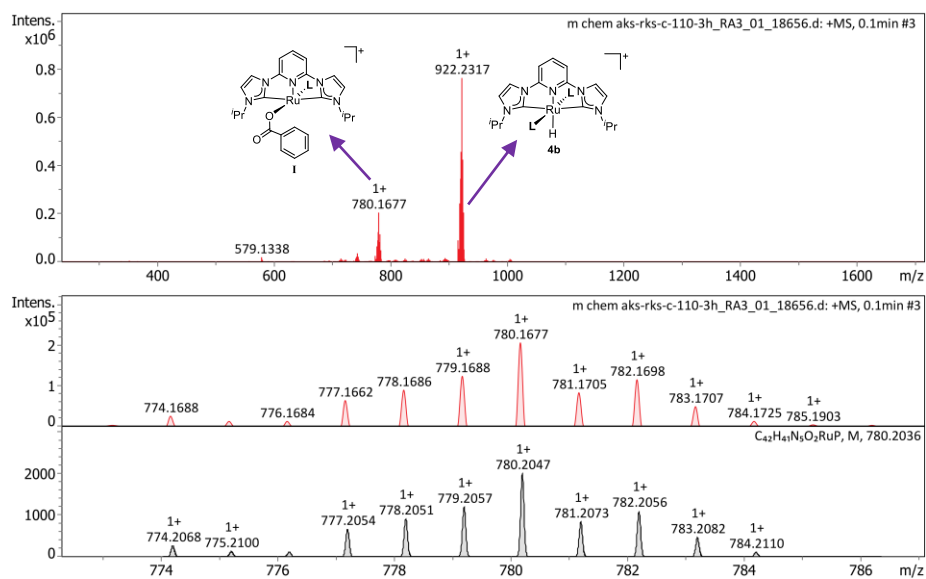
Figure 3.9. LCMS spectrogram of the catalytic reaction mixture with benzaldehyde and catalyst **4b** formed intermediate **I** ($L = PPh_3$).

3.4.8. Formation of other intermediates I, II, and III

Other intermediates **I**, **II**, and **III** are formed during the catalytic reactions (Figure **3.8**). Intermediate **I** also appeared in LCMS during the reaction of benzaldehyde with Ru hydride catalyst **4b** (Figure **3.9**). This information suggests that the ortho C-H activation of benzaldehyde takes place, generating intermediate **D**, which further reacts with moisture (while recording mass data) and appears as intermediate **I** (Figure **3.9**).
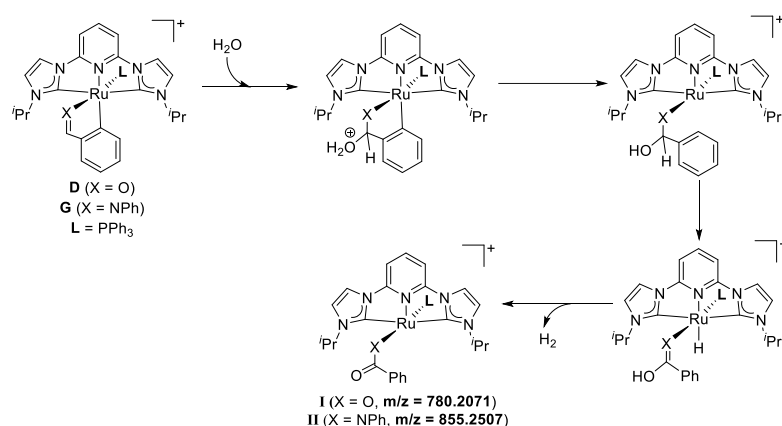
Figure 3.10. Plausible mechanism for the formation of intermediates **I** and **II** in the catalytic reaction mixture by complex **3b**.
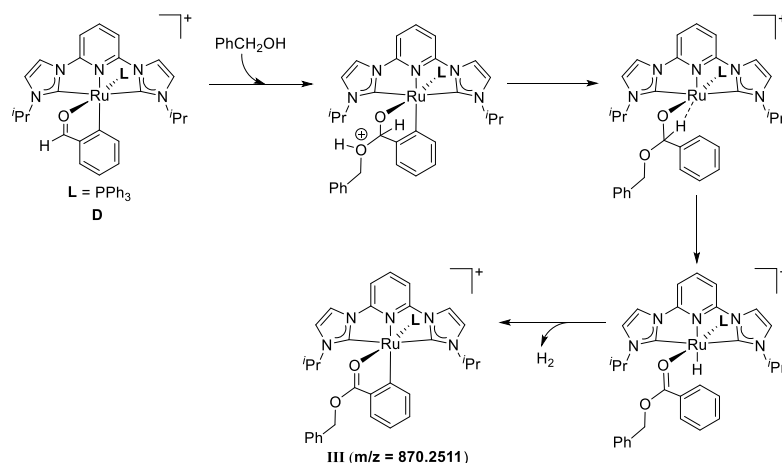
Figure 3.11. Plausible mechanism for the formation of intermediate **III** in the catalytic reaction mixture by complex **3b**.

3.5. References

1. Belowich M. E., Stoddart J. F. (2012), Dynamic imine chemistry, Chem. Soc. Rev., 41(6), 2003-2024 (DOI: 10.1039/C2CS15305J).

2. Broomfield L. M., Wu Y., Martin E., Shafir A. (2015), Phosphino-amine (PN) Ligands for Rapid Catalyst Discovery in Ruthenium-Catalyzed Hydrogen-Borrowing Alkylation of Anilines: A Proof of Principle, Adv. Synth. Catal., 357(16-17), 3538-3548 (DOI: 10.1002/adsc.201500562).

3. Mastalir M., Glatz M., Pittenauer E., Allmaier G., Kirchner K. (2019), Rhenium-Catalyzed Dehydrogenative Coupling of Alcohols and Amines to Afford Nitrogen-Containing Aromatics and More, Org. Lett., 21(4), 1116-1120 (DOI: 10.1021/acs.orglett.9b00034).

4. Marichev K. O., Takacs J. M. (2016), Ruthenium-Catalyzed Amination of Secondary Alcohols Using Borrowing Hydrogen Methodology, ACS Catal., 6(4), 2205-2210 (DOI: 10.1021/acscatal.6b00175).

5. Leonard J., Blacker A. J., Marsden S. P., Jones M. F., Mulholland K. R., Newton R. (2015), A Survey of the Borrowing Hydrogen Approach to the Synthesis of some Pharmaceutically Relevant Intermediates, Org. Process Res. Dev., 19(10), 1400-1410 (DOI: 10.1021/acs.oprd.5b00199).

6. Liu H., Chuah G.-K., Jaenicke S. (2012), *N*-alkylation of amines with alcohols over alumina-entrapped Ag catalysts using the "borrowing hydrogen" methodology, J. Catal., 292, 130-137 (DOI: 10.1016/j.jcat.2012.05.007).

7. Elangovan S., Neumann J., Sortais J.-B., Junge K., Darcel C., Beller M. (2016), Efficient and selective *N*-alkylation of amines with alcohols catalysed by manganese pincer complexes, Nat. Commun., 7(1), 12641 (DOI: 10.1038/ncomms12641).

8. Tan D.-W., Li H.-X., Zhang M.-J., Yao J.-L., Lang J.-P. (2017), Acceptorless Dehydrogenation of Alcohols Catalyzed by CuI *N*-Heterocycle Thiolate Complexes, ChemCatChem, 9(6), 1113-1118 (DOI: 10.1002/cctc.201601459).

9. Ruiz-Castillo P., Buchwald S. L. (2016), Applications of Palladium-Catalyzed C–N Cross-Coupling Reactions, Chem. Rev., 116(19), 12564-12649 (DOI: 10.1021/acs.chemrev.6b00512).

10. Dutta I., Sarbajna A., Pandey P., Rahaman S. M. W., Singh K., Bera J. K. (2016), Acceptorless Dehydrogenation of Alcohols on a Diruthenium(II, II) Platform, Organometallics, 35(10), 1505-1513 (DOI: 10.1021/acs.organomet.6b00085).

11. Miao Y., Samuelsen S. V., Madsen R. (2021), Vanadium- and Chromium-Catalyzed Dehydrogenative Synthesis of Imines from Alcohols and Amines, Organometallics, 40(9), 1328-1335 (DOI: 10.1021/acs.organomet.1c00123).

12. Li R.-J., Ling C., Lv W.-R., Deng W., Yao Z.-J. (2021), Cyclometalated Half-Sandwich Iridium(III) Complexes: Synthesis, Structure, and Diverse Catalytic Activity in Imine Synthesis Using Air as the Oxidant, Inorg. Chem., 60(7), 5153-5162 (DOI: 10.1021/acs.inorgchem.1c00174).

13. Luque-Urrutia J. A., Solà M., Milstein D., Poater A. (2019), Mechanism of the Manganese-Pincer-Catalyzed Acceptorless Dehydrogenative Coupling of Nitriles and Alcohols, J. Am. Chem. Soc., 141(6), 2398-2403 (DOI: 10.1021/jacs.8b11308).

14. Mastalir M., Glatz M., Gorgas N., Stöger B., Pittenauer E., Allmaier G., Veiros L. F., Kirchner K. (2016), Divergent Coupling of Alcohols and Amines Catalyzed by Isoelectronic Hydride MnI and FeII PNP Pincer Complexes, Chem. Eur. J., 22(35), 12316-12320 (DOI: 10.1002/chem.201603148).

15. Layer R. W. (1963), The Chemistry of Imines, Chem. Rev., 63(5), 489-510 (DOI: 10.1021/cr60225a003).

16. Sindhuja E., Ramesh R. (2014), Direct synthesis of imines from primary alcohols and amines using an active ruthenium(II) NNN-pincer complex, Tetrahedron Lett., 55(40), 5504-5507 (DOI: 10.1016/j.tetlet.2014.08.035).

17. Choudhury L. H., Parvin T. (2011), Recent advances in the chemistry of imine-based multicomponent reactions (MCRs), Tetrahedron, 67(43), 8213-8228 (DOI: 10.1016/j.tet.2011.07.020).

18. Martin S. F. (2009), Recent applications of imines as key intermediates in the synthesis of alkaloids and novel nitrogen heterocycles, Pure Appl. Chem., 81(2), 195-204 (DOI: 10.1351/PAC-CON-08-07-03).

19. Zhang J., Balaraman E., Leitus G., Milstein D. (2011), Electron-Rich PNP- and PNN-Type Ruthenium(II) Hydrido Borohydride Pincer Complexes, Synthesis, Structure, and Catalytic Dehydrogenation of Alcohols and Hydrogenation of Esters, Organometallics, 30(21), 5716-5724 (DOI: 10.1021/om200595m).

20. Zell T., Milstein D. (2015), Hydrogenation and Dehydrogenation Iron Pincer Catalysts Capable of Metal–Ligand Cooperation by Aromatization/Dearomatization, Acc. Chem. Res., 48(7), 1979-1994 (DOI: 10.1021/acs.accounts.5b00027).

21. Ryabchuk P., Agapova A., Kreyenschulte C., Lund H., Junge H., Junge K., Beller M. (2019), Heterogeneous nickel-catalysed reversible, acceptorless dehydrogenation of *N*-heterocycles for hydrogen storage, Chem. Commun., 55(34), 4969-4972 (DOI: 10.1039/C9CC00918C).

22. Cui X., Li W., Junge K., Fei Z., Beller M., Dyson P. J. (2020), Selective Acceptorless Dehydrogenation of Primary Amines to Imines by Core-Shell Cobalt Nanoparticles, Angew. Chem. Int. Ed., 59(19), 7501-7507 (DOI: 10.1002/anie.201915526).

23. Kawahara R., Fujita K., Yamaguchi R. (2012), Dehydrogenative Oxidation of Alcohols in Aqueous Media Using Water-Soluble

and Reusable Cp*Ir Catalysts Bearing a Functional Bipyridine Ligand, J. Am. Chem. Soc., 134(8), 3643-3646 (DOI: 10.1021/ja210857z).

24. Fujita K., Tamura R., Tanaka Y., Yoshida M., Onoda M., Yamaguchi R. (2017), Dehydrogenative Oxidation of Alcohols in Aqueous Media Catalyzed by a Water-Soluble Dicationic Iridium Complex Bearing a Functional *N*-Heterocyclic Carbene Ligand without Using Base, ACS Catal., 7(10), 7226-7230 (DOI: 10.1021/acscatal.7b02560).

25. Michlik S., Kempe R. (2013), Regioselectively Functionalized Pyridines from Sustainable Resources, Angew. Chem. Int. Ed., 52(24), 6326-6329 (DOI: 10.1002/anie.201301919).

26. Cherepakhin V., Williams T. J. (2018), Iridium Catalysts for Acceptorless Dehydrogenation of Alcohols to Carboxylic Acids: Scope and Mechanism, ACS Catal., 8(5), 3754-3763 (DOI: 10.1021/acscatal.8b00105).

27. Wang Z., Pan B., Liu Q., Yue E., Solan G. A., Ma Y., Sun W.-H. (2017), Efficient acceptorless dehydrogenation of secondary alcohols to ketones mediated by a PNN-Ru(II) catalyst, Catal. Sci. Technol., 7(8), 1654-1661 (DOI: 10.1039/C7CY00342K).

28. Gunanathan C., Milstein D. (2014), Bond Activation and Catalysis by Ruthenium Pincer Complexes, Chem. Rev., 114(24), 12024-12087 (DOI: 10.1021/cr5002782).

29. Fuse H., Mitsunuma H., Kanai M. (2020), Catalytic Acceptorless Dehydrogenation of Aliphatic Alcohols, J. Am. Chem. Soc., 142(9), 4493-4499 (DOI: 10.1021/jacs.0c00123).

30. Díez-González S., Marion N., Nolan S. P. (2009), *N*-Heterocyclic Carbenes in Late Transition Metal Catalysis, Chem. Rev., 109(8), 3612-3676 (DOI: 10.1021/cr900074m).

31. Siddiki S. M. A. H., Toyao T., Shimizu K. (2018), Acceptorless dehydrogenative coupling reactions with alcohols over heterogeneous catalysts, Green Chem., 20(13), 2933-2952 (DOI: 10.1039/C8GC00451J).

32. Nguyen D. H., Trivelli X., Capet F., Paul J.-F., Dumeignil F., Gauvin R. M. (2017), Manganese Pincer Complexes for the Base-Free, Acceptorless Dehydrogenative Coupling of Alcohols to Esters: Development, Scope, and Understanding, ACS Catal., 7(3), 2022-2032 (DOI: 10.1021/acscatal.6b03554).

33. Wei Z., de Aguirre A., Junge K., Beller M., Jiao H. (2018), Benzyl Alcohol Dehydrogenative Coupling Catalyzed by Defined Mn and Re PNP Pincer Complexes-A Computational Mechanistic Study, Eur. J. Inorg. Chem., 2018(42), 4643-4657 (DOI: 10.1002/ejic.201800674).

34. Gunanathan C., Milstein, D. (2008), Selective Synthesis of Primary Amines Directly from Alcohols and Ammonia, Angew. Chem. Int. Ed., 47(45), 8661-8664 (DOI: 10.1002/anie.200803229).

35. Maggi A., Madsen R. (2012), Dehydrogenative Synthesis of Imines from Alcohols and Amines Catalyzed by a Ruthenium *N*-Heterocyclic Carbene Complex, Organometallics, 31(1), 451-455 (DOI: 10.1021/om201095m).

36. Musa S., Fronton S., Vaccaro L., Gelman D. (2013), Bifunctional Ruthenium(II) PCP Pincer Complexes and Their Catalytic Activity in Acceptorless Dehydrogenative Reactions, Organometallics, 32(10), 3069-3073 (DOI: 10.1021/om400285r).

37. Eizawa A., Nishimura S., Arashiba K., Nakajima K., Nishibayashi, Y. (2018), Synthesis of Ruthenium Complexes Bearing PCP-Type Pincer Ligands and Their Application to Direct Synthesis of Imines from Amines and Benzyl Alcohol, Organometallics, 37(18), 3086-3092 (DOI: 10.1021/acs.organomet.8b00465).

38. Maji M., Chakrabarti K., Paul B., Roy B. C., Kundu S. (2018), Ruthenium(II)-NNN-Pincer-Complex-Catalyzed Reactions Between Various Alcohols and Amines for Sustainable C−N and C−C Bond Formation, Adv. Synth. Catal., 360(4), 722-729 (DOI: 10.1002/adsc.201701117).

39. Garg N. K., Tan M., Johnson M. T., Wendt O. F. (2023), Highly Efficient Base Catalyzed *N*-alkylation of Amines with Alcohols and β-Alkylation of Secondary Alcohols with Primary Alcohols, ChemCatChem, e202300741 (DOI: 10.1002/cctc.202300741).

40. Himmelbauer D., Talmazan R., Weber S., Pecak J., Thun-Hohenstein A., Geissler M.-S., Pachmann L., Pignitter M., Podewitz M., Kirchner K. (2023), No Transition Metals Required - Oxygen Promoted Synthesis of Imines from Primary Alcohols and Amines under Ambient Conditions, Chem. Eur. J., 29(29), e202300094 (DOI: 10.1002/chem.202300094).

41. Kozlov A. S., Afanasyev O. I., Chusov D. (2022), Borrowing hydrogen amination: Whether a catalyst is required?, J. Catal., 413, 1070-1076 (DOI: 10.1016/j.jcat.2022.08.014).

42. Yadav D., Singh R. K., Misra S., Singh A. K. (2022), Ancillary ligand effects and microwave-assisted enhancement on the catalytic performance of cationic ruthenium(II)-CNC pincer complexes for acceptorless alcohol dehydrogenation, Appl. Organomet. Chem., e6756 (DOI: 10.1002/aoc.6756).

43. Lu C., Guo Y., Yan J., Luo Z., Luo H.-B., Yan M., Huang L., Li X. (2013), Design, Synthesis, and Evaluation of Multitarget-Directed Resveratrol Derivatives for the Treatment of Alzheimer's Disease, J. Med. Chem., 56(14), 5843-5859 (DOI: 10.1021/jm400567s).

44. Chai H., Yu K., Liu B., Tan W., Zhang G. (2020), A Highly Selective Manganese-Catalyzed Synthesis of Imines under Phosphine-Free Conditions, Organometallics, 39(1), 217-226 (DOI: 10.1021/acs.organomet.9b00769).

45. Masdemont J., Luque-Urrutia J. A., Gimferrer M., Milstein D., Poater A. (2019), Mechanism of Coupling of Alcohols and Amines To Generate Aldimines and H_2 by a Pincer Manganese Catalyst, ACS Catal., 9(3), 1662-1669 (DOI: 10.1021/acscatal.8b04175).

46. Donthireddy S. N. R., Singh V. K., Rit A. (2022), A heteroditopic NHC and phosphine ligand supported ruthenium(II)-complex: an effective catalyst for the *N*-alkylation of amides using alcohols, Catal. Sci. Technol., 12(12), 4050-4056 (DOI: 10.1039/D2CY00544A).

47. Murai S., Kakiuchi F., Sekine S., Tanaka Y., Kamatani A., Sonoda M., Chatani N. (1993), Efficient catalytic addition of aromatic carbon-hydrogen bonds to olefins, Nature, 366(6455), 529-531, (DOI: 10.1038/366529a0).

48. Murai S., Kakiuchi F., Sekine S., Tanaka Y., Kamatani A., Sonoda M., Chatani N. (1994), Catalytic C-H/olefin coupling, Pure Appl. Chem., 66(7), 1527-1534 (DOI: 10.1351/pac199466071527).

49. Kakiuchi F., Tanaka Y., Sato T., Chatani N., Murai S. (1995), Catalytic Addition of Olefinic C–H Bonds to Olefins, Chem. Lett., 24(8), 679-680 (DOI: 10.1246/cl.1995.679).

50. Arockiam P. B., Bruneau C., Dixneuf P. H. (2012), Ruthenium(II)-Catalyzed C–H Bond Activation and Functionalization, Chem. Rev., 112(11), 5879-5918 (DOI: 10.1021/cr300153j).

51. Yadav D., Misra S., Kumar D., Singh S., Singh A. K. (2021), Cationic ruthenium(II)-NHC pincer complexes: Synthesis, characterisation and catalytic activity for transfer hydrogenation of ketones, Appl. Organomet. Chem., 35(8), e6287 (DOI: 10.1002/aoc.6287).

52. Yadav D., Singh R. K., Singh S., Shirage P. M., Singh A. K. (2021), Cationic ruthenium(II)-NHC pincer complexes with hemilabile COD: Solid-state structural characterization and theoretical study of an η^2-(E,Z)-COD ligand, J. Organomet. Chem., 953, 122061 (DOI: 10.1016/j.jorganchem.2021.122061).

53. Neese F. (2012), The ORCA program system, WIREs Comput. Mol. Sci., 2(1), 73-78 (DOI: 10.1002/wcms.81).

54. Neese F., Wennmohs F., Becker U., Riplinger C. (2020), The ORCA quantum chemistry program package, J. Chem. Phys., 152(22), 224108 (DOI: 10.1063/5.0004608).

55. Neese F. (2022), Software update: The ORCA program system-Version 5.0, WIREs Comput. Mol. Sci., 12(5), e1606 (DOI: 10.1002/wcms.1606).

56. Singh R. K., Yadav D., Misra S., Singh A. K. (2023), Role of ancillary ligands in selectivity towards acceptorless dehydrogenation versus dehydrogenative coupling of alcohols and amines catalyzed by cationic ruthenium(II)-CNC pincer complexes, Dalton Trans., 52(43), 15878-15895 (DOI: 10.1039/D3DT03149G).

57. Dornan L. M., Muldoon M. J. (2015), A highly efficient palladium(II)/polyoxometalate catalyst system for aerobic oxidation of alcohols, Catal. Sci. Technol., 5(3), 1428-1432 (DOI: 10.1039/C4CY01632G).

58. Marenich A. V., Cramer C. J., Truhlar D. G. (2009), Universal Solvation Model Based on Solute Electron Density and on a Continuum Model of the Solvent Defined by the Bulk Dielectric Constant and Atomic Surface Tensions, J. Phys. Chem. B, 113(18), 6378-6396 (DOI: 10.1021/jp810292n).

59. Mardirossian N., Head-Gordon M. (2016), ωB97M-V: A combinatorially optimized, range-separated hybrid, meta-GGA density functional with VV10 nonlocal correlation, J. Chem. Phys., 144(21), 214110 (DOI: 10.1063/1.4952647).

60. Martin R. L., Hay P. J., Pratt L. R. (1998), Hydrolysis of Ferric Ion in Water and Conformational Equilibrium, J. Phys. Chem. A, 102(20), 3565-3573 (DOI: 10.1021/jp980229p).

Chapter 4

Syntheses and Characterization of Cationic Ru(II)-CNC Pincer Complexes with Multiple NHC Donor Ligands

4.1. Introduction

The Pincer ligands have found more attention due to their enormous properties that influence the behaviour of the metal centres of the resulting complexes [1, 2]. It coordinates with the metal centre through three adjacent coplanar sites with a meridional geometry. The involvement of the pincer ligand has greatly influenced the understanding of the process of various organometallic and inorganic systems [3]. In homogeneous catalysis, pincer ligands play a crucial role by enhancing chemical and thermal stability, thereby reducing metal leaching during the catalytic cycle [4]. Moreover, these ligands offer the flexibility to adjust electronic and steric properties around the metal centre and expand their range of applications [5].

NHCs have found considerable attention as a substitute for phosphines, emerging as privileged ligands in the field of organometallic, inorganic, and organic chemistry [6–10]. NHC pincer carbene ligands are particularly intriguing derivatives, capable of inducing a significant entropic chelate effect, yielding a variety of more stable complexes with exciting chemical properties [11]. In this regard, chelation significantly influences the electronic properties of the metal, thereby modulating catalytic and photoelectronic properties [12, 13]. Over the past decades, NHC-based metal complexes have been broadly explored due to their wide applications in various organic transformations. Ruthenium pincer complexes are one of the most effective catalysts for important organic transformations, owing to

their stability and availability in various stable oxidation states and coordination geometries [4, 14–16].

Ruthenium(II) polypyridine complexes, along with those of other transition metals, have been extensively studied for the synthesis of environmentally friendly fuels and their precursors, such as CO, HCOOH, and CH_4 derived from CO_2 [17–21]. Hydrogen is an extremely engaging fuel because of its high energy content, and can be obtained by water oxidation [22]. NHC and pyridine rings have been combined to form bidentate, tridentate, and tetradentate ligands, and their metal complexes are highly active for CO_2 reduction and water oxidation catalysis [23, 24]. Mechanistic study of water oxidation revealed the generation of higher oxidation states, $Ru^{IV}(OH_2)$ and $Ru^{V/VI}=O$ intermediates, during the catalytic process [19, 25, 26]. Therefore, increasing the nucleophilic character of the metal through ligand modifications might help to stabilize these intermediates. Metal complexes featuring NHC and pyridine ligands play a crucial role in enhancing the electron density at the metal centre, exhibiting various redox states, considered an attractive possibility for potential water oxidation catalysts [26]. In particular, these characteristics of metal complexes can also be beneficial for the catalytic conversion of CO_2 to usable fuel precursors [27]. According to literature reports, the hydricity of the transition metal complexes is an activity descriptor for water-splitting and CO_2 reduction [19, 23, 26, 28]. Therefore, it is expected that the pyridine-functionalized NHC ligand system may increase the hydricity of the metal complex, which could be better for CO_2 reduction or similar types of transformations.

Metal complexes with pyridine and NHC ligands have shown high efficiency in a wide range of conversions, including H_2O oxidation and CO_2 reduction [23, 24, 29]. In 2008, Thummel reported the single-site mononuclear Ru(II) complexes with bipyridine, terpyridine, and polypyridine ligands, similarly, monomeric ruthenium-aqua complexes with polypyridine and NHC were described

by Meyer and co-workers for catalytic oxidation of H_2O [24, 26]. Parallel to this, a similar class of metal complexes is well explored as an efficient catalyst for CO_2 reduction. In recent years, Arikawa demonstrated the fixation of atmospheric carbon dioxide while Papish reported the selective carbon dioxide reduction using Ru(II) complexes of pyridinol and NHC-based pincers [30, 31]. Ru(II) pincer complexes were well explored in different organic transformations with excellent selectivity [4]. Previously, Danopoulos [32] and Peris [33] investigated the Ru(II)-CNC pincer complexes for transfer hydrogenation and oxidative cleavage of olefins. Our group recently described the Ru(II)-CNC pincer complexes for different catalytic organic transformations with excellent selective products [34–36]. Some selected active ruthenium catalysts for different catalytic reactions are shown in Figure **4.1**. More recently, we have reported the base-free synthesis of a simple Ru(III)-NHC complex of the type [Ru(CN)(H_2O)Cl_3] (CN = a bidentate, pyridine-carbene ligand) and their use as a precursor to prepare new ruthenium complexes [37].
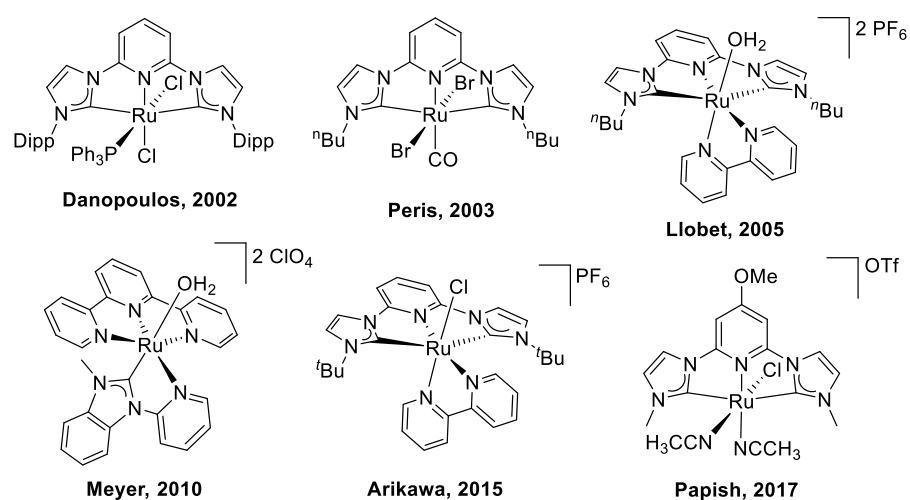
Figure 4.1. Some selected active ruthenium pincer catalysts for different catalytic reactions were previously reported.

Herein, we report a library of electron-rich cationic Ru(II)-CNC pincer complexes with multiple NHC carbene donor ligands [Ru(CNC^{Me})(CN^{Me})I]PF$_6$ **(7a)**, [Ru(CNC^{i-Pr})(CN^{Me})I]PF$_6$ **(7b)**,

[Ru(CNC^{Cy})(CN^{Me})I]PF$_6$ **(7c)**, [Ru(CNC$^{t\text{-}Bu}$)(CN^{Me})I]PF$_6$ **(7d)**, [Ru(CNC^{Me})(CN$^{i\text{-}Pr}$)I]PF$_6$ **(8a)**, [Ru(CNC$^{i\text{-}Pr}$)(CN$^{i\text{-}Pr}$)I]PF$_6$ **(8b)**, [Ru(CNC^{Cy})(CN$^{i\text{-}Pr}$)I]PF$_6$ **(8c)**, [Ru(CNC$^{t\text{-}Bu}$)(CN$^{i\text{-}Pr}$)I]PF$_6$ **(8d)**, [Ru(CNC^{Me})(Py-Bim^{Me})I]PF$_6$ **(9a)**, and [Ru(CNC^{Me})(3MePy-Im^{Me})I]PF$_6$ **(10a)** with smaller and bulky *N*-wingtips based CNC pincer ligands. A simple procedure for synthesized Ru(II)-CNC pincer complexes by reacting a bidentate ruthenium precursor with a CNC pincer ligand under refluxed conditions.

4.2. Results and Discussion

4.2.1. Synthesis of ligand precursors

CNC pincer ligand precursors (CNC^{Me}·2HBr = 2,6-bis[3-(methyl)imidazolium]pyridine dibromide and (CNC$^{i\text{-}Pr}$·2HBr = 2,6-bis[3-(isopropyl)imidazolium]pyridine dibromide and CNC^{Cy}·2HBr = 2,6-bis[3-(cyclohexyl)imidazolium]pyridine dibromide) and CNC$^{t\text{-}Bu}$·2HBr = 2,6-bis[3-(*tert*-butyl)imidazolium]pyridine dibromide) were prepared according to the reported procedure in the literature using 2,6-dibromopyridine and different alkyl-substituted imidazoles [38, 39].

4.2.2. Synthesis and characterization of cationic Ru(II)-CNC pincer complexes (7a-10a)

The reaction of bidentate ruthenium precursors and CNC^{Me}·2HBr pincer in ethylene glycol under reflux conditions, followed by ion exchange with the saturated solution of KPF$_6$, afforded complexes [Ru(CNC^{Me})(CN^{Me})I]PF$_6$ **(7a)**, [Ru(CNC^{Me})(CN$^{i\text{-}Pr}$)I]PF$_6$ **(8a)**, [Ru(CNC^{Me})(Py-Bim^{Me})I]PF$_6$ **(9a)**, and [Ru(CNC^{Me})(3MePy-Im^{Me})I]PF$_6$ **(10a)** (Scheme **4.1**). The addition of excess sodium iodide was necessary to avoid forming products with different halides in the coordination sphere. The ^{1}H NMR spectrum of the CNC^{Me}·2HBr ligand precursor displays a singlet at 10.59 ppm corresponding to the

imidazolium proton. The absence of this peak in the spectrum confirms the generation of the carbene during complex formation. All new complexes have been characterized by multinuclear NMR and HRMS techniques, and the single-crystal X-ray diffraction technique has determined solid-state structures of complex **7a**.
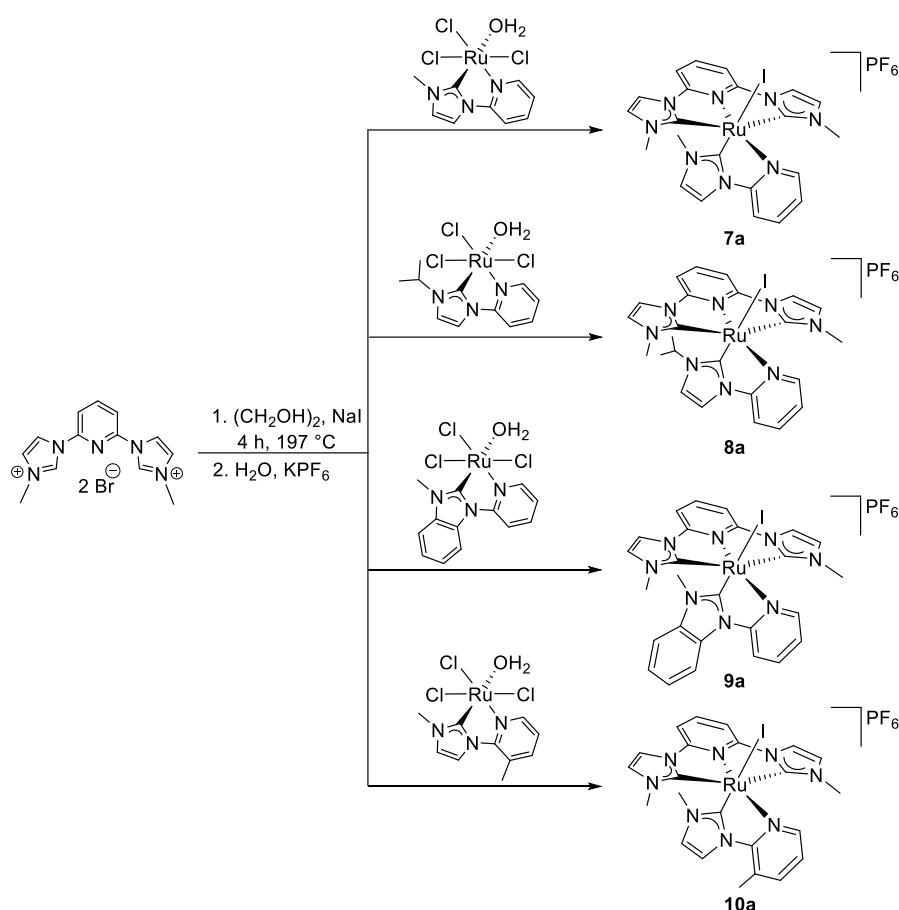
Scheme 4.1. Syntheses of cationic Ru(II)-CNC pincer complexes **7a-10a**.

The ^{1}H and ^{13}C NMR spectra of complex **7a** in the dmso-d$_6$ show two sets of signals for each of the protons expected, indicating the existence of two species in solution. This could be due to the existence of *cis/trans* isomers with respect to the two pyridine units, or due to a ligand substitution by a dmso-d$_6$ molecule resulting in an equilibrium between two forms. Structurally similar complexes with terpyridine ligands have been reported to give *cis/trans*-isomers concerning the two pyridine units by the Rodríguez group [40].

Luckily, we got the crystal structure of *cis*-**7a** as a kinetic product and formed only at lower reflux temperatures. The *trans* isomer is the major thermodynamic product formed only at reflux conditions, and its structure was determined using the single-crystal X-ray diffraction technique. The solid-state structures of **7a** show the species that have pyridine-pyridine *trans* to each other; the substitution of a labile ligand by a dmso-d$_6$ molecule seems more feasible in this case. Two possibilities for substitution can be considered, either iodide dissociated from the metal centre or hemilabile pyridine of the bidentate ligand dissociated from the metal centre. If bidentate hemilabile pyridine has dissociated from the metal centre, then the *ortho* proton of the pyridine ligand would be expected to show a further upfield shifted signal, which is not the case here. Further, the iodide ligand *trans* to an NHC ligand is expected to be labile. Therefore, we believe iodide substitution by a nucleophilic dmso-d$_6$ solvent molecule. The ^{1}H NMR spectrum of complex (**11a** vide infra) in dmso-d$_6$ confirmed this hypothesis, which shows that the acetonitrile was dissociated from the metal centre, and a new species **7a'** was generated with the free acetonitrile signal (Figure **4.2**). The ^{1}H NMR signals of complex (**11a** vide infra) were perfectly matched with the one set of signals of complex **7a** while recording the ^{1}H NMR in dmso-d$_6$ (Figure **4.3**). This information supports the clear indication of *in-situ* generation of complex **7a'**. Furthermore, to confirm this assumption, NMR spectra of this complex have been recorded in less nucleophilic, non-coordinating solvent, acetone-d$_6$, which shows only one species in the solution. Figures **4.2** and **4.4** show the ^{1}H NMR spectra of **7a** in dmso-d$_6$ and acetone-d$_6$, respectively, confirming only one molecular species in the acetone-d$_6$ solution. The formation of only the *trans* isomer in acetone-d$_6$ could be explained as it is favoured due to the steric effects of *N*-alkyl substituents in the plane of the CNC pincer ligand. Additionally, for the *cis*-isomer, the *N*-alkyl substituents of the bidentate CN ligand will be closer to the *N*-alkyl substituents of the

CNC ligand, while in the *trans*-isomer, they are away, making the pyridine-pyridine *trans*-isomer relatively less crowded.

Figure 4.2. ¹H NMR spectrum of complex **7a** recorded in dmso-d₆ showing two distinct species in solution with ratios of **7a** (45%) and **7a'** (55%).

Figure 4.3. ¹H NMR spectrum of complex **11a** in dmso-d₆ supporting the *in-situ* generation of complex **7a'** with dissociated acetonitrile.

Figure 4.4. ^{1}H NMR spectrum of complex **7a** recorded in acetone-d$_6$.

In ^{1}H NMR spectra of complexes **7a**, **8a**, **9a**, and **10a**, exhibit doublets for *ortho* protons of the pyridine ring of bidentate ligand at 10.51, 10.52, 10.68, and 10.57 ppm, respectively, similar to the previously reported complex [Ru(CNC$^{n\text{-Bu}}$)(CN$^{n\text{-Bu}}$)Br]PF$_6$ [41]. The CNC methyl proton of pincer complexes **7a**, **8a**, **9a**, and **10a** was obtained as a singlet at 3.14, 3.14, 3.15, and 3.13 ppm. The other aliphatic protons of complexes **7a** and **10a** appeared as a singlet for the *N*-Methyl bidentate proton at 2.70 and 2.69 ppm, while another singlet for the 3-methyl pyridine of complex **10a** at 2.90 ppm. The isopropyl protons of the bidentate CN ligand of complex **8a** appear at 2.88 – 2.81 ppm for the methine proton and a doublet for the methyl proton at 0.82 ppm. The methyl proton of Py-Bim$^{\text{Me}}$ of the bidentate ligand in complex **9a** appeared at 2.89 ppm. In the ^{13}C NMR spectra of complexes **7a**, **8a**, **9a**, and **10a**, the carbene carbon for CNC pincer ligand appeared at 195.44, 195.58, 194.00, and 195.48 ppm and bidentate ligand carbene signal at 191.08, 188.96, 203.32, and 192.63 ppm, respectively, similar to the previously reported complex [Ru(CNC$^{n\text{-Bu}}$)(CN$^{n\text{-Bu}}$)Br]PF$_6$ [41]. Carbene signals have been identified by comparing the ^{13}C NMR spectra of the set of complexes

containing the same pincer ligand CNC^{Me} but different CN ligands (e.g., complexes **7a** and **8a**, having CNC^{Me} but different CN^{Me} or CN^{iPr} ligands). ^{31}P NMR spectrum shows peaks at -144.24, -144.20, -144.22, and -144.25 ppm for PF$_6^-$ counterion, and their splitting as a septate due to coupling with six ^{19}F nuclei. Complexes **7a**, **8a**, **9a**, and **10a**, in acetonitrile, displayed the ESI$^+$ HRMS signal at m/z 627.0079, 655.0365, 677.0214, and 641.0232, respectively, assigned to [M-PF$_6$]$^+$.

4.2.3. Description of the crystal structures of complexes 7a and *cis*-7a

The solid-state structure and geometry around the ruthenium centre in **7a** have been confirmed by the single-crystal X-ray diffraction technique and their structural parameters and final refinements for the complexes are given in Table **4.1**. Some selected bond lengths and bond angles are given in Table **4.2**. It crystallized in a monoclinic with P2$_1$/c space group, and the structure revealed two almost planar five-membered metallacycles of the CNC pincer ligand, one five-membered metallacycles of the CN^{Me} bidentate ligand, and I$^-$ ion occupies the sixth coordination position around the ruthenium centre with octahedral geometry (Figure **4.5**). The CNC pincer ligand occupies three meridional sites with C1-Ru1-C2 angle of 154.7(6)° and their bite angle of N1-Ru1-C1 is 76.9(5)°, while with bidentate ligand the bite angle of N2-Ru1-C3 is 77.5(6)°, similar to previously reported complexes [36]. The Ru-I bond *trans* to carbene is fairly weak and labile, confirmed by the synthesis of complexes, where the iodo group was replaced by dmso-d$_6$ while recording the NMR spectra. The Ru-I bond length is 2.8185 Å, longer than the previously reported complexes Ru-I, 2.7671 Å [42], which suggests a lower degree of back donation from ruthenium to the iodo group and is reasoned to be more labile. The bond lengths of Ru-N of the pyridine group (~1.9 - 2.1 Å) [36] and Ru–C(NHC) (~1.9- 2.1 Å) [36] are similar to the previously reported metal complexes [37].

Figure 4.5. Single crystal X-ray structure of complex **7a**. All hydrogen atoms and one PF_6^- counter-anion are omitted for clarity. Selected bond lengths (Å) and angles (°): Ru1-C1, 2.041(12); Ru1-C2, 2.053(15); Ru1-C3, 2.001(13); Ru1-N1, 2.002(11); Ru1-N2, 2.111(12); Ru1-I1, 2.8185(14), N1-Ru1-C1, 76.9(5); C2-Ru1-I1, 91.8(4); N2-Ru1-C1, 104.3(5); C1-Ru1-C2, 154.7(6); C3-Ru1-I1, 171.8(5); N1-Ru1-N2, 175.8(5) and N2-Ru1-C3, 77.5(6).
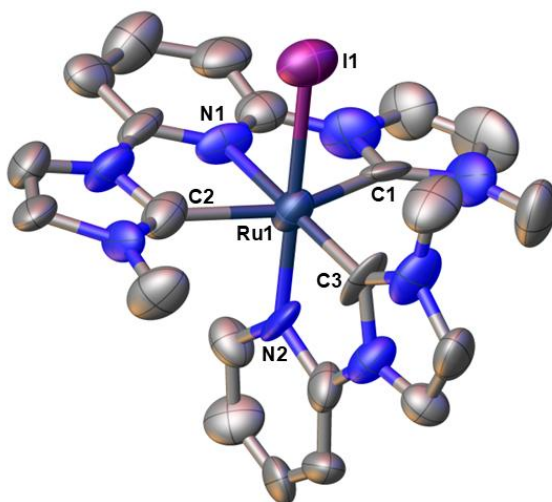
Figure 4.6. Single crystal X-ray structure of complex ***cis*-7a**. All hydrogen atoms and one PF_6^- counter-anion are omitted for clarity. Selected bond lengths (Å) and angles (°): Ru1-C1, 2.09(2); Ru1-C2, 2.10(2); Ru1-C3, 2.020(13); Ru1-N1, 2.031(12); Ru1-N2, 2.027(16);

Ru1-I1, 2.729(3), N1-Ru1-C1, 76.0(6); C2-Ru1-I1, 87.0(5); N2-Ru1-C1, 92.4(5); C1-Ru1-C2, 152.3(7); C3-Ru1-I1, 99.0(6) and N1-Ru1-N2, 98.1(6).

Table 4.1. Crystal data and structure refinement parameters of complexes **7a** and *cis*-**7a**.

	7a	*cis*-**7a**
Empirical formula	$C_{22}H_{22}N_8RuIPF_6$	$C_{22}H_{22}N_8RuIPF_6$
T/K	293(2)	293(2)
Crystal System	monoclinic	monoclinic
Space Group	$P2_1/c$	$P2_1/c$
a/Å	15.0771(5)	16.0081(9)
b/Å	10.9379(5)	13.6413(7)
c/Å	16.8084(6)	15.4884(11)
α/°	90	90
β/°	104.553(4)	115.284(8)
γ/°	90	90
V/Å³	2682.97(19)	3058.2(4)
Z	4	4
ρ_{calc}g/cm³	1.910	1.675
λ/Å (Cu-Kα)	1.54184	1.54184
Reflections Collected	10376	13513
Data/restr./param.	4767/0/355	5804/0/356
R (int)	0.1243	0.1714
Final R indices [I>2σ(I)]	$R_1 = 0.1166$, $wR_2 = 0.3174$	$R_1 = 0.1479$, $wR_2 = 0.3601$
R indices (all data)	$R_1 = 0.1579$, $wR_2 = 0.3690$	$R_1 = 0.2204$, $wR_2 = 0.4344$
GOF on F2	1.039	1.158

The crystal structure of *cis*-**7a** is similar to the complex **7a** instead of pyridine-pyridine *cis* to each other, this arrangement is more unstable and crowded (Figure **4.6**). It crystallized in a monoclinic,

P2$_1$/c space group with octahedral geometry around the ruthenium centre. Luckily, we got the crystal structure of *cis*-**7a**, which forms at lower reflux temperatures, and its diffraction quality is inferior and insufficient to discuss bond parameters. The molecular structure of this crystal has some disorder, shown only for the structural arrangement. The crystallographic data and structural refinement parameters of complex *cis*-**7a** are given in Table **4.1**, while bond lengths and bond angles are in Table **4.2**.

Table 4.2. Selected bond lengths and bond angles of complexes **7a** and *cis*-**7a**.

Complex	Bond lengths (Å)	Bond angles (°)
7a	Ru1-C1, 2.041(12) Ru1-C2, 2.053(15) Ru1-C3, 2.001(13) Ru1-N1, 2.002(11) Ru1-N2, 2.111(12) Ru1-I1, 2.8185(14)	C1-Ru1-I1, 86.8(3) C1-Ru1-C3, 89.7(6) C1-Ru1-N2, 104.3(5) C1-Ru1-C2, 154.7(6) C1-Ru1-N1, 76.9(5) C2-Ru1-I1, 91.8(4) C2-Ru1-C3, 94.6(6) C2-Ru1-N2, 101.0(6) C3-Ru1-I1, 171.8(5) N1-Ru1-I1, 87.9(3) N1-Ru1-C3, 98.6(6) N1-Ru1-N2, 175.8(5) N1-Ru1-C2, 77.8(5) N2-Ru1-I1, 96.1(4) N2-Ru1-C3, 77.5(6)
cis-**7a**	Ru1-C1, 2.09(2) Ru1-C2, 2.10(2) Ru1-C3, 2.020(13) Ru1-N1, 2.031(12) Ru1-N2, 2.027(16) Ru1-I1, 2.729(2)	C1-Ru1-I1, 88.8(4) C3-Ru1-C1, 101.9(6) N2-Ru1-C1, 92.4(5) C1-Ru1-C2, 152.3(7) N1-Ru1-C1, 76.0(6) C2-Ru1-I1, 87.0(5) C3-Ru1-C2, 105.8(7) N2-Ru1-C2, 92.2(6) C3-Ru1-I1, 99.0(6) N1-Ru1-I1, 82.9(4) C3-Ru1-N1, 177.2(6) N1-Ru1-N2, 98.1(6) N1-Ru1-C2, 76.3(7) N2-Ru1-I1, 178.6(4) C3-Ru1-N2, 80.1(8)

4.2.4. Synthesis and Characterization of cationic Ru(II)-CNC pincer complexes (7b-8d) with bulky *N*-wingtip

The synthesis of novel Ru(II) complexes with bulky *N*-wingtip was followed by a similar reaction procedure as discussed earlier via the treatment of ruthenium precursors [Ru(CN$^{R'}$)(H$_2$O)Cl$_3$] (R' = Me, ^{i}Pr), with pincer ligand precursors CNC^R·2HBr (R = ^{i}Pr, Cy, and ^{t}Bu) afforded complexes [Ru(CNC$^{i\text{-}Pr}$)(CN^{Me})I]PF$_6$ (**7b**), [Ru(CNC^{Cy})(CN^{Me})I]PF$_6$ (**7c**), [Ru(CNC$^{t\text{-}Bu}$)(CN^{Me})I]PF$_6$ (**7d**), [Ru(CNC$^{i\text{-}Pr}$)(CN$^{i\text{-}Pr}$)I]PF$_6$ (**8b**), [Ru(CNC^{Cy})(CN$^{i\text{-}Pr}$)I]PF$_6$ (**8c**), and [Ru(CNC$^{t\text{-}Bu}$)(CN$^{i\text{-}Pr}$)I]PF$_6$ (**8d**) (Scheme **4.2**). ^{1}H NMR spectra of pincer ligand precursors CNC^{iPr}·2HBr, CNC^{Cy}·2HBr, and CNC^{tBu}·2HBr exhibit a singlet for the imidazolium proton at 10.72, 10.55, and 10.25 ppm, respectively. The absence of the imidazolium proton peak in the ^{1}H NMR spectrum indicates the generation of the carbene during complex formation. All new complexes have been characterized by multinuclear NMR and HRMS techniques, and the single-crystal X-ray diffraction technique has confirmed the solid-state structure of complexes **7b** and **7c**.
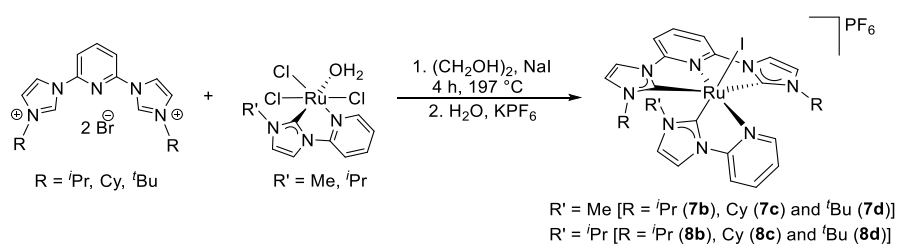
Scheme 4.2. Syntheses of cationic Ru(II)-CNC pincer complexes **7b-8d** with bulky *N*-wingtip.

In the NMR spectra of these complexes, two sets of signals appear in dmso-d$_6$, similarly with lower *N*-wingtip complexes (**7a-10a**). One set of signals appeared for complex **7b**, while the other one for *in-situ* generated dmso-d$_6$ coordinated species **7b'** (Figure **4.7**). This observation was confirmed earlier in the lower *N*-wingtip complex **7a**. This assumption was further confirmed by the ^{1}H NMR

spectrum of complex (**11b** vide infra), which was recorded in dmso-d_6 and shows that the acetonitrile was dissociated from the metal centre, and a new species **7b'** was generated with the free acetonitrile signal (Figure **4.8**). In both the NMR spectra, the one set of signals was perfectly matched and confirmed the existence of *in-situ* generated dmso-d_6 coordinated species **7b'**. Additionally, upon recording the NMR spectra of complex **7b** in less nucleophilic, non-coordinating solvent acetone-d_6, which shows the existence of only one species in solution (Figure **4.9**).

In ^{1}H NMR spectra of complexes **7b** and **8b**, doublets for *ortho* protons of the pyridine ring of the bidentate ligand are observed at 10.51 and 10.54 ppm, respectively, similar to the previously reported complex [Ru(CNC$^{n\text{-}Bu}$)(CN$^{n\text{-}Bu}$)Br]PF$_6$ [41]. The isopropyl group of pincer ligand gives one multiplet at 3.54 – 3.46 (**7b**) and 3.48 – 3.40 (**8b**) ppm for methine proton and two doublets for both the methyl groups at 1.34 (**7b**), 1.31 (**8b**), 0.91(**7b**), and 0.89 (**8b**) ppm. In complex **7b**, a singlet for the bidentate methyl proton at 2.72 ppm, while in complex 8b, the isopropyl protons of the bidentate CN ligand appear at 2.96 – 2.90 ppm for the methine proton and a doublet for the methyl proton at 0.82 ppm. In the ^{13}C NMR spectrum, the carbene signals of complexes **7b** and **8b** show at 193.87 and 194.07 ppm for CNC and 191.59 and 189.81 ppm for CN bidentate ligand, respectively, similar to previously reported ruthenium complex [41]. We have assigned the peaks for ^{13}C NMR by comparing the spectra of a set of complexes containing the same CNC but different CN ligands (e.g., complexes **7b** and **8b**, having CNC$^{i\text{-}Pr}$ but different CN^{Me} or CN$^{i\text{-}Pr}$ ligands, respectively). The signal showing a significant change in chemical shift upon the change in the *N*-alkyl group of the CN ligand has been assigned as the carbene signal of the CN ligand. ^{31}P NMR spectrum shows peaks at -144.24, and -144.23 ppm for PF$_6^-$ counterion, and their splitting as a septate due to coupling with six ^{19}F nuclei. Complexes **7b** and **8b**, in acetonitrile, displayed the ESI$^+$

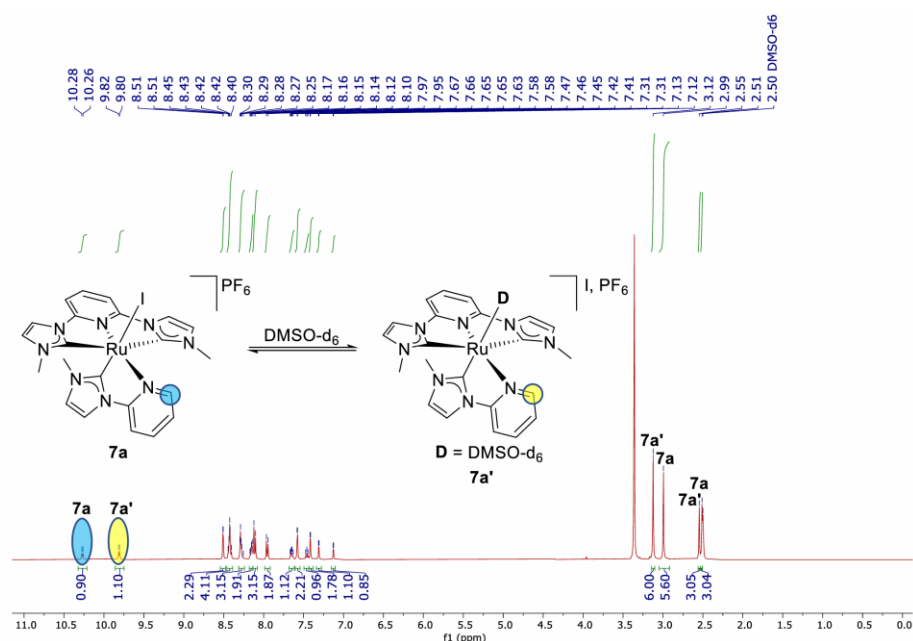HRMS signal at m/z 683.0699 and 711.0995, respectively, assigned to $[M-PF_6]^+$.
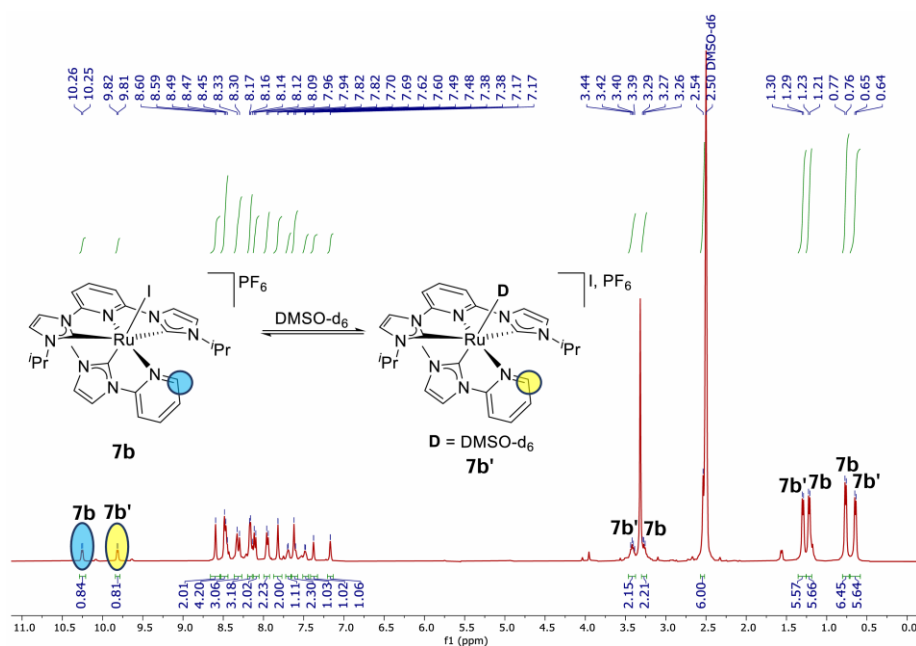
Figure 4.7. ^{1}H NMR spectrum of complex **7b** recorded in dmso-d_6 showing two distinct species in solution with ratios of **7b** (51%) and **7b'** (49%).
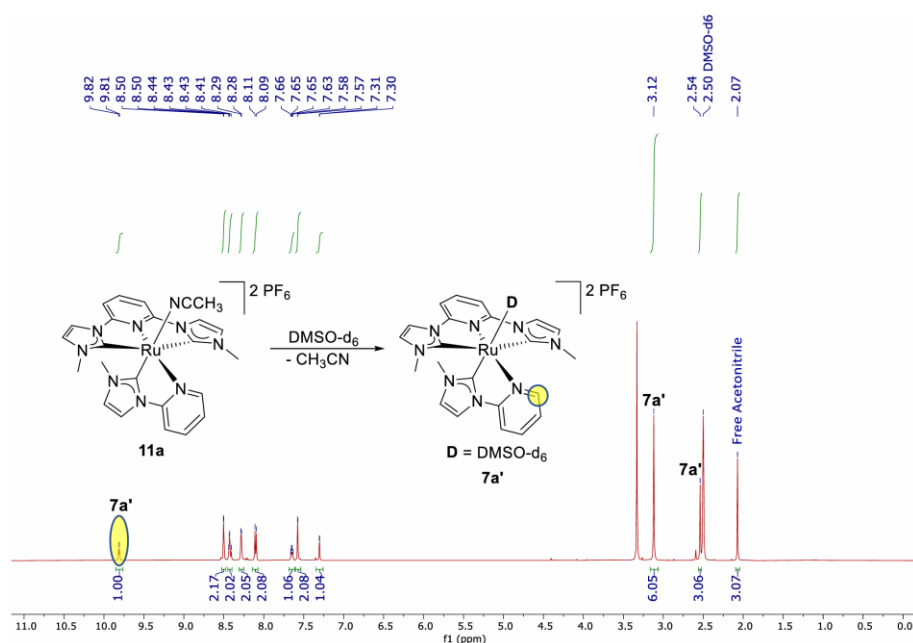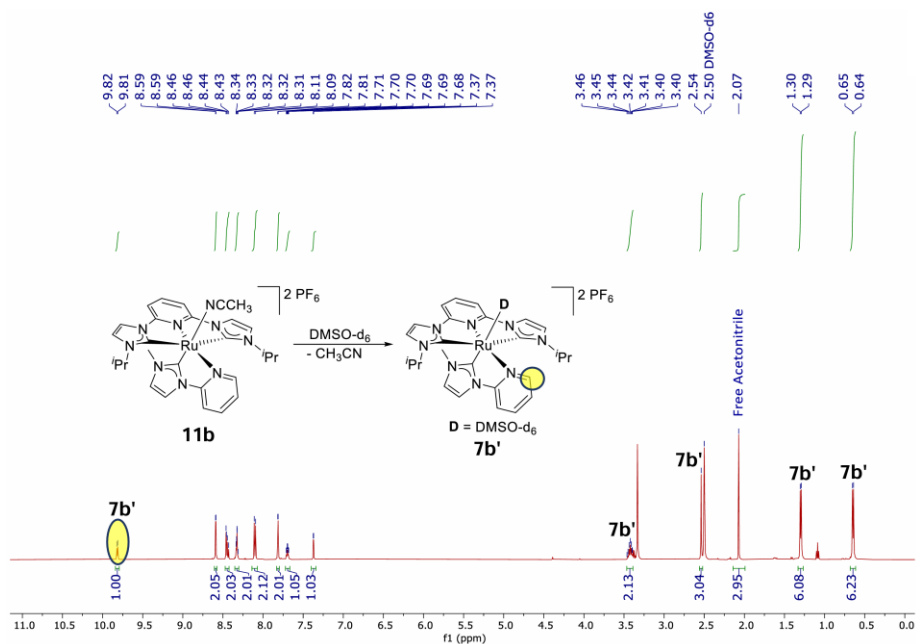

Figure 4.8. ^{1}H NMR spectrum of complex **11b** in dmso-d_6 supporting the *in-situ* generation of complex **7b'** with dissociated acetonitrile.
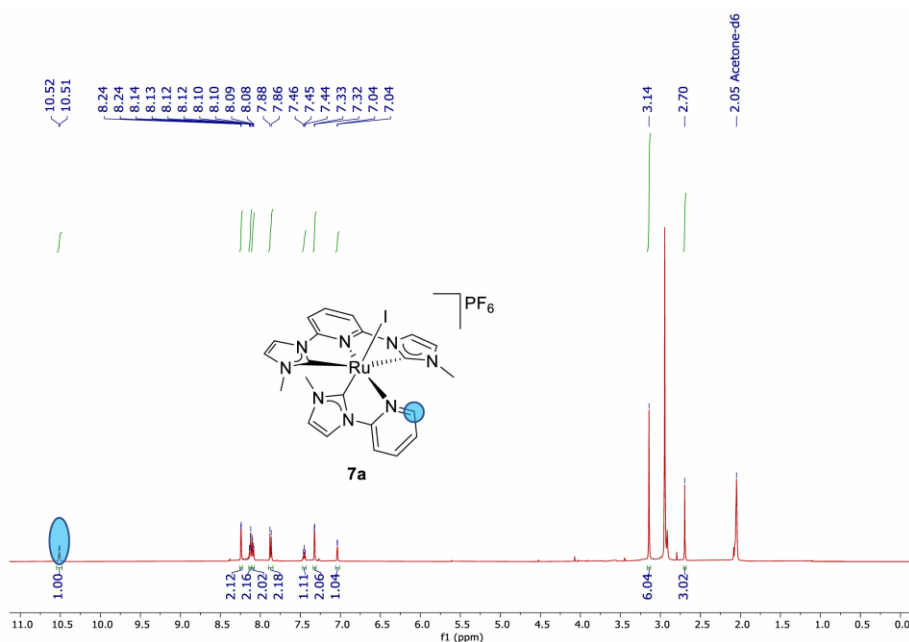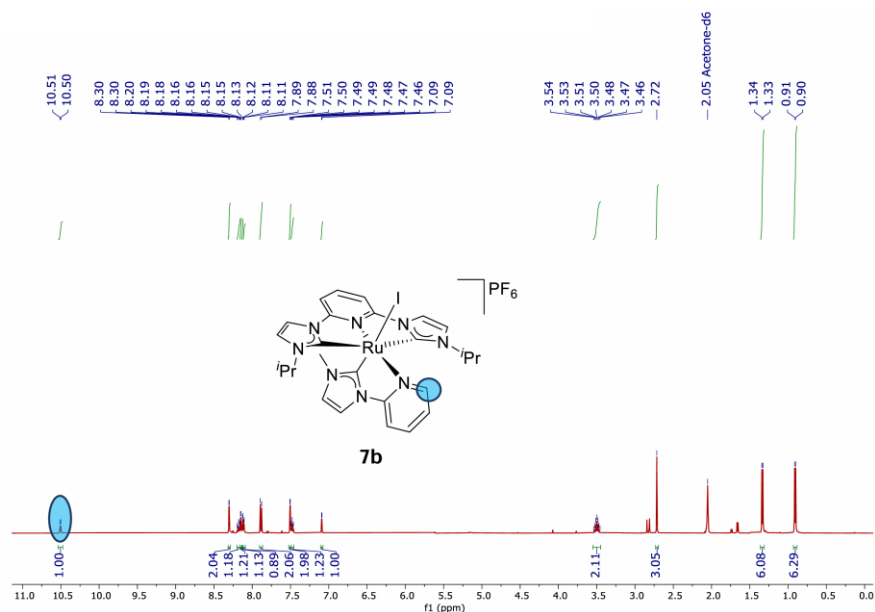
Figure 4.9. ¹H NMR spectrum of complex **7b** recorded in acetone-d₆.

The ¹H NMR spectrum of complexes **7c** and **8c** show a doublet for *ortho* protons of bidentate ligand at 10.57 and 10.59 ppm, similar to the previously reported complex [Ru(CNC$^{n\text{-Bu}}$)(CN$^{n\text{-Bu}}$)Br]PF₆ [41]. The aliphatic proton of cyclohexyl for methine proton appears as a multiplet at 3.11 – 3.05 ppm and 2.91 – 2.84 ppm, and the other peaks for cyclohexyl appear at their expected position in the aliphatic region. The methyl proton of bidentate ligand in complex **7c** appears at 2.71 ppm, while the isopropyl group of complex **8c** appears as a multiplet at 3.04 – 3.02 ppm for methine proton and a doublet for methyl proton at 0.81 ppm. In the ¹³C NMR spectrum of **7c** and **8c**, the carbene carbon signals appear at 193.99 and 194.09 ppm for CNC and CN bidentate ligand at 191.91 and 190.04 ppm, similar to **7b** and **8b**, and previously reported ruthenium complex [41]. ³¹P NMR spectrum shows peaks at -144.25 and -144.24 ppm for PF₆⁻ counterion, and their splitting as a septate due to coupling with six ¹⁹F nuclei. HRMS of complexes **7c** and **8c**, in acetonitrile displayed ESI⁺ signals at m/z 763.1314 and 791.1618, respectively, assigned to [M-PF₆]⁺.

In the ¹H NMR spectrum of complexes **7d** and **8d**, a doublet appears at 10.14 and 10.21 ppm for the *ortho* protons of the pyridine

ring of the bidentate ligand. A singlet appears at 1.16 and 1.15 ppm for the aliphatic proton of the *t*-butyl group, respectively. The bidentate methyl proton of **7d** resonates at 2.73 ppm, while the isopropyl proton of **8d** appears as a multiplet at 2.96 – 2.90 ppm for methine proton and a doublet at 0.82 ppm for methyl protons. The CNC carbene carbon signals in ^{13}C NMR appear at 189.90 and 190.10 ppm for **7d** and **8d**, respectively, while the carbene signals for CN ligand appear at 192.32 and 190.52 ppm for **7d** and **8d**, respectively. ^{31}P NMR spectrum shows peaks at -144.23 and -144.22 ppm for PF_6^- counterion, and their splitting as a septate due to coupling with six ^{19}F nuclei. The HRMS of complexes **7d** and **8d**, in acetonitrile show an ESI$^+$ signal at m/z 711.0997 and 739.1301, respectively, assigned to $[M-PF_6]^+$.

4.2.5. Description of the crystal structure of complexes 7b and 7c

The molecular structures of complexes **7b** and **7c** have been confirmed by X-ray crystal diffraction analysis, and their structural parameters and final refinements for the complexes are given in Table **4.3**. Some selected bond lengths and bond angles are shown in Table **4.4**.
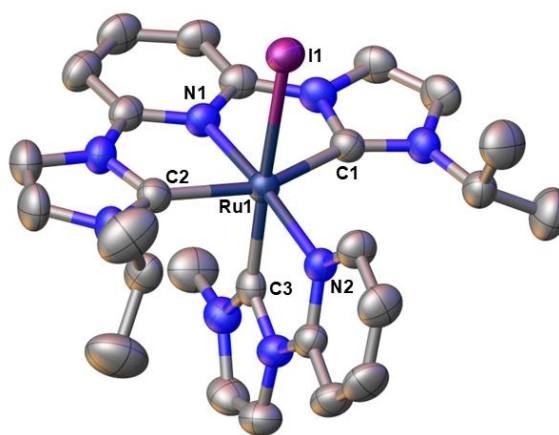
Figure 4.10. Single crystal X-ray structure of complex **7b**. All hydrogen atoms and one PF_6^- counter-anion are omitted for clarity. Selected bond lengths (Å) and angles (°): Ru1-C1, 2.059(2); Ru1-C2,

2.055(3); Ru1-C3, 1.984(3); Ru1-N1, 2.003(2); Ru1-N2, 2.114(2); Ru1-I1, 2.8149(3), C1-Ru1-N1, 77.79(9); C2-Ru1-I1, 88.18(8); C1-Ru1-N2, 105.47(9); C1-Ru1-C2, 155.28(10); C3-Ru1-I1, 173.21(8) and N1-Ru1-N2, 175.07(9).
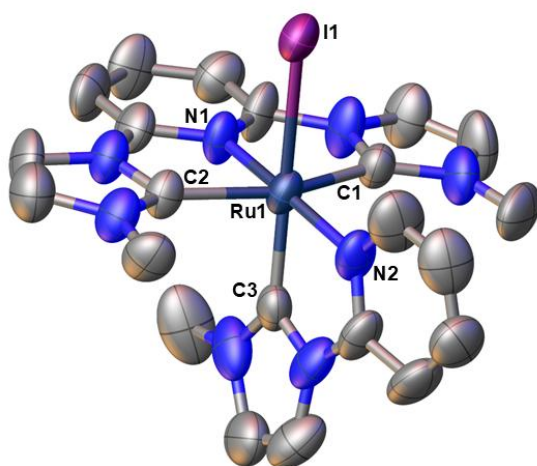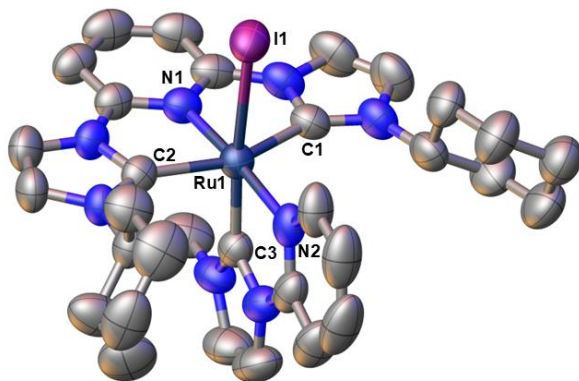

Figure 4.11. Single crystal X-ray structure of complex **7c**. All hydrogen atoms and one PF_6^- counter-anion are omitted for clarity. Selected bond lengths (Å) and angles (°): Ru1-C1, 2.047(6); Ru1-C2, 2.054(6); Ru1-C3, 1.964(6); Ru1-N1, 1.993(5); Ru1-N2, 2.095(5); Ru1-I1, 2.8148(7), C1-Ru1-N1, 77.9(2); C2-Ru1-I1, 90.28(15); C1-Ru1-N2, 105.0(2); C1-Ru1-C2, 155.3(2); C2-Ru1-N2, 99.69(19); C2-Ru1-C3, 92.2(2); C3-Ru1-I1, 173.63(17); N2-Ru1-I1, 96.30(15) and N1-Ru1-N2, 175.5(2).

Complexes **7b** and **7c** crystallized in a monoclinic system with a P2$_1$/c space group with a ruthenium metal center in a distorted octahedral geometry. The structure of both the complexes **7b** and **7c** consists of two almost planar five-membered metallacycles of the CNC pincer ligand, one five-membered metallacycle of the CN^{Me} ligand, and I$^-$ ion, which occupies the sixth coordination position around the ruthenium atom (Figure **4.10** and **4.11**). The CNC ligand is a tridentate chelating ligand that occupies three meridional sites with C1-Ru1-C2 angles 155.28(10)° in **7b** and 155.3(2)° in **7c**, and their bite angles of C1-Ru1-N1 are 77.79(9)° in **7b** and 77.9(2)° in **7c**, while CN ligand is

bidentate ligand occupies two sites at the ruthenium center, in which pyridine-pyridine are *trans* to each other with bite angles of N2-Ru1-C3 are 77.48(10)° in **7b** and 77.5(2)° in **7c**, similar to our previously reported complexes [36]. Notably, the Ru-I bond trans to carbene with bond lengths 2.8149 Å in **7b** and 2.8148 Å in **7c**, are longer than a previously reported complex Ru-I, 2.7671 Å [42], indicating the labile nature of the iodide ligand due to the greater trans effect of the carbenes. The bond lengths of Ru-N of the pyridine group (~1.9 - 2.1 Å) [36] are similar to the previously reported metal complexes whereas Ru–C(NHC) bond lengths (~1.9 - 2.1 Å) [36] are also similar to the analogous complexes [37].

Table 4.3. Crystal data and structure refinement parameters of complexes **7b** and **7c**.

	7b	7c
Empirical formula	$C_{27}H_{34}N_8ORuIPF_6$	$C_{32}H_{38}N_8RuIPF_6$
T/K	300	300
Crystal System	monoclinic	monoclinic
Space Group	$P2_1/c$	$P2_1/c$
a/Å	9.4855(2)	9.4252(9)
b/Å	25.4311(6)	22.344(2)
c/Å	13.8955(4)	17.0298(18)
α/°	90	90
β/°	95.388(3)	90.948(4)
γ/°	90	90
V/Å³	3337.15(14)	3585.9(6)
Z	4	4
ρ_{calc}g/cm³	1.711	1.681
λ/Å (Mo-Kα)	0.71073	0.71073
Reflections Collected	38907	42475
Data/restr./param.	8765/0/393	7870/0/443
R (int)	0.0386	0.0752
Final R indices [I>2σ(I)]	$R_1 = 0.0354$, $wR_2 = 0.0867$	$R_1 = 0.0526$, $wR_2 = 0.1039$
R indices (all data)	$R_1 = 0.0508$, $wR_2 = 0.0914$	$R_1 = 0.1085$, $wR_2 = 0.1247$
GOF on F2	1.079	1.028

Table 4.4. Selected bond lengths and bond angles of complexes **7b** and **7c**.

Complex	Bond lengths (Å)	Bond angles (°)
7b	Ru1-C1, 2.059(2) Ru1-C2, 2.055(3) Ru1-C3, 1.984(3) Ru1-N1, 2.003(2) Ru1-N2, 2.114(2) Ru1-I1, 2.8149(3)	C1-Ru1-I1, 88.64(8) C1-Ru1-C3, 95.10(10) C1-Ru1-N2, 105.47(9) C1-Ru1-C2, 155.28(10) C1-Ru1-N1, 77.79(9) C2-Ru1-I1, 88.18(8) C2-Ru1-C3, 90.74(10) C2-Ru1-N2, 99.24(9) C3-Ru1-I1, 173.21(8) N1-Ru1-I1, 87.64(7) N1-Ru1-C3, 98.67(10) N1-Ru1-N2, 175.07(9) N1-Ru1-C2, 77.59(10) N2-Ru1-I1, 96.08(6) N2-Ru1-C3, 77.48(10)
7c	Ru1-C1, 2.047(6) Ru1-C2, 2.054(6) Ru1-C3, 1.964(6) Ru1-N1, 1.993(5) Ru1-N2, 2.095(5) Ru1-I1, 2.8148(7)	C1-Ru1-I1, 87.48(16) C1-Ru1-C3, 92.7(2) C1-Ru1-N2, 105.0(2) C1-Ru1-C2, 155.3(2) C1-Ru1-N1, 77.9(2) C2-Ru1-I1, 90.28(15) C2-Ru1-C3, 92.2(2) C2-Ru1-N2, 99.69(19) C3-Ru1-I1, 173.63(17) N1-Ru1-I1, 87.20(13) N1-Ru1-C3, 99.1(2) N1-Ru1-N2, 175.5(2) N1-Ru1-C2, 77.5(2) N2-Ru1-I1, 96.30(15) N2-Ru1-C3, 77.5(2)

4.3. Conclusion

In summary, a series of new electron-rich, phosphine-free complexes $[Ru(CNC^{Me})(CN^{Me})I]PF_6$ (**7a**), $[Ru(CNC^{i-Pr})(CN^{Me})I]PF_6$ (**7b**), $[Ru(CNC^{Cy})(CN^{Me})I]PF_6$ (**7c**), $[Ru(CNC^{t-Bu})(CN^{Me})I]PF_6$ (**7d**), $[Ru(CNC^{Me})(CN^{i-Pr})I]PF_6$ (**8a**), $[Ru(CNC^{i-Pr})(CN^{i-Pr})I]PF_6$ (**8b**), $[Ru(CNC^{Cy})(CN^{i-Pr})I]PF_6$ (**8c**), $[Ru(CNC^{t-Bu})(CN^{i-Pr})I]PF_6$ (**8d**), $[Ru(CNC^{Me})(Py-Bim^{Me})I]PF_6$ (**9a**), and $[Ru(CNC^{Me})(3MePy-Im^{Me})I]PF_6$ (**10a**) have been synthesized and characterized. These complexes feature multiple *N*-heterocyclic carbene (NHC) ligands,

with CNC (2,6-bis(alkylimidazol-2-ylidene)-pyridine) and CN [(2-(3-alkylimidazol-2-ylidene)-pyridine), (2-(3-methylbenzaimidazol-2-ylidene)-pyridine) and (2-(3-methylimidazol-2-ylidene)-3-methyl-pyridine)] as key ligands. The spectroscopic characterization of all complexes was performed using multinuclear NMR and high-resolution mass spectrometry (HRMS) and the molecular structures of $[Ru(CNC^{Me})(CN^{Me})I]PF_6$ (**7a**), $[Ru(CNC^{i\text{-}Pr})(CN^{Me})I]PF_6$ (**7b**) and $[Ru(CNC^{Cy})(CN^{Me})I]PF_6$ (**7c**) have been confirmed by single-crystal X-ray diffraction technique. The existence of only one isomer was confirmed by the spectral studies of $[Ru(CNC^{Me})(CN^{Me})I]PF_6$ (**7a**) and $[Ru(CNC^{Me})(CN^{Me})CH_3CN]PF_6$ (**11a** vide infra) complexes, further confirmed by the NMR spectra of complexes have been recorded in less nucleophilic, non-coordinating solvent acetone-d_6 which shows only one species in the solution.

4.4. Experimental Section

4.4.1. General Considerations

All reactions were carried out under an inert atmosphere using the standard Schlenk line techniques. Solvents were purchased from S. D. Fine-Chem Limited and purified by distillation under an inert atmosphere. $[Ru(CN^{Me})(H_2O)Cl_3]$, $[Ru(CN^{i\text{-}Pr})(H_2O)Cl_3]$, $[Ru(Py-Bim^{Me})(H_2O)Cl_3]$ and $[Ru(3MePy-Im^{Me})(H_2O)Cl_3]$ precursors were prepared by our research group using $RuCl_3 \cdot 3H_2O$ [37, 43]. $RuCl_3 \cdot 3H_2O$ was purchased from Sigma-Aldrich. Deuterated acetone (Acetone-d_6) and deuterated dimethyl sulphoxide (DMSO-d_6) were purchased from EURISOtop or Sigma-Aldrich. NMR spectra were recorded on Bruker Avance (III) spectrometer and Bruker Avance NEO spectrometer operating at 400 and 500 MHz for ^1H, 162 and 202 MHz for ^{31}P, and 101 and 126 MHz for ^{13}C NMR, respectively. NMR chemical shifts are reported in ppm and referenced to the solvent peaks for ^1H (acetone-d_6, δ 2.05 and DMSO-d_6 δ 2.50 ppm) and ^{13}C (natural abundance of ^{13}C in acetone-d_6, δ 29.84 and δ 206.26 and DMSO-d_6 δ

39.52 ppm). ^{31}P NMR chemical shifts are referenced to an external 85% H_3PO_4 standard as 0 ppm. Multiplicities are given as s (singlet), d (doublet), t (triplet), and m (multiplet), and the coupling constants J are given in hertz. The mass chromatograms were recorded on Bruker-Daltonics-MicroTOF-QII mass spectrometer in HPLC grade acetonitrile. Elemental analysis was carried out on a Thermo Fischer Scientific FLASH 2000 (formerly the Flash EA1112) is the CHNS-O elemental analyzer.

4.4.2. Preparation of ligand Precursor

The bidentate ligand precursors (Py-Im[Me] or CN[Me] = 3-methyl-1-(pyridine-2-yl)imidazol-2-ylidene, Py-Im[i-Pr] or CN[i-Pr] = 3-isopropyl-1-(pyridine-2-yl)imidazol-2-ylidene, Py-Bim[Me] = 3-methyl-1-(pyridine-2-yl)benzimidazol-2-ylidene, and 3MePy-Im[Me] = 3-methyl-1-(3-methylpyridine-2-yl)imidazol-2-ylidene) were synthesized by the previously reported procedures [44–47]. The preparation of different alkyl-substituted pincer ligands (CNC[Me]·2HBr = 2,6-bis[3-(methyl)imidazolium]pyridine dibromide, CNC[i-Pr]·2HBr = 2,6-bis[3-(isopropyl)imidazolium]pyridine dibromide, CNC[Cy]·2HBr = 2,6-bis[3-(cyclohexyl)imidazolium]pyridine dibromide, and CNC[t-Bu]·2HBr = 2,6-bis[3-(*tert*-butyl)imidazolium]pyridine dibromide) was based on the previously reported method [38, 39].

4.4.3. General Procedure for the synthesis of metal complexes

An oven-dried Schlenk tube with a magnetic stirring bar was charged with ligand precursor (1 equiv.), ruthenium precursor (1 equiv.), and NaI (0.149 g, 1mmol) in ethylene glycol (10 mL), the resulted mixture was refluxed under N_2 atmosphere for 4 h. After the reaction was completed, cooled to room temperature and added an aqueous solution of KPF_6 (0.184 g, 1 mmol, 10 mL water), then stirred for 2 min at room temperature. A desired complex was precipitated out, filtered the precipitate, washed with H_2O, and dried under vacuum.

4.4.3.1. Synthesis of Complex (7a) [Ru(CNC^{Me})(CN^{Me})I]PF$_6$

Complex (**7a**) was prepared by the general procedure of complex synthesis, from 2,6-bis[3-(methyl)imidazolium]pyridine dibromide (0.100 g, 0.25 mmol) and [Ru(CN^{Me})(H$_2$O)Cl$_3$] (0.096 g, 0.25 mmol) to give the desired complex as a yellowish orange solid. The X-ray quality crystals of complex **7a** and *cis*-**7a** were obtained by slow diffusion of diethyl ether in methanol solution at 4 ˚C. Yield = 0.129 g (67%). ^{1}H NMR (400 MHz, DMSO-d$_6$, complex **7a** : **7a'** ratio 45 : 55) δ 10.27 (d, J = 5.7 Hz, 1H) (**7a**), 9.81 (d, J = 5.8 Hz, 1H) (**7a'**), 8.51 (d, J = 1.9 Hz, 2H), 8.45 – 8.40 (m, 4H), 8.30 – 8.25 (m, 3H), 8.17 – 8.14 (m, 2H), 8.11 (d, J = 8.3 Hz, 3H), 7.96 (d, J = 8.1 Hz, 2H), 7.67 – 7.63 (m, 1H), 7.58 (d, J = 2.0 Hz, 2H), 7.47 – 7.45 (m, 1H), 7.42 (d, J = 2.1 Hz, 2H), 7.31 (d, J = 2.3 Hz, 1H), 7.13 (d, J = 2.2 Hz, 1H), 3.12 (s, 6H) (**7a'**), 2.99 (s, 6H) (**7a**), 2.55 (s, 3H) (**7a'**), 2.51 (s, 3H) (**7a**). ^{13}C NMR (126 MHz, DMSO-d$_6$) δ 193.30, 188.90, 187.04, 183.34, 156.06, 153.56, 153.38, 152.49, 152.13, 151.93, 141.56, 139.00, 137.76, 136.92, 125.98, 125.37, 124.55, 124.23, 122.49, 121.24, 118.67, 117.59, 117.09, 116.40, 115.26, 112.72, 107.95, 105.46, 35.84, 35.31, 34.17, 33.73. ^{31}P NMR (202 MHz, DMSO-d$_6$) δ -144.20. ^{1}H NMR (500 MHz, Acetone-d$_6$) δ 10.51 (d, J = 5.8 Hz, 1H), 8.24 (d, J = 2.2 Hz, 2H), 8.14 – 8.12 (m, 2H), 8.10 – 8.08 (m, 2H), 7.87 (d, J = 8.1 Hz, 2H), 7.45 (t, J = 6.4 Hz, 1H), 7.32 (d, J = 2.2 Hz, 2H), 7.04 (d, J = 2.3 Hz, 1H), 3.14 (s, 6H), 2.70 (s, 3H). ^{13}C NMR (126 MHz, Acetone-d$_6$) δ 195.44, 191.08, 157.87, 154.99, 153.38, 138.39, 137.74, 125.18, 124.97, 121.98, 117.52, 115.68, 111.85, 106.17, 36.24, 34.72. ^{31}P NMR (202 MHz, Acetone-d$_6$) δ -144.24. HRMS for [M-PF$_6$]$^+$ [C$_{22}$H$_{22}$N$_8$RuI] calculated - 627.0056, found - 627.0079. Anal. Calcd. for [C$_{22}$H$_{22}$N$_8$RuI]PF$_6$: C 34.25, H 2.87, N 14.53, found: C 34.34, H 2.49, N 14.77%.

4.4.3.2. Synthesis of Complex (8a) [Ru(CNC^{Me})(CN$^{i\text{-}Pr}$)I]PF$_6$

Complex (**8a**) was prepared by the general procedure of complex synthesis, from 2,6-bis[3-(methyl)imidazolium]pyridine dibromide

(0.100 g, 0.25 mmol) and [Ru(CN$^{i\text{-}Pr}$)(H$_2$O)Cl$_3$] (0.103 g, 0.25 mmol) to give the desired complex as a brown-yellow solid. Yield = 0.130 g (65%). ^{1}H NMR (500 MHz, Acetone-d$_6$) δ 10.52 (d, J = 5.8 Hz, 1H), 8.26 (d, J = 2.2 Hz, 2H), 8.20 (d, J = 2.5 Hz, 1H), 8.15 – 8.13 (m, 1H), 8.12 – 8.10 (m, 2H), 7.88 (d, J = 8.1 Hz, 2H), 7.46 – 7.43 (m, 1H), 7.35 (d, J = 2.2 Hz, 2H), 7.26 (d, J = 2.5 Hz, 1H), 3.14 (s, 6H), 2.88 – 2.81 (m, 1H), 0.82 (d, J = 6.8 Hz, 6H). ^{13}C NMR (126 MHz, Acetone-d$_6$) δ 195.58, 188.96, 157.86, 154.94, 153.18, 138.68, 137.81, 125.20, 121.90, 119.16, 117.44, 116.94, 111.91, 106.01, 50.40, 36.23, 22.28. ^{31}P NMR (202 MHz, Acetone-d$_6$) δ -144.20. HRMS for [M-PF$_6$]$^+$ [C$_{24}$H$_{26}$N$_8$RuI] calculated - 655.0369, found - 655.0365. Anal. Calcd. for [C$_{24}$H$_{26}$N$_8$RuI]PF$_6$: C 36.06, H 3.28, N 14.02, found: C 36.39, H 3.19, N 13.89%.

4.4.3.3. Synthesis of Complex (9a) [Ru(CNC^{Me})(Py-Bim^{Me})I]PF$_6$

Complex (**9a**) was prepared by the general procedure of complex synthesis, from 2,6-bis[3-(methyl)imidazolium]pyridine dibromide (0.036 g, 0.11 mmol) and [Ru(Py-Bim^{Me})(H$_2$O)Cl$_3$] (0.050 g, 0.11 mmol) to give the desired complex as a green-yellow solid. Yield = 0.042 g (46%). ^{1}H NMR (500 MHz, Acetone-d$_6$) δ 10.68 (d, J = 5.2 Hz, 1H), 8.58 (d, J = 8.4 Hz, 1H), 8.30 – 8.24 (m, 4H), 8.21 – 8.17 (m, 1H), 7.94 (d, J = 8.2 Hz, 2H), 7.52 – 7.49 (m, 1H), 7.41 – 7.35 (m, 3H), 7.31 (d, J = 2.2 Hz, 2H), 3.15 (s, 6H), 2.89 (s, 3H). ^{13}C NMR (126 MHz, Acetone-d$_6$) δ 203.32, 194.00, 158.40, 154.80, 154.09, 139.13, 138.15, 137.31, 131.65, 125.13, 124.91, 123.99, 121.60, 117.67, 112.84, 112.02, 110.33, 106.63, 36.31, 31.29. ^{31}P NMR (202 MHz, Acetone-d$_6$) δ -144.22. HRMS for [M-PF$_6$]$^+$ [C$_{26}$H$_{24}$N$_8$RuI] calculated - 677.0213, found - 677.0214. Anal. Calcd. for [C$_{26}$H$_{24}$N$_8$RuI]PF$_6$: C 38.02, H 2.94, N 13.64, found: C 38.43, H 2.61, N 13.57%.

4.4.3.4. Synthesis of Complex (10a) [Ru(CNC^Me)(3MePy-Im^Me)I]PF$_6$

Complex (**10a**) was prepared by the general procedure of complex synthesis, from 2,6-bis[3-(methyl)imidazolium]pyridine dibromide (0.044 g, 0.11 mmol), [Ru(3MePy-Im^Me)(H$_2$O)Cl$_3$] (0.044 g, 0.11 mmol) to give the desired complex as a brownish-green solid. Yield = 0.049 g (57%). ^{1}H NMR (500 MHz, Acetone-d$_6$) δ 10.57 (d, J = 5.5 Hz, 1H), 8.25 (d, J = 2.2 Hz, 2H), 8.21 (d, J = 2.5 Hz, 1H), 8.10 (t, J = 8.1 Hz, 1H), 7.94 (d, J = 6.2 Hz, 1H), 7.87 (d, J = 8.2 Hz, 2H), 7.34 – 7.31 (m, 3H), 7.03 (d, J = 2.4 Hz, 1H), 3.13 (s, 6H), 2.90 (s, 3H), 2.69 (s, 3H). ^{13}C NMR (126 MHz, Acetone-d$_6$) δ 195.48, 192.63, 156.32, 154.93, 152.46, 140.99, 138.38, 124.96, 124.26, 123.59, 121.39, 118.80, 117.53, 106.22, 36.25, 34.79, 20.98. ^{31}P NMR (202 MHz, Acetone-d$_6$) δ -144.25. HRMS for [M-PF$_6$]$^+$ [C$_{23}$H$_{24}$N$_8$RuI] calculated - 641.0212, found - 641.0232. Anal. Calcd. for [C$_{23}$H$_{24}$N$_8$RuI]PF$_6$: C 35.17, H 3.08, N 14.27, found: C 35.41, H 2.91, N 14.65%.

4.4.3.5. Synthesis of Complex (7b) [Ru(CNC^{i-Pr})(CN^Me)I]PF$_6$

Complex (**7b**) was prepared by the general procedure of complex synthesis, from 2,6-bis[3-(isopropyl)imidazolium]pyridine dibromide (0.114 g, 0.25 mmol) and [Ru(CN^Me)(H$_2$O)Cl$_3$] (0.096 g, 0.25 mmol) to give the desired complex as a dark yellow solid. The X-ray quality crystals of **7b** were obtained by slow diffusion of diethyl ether in methanol solution at 0 ˚C. Yield = 0.139 g (67%). ^{1}H NMR (500 MHz, DMSO-d$_6$, complex **7b** : **7b'** ratio 51 : 49) δ 10.25 (d, J = 5.5 Hz, 1H) (**7b**), 9.81 (d, J = 5.7 Hz, 1H) (**7b'**), 8.60 – 8.59 (m, 2H), 8.49 – 8.45 (m, 4H), 8.33 – 8.30 (m, 3H), 8.17 – 8.14 (m, 3H), 8.11 (d, J = 8.1 Hz, 2H), 7.95 (d, J = 7.9 Hz, 2H), 7.82 (m, 2H), 7.70 – 7.69 (m, 1H), 7.61 (d, J = 7.8 Hz, 2H), 7.49 – 7.48 (m, 1H), 7.38 (m, 1H), 7.17 (m, 1H), 3.44 – 3.39 (m, 2H) (**7b'**), 3.29 – 3.26 (m, 2H) (**7b**), 2.54 (s, 6H), 1.30 (d, J = 6.4 Hz, 6H) (**7b'**), 1.22 (d, J = 6.4 Hz, 6H) (**7b**), 0.76 (d, J = 6.4 Hz, 6H) (**7b**), 0.64 (d, J = 6.3 Hz, 6H) (**7b'**). ^{13}C NMR (126 MHz,

DMSO-d$_6$) δ 191.64, 189.39, 185.20, 183.54, 156.21, 153.39, 153.22, 152.77, 152.17, 152.06, 141.74, 139.44, 137.88, 137.25, 126.64, 124.97, 122.83, 121.17, 120.26, 119.46, 119.11, 117.66, 115.94, 115.00, 112.37, 110.90, 108.00, 105.41, 51.98, 51.24, 34.33, 33.82, 22.82, 22.05, 22.02, 21.15. ^{31}P NMR (202 MHz, DMSO-d$_6$) δ -144.18. ^{1}H NMR (500 MHz, Acetone-d$_6$) δ 10.51 (d, J = 5.3 Hz, 1H), 8.30 (d, J = 2.2 Hz, 2H), 8.20 – 8.16 (m, 1H), 8.15 (d, J = 2.3 Hz, 1H), 8.12 (d, J = 2.5 Hz, 1H), 8.11 (d, J = 2.7 Hz, 1H), 7.89 (d, J = 8.2 Hz, 2H), 7.50 (d, J = 2.3 Hz, 2H), 7.50 – 7.46 (m, 1H), 7.09 (d, J = 2.3 Hz, 1H), 3.54 – 3.46 (m, 2H), 2.72 (s, 3H), 1.34 (d, J = 6.8 Hz, 6H), 0.91 (d, J = 6.9 Hz, 6H). ^{13}C NMR (126 MHz, Acetone-d$_6$) δ 193.87, 191.59, 158.08, 154.86, 153.52, 138.48, 137.99, 125.62, 121.98, 119.54, 118.12, 115.52, 111.68, 106.13, 52.66, 34.83, 22.74, 22.58. ^{31}P NMR (202 MHz, Acetone-d$_6$) δ -144.24 (s). HRMS for [M-PF$_6$]$^+$ [C$_{26}$H$_{30}$N$_8$RuI] calculated - 683.0683, found - 683.0699. Anal. Calcd. for [C$_{26}$H$_{30}$N$_8$RuI]PF$_6$: C 37.74, H 3.65, N 13.54, found: C 37.48, H 3.38, N 13.27%.

4.4.3.6. Synthesis of Complex (8b) [Ru(CNC$^{i\text{-}Pr}$)(CN$^{i\text{-}Pr}$)I]PF$_6$

Complex (**8b**) was prepared by the general procedure of complex synthesis, from 2,6-bis[3-(isopropyl)imidazolium]pyridine dibromide (0.114 g, 0.25 mmol) and [Ru(CN$^{i\text{-}Pr}$)(H$_2$O)Cl$_3$] (0.103 g, 0.25 mmol) to give the desired complex as a light yellow solid. Yield = 0.127 g (59 %). ^{1}H NMR (500 MHz, Acetone-d$_6$) δ 10.54 (d, J = 6.0 Hz, 1H), 8.34 (d, J = 2.5 Hz, 2H), 8.27 (d, J = 2.5 Hz, 1H), 8.20 – 8.13 (m, 3H), 7.90 (d, J = 8.1 Hz, 2H), 7.53 (d, J = 2.4 Hz, 2H), 7.46 (t, J = 6.5 Hz, 1H), 7.34 (d, J = 2.5 Hz, 1H), 3.48 – 3.40 (m, 2H), 2.96 – 2.90 (m, 1H), 1.31 (d, J = 6.8 Hz, 6H), 0.89 (d, J = 7.2 Hz, 6H), 0.82 (d, J = 7.3 Hz, 6H). ^{13}C NMR (126 MHz, Acetone-d$_6$) δ 194.07, 189.81, 158.38, 154.85, 153.38, 138.74, 138.09, 121.92, 119.77, 119.66, 118.14, 116.90, 111.74, 105.99, 52.60, 50.54, 22.67, 22.60, 22.23. ^{31}P NMR (202 MHz, Acetone-d$_6$) δ -144.23. HRMS for [M-PF$_6$]$^+$ [C$_{28}$H$_{34}$N$_8$RuI] calculated - 711.0996, found - 711.0995. Anal. Calcd. for

$[C_{28}H_{34}N_8RuI]PF_6$: C 39.31, H 4.01, N 13.10, found: C 39.45, H 3.89, N 12.93%.

4.4.3.7. Synthesis of Complex (7c) [Ru(CNC^{Cy})(CN^{Me})I]PF$_6$

Complex (**7c**) was prepared by the general procedure of complex synthesis, from 2,6-bis[3-(cyclohexyl)imidazolium]pyridine dibromide (0.134 g, 0.25 mmol) and [Ru(CN^{Me})(H$_2$O)Cl$_3$] (0.096 g, 0.25 mmol) to give the desired complex as a greenish-yellow solid. The X-ray quality crystals of **7c** were obtained by slow diffusion of diethyl ether in methanol solution at 0 ˚C. Yield = 0.147 g (65%). ^{1}H NMR (500 MHz, Acetone-d$_6$) δ 10.57 (d, J = 5.7 Hz, 1H), 8.29 (d, J = 2.2 Hz, 2H), 8.24 (m, 2H), 8.19 (d, J = 2.3 Hz, 1H), 8.13 (t, J = 8.1 Hz, 1H), 7.88 (d, J = 8.2 Hz, 2H), 7.60 (m, 1H), 7.48 (d, J = 2.3 Hz, 2H), 7.10 (d, J = 2.3 Hz, 1H), 3.11 – 3.05 (m, 2H), 2.71 (s, 3H), 1.75 – 1.73 (m, 2H), 1.60 – 1.49 (m, 5H), 1.47 – 1.44 (m, 4H), 1.07 – 1.03 (m, 5H), 0.88 – 0.82 (m, 2H), 0.54 – 0.46 (m, 2H). ^{13}C NMR (126 MHz, Acetone-d$_6$) δ 193.99, 191.91, 158.40, 154.87, 153.58, 138.55, 137.93, 125.66, 122.40, 120.09, 118.06, 115.45, 111.92, 106.16, 60.34, 34.87, 33.80, 33.31, 26.26, 26.23, 25.40. ^{31}P NMR (202 MHz, Acetone-d$_6$) δ -144.25. HRMS for [M-PF$_6$]$^+$ [C$_{32}$H$_{38}$N$_8$RuI] calculated -763.1311, found - 763.1314. Anal. Calcd. for [C$_{32}$H$_{38}$N$_8$RuI]PF$_6$: C 42.35, H 4.22, N 12.35, found: C 42.48, H 4.18, N 12.59%.

4.4.3.8. Synthesis of Complex (8c) [Ru(CNC^{Cy})(CN$^{i\text{-}Pr}$)I]PF$_6$

Complex (**8c**) was prepared by the general procedure of complex synthesis, from 2,6-bis[3-(cyclohexyl)imidazolium]pyridine dibromide (0.134 g, 0.25 mmol) and [Ru(CN$^{i\text{-}Pr}$)(H$_2$O)Cl$_3$] (0.103 g, 0.25 mmol) to give the desired complex as a greenish-yellow solid. Yield = 0.136 g (58%). ^{1}H NMR (500 MHz, Acetone-d$_6$) δ 10.59 (d, J = 5.9 Hz, 1H), 8.31 (d, J = 2.3 Hz, 2H), 8.30 (d, J = 2.5 Hz, 1H), 8.26 (d, J = 1.7 Hz, 1H), 8.16 – 8.15 (m, 1H), 8.13 (d, J = 8.1 Hz, 1H), 7.89 (d, J = 8.2 Hz, 2H), 7.58 – 7.55 (m, 1H), 7.50 (d, J = 2.3 Hz, 2H), 7.33 (d, J = 2.4 Hz, 1H), 3.04 – 3.02 (m, 1H), 2.91 – 2.84 (m, 2H), 1.74 – 1.70 (m, 3H),

1.60 – 1.55 (m, 5H), 1.47 – 1.42 (m, 4H), 1.06 – 0.97 (m, 4H), 0.81 (d, J = 6.9 Hz, 6H), 0.78 – 0.74 (m, 2H), 0.58 – 0.49 (m, 2H). ^{13}C NMR (126 MHz, Acetone-d_6) δ 194.09, 190.04, 158.57, 154.80, 153.37, 138.82, 137.99, 122.26, 120.32, 119.73, 118.03, 116.72, 111.99, 106.00, 60.29, 50.55, 33.77, 33.23, 26.24, 26.18, 25.62, 25.31, 22.18. ^{31}P NMR (202 MHz, Acetone-d_6) δ -144.24. HRMS for [M-PF$_6$]$^+$ [C$_{34}$H$_{42}$N$_8$RuI] calculated -791.1624, found - 791.1618. Anal. Calcd. for [C$_{34}$H$_{42}$N$_8$RuI]PF$_6$: C 43.64, H 4.52, N 11.98, found: C 43.39, H 4.29, N 12.17%.

4.4.3.9. Synthesis of Complex (7d) [Ru(CNC$^{t\text{-Bu}}$)(CN^{Me})I]PF$_6$

Complex (**7d**) was prepared by the general procedure of complex synthesis, from 2,6-bis[3-(*tert*-Butyl)imidazolium]pyridine dibromide (0.121 g, 0.25 mmol) and [Ru(CN^{Me})(H$_2$O)Cl$_3$] (0.096 g, 0.25 mmol) to give the desired complex as a greenish-yellow solid. Yield = 0.129 g (60%). ^{1}H NMR (500 MHz, Acetone-d_6) δ 10.14 (d, J = 5.9 Hz, 1H), 8.33 (d, J = 2.2 Hz, 2H), 8.20 – 8.15 (m, 2H), 8.13 – 8.11 (m, 3H), 7.99 (d, J = 8.2 Hz, 2H), 7.57 (d, J = 2.2 Hz, 2H), 7.10 (d, J = 2.1 Hz, 1H), 2.73 (s, 3H), 1.16 (s, 18H). ^{13}C NMR (126 MHz, Acetone-d_6) δ 192.32, 189.90, 159.83, 154.66, 154.52, 138.68, 138.35, 126.29, 122.33, 121.77, 116.09, 115.63, 111.95, 106.55, 58.20, 34.81, 31.05. ^{31}P NMR (202 MHz, Acetone-d_6) δ -144.23. HRMS for [M-PF$_6$]$^+$ [C$_{28}$H$_{34}$N$_8$RuI] calculated -711.0996, found - 711.0997. Anal. Calcd. for [C$_{28}$H$_{34}$N$_8$RuI]PF$_6$: C 39.31, H 4.01, N 13.10, found: C 39.69, H 4.32, N 13.28%.

4.4.3.10. Synthesis of Complex (8d) [Ru(CNC$^{t\text{-Bu}}$)(CN$^{i\text{-Pr}}$)I]PF$_6$

Complex (**8d**) was prepared by the general procedure of complex synthesis, from 2,6-bis[3-(*tert*-Butyl)imidazolium]pyridine dibromide (0.121 g, 0.25 mmol) and [Ru(CN$^{i\text{-Pr}}$)(H$_2$O)Cl$_3$] (0.103 g, 0.25 mmol) to give the desired complex as a greenish-yellow solid. Yield = 0.124 g (56%). ^{1}H NMR (500 MHz, Acetone-d_6) δ 10.21 (d, J = 5.9 Hz, 1H), 8.35 (d, J = 2.4 Hz, 2H), 8.22 (d, J = 2.7 Hz, 1H), 8.20 (d, J = 2.4 Hz,

1H), 8.16 – 8.13 (m, 1H), 8.11 – 8.08 (m, 1H), 8.00 (d, J = 8.1 Hz, 2H), 7.59 (d, J = 2.4 Hz, 2H), 7.53 (t, J = 6.4 Hz, 1H), 7.33 (d, J = 2.5 Hz, 1H), 2.96 – 2.90 (m, 1H), 1.15 (s, 18H), 0.82 (d, J = 6.8 Hz, 6H). ^{13}C NMR (126 MHz, Acetone-d_6) δ 190.52, 190.10, 160.09, 158.56, 154.55, 138.90, 138.40, 122.59, 121.76, 120.22, 117.04, 116.06, 111.97, 106.36, 58.16, 50.36, 31.02, 22.31. ^{31}P NMR (202 MHz, Acetone-d_6) δ -144.22. HRMS for $[M-PF_6]^+$ $[C_{30}H_{38}N_8RuI]$ calculated -739.1310, found - 739.1301. Anal. Calcd. for $[C_{30}H_{38}N_8RuI]PF_6$: C 40.78, H 4.33, N 12.68, found: C 40.53, H 4.14, N 12.36%.

4.4.4. X-ray data collection and structure refinement

The crystallographic data of complexes **7a** and ***cis*-7a** were recorded on a dual-core Agilent Technologies (Oxford Diffraction) Super Nova CCD System using a graphite-monochromated Cu Kα radiation (λ = 1.54184 Å) source at room temperature. The other complexes **7b** and **7c** were recorded at room temperature on a Rigaku Oxford Diffractometer XtaLAB Synergy-I with HyPix-Bantam detector and Bruker APEX-II CCD detector with graphite-monochromated Mo Kα radiation (λ = 0.71073 Å), respectively. The data collection was evaluated with the help of CrysAlisPro CCD software. Using Olex2 [48], the structure was solved with the SHELXT [49] structure solution program using Intrinsic Phasing and refined with the SHELXL [50] refinement package using least squares minimization final refinement included atomic positions for all the atoms, anisotropic thermal parameters for all the non-hydrogen atoms, and isotropic thermal parameters for all the hydrogen atoms. For complex **7b**, a solvent mask was calculated, and 68 electrons were found in a volume of 474 Å^3 in one void per unit cell. This is consistent with the presence of one methanol solvent molecule per asymmetric unit which accounts for 72 electrons per unit cell. Structural parameters and final refinements for the complexes are given in Table **4.1** (**7a** and ***cis*-7a**), and Table **4.3** (**7b** and **7c**). Selected bond lengths and bond angles of complexes are given in Table **4.2** (**7a** and ***cis*-7a**) and Table **4.4** (**7b** and **7c**).

4.4.5. Characterisation data of ligand and metal complexes
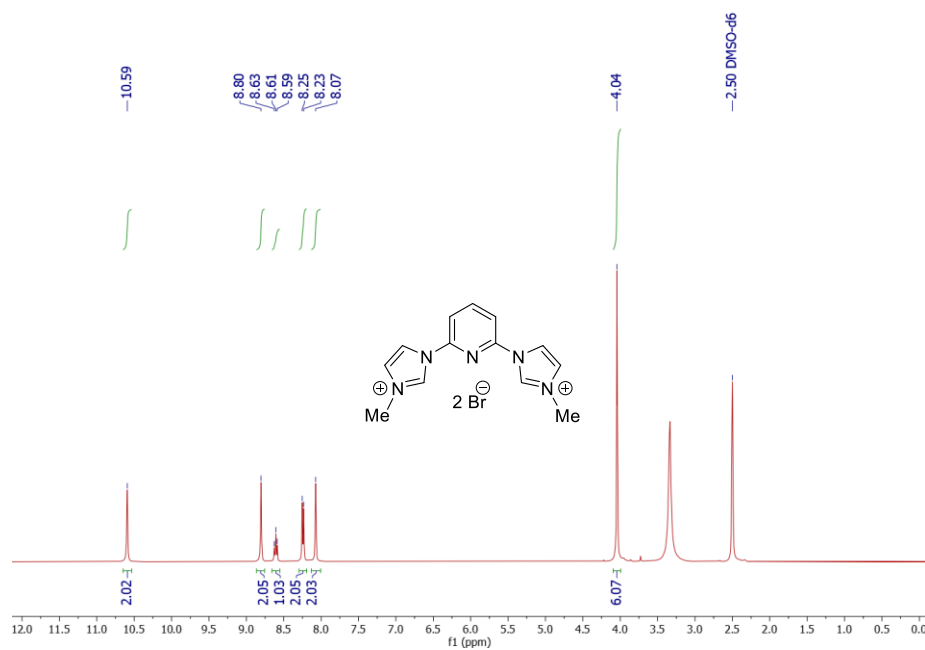
Figure 4.12. ^{1}H NMR spectrum of **CNC^Me·2HBr**.
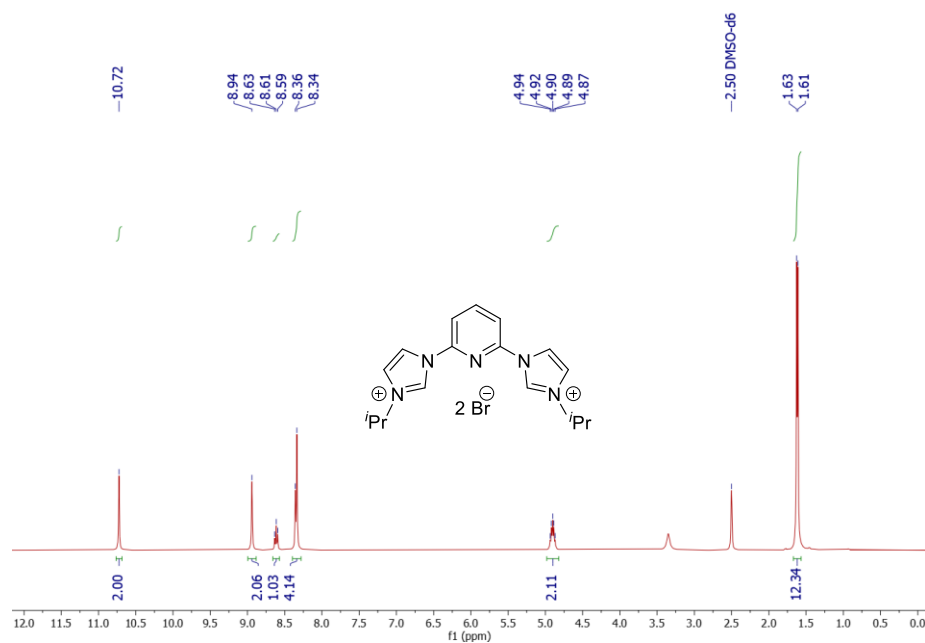
Figure 4.13. ^{1}H NMR spectrum of **CNC^i-Pr·2HBr**.
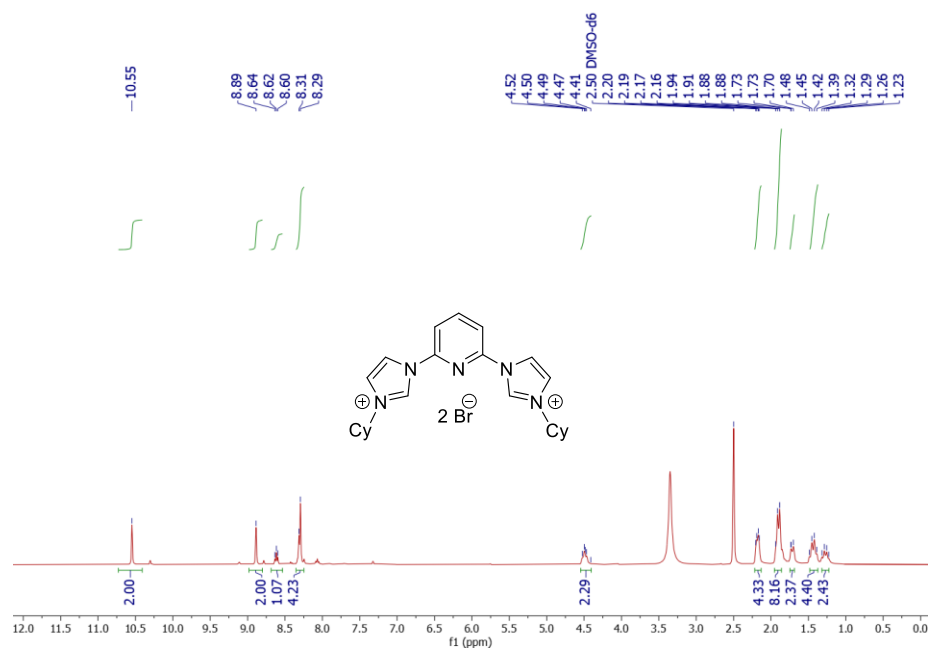
Figure 4.14. ^{1}H NMR spectrum of **CNC^{Cy}·2HBr**.
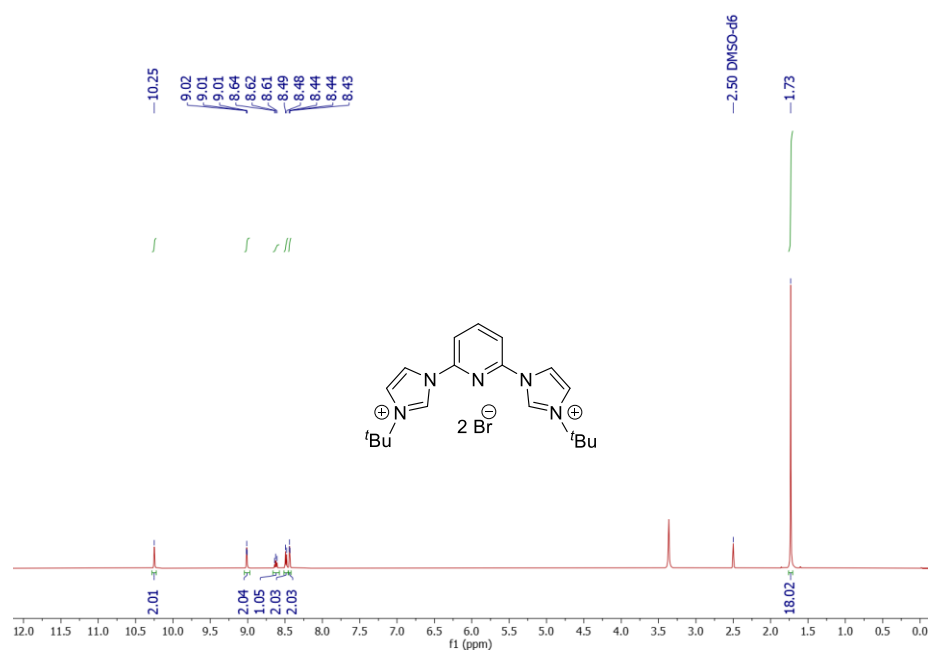
Figure 4.15. ^{1}H NMR spectrum of **CNC$^{t\text{-Bu}}$·2HBr**.
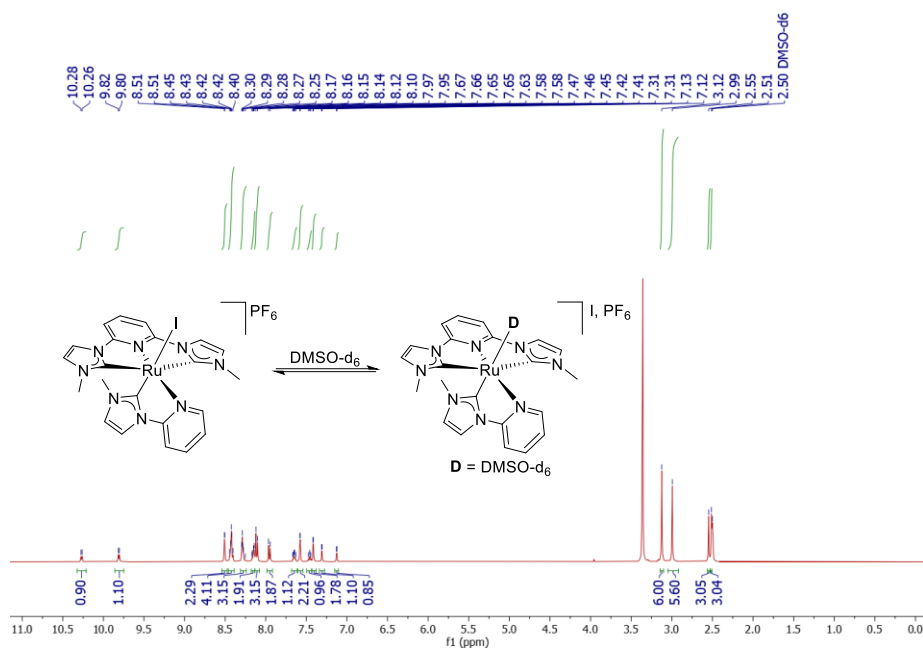
Figure 4.16. ^{1}H NMR spectrum of complex **7a** in dmso-d$_6$.
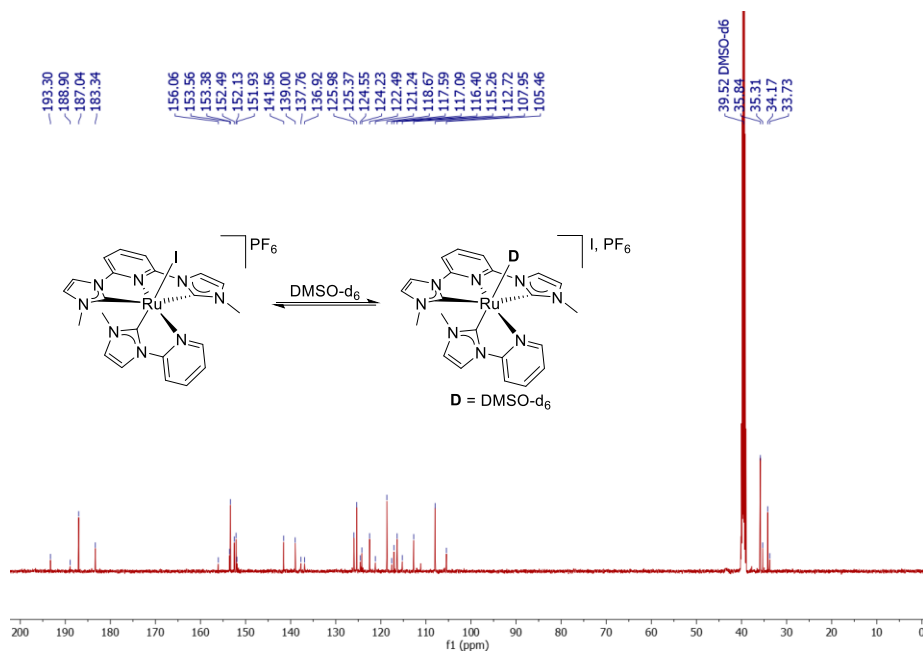
Figure 4.17. ^{13}C NMR spectrum of complex **7a** in dmso-d$_6$.
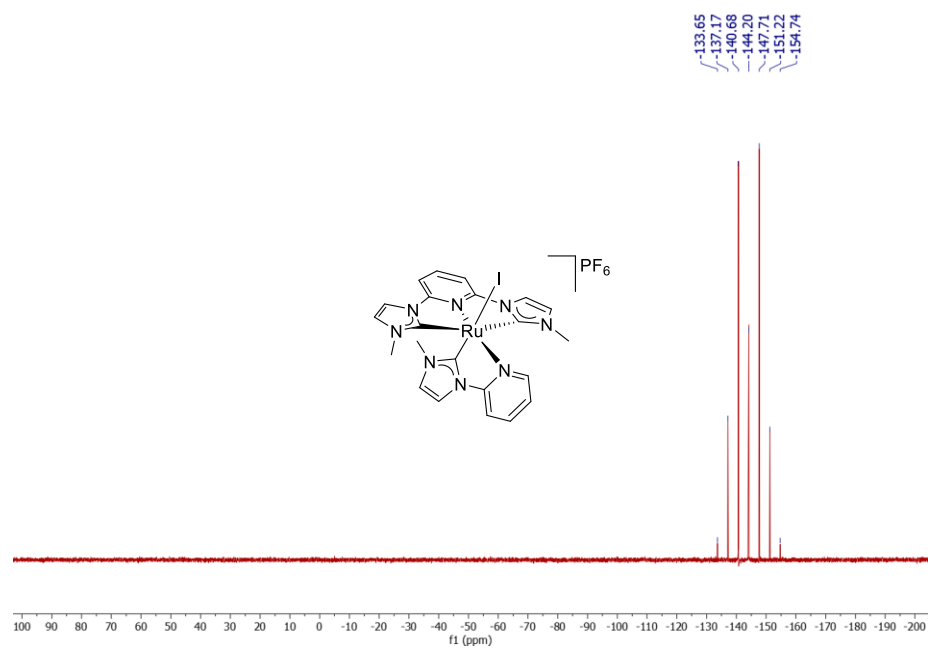
Figure 4.18. ^{31}P NMR spectrum of complex **7a** in dmso-d$_6$.
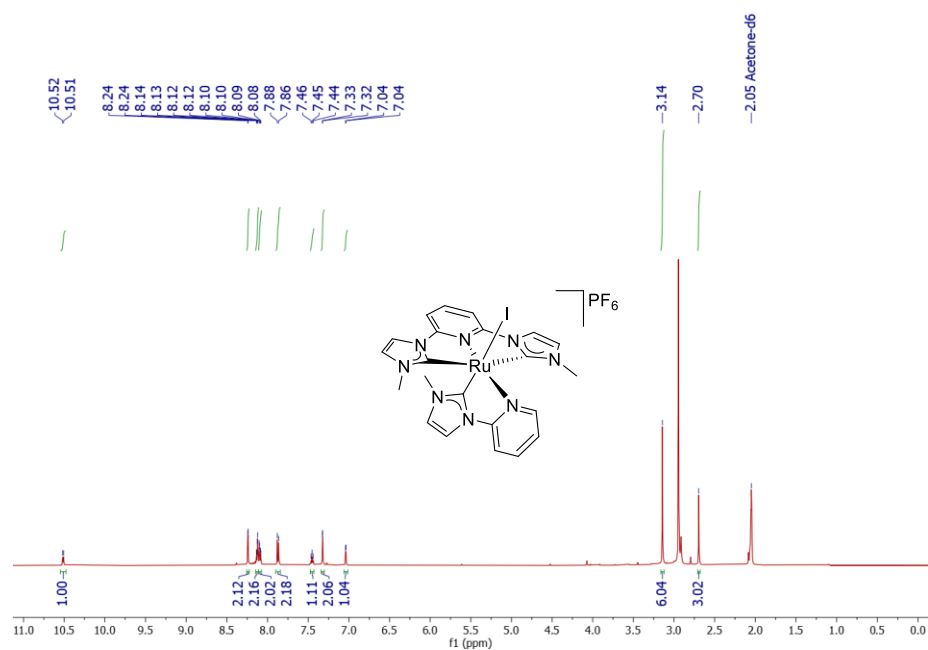
Figure 4.19. ^{1}H NMR spectrum of complex **7a** in acetone-d$_6$.
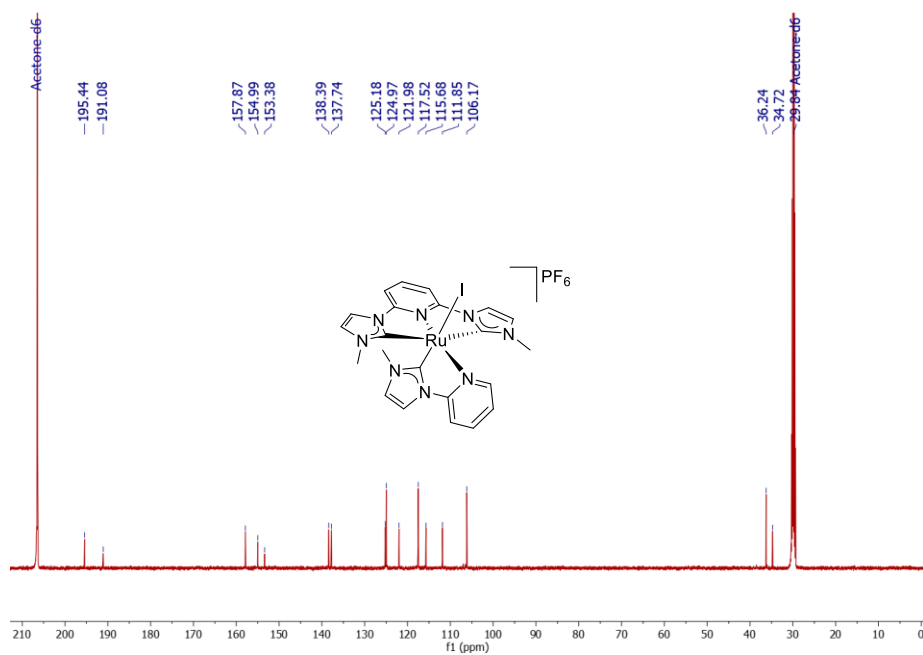
Figure 4.20. ^{13}C NMR spectrum of complex **7a** in acetone-d$_6$.
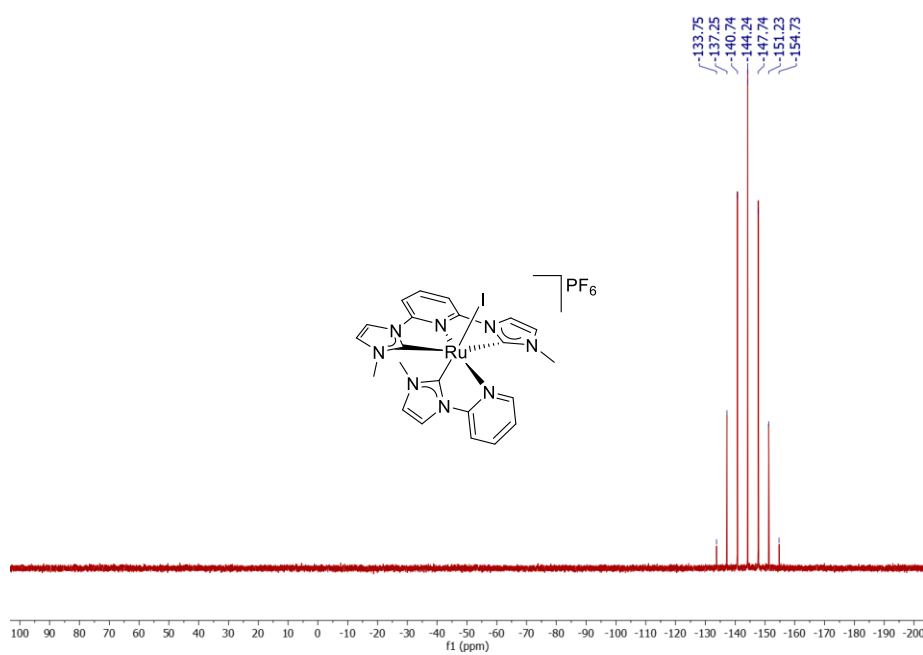
Figure 4.21. ^{31}P NMR spectrum of complex **7a** in acetone-d$_6$.
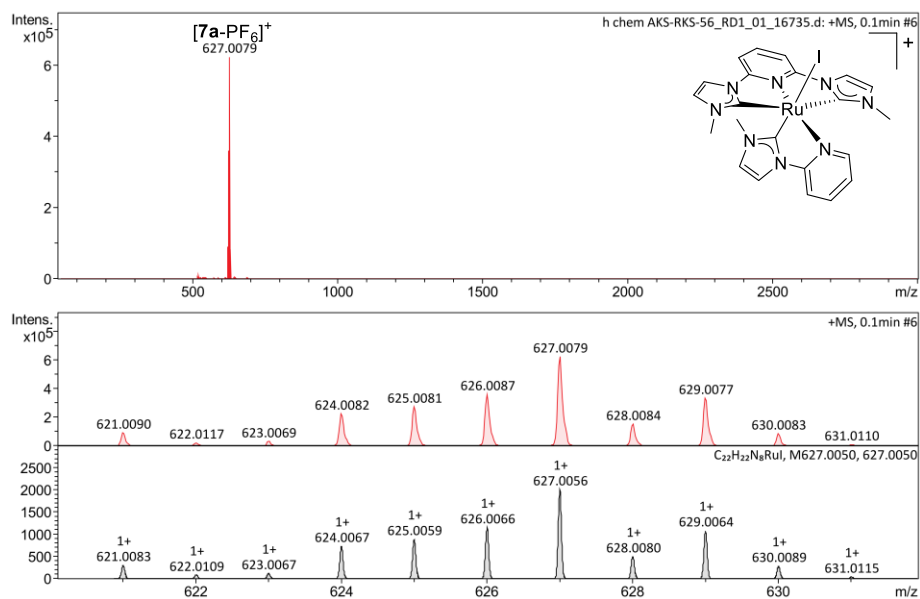
Figure 4.22. HRMS spectrogram of complex **7a**.
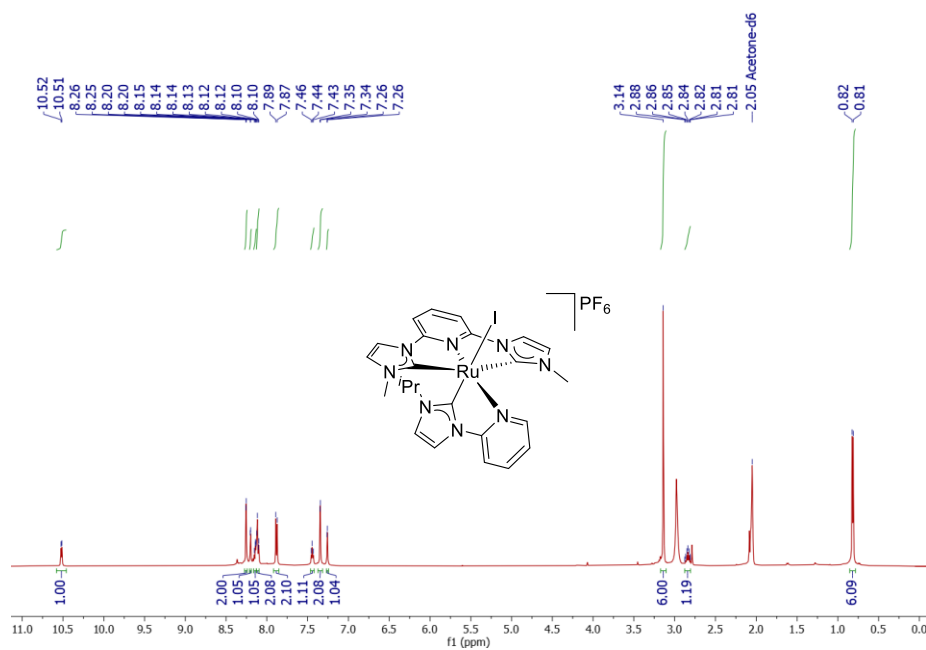
Figure 4.23. ^{1}H NMR spectrum of complex **8a** in acetone-d$_6$.
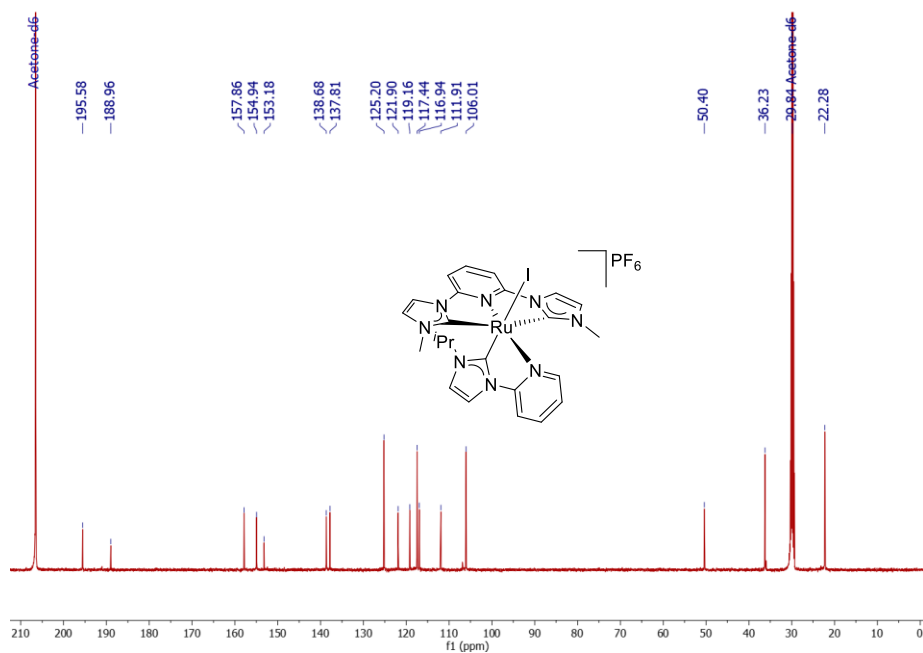
Figure 4.24. ^{13}C NMR spectrum of complex **8a** in acetone-d$_6$.
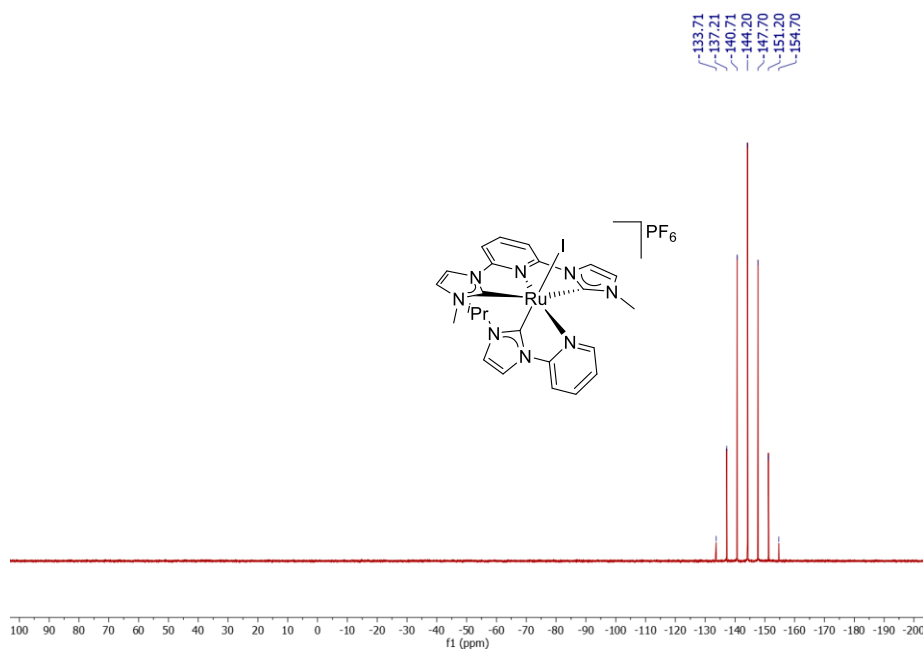
Figure 4.25. ^{31}P NMR spectrum of complex **8a** in acetone-d$_6$.
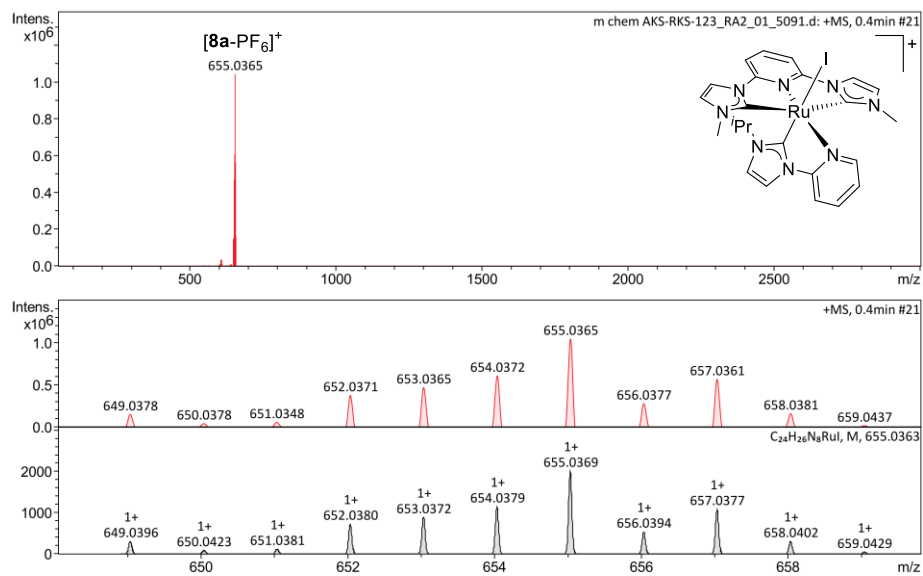
Figure 4.26. HRMS spectrogram of complex **8a**.
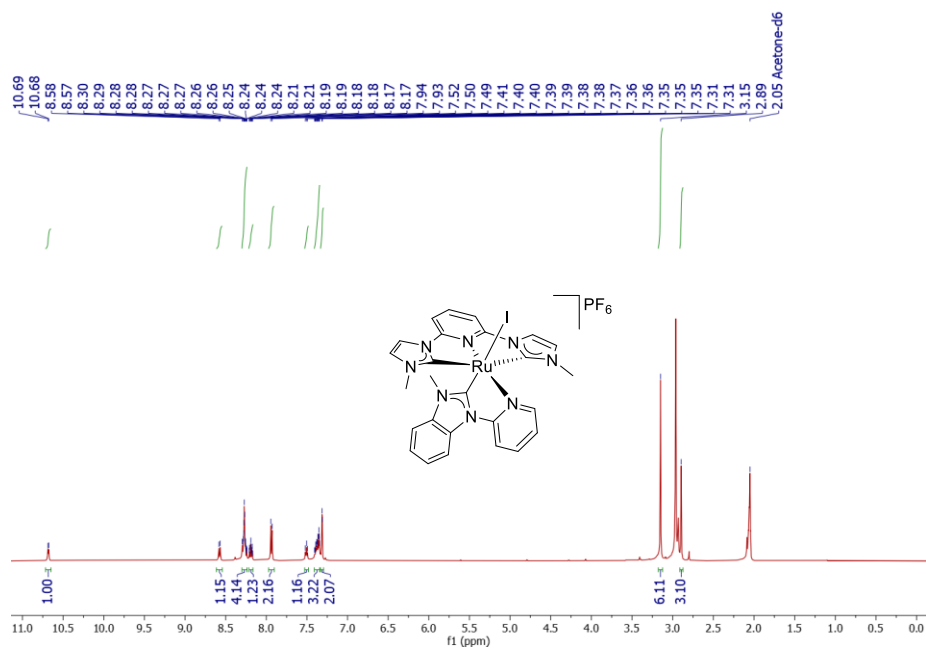
Figure 4.27. ^{1}H NMR spectrum of complex **9a** in acetone-d[6].

159
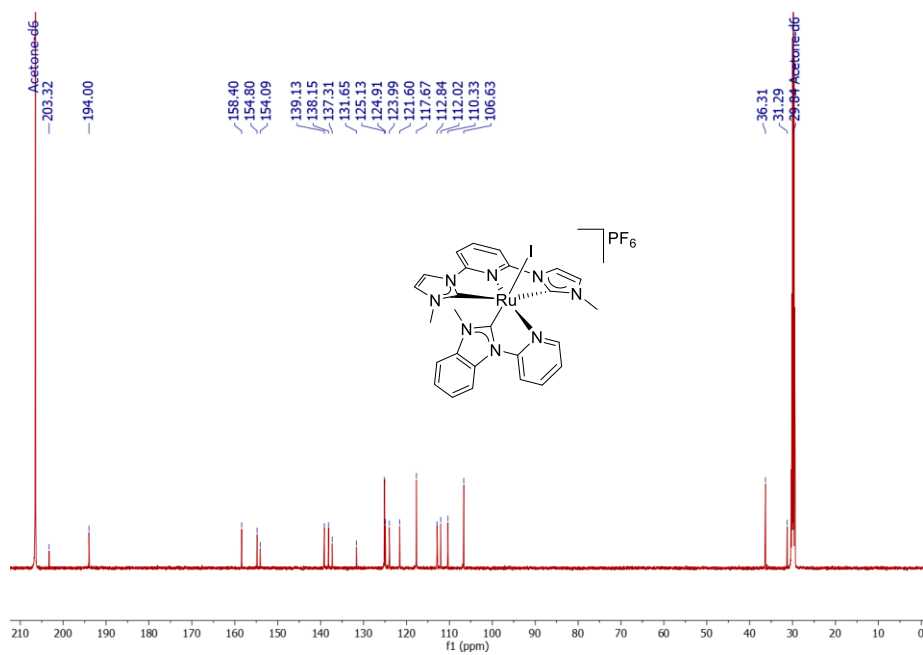
Figure 4.28. ^{13}C NMR spectrum of complex **9a** in acetone-d$_6$.
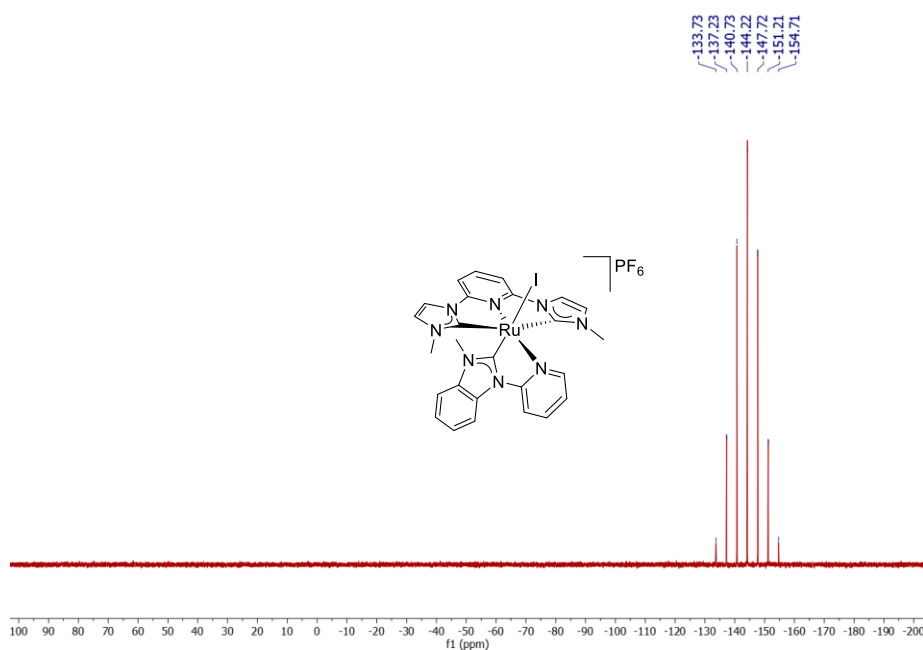
Figure 4.29. ^{31}P NMR spectrum of complex **9a** in acetone-d$_6$.
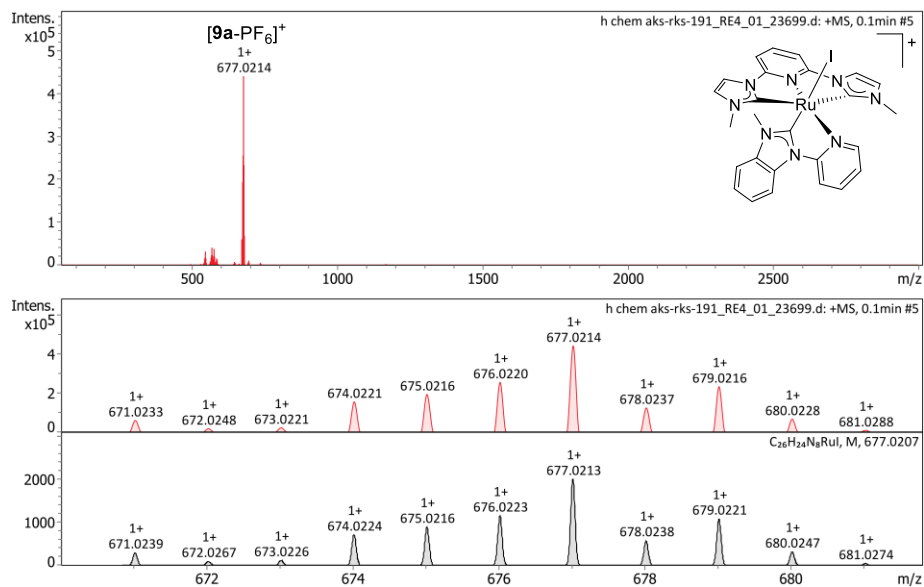
Figure 4.30. HRMS spectrogram of complex **9a** in acetone-d$_6$.
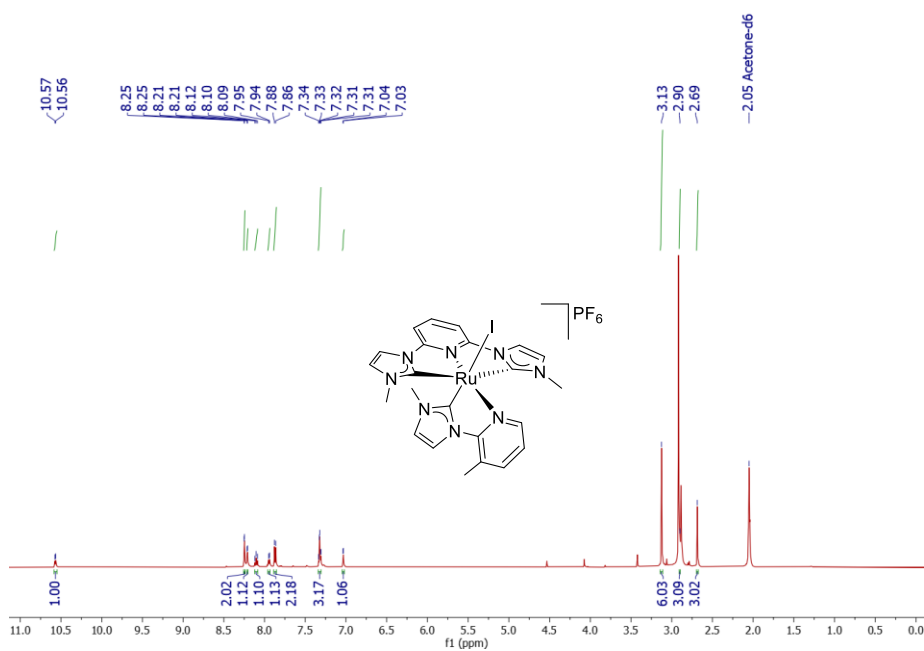
Figure 4.31. ^{1}H NMR spectrum of complex **10a** in acetone-d$_6$.

161
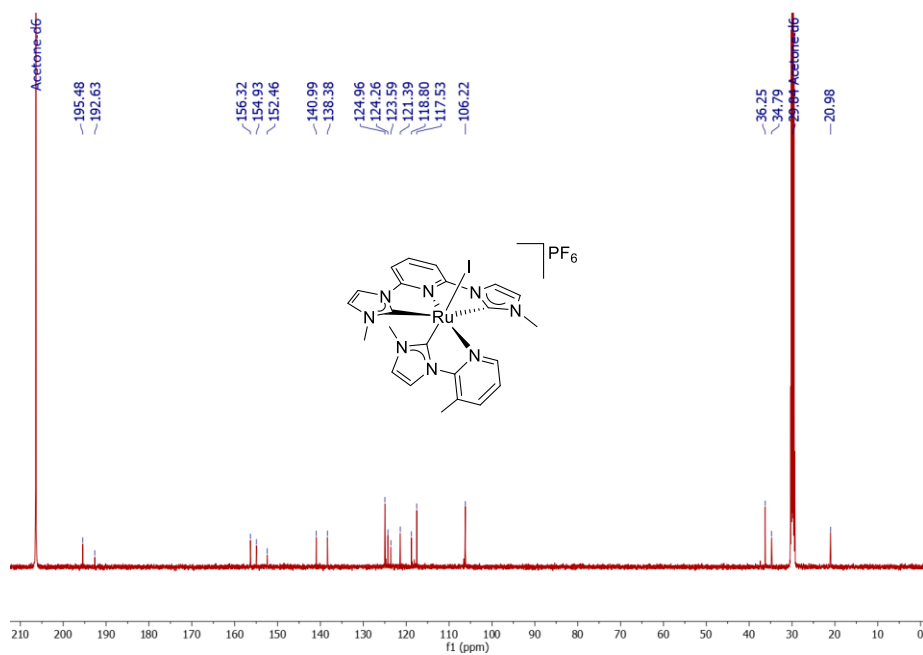
Figure 4.32. ^{13}C NMR spectrum of complex **10a** in acetone-d$_6$.
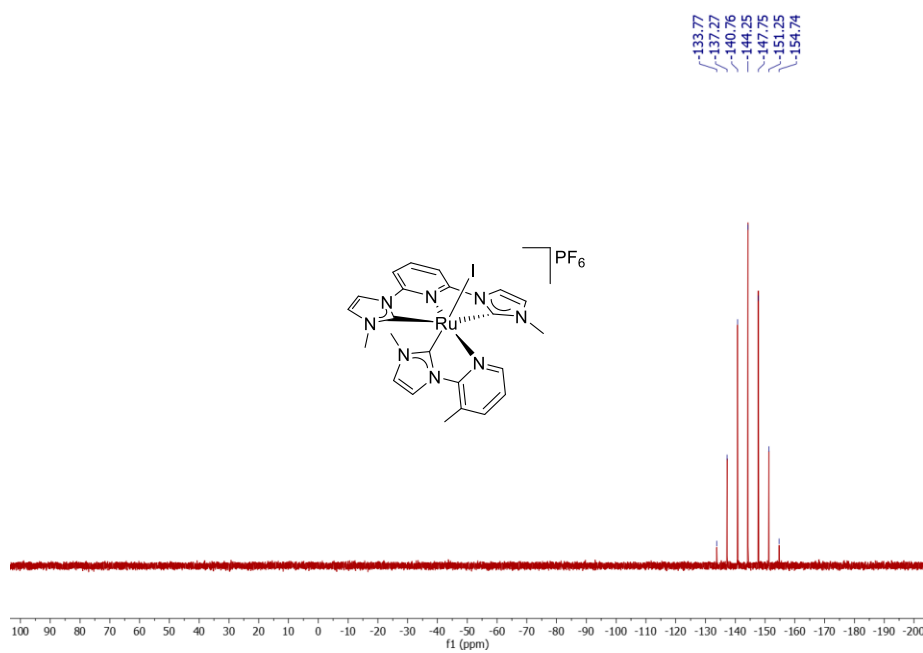
Figure 4.33. ^{31}P NMR spectrum of complex **10a** in acetone-d$_6$.
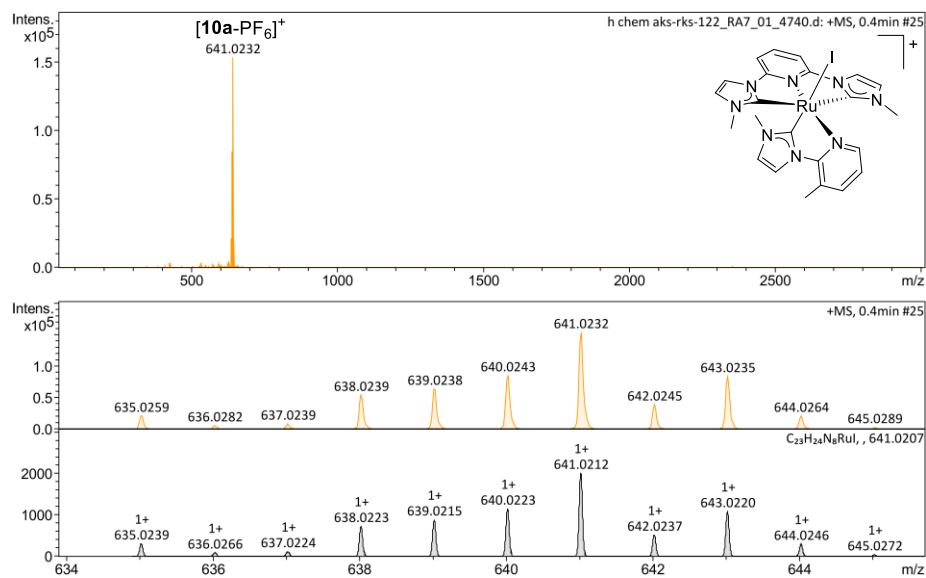
Figure 4.34. HRMS spectrogram of complex **10a**.
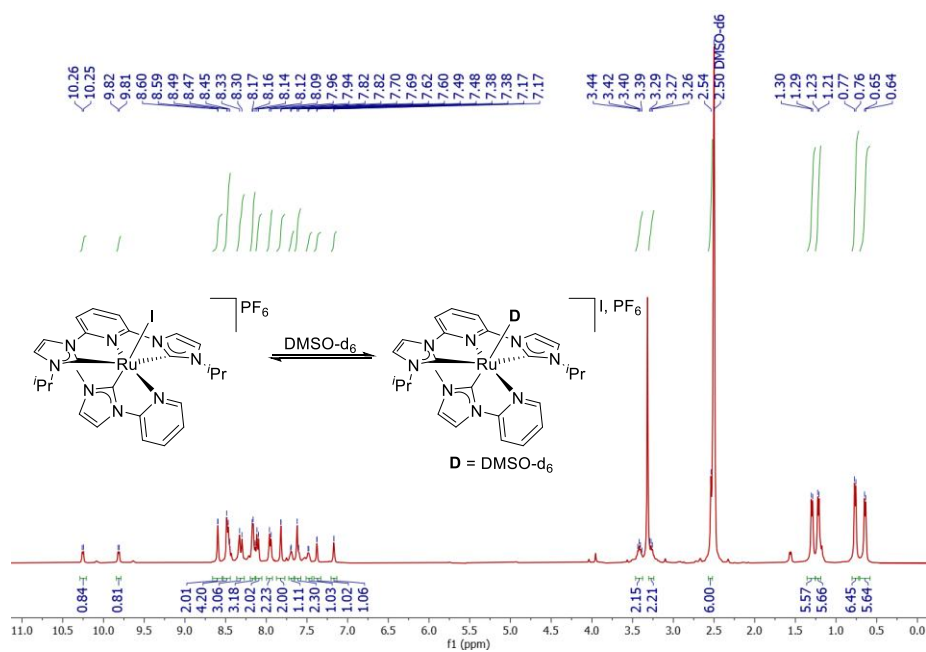
Figure 4.35. ^{1}H NMR spectrum of complex **7b** in dmso-d$_6$.

163
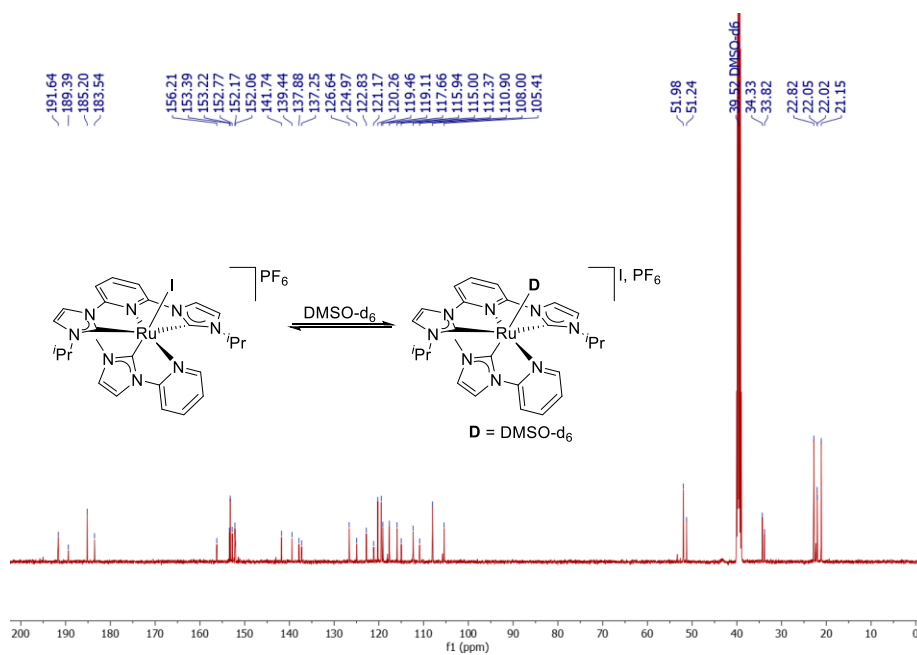
Figure 4.36. ^{13}C NMR spectrum of complex **7b** in dmso-d$_6$.
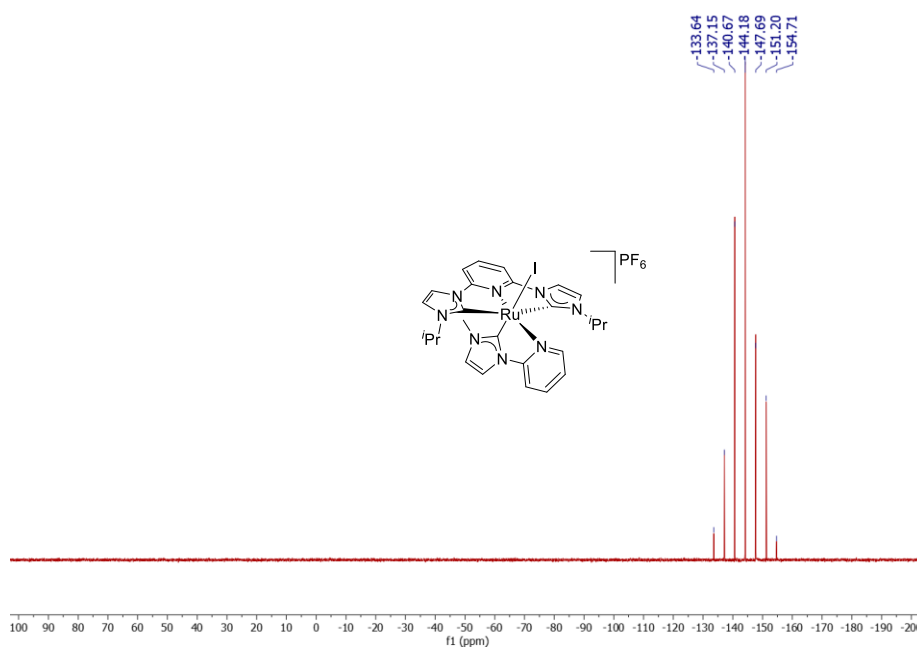
Figure 4.37. ^{31}P NMR spectrum of complex **7b** in dmso-d$_6$.
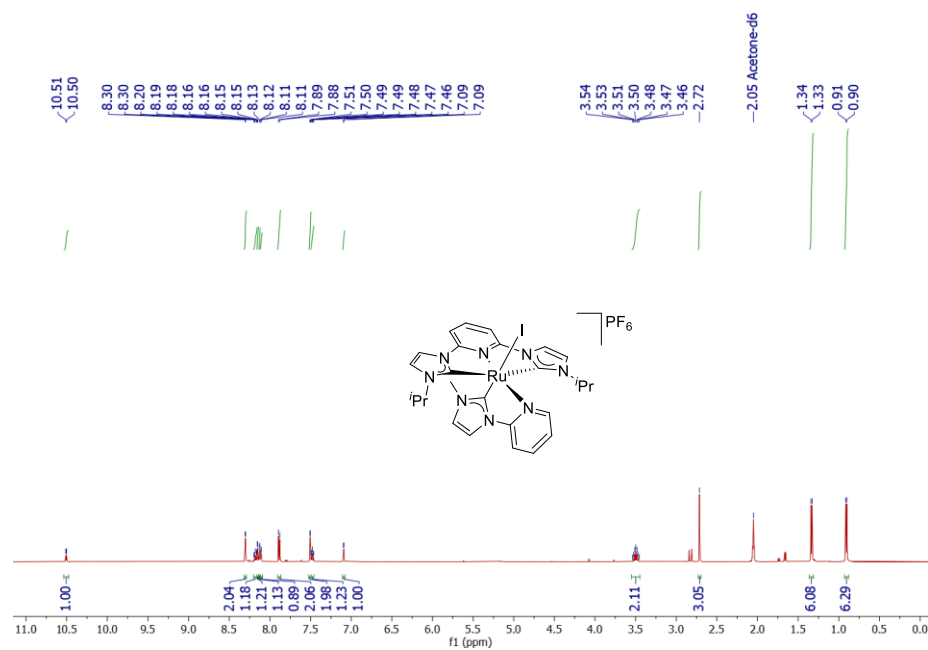
Figure 4.38. ^{1}H NMR spectrum of complex **7b** in acetone-d$_6$.
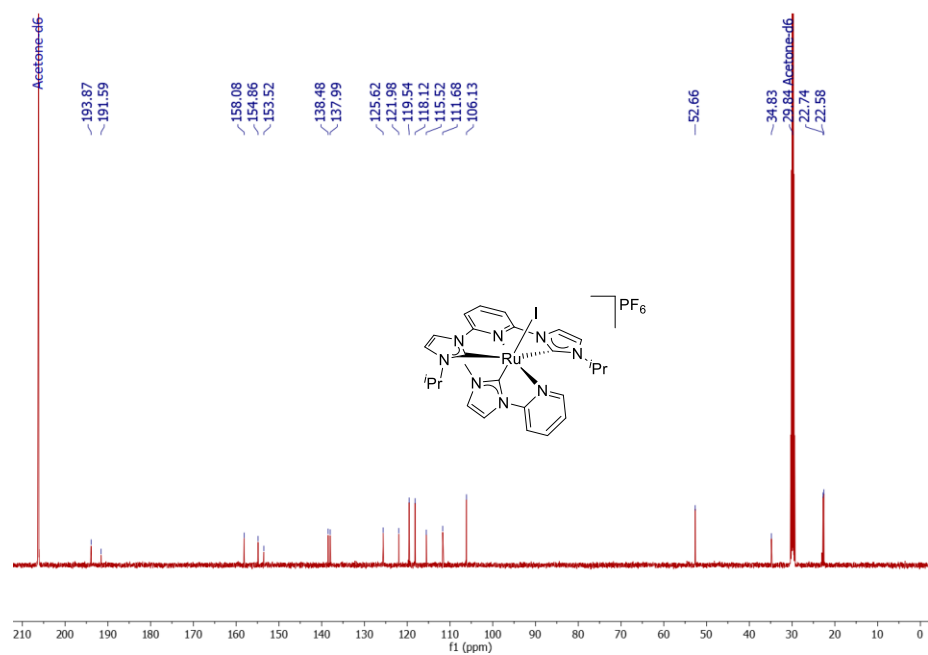
Figure 4.39. ^{13}C NMR spectrum of complex **7b** in acetone-d$_6$.

Figure 4.40. ^{31}P NMR spectrum of complex **7b** in acetone-d$_6$.

Figure 4.41. HRMS spectrogram of complex **7b**.

166
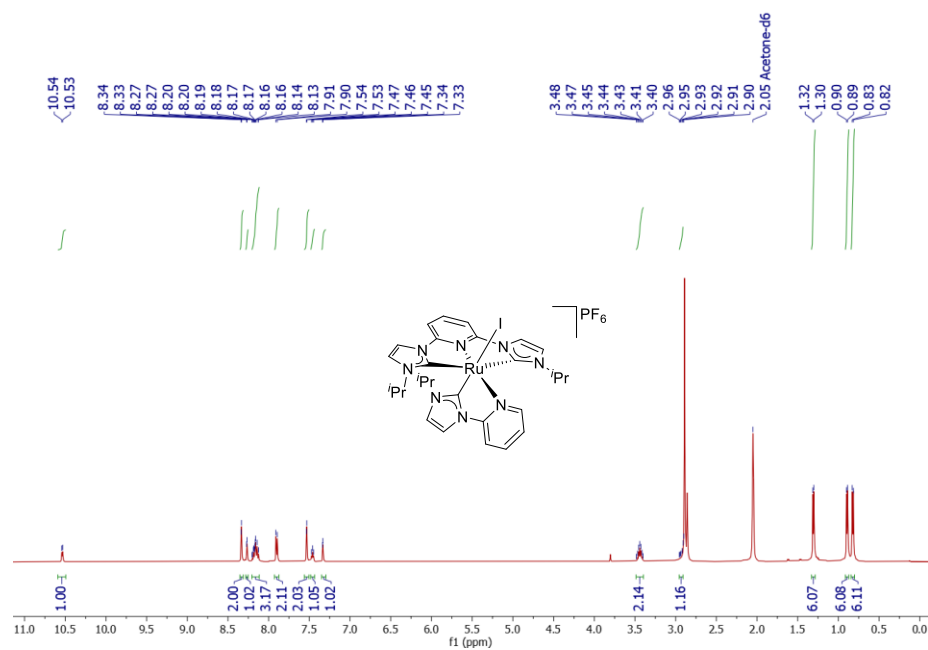
Figure 4.42. ^{1}H NMR spectrum of complex **8b** in acetone-d$_6$.
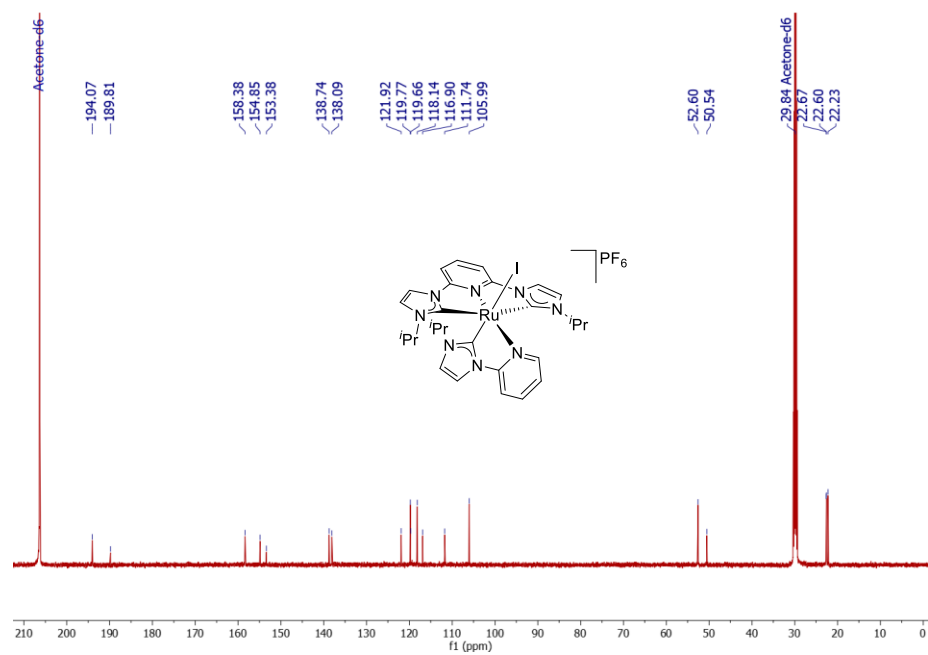
Figure 4.43. ^{13}C NMR spectrum of complex **8b** in acetone-d$_6$.
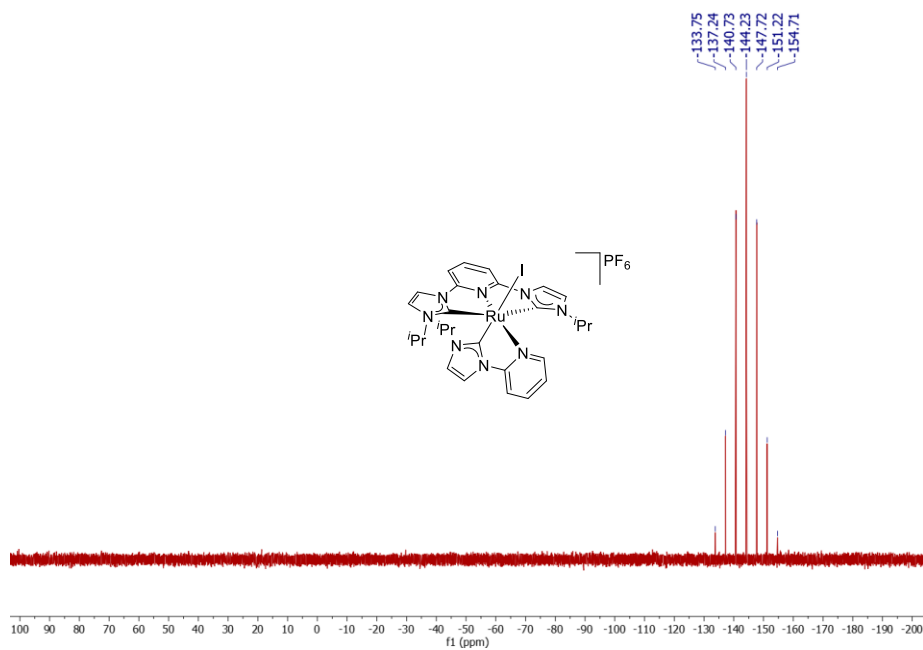
Figure 4.44. ^{31}P NMR spectrum of complex **8b** in acetone-d$_6$.
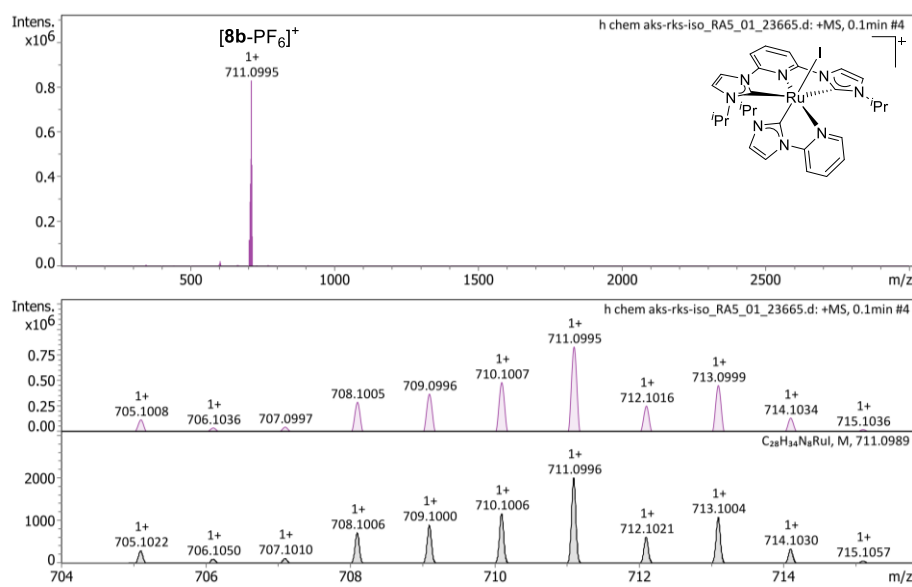
Figure 4.45. HRMS spectrogram of complex **8b**.

168
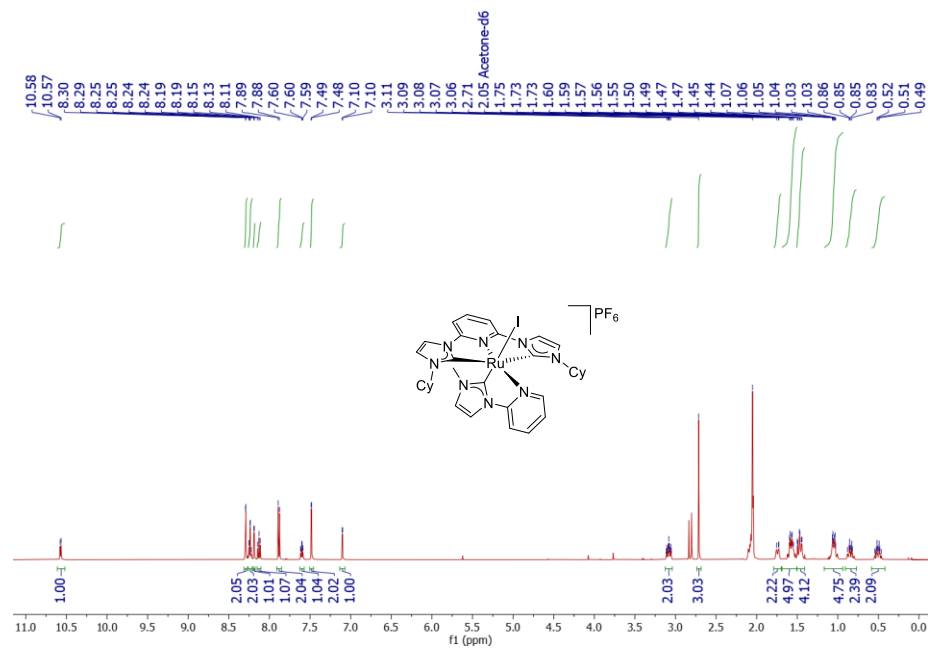
Figure 4.46. ^{1}H NMR spectrum of complex **7c** in acetone-d$_6$.
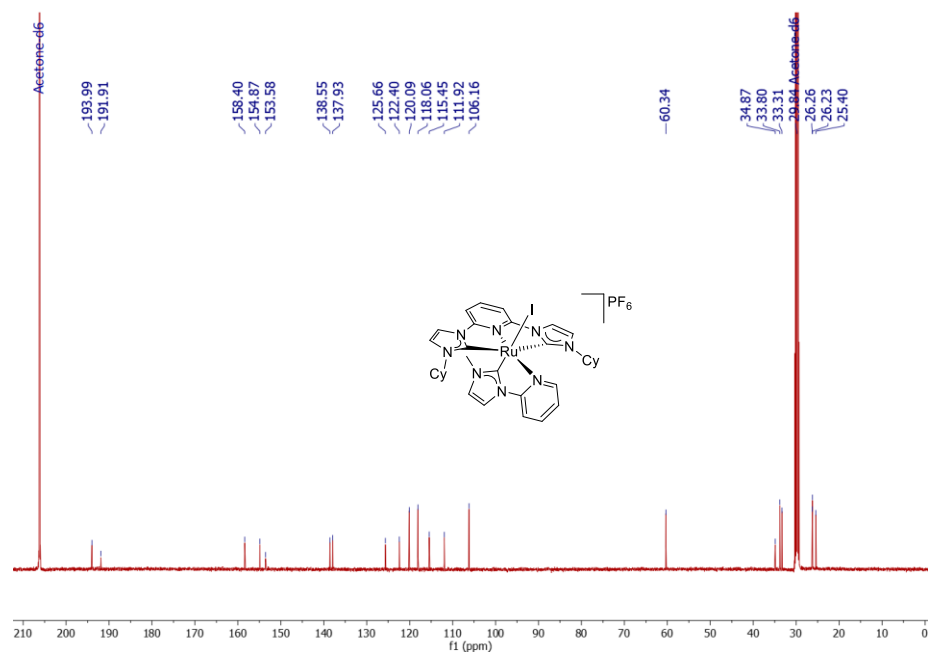
Figure 4.47. ^{13}C NMR spectrum of complex **7c** in acetone-d$_6$.
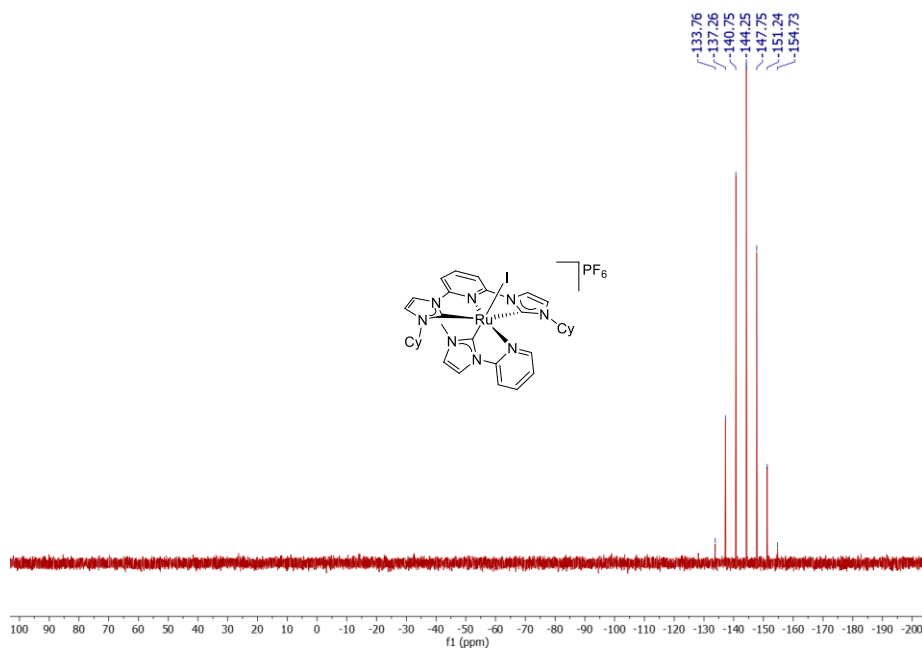
Figure 4.48. ^{31}P NMR spectrum of complex **7c** in acetone-d_6.
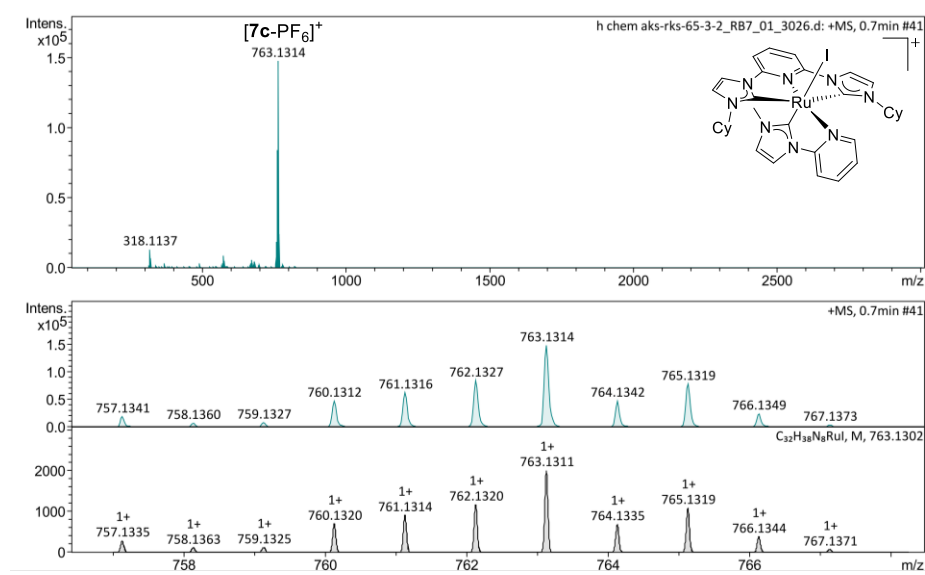
Figure 4.49. HRMS spectrogram of complex **7c**.
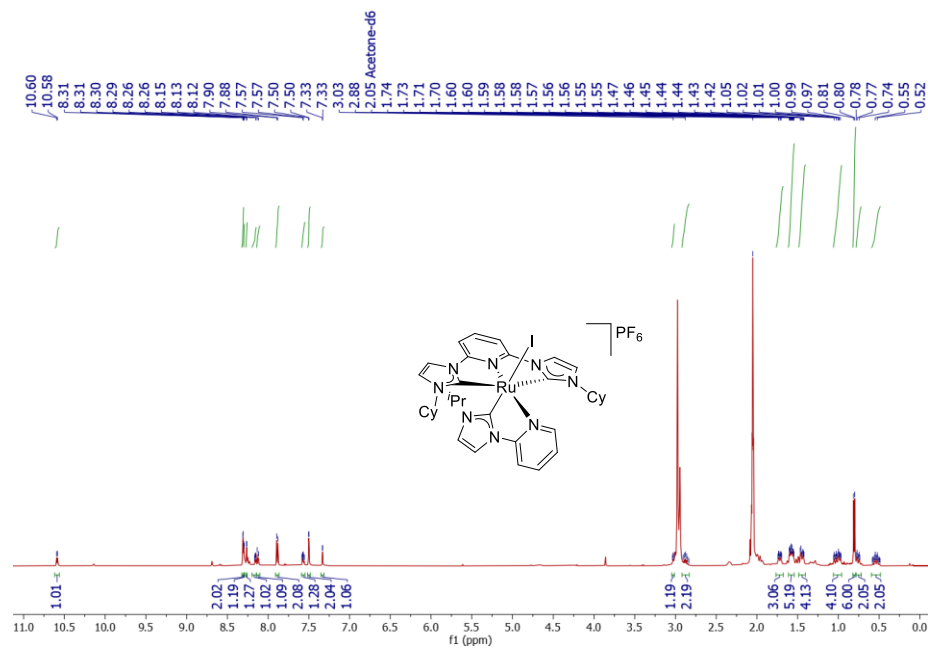
Figure 4.50. ^{1}H NMR spectrum of complex **8c** in acetone-d$_6$.
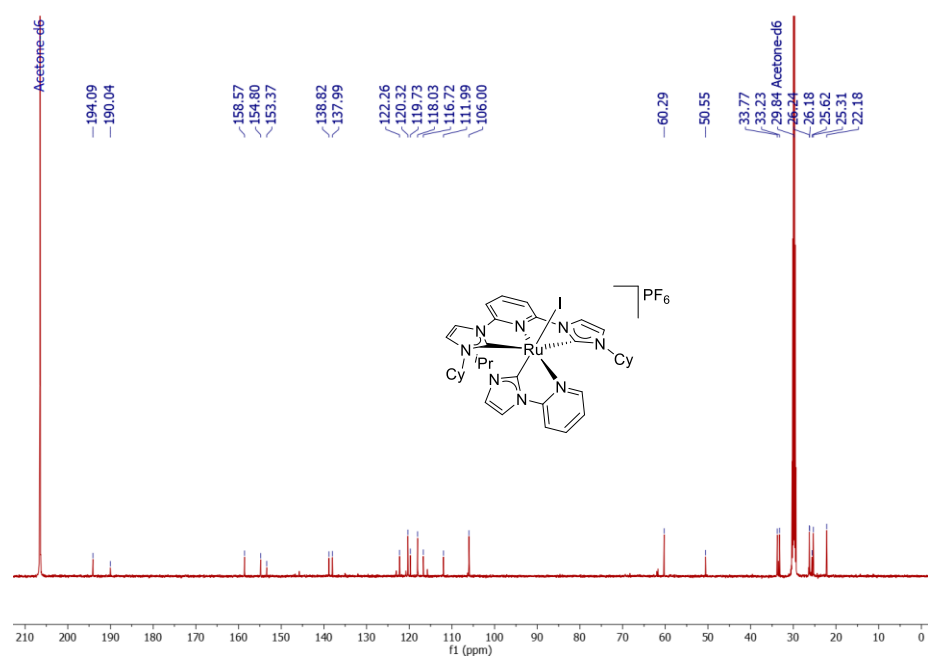
Figure 4.51. ^{13}C NMR spectrum of complex **8c** in acetone-d$_6$.
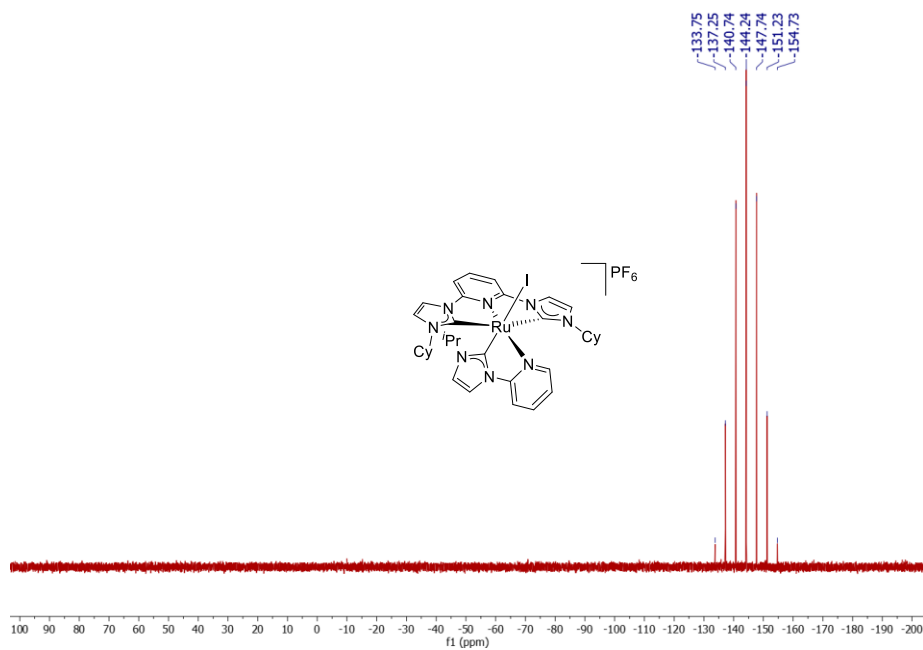
Figure 4.52. ^{31}P NMR spectrum of complex **8c** in acetone-d$_6$.
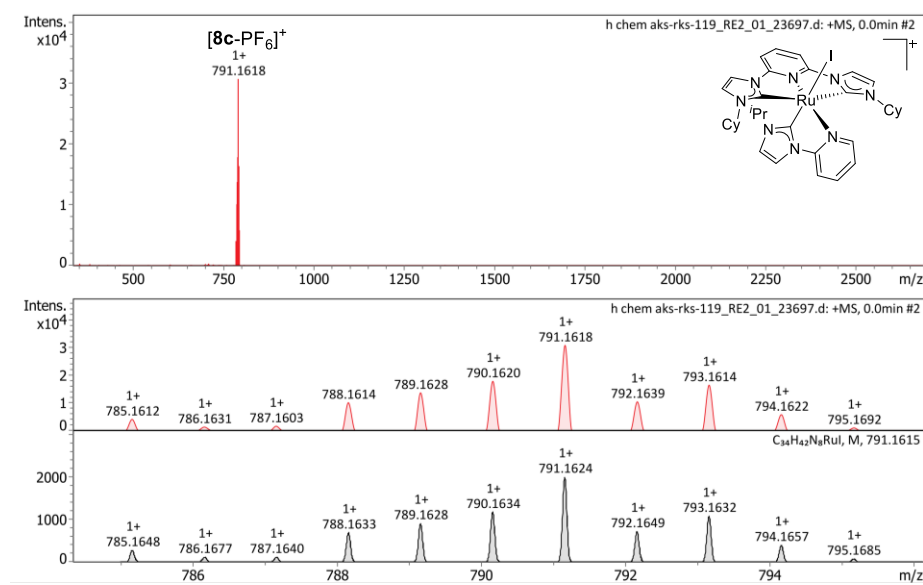
Figure 4.53. HRMS spectrogram of complex **8c**.
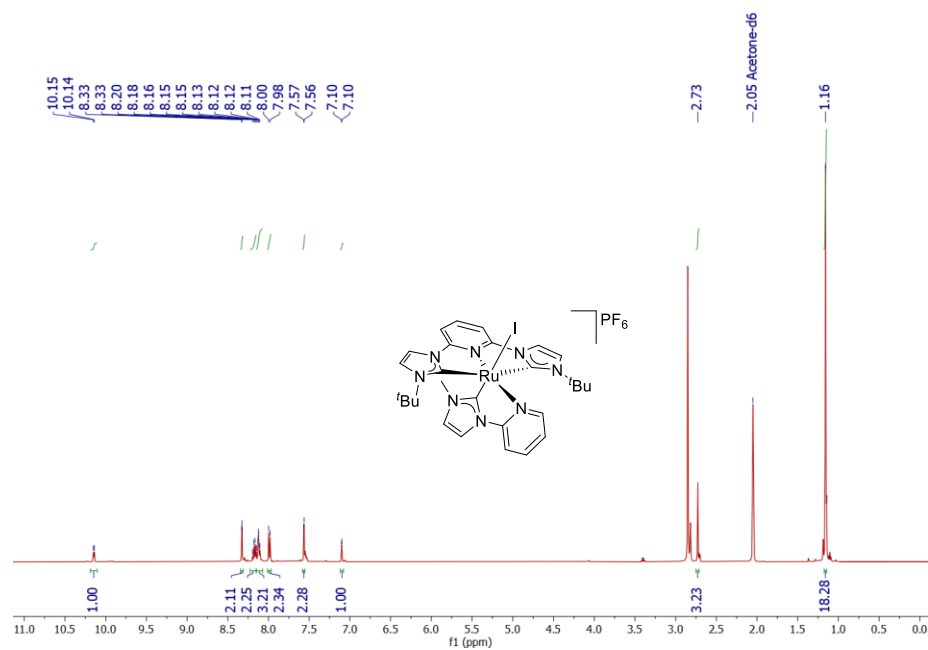
Figure 4.54. ^{1}H NMR spectrum of complex **7d** in acetone-d$_6$.
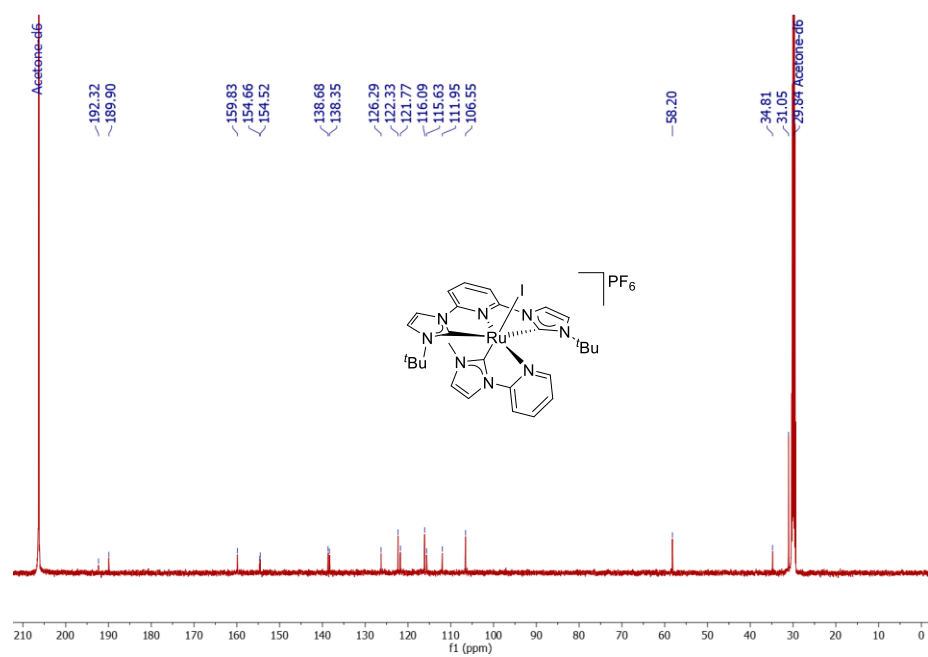
Figure 4.55. ^{13}C NMR spectrum of complex **7d** in acetone-d$_6$.
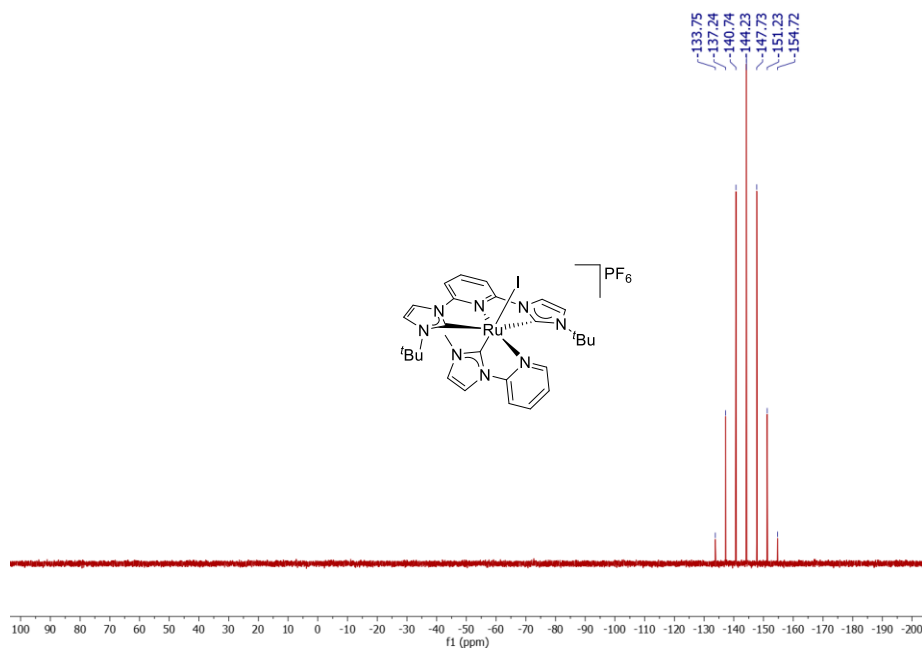
Figure 4.56. ^{31}P NMR spectrum of complex **7d** in acetone-d$_6$.
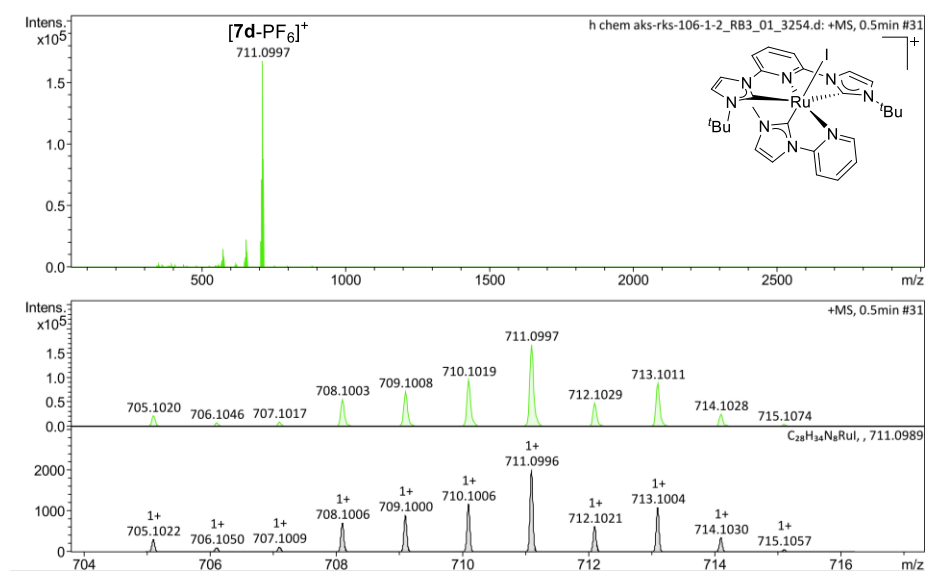
Figure 4.57. HRMS spectrogram of complex **7d**.
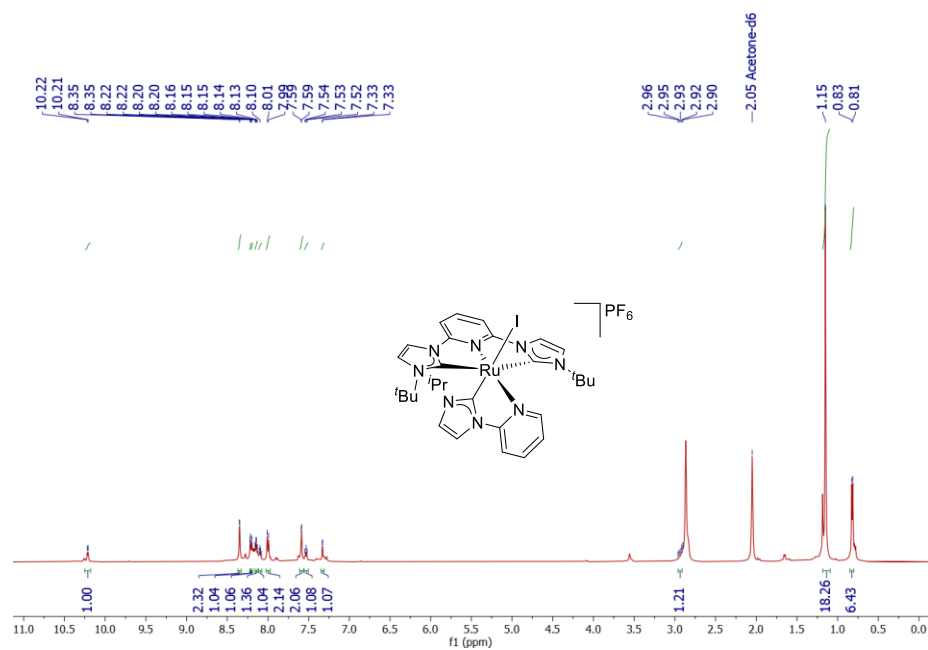
Figure 4.58. ^{1}H NMR spectrum of complex **8d** in acetone-d$_6$.
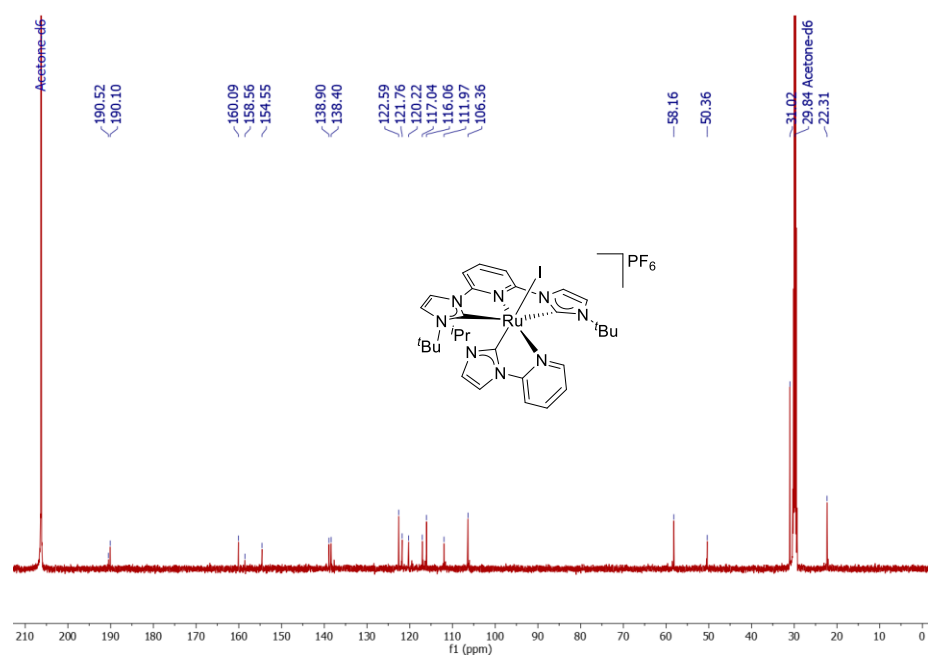
Figure 4.59. ^{13}C NMR spectrum of complex **8d** in acetone-d$_6$.
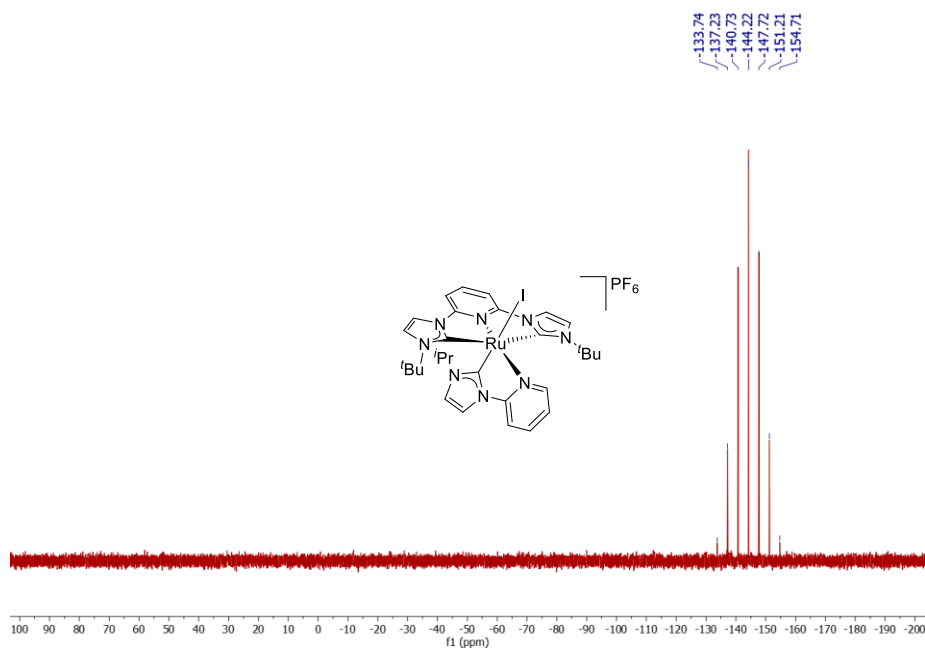
Figure 4.60. ^{31}P NMR spectrum of complex **8d** in acetone-d$_6$.
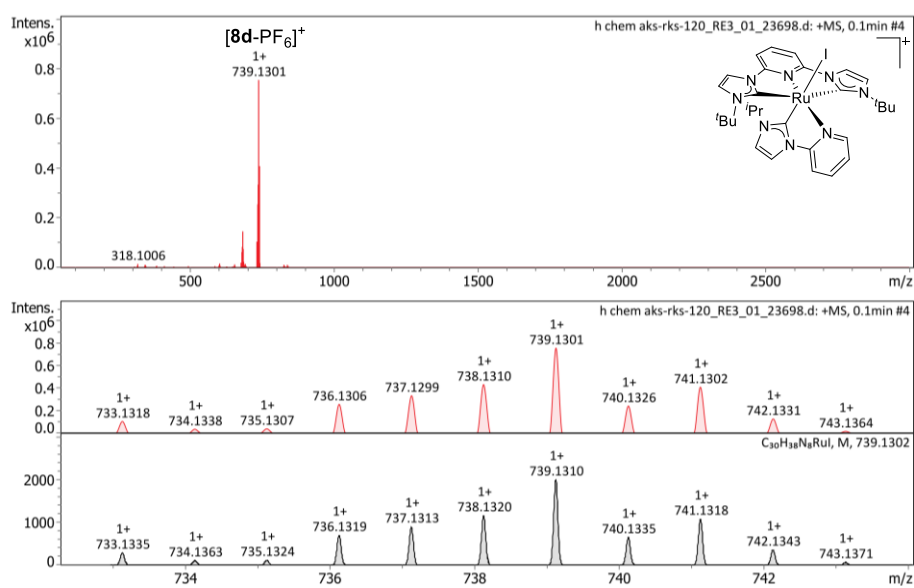
Figure 4.61. HRMS spectrogram of complex **8d**.

4.5. References

1. Lawrence M. A. W., Green K.-A., Nelson P. N., Lorraine S. C. (2018), Review: Pincer ligands-Tunable, versatile and applicable, Polyhedron, 143, 11-27 (DOI: 10.1016/j.poly.2017.08.017).

2. Piccirilli L., Lobo Justo Pinheiro D., Nielsen M. (2020), Recent Progress with Pincer Transition Metal Catalysts for Sustainability, Catalysts, 10(7), 773 (DOI: 10.3390/catal10070773).

3. Peris E., Crabtree R. H. (2018), Key factors in pincer ligand design, Chem. Soc. Rev., 47(6), 1959-1968 (DOI: 10.1039/C7CS00693D).

4. Gunanathan C., Milstein D. (2014), Bond Activation and Catalysis by Ruthenium Pincer Complexes, Chem. Rev., 114(24), 12024-12087 (DOI: 10.1021/cr5002782).

5. Valdés H., García-Eleno M. A., Canseco-Gonzalez D., Morales-Morales D. (2018), Recent Advances in Catalysis with Transition-Metal Pincer Compounds, ChemCatChem, 10(15), 3136-3172 (DOI: 10.1002/cctc.201702019).

6. Hopkinson M. N., Richter C., Schedler M., Glorius F. (2014), An overview of *N*-heterocyclic carbenes, Nature, 510(7506), 485-496 (DOI: 10.1038/nature13384).

7. Díez-González S., Marion N., Nolan S. P. (2009), *N*-Heterocyclic Carbenes in Late Transition Metal Catalysis, Chem. Rev., 109(8), 3612-3676 (DOI: 10.1021/cr900074m).

8. Jacobsen H., Correa A., Poater A., Costabile C., Cavallo L. (2009), Understanding the M(NHC) (NHC=*N*-heterocyclic carbene) bond, Coord. Chem. Rev., 253(5), 687-703 (DOI: 10.1016/j.ccr.2008.06.006).

9. Nesterov V., Reiter D., Bag P., Frisch P., Holzner R., Porzelt A., Inoue S. (2018), NHCs in Main Group Chemistry, Chem. Rev., 118(19), 9678-9842 (DOI: 10.1021/acs.chemrev.8b00079).

10. Zhao Q., Meng G., Nolan S. P., Szostak M. (2020), *N*-Heterocyclic Carbene Complexes in C–H Activation Reactions, Chem. Rev., 120(4), 1981-2048 (DOI: 10.1021/acs.chemrev.9b00634).

11. Andrew R. E., González-Sebastián L., Chaplin A. B. (2016), NHC-based pincer ligands: carbenes with a bite, Dalton Trans., 45(4), 1299-1305 (DOI: 10.1039/C5DT04429D).

12. de Frémont P., Marion N., Nolan S. P. (2009), Carbenes: Synthesis, properties, and organometallic chemistry, Coord. Chem. Rev., 253(7), 862-892 (DOI: 10.1016/j.ccr.2008.05.018).

13. Fantasia S., Petersen J. L., Jacobsen H., Cavallo L., Nolan S. P. (2007), Electronic Properties of *N*-Heterocyclic Carbene (NHC) Ligands: Synthetic, Structural, and Spectroscopic Studies of (NHC)Platinum(II) Complexes, Organometallics, 26(24), 5880-5889 (DOI: 10.1021/om700857j).

14. Younus H. A., Ahmad N., Su W., Verpoort F. (2014), Ruthenium pincer complexes: Ligand design and complex synthesis, Coord. Chem. Rev., 276, 112-152 (DOI: 10.1016/j.ccr.2014.06.016).

15. Fogler E., Balaraman E., Ben-David Y., Leitus G., Linda, Shimon J. W., Milstein D. (2011), New CNN-Type Ruthenium Pincer NHC Complexes, Mild, Efficient Catalytic Hydrogenation of Esters, Organometallics, 30(14), 3826-3833 (DOI: 10.1021/om200367j).

16. Younus H. A., Su W., Ahmad N., Chen S., Verpoort F. (2015), Ruthenium Pincer Complexes: Synthesis and Catalytic Applications, Adv. Synth. Catal., 357(2-3), 283-330 (DOI: 10.1002/adsc.201400777).

17. Ishida H., Tanaka K., Tanaka T. (1987), Electrochemical CO_2 reduction catalyzed by ruthenium complexes $[Ru(bpy)_2(CO)_2]^{2+}$ and $[Ru(bpy)_2(CO)Cl]^+$, Effect of pH on the formation of CO and $HCOO^-$, Organometallics, 6(1), 181-186, (DOI: 10.1021/om00144a033).

18. Ishida H., Terada T., Tanaka K., Tanaka T. (1990), Photochemical carbon dioxide reduction catalyzed by bis(2,2'-bipyridine)dicarbonylruthenium(2+) using triethanolamine and 1-benzyl-1,4-dihydronicotinamide as an electron donor, Inorg. Chem., 29(5), 905-911 (DOI: 10.1021/ic00330a004).

19. Kärkäs M. D., Verho O., Johnston E. V., Åkermark B. (2014), Artificial Photosynthesis: Molecular Systems for Catalytic Water Oxidation, Chem. Rev., 114(24), 11863-12001 (DOI: 10.1021/cr400572f).

20. Tamaki Y., Morimoto T., Koike K., Ishitani O. (2012), Photocatalytic CO_2 reduction with high turnover frequency and selectivity of formic acid formation using Ru(II) multinuclear complexes, Proc. Natl. Acad. Sci., 109(39), 15673-15678 (DOI: 10.1073/pnas.1118336109).

21. Suzuki T. M., Tanaka H., Morikawa T., Iwaki M., Sato S., Saeki S., Inoue M., Kajino T., Motohiro T. (2011), Direct assembly synthesis of metal complex-semiconductor hybrid photocatalysts anchored by phosphonate for highly efficient CO_2 reduction, Chem. Commun., 47(30), 8673-8675 (DOI: 10.1039/C1CC12491A).

22. Blakemore J. D., Crabtree R. H., Brudvig G. W. (2015), Molecular Catalysts for Water Oxidation, Chem. Rev., 115(23), 12974-13005 (DOI: 10.1021/acs.chemrev.5b00122).

23. Boudreaux C. M., Liyanage N. P., Shirley H., Siek S., Gerlach D. L., Qu F., Delcamp J. H., Papish E. T. (2017), Ruthenium(II) complexes of pyridinol and *N*-heterocyclic carbene derived pincers as robust catalysts for selective carbon dioxide reduction, Chem. Commun., 53(81), 11217-11220 (DOI: 10.1039/C7CC05706G).

24. Tseng H.-W., Zong R., Muckerman J. T., Thummel R. (2008), Mononuclear Ruthenium(II) Complexes That Catalyze Water Oxidation, Inorg. Chem., 47(24), 11763-11773 (DOI: 10.1021/ic8014817).

25. Concepcion J. J., Jurss J. W., Templeton J. L., Meyer T. J. (2008), One Site is Enough. Catalytic Water Oxidation by $[Ru(tpy)(bpm)(OH_2)]^{2+}$ and $[Ru(tpy)(bpz)(OH_2)]^{2+}$, J. Am. Chem. Soc., 130(49), 16462-16463 (DOI: 10.1021/ja8059649).

26. Concepcion J. J., Jurss J. W., Norris M. R., Chen Z., Templeton J. L., Meyer T. J. (2010), Catalytic Water Oxidation by Single-Site Ruthenium Catalysts, Inorg. Chem., 49(4), 1277-1279 (DOI: 10.1021/ic901437e).

27. Robert M. (2016), Running the Clock: CO_2 Catalysis in the Age of Anthropocene, ACS Energy Lett., 1(1), 281-282 (DOI: 10.1021/acsenergylett.6b00159).

28. Sato S., Arai T., Morikawa T., Uemura K., Suzuki T. M., Tanaka H., Kajino T. (2011), Selective CO_2 Conversion to Formate Conjugated with H_2O Oxidation Utilizing Semiconductor/Complex Hybrid Photocatalysts, J. Am. Chem. Soc., 133(39), 15240-15243 (DOI: 10.1021/ja204881d).

29. Masllorens E., Rodríguez M., Romero I., Roglans A., Parella T., Benet-Buchholz J., Poyatos M., Llobet A. (2006), Can the Disproportion of Oxidation State III Be Favored in $Ru^{II}-OH_2/Ru^{IV}=O$ Systems?, J. Am. Chem. Soc., 128(16), 5306-5307 (DOI: 10.1021/ja057733+).

30. Arikawa Y., Nakamura T., Ogushi S., Eguchi K., Umakoshi K. (2015), Fixation of atmospheric carbon dioxide by ruthenium complexes bearing an NHC-based pincer ligand: formation of a methylcarbonato complex and its methylation, Dalton Trans., 44(12), 5303-5305 (DOI: 10.1039/C5DT00476D).

31. Hunt L. A., Das S., Lamb R. W., Nugegoda D., Curiac C., Figgins M. T., Lambert E. C., Qu F., Hammer N. I., Delcamp J. H., Webster C. E., Papish E. T. (2023), Ruthenium (II) Complexes of CNC Pincers and Bipyridine in the Photocatalytic CO_2 Reduction Reaction to CO Using Visible Light: Catalysis, Kinetics, and Computational Insights, ACS Catal., 13(9), 5986-5999 (DOI: 10.1021/acscatal.2c05459).

32. Danopoulos A. A., Winston S., Motherwell W. B. (2002), Stable *N*-functionalised 'pincer' bis carbene ligands and their ruthenium complexes; synthesis and catalytic studies, Chem. Commun., (13), 1376-1377 (DOI: 10.1039/B202814J).

33. Poyatos M., Mata J. A., Falomir E., Crabtree R. H., Peris E. (2003), New Ruthenium(II) CNC-Pincer Bis(carbene) Complexes: Synthesis and Catalytic Activity, Organometallics, 22(5), 1110-1114 (DOI: 10.1021/om020817w).

34. Yadav D., Singh R. K., Misra S., Singh A. K. (2022), Ancillary ligand effects and microwave-assisted enhancement on the catalytic performance of cationic ruthenium(II)-CNC pincer complexes for acceptorless alcohol dehydrogenation, Appl. Organomet. Chem., e6756 (DOI: 10.1002/aoc.6756).

35. Yadav D., Singh R. K., Singh S., Shirage P. M., Singh A. K. (2021), Cationic ruthenium(II)-NHC pincer complexes with hemilabile COD: Solid-state structural characterization and theoretical study of an η^2-(E,Z)-COD ligand, J. Organomet. Chem., 953, 122061 (DOI: 10.1016/j.jorganchem.2021.122061).

36. Yadav D., Misra S., Kumar D., Singh S., Singh A. K. (2021), Cationic ruthenium(II)-NHC pincer complexes: Synthesis, characterisation and catalytic activity for transfer hydrogenation of ketones, Appl. Organomet. Chem., 35(8), e6287 (DOI: 10.1002/aoc.6287).

37. Shahid N., Singh R. K., Srivastava N., Singh A. K. (2023), Base-free synthesis of benchtop stable Ru(III)-NHC complexes from $RuCl_3 \cdot 3H_2O$ and their use as precursors for Ru(II)-NHC complexes, Dalton Trans., 52(13), 4176-4185, (DOI: 10.1039/D3DT00243H).

38. Andrade G. A., DiMeglio J. L., Guardino E. T., Yap G. P. A., Rosenthal J. (2017), Synthesis and structure of palladium(II) complexes supported by bis-NHC pincer ligands for the electrochemical activation of CO_2, Polyhedron, 135, 134-143, (DOI: 10.1016/j.poly.2017.06.018).

39. Nielsen D. J., Cavell K. J., Skelton B. W., White A. H. (2006), Methyl-palladium(II) complexes of pyridine-bridged bis(nucleophilic heterocyclic carbene) ligands: Substituent effects on structure, stability, and catalytic performance, Inorg. Chim. Acta, 359(6), 1855-1869 (DOI: 10.1016/j.ica.2005.07.049).

40. Dakkach M., Atlamsani A., Parella T., Fontrodona X., Romero I., Rodríguez M. (2013), New Aqua *N*-Heterocyclic Carbene Ru(II) Complexes with Two-Electron Process as Selective Epoxidation Catalysts: An Evaluation of Geometrical and Electronic Effects, Inorg. Chem., 52(9), 5077-5087 (DOI: 10.1021/ic302863h).

41. Vaquer L., Miró P., Sala X., Bozoglian F., Masllorens E., Benet-Buchholz J., Fontrodona X., Parella T., Romero I., Roglans A., Rodríguez M., Bo C., Llobet A. (2013), Understanding Electronic Ligand Perturbation over Successive Metal-Based Redox Potentials in Mononuclear Ruthenium-Aqua Complexes, ChemPlusChem, 78(3), 235-243 (DOI: 10.1002/cplu.201200268).

42. Naziruddin A. R., Huang Z.-J., Lai W.-C., Lin W.-J., Hwang W.-S. (2013), Ruthenium(II) carbonyl complexes bearing CCC-pincer bis-(carbene) ligands: synthesis, structures and activities toward recycle transfer hydrogenation reactions, Dalton Trans., 42(36), 13161-13171 (DOI: 10.1039/C3DT51161H).

43. Shahid N., Budhija V., Singh A. K. (2024), Halide-Assisted Electrophilic C–H Activation in Aqueous Acid and Salt Solutions for the Synthesis of Ru(III)-Abnormal NHC Complexes, Organometallics, 43(19), 2243-2255 (DOI: 10.1021/acs.organomet.4c00273).

44. Barbante G. J., Francis P. S., Hogan C. F., Kheradmand P. R., Wilson D. J. D., Barnard P. J. (2013), Electrochemiluminescent Ruthenium(II) *N*-Heterocyclic Carbene Complexes: a Combined Experimental and Theoretical Study, Inorg. Chem., 52(13), 7448-7459 (DOI: 10.1021/ic400263r).

45. Stanton III C. J., Machan C. W., Vandezande J. E., Jin T., Majetich G. F., Schaefer III H. F., Kubiak C. P., Li G., Agarwal J.

(2016), Re(I) NHC Complexes for Electrocatalytic Conversion of CO_2, Inorg. Chem., 55(6), 3136-3144, (DOI: 10.1021/acs.inorgchem.6b00079).

46. Nirmala M., Viswanathamurthi P. (2016), Ruthenium(II) complexes bearing pyridine-functionalized *N*-heterocyclic carbene ligands: Synthesis, structure and catalytic application over amide synthesis, J. Chem. Sci., 128(11), 1725-1735 (DOI: 10.1007/s12039-016-1169-y).

47. Ghorai D., Dutta C., Choudhury J. (2016), Switching of "Rollover Pathway" in Rhodium(III)-Catalyzed C–H Activation of Chelating Molecules, ACS Catal., 6(2), 709-713 (DOI: 10.1021/acscatal.5b02540).

48. Dolomanov O. V., Bourhis L. J., Gildea R. J., Howard J. A. K., Puschmann H. (2009), OLEX2: a complete structure solution, refinement and analysis program, J. Appl. Cryst., 42(2), 339-341 (DOI: 10.1107/S0021889808042726).

49. Sheldrick G. M. (2015), SHELXT - Integrated space-group and crystal-structure determination, Acta Cryst. Sect. A: Found. Adv., 71(1), 3-8 (DOI: 10.1107/S2053273314026370).

50. Sheldrick G. M. (2015), Crystal structure refinement with SHELXL, Acta Cryst. Sect. C: Struct. Chem., 71(1), 3-8 (DOI: 10.1107/S2053229614024218).

Chapter 5

Cationic Ru(II)-CNC Pincer Complexes as Phosphine-free Catalysts for Nitrile Hydration to Amides in Aqueous Medium

5.1. Introduction

NHCs containing ruthenium complexes are remarkably useful in catalytic applications, providing efficient methods for converting renewable resources and synthesizing valuable products [1–4]. These complexes have been effectively used in various organic transformations, including (de)hydrogenation, cross-coupling reactions, metathesis, and C-H activation [5–10]. NHC ligands have unique steric and electronic properties, combined with the tunable reactivity of ruthenium, which allows these complexes to participate in diverse bond activations and transformations [11, 12]. This versatility makes Ru-NHC complexes essential tools in synthetic chemistry, particularly as phosphine-free catalysts, facilitating the efficient synthesis of complex molecules and promoting sustainable and environmentally friendly processes [13–16]. Phosphine ligands are frequently used in conventional transition metal catalysts to stabilize the metal centre and control reactivity. However, phosphine ligands can present several drawbacks, such as toxicity, air and moisture sensitivity, and limited ligand tunability [17, 18]. In contrast, Ru-NHC complexes offer a desirable alternative as phosphine-free catalysts, providing exceptional stability, selectivity, and reactivity [19–22]. These catalysts can transform various synthetic methodologies and promote more sustainable and environment-friendly chemical processes.

Amides are critically important in chemical and biological systems and are widely utilized as synthetic intermediates in pharmaceuticals, materials science, polymer chemistry, and fine chemical production [23–26]. Several synthetic methods have been developed to synthesise amides, with the condensation of carboxylic acids and amines being one of the most convenient approaches [24–27]. Among the several strategies explored, the hydration of nitriles stands out as a sustainable and environment-friendly method due to its lack of toxic byproducts [27]. However, traditional methods for nitrile hydration have faced challenges, such as harsh reaction conditions involving highly alkaline or acidic media, which are neither sustainable nor practical from an environmental perspective [28–30]. Additionally, the overhydrolysis of amides into carboxylic acids or ammonium carboxylates limits the applicability of this method, mainly when additional sensitive functional groups are present [28, 29]. Consequently, developing atom-efficient catalytic procedures that prevent overhydration is a highly desirable goal in modern chemistry.
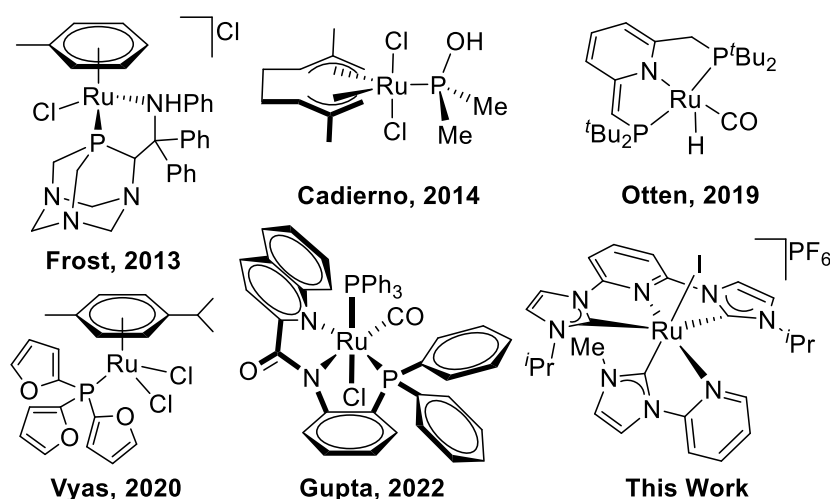
Figure 5.1. Some selected active ruthenium catalysts for nitrile hydration.

Several transition metal-based catalysts have been reported for the hydration of nitriles, facilitating the direct nucleophilic addition of water to a nitrile bond, resulting in the formation of amides [31–35].

Ruthenium complexes have been identified as very effective catalysts, offering enhanced selectivity and efficiency for nitrile hydration under mild conditions [36–39]. For the hydration of nitriles, a library of ruthenium-based catalysts has been reported, which typically requires higher catalyst loading (2–5 mol%) and higher temperatures (80–100 ˚C) [40–44]. Cadierno explored ruthenium catalysts for nitrile hydration with lower catalyst loadings (1 mol%) in an aqueous medium [45]. More recently, Otten [46] and Gupta [47] described the ruthenium-catalyzed hydration of nitriles using pincer and tridentate ligands under mild reaction conditions. Some selected active ruthenium catalysts for nitrile hydration are shown in Figure **5.1**. Additionally, other transition metals, such as Rh [48, 49], Ir [50], Os [51], Au [52], and Pt [53], with or without additives, have also been investigated for nitrile hydration under mild reaction conditions.

R = Me (**7a**), R = ^{i}Pr (**7b**)
R = Cy (**7c**), R = ^{t}Bu (**7d**)

R = Me (**8a**), R = ^{i}Pr (**8b**)
R = Cy (**8c**), R = ^{t}Bu (**8d**)

9a

10a
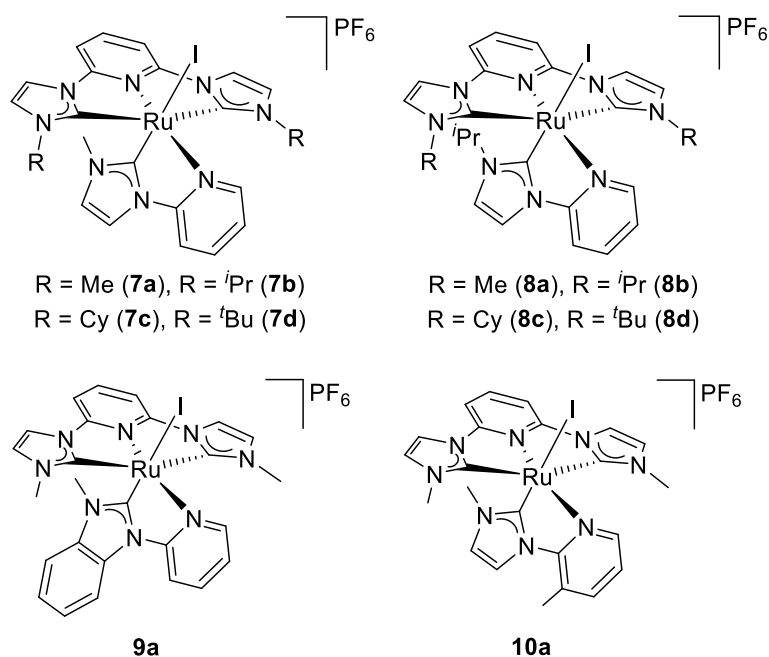
Figure 5.2. Cationic Ru(II)-CNC pincer complexes in this study.

Ru(II)-CNC pincer complexes have been extensively studied in catalysis, yet their application in nitrile hydration still needs to be explored [54, 55]. Thus, investigating the catalytic reactivity of cationic Ru(II)-CNC pincer complexes for this specific transformation

is highly beneficial. Herein, we report the catalytic application of cationic Ru(II)-CNC pincer complexes as phosphine free catalysts [Ru(CNC^{Me})(CN^{Me})I]PF$_6$ (**7a**), [Ru(CNC$^{i\text{-}Pr}$)(CN^{Me})I]PF$_6$ (**7b**), [Ru(CNC^{Cy})(CN^{Me})I]PF$_6$ (**7c**), [Ru(CNC$^{t\text{-}Bu}$)(CN^{Me})I]PF$_6$ (**7d**), [Ru(CNC^{Me})(CN$^{i\text{-}Pr}$)I]PF$_6$ (**8a**), [Ru(CNC$^{i\text{-}Pr}$)(CN$^{i\text{-}Pr}$)I]PF$_6$ (**8b**), [Ru(CNC^{Cy})(CN$^{i\text{-}Pr}$)I]PF$_6$ (**8c**), [Ru(CNC$^{t\text{-}Bu}$)(CN$^{i\text{-}Pr}$)I]PF$_6$ (**8d**), [Ru(CNC^{Me})(Py-Bim^{Me})I]PF$_6$ (**9a**), and [Ru(CNC^{Me})(3MePy-Im^{Me})I]PF$_6$ (**10a**) for hydration of nitriles under mild reaction conditions in an aqueous medium that afforded excellent yield (Figure **5.2**).

5.2. Results and Discussion

All the synthesized novel ruthenium pincer complexes were investigated for the catalytic application for the hydration of nitriles under mild reaction conditions in an aqueous medium.

5.2.1. Catalytic application for hydration of nitriles

Cationic Ru(II)-CNC pincer complexes were examined for catalytic application in the hydration of nitriles. Initially, we have taken benzonitrile as a model substrate with a catalytic amount of base and ruthenium catalyst in an aqueous medium. GCMS monitored the conversion to evaluate the catalytic reactivity of pincer complexes. Using 1 mmol of benzonitrile with 1 mol % catalyst **7b** and a catalytic amount of NaOH (20 mol%) at 60 ˚C for 6 h afforded maximum catalytic reactivity than other catalysts >99% (Table 5.1, Entry 5). Using similar reaction conditions for catalysts **7a**, **8a**, **9a**, and **10a** with smaller alkyl *N*-wingtip pincer complexes shows good to moderate catalytic reactivity with 87%, 85%, 64%, and 69% (Table 5.1, Entries 1-4) conversion as compared to catalyst **7b**, while with bulky *N*-wingtip pincer catalysts in similar reaction conditions **8b**, **7c**, **8c**, **7d**, and **8d** shows conversion of 96%, 72%, 73%, 62%, and 61% (Table 5.1, Entries 18-22). Further, decreasing the amount of NaOH with 10

and 15 mol% under similar reaction conditions shows lower catalytic reactivity than 20 mol% of NaOH with 77% and 89% conversions (Table 5.1, Entries 6-7). The catalytic reactivity was investigated with different bases such as KOH, NaHCO$_3$, and Na$_2$CO$_3$, which show lower reactivity as compared to NaOH and afforded good to moderate conversions of 95%, 27%, and 40% (Table 5.1, Entries 8-10). Under similar reaction conditions with a lower catalyst loading of 0.5 mol%, the catalytic reactivity decreased and showed almost half conversion 54%, although, increasing the reaction time (12 h) also affords only 76% conversion (Table 5.1, Entries 16-17). By decreasing the reaction time from 6 h to 2 h and 4 h, the conversion was also affected, and the reactivity was decreased to 53% and 77% conversions (Table 5.1, Entries 11-12). Further, investigation of the reactivity at lower temperatures from 30 ˚C, 40 ˚C, and 50 ˚C, the reactivity again decreases due to the lower solubility of the catalyst. It shows good to moderate reactivity with 17%, 38%, and 76% conversions (Table 5.1, Entries 13-15). Additionally, the reactivity was also investigated with similar reaction conditions with no catalyst loading, showing 20% conversion (Table 5.1, Entry 24), and without base, 17% conversion (Table 5.1, Entry 23). Furthermore, no such catalytic reactivity was observed upon investigation with similar reaction conditions without base and catalyst (Table 5.1, Entry 25).

5.2.2. Substrate scope for hydration of nitriles

Hydration of nitriles, including several aromatic substituted nitriles, heterocyclic nitriles, and aliphatic nitriles, was explored under the optimized reaction conditions. It was observed that complex **7b** typically produces high yields and works well as a precatalyst for a variety of substrates. A variety of substrates containing electron-donating or electron-withdrawing groups in the aryl group of nitriles reacted smoothly under optimized reaction conditions to produce high yields of the amides product (Scheme **5.1**). All the amide products

189

were characterized by NMR spectroscopy and compared with the previously reported NMR spectra. Hydration of benzonitrile gave an excellent yield of 93% with maximum selectivity for benzamide (**IIa**), which is also used as a model substrate. Similarly, 3-methylbenzonitrile, 4-methylbenzonitrile, 3-methoxybenzonitrile, and 4-methoxybenzonitrile gave good yields of amides as a sole product with 76%, 82%, 73%, and 87%, respectively (**IIb–IIe**). 2-aminobenzonitrile, 3-aminobenzonitrile, and 4-aminobenzonitrile have also afforded good yields as 71%, 46%, and 81%, respectively (**IIf–IIh**). However, 4-cyanobenzaldehyde shows poor reactivity after increasing temperature and time of the reaction, 48% yield (**IIj**). Similarly, methyl 4-cyanobenzoate shows poor catalytic reactivity and gave a lower isolated yield of 53% (**IIk**). However, 4-hydroxybenzonitrile (**Ii**) and 4-cyanobenzoic acid (**Il**) do not show any reactivity under the optimized reaction conditions. Further, 2-nitrobenzonitrile, 3-nitrobenzonitrile, and 4-nitrobenzonitrile gave good isolated yields of 48%, 77%, and 74%, respectively (**IIm–IIo**) under similar reaction conditions. Halogen-substituted nitriles i.e., 2-chlorobenzonitrile and 2-bromobenzonitrile shows good reactivity and afforded good isolated yields 65% (**IIp**) and 62% (**IIq**), while 4-chlorobenzonitrile, 4-bromobenzonitrile and 4-iodobenzonitrile also afforded better yields 81%, 75%, and 77%, respectively (**IIr–IIt**). 2-naphthonitrile also reacted well and gave a better yield under similar reaction conditions, 89% (**IIu**). However, cinnamonitrile afforded cinnamamide products with a lower yield than other aryl amide products by 57% (**IIv**). Additionally, we explored the reactivity of heterocyclic nitriles, i.e., 3-cyanopyridine, 4-cyanopyridine, and 2-thiophenecarbonitrile under similar reaction conditions, which afforded good yields viz; 62%, 67%, and 85%, respectively (**IIw–IIy**). The product of 3-cyanopyridine is nicotinamide (**IIw**), a biologically active compound with anti-inflammatory properties, and is helpful for those with inflammatory skin problems [56, 57]. However, aliphatic nitriles such as butyronitrile gave a poor yield of 34% (**IIz**).

Table 5.1. Screening of catalyst optimization in an aqueous medium for hydration of benzonitrile.
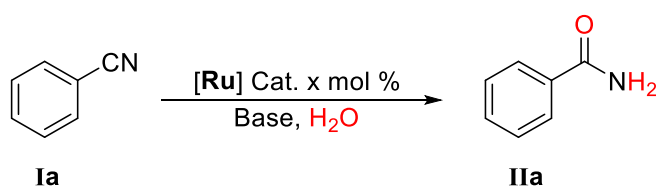
Entry[a]	Catalyst (mol%)	Base (mol%)	Temp. (°C), time (h)	Conversion[b] (%)	TON[c]/ TOF[d](h^{-1})
1.	**7a** (1)	NaOH (20)	60/6	87(82)	87/14
2.	**8a** (1)	NaOH (20)	60/6	85(81)	85/14
3.	**9a** (1)	NaOH (20)	60/6	64(59)	64/11
4.	**10a** (1)	NaOH (20)	60/6	69(63)	69/11
5.	**7b (1)**	**NaOH (20)**	**60/6**	**>99(93)**	**99/16**
6.	**7b** (1)	NaOH (10)	60/6	77	77/13
7.	**7b** (1)	NaOH (15)	60/6	89	89/15
8.	**7b** (1)	KOH (20)	60/6	95	95/16
9.	**7b** (1)	NaHCO$_3$ (20)	60/6	27	27/4
10.	**7b** (1)	Na$_2$CO$_3$ (20)	60/6	40	40/7
11.	**7b** (1)	NaOH (20)	60/2	53	53/26
12.	**7b** (1)	NaOH (20)	60/4	77	77/19
13.	**7b** (1)	NaOH (20)	30/6	17	17/3
14.	**7b** (1)	NaOH (20)	40/6	38	38/6
15.	**7b** (1)	NaOH (20)	50/6	76	76/13
16.	**7b** (0.5)	NaOH (20)	60/6	54	108/18
17.	**7b** (0.5)	NaOH (20)	60/12	76	152/13
18.	**8b** (1)	NaOH (20)	60/6	96(89)	96/16
19.	**7c** (1)	NaOH (20)	60/6	72(64)	72/12
20.	**8c** (1)	NaOH (20)	60/6	73(66)	73/12
21.	**7d** (1)	NaOH (20)	60/6	62(57)	62/10
22.	**8d** (1)	NaOH (20)	60/6	61(54)	61/10
23.	**7b** (1)	-	60/6	17	17/3

24.	-	NaOH (20)	60/6	20	0
25.	-	-	60/6	0	0

[a]Reaction conditions: Benzonitrile (1 mmol), Catalyst (1 mol %), Base, H_2O (5 mL) under an open-air condition. [b]Conversion was determined by gas chromatography (GCMS) without an internal standard and isolated yield after the work-up is given in parentheses. [c]TON = [(Number of moles of substrate converted)/(Number of moles of catalyst)] at the end of the reaction. [d]TOF = [(TON)/hour].

Scheme 5.1. The substrate scope of nitrile hydration from catalyst **7b**[a].
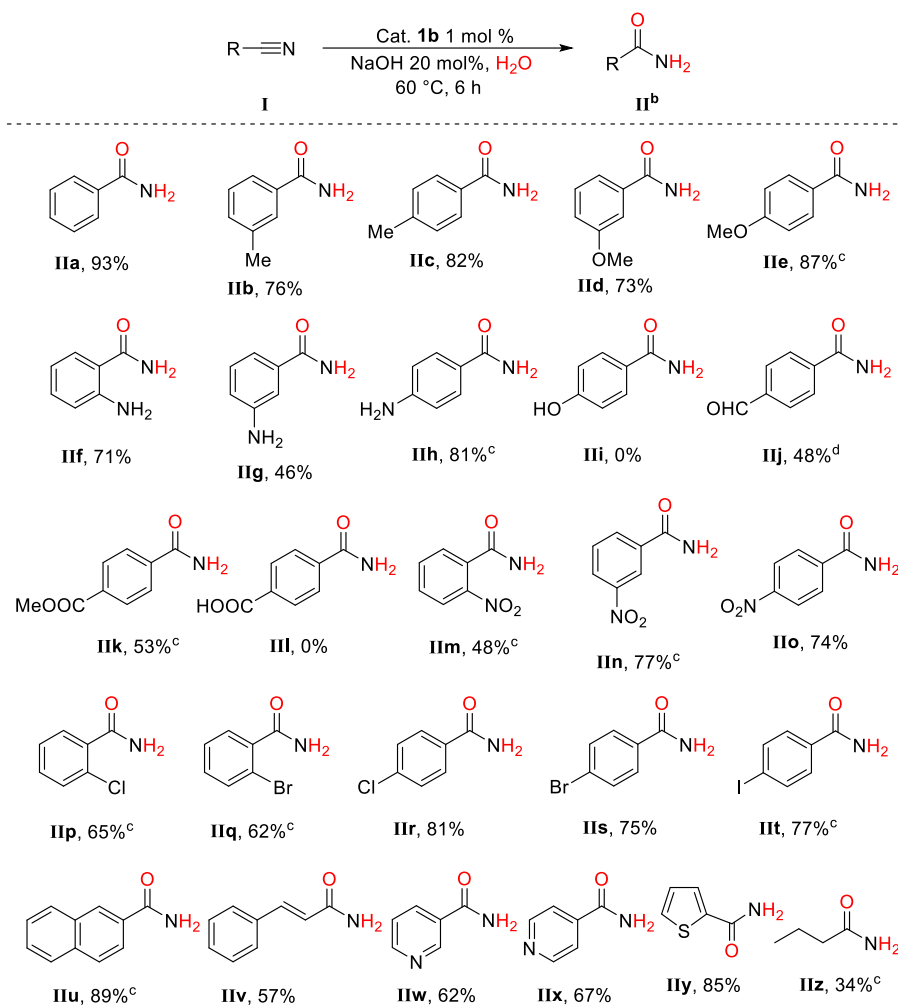
[a]Reaction conditions: Nitrile (1 mmol), Catalyst (1 mol %), NaOH (20 mol%), H_2O (5 mL) under an open-air condition at 60 ˚C for 6h. [b]Isolated yield. [c]0.5 ml isopropanol was used due to the poor solubility of the reactant in H_2O. [d]Reaction at 80 ˚C for 24 hours.

5.2.3. Mechanism for hydration of nitrile

The hydration of nitriles catalyzed by transition metal complexes has been shown to follow slightly different mechanisms and involve different types of intermediates depending on the catalyst precursor

[46, 58, 59]. Recently, ruthenium complexes based on amide-phosphine pincer ligands were shown to catalyzed the base-free hydration of nitriles via Ru–H···H–OH dihydrogen bonding interaction in the catalytic cycle [47]. We analysed our catalytic samples using mass spectrometry to get some insight into the reaction mechanism and reactive intermediates. ESI-MS analysis of the catalytic mixture reveals the formation of a Ru-OH species, **A** in the first hour of the reaction (Figure **5.5**). Otten and coworkers have reported the hydration of nitriles catalyzed by ruthenium pincer complexes through a metal-ligand cooperative effect in the catalytic cycle and the appearance of a Ru-OH species during the catalysis [46]. Further, the nitrile-bound species **B** is detected in the mass spectrum of the catalytic mixture after three hours (Figure **5.6**). A plausible mechanism starting from the most efficient precatalyst **7b** and involving an active intermediate Ru-hydroxy complex **A** is proposed in Figure **5.3**.

The catalytic reaction of hydration of nitriles involves a preliminary step that begins with the generation of ruthenium hydroxy species **A** by the reaction of complex **7b** with the base (NaOH or KOH) or base + water (Na_2CO_3 or $NaHCO_3$), which gives a peak at m/z 573.1689. During our attempts to isolate or characterize the intermediate **A**, it was realized that this species is stable only in the presence of higher equivalents of base. An NMR tube experiment in dmso-d_6 containing **7b** with two equivalents of KOH shows only ~10% of a new species in addition to the signals of the starting complex (Figure **5.7**). However, we are able to get convincing HRMS data for the in situ generated species **A** under catalytic conditions but without nitrile substrate (Figure **5.8**). Further, an intermediate **B,** which appears in LCMS at m/z 676.2123, is formed via dissociation of a hemilabile pyridine of the bidentate ligand, followed by coordination of benzonitrile. The nucleophilic attack of hydroxide at the electrophilic centre of benzonitrile generates intermediate **C** with an iminolate ligand. Further, rearrangement of the iminolate to amido and

193

coordination of a water molecule gives intermediate **D**, which undergoes protonolysis to give the final amide products and regenerates the active catalyst **A**. Metal-hydroxy intermediates, similar to **B** and **C**, have been previously reported for the hydration of nitriles using other metal complexes [51, 58, 60] which follow a similar mechanism.
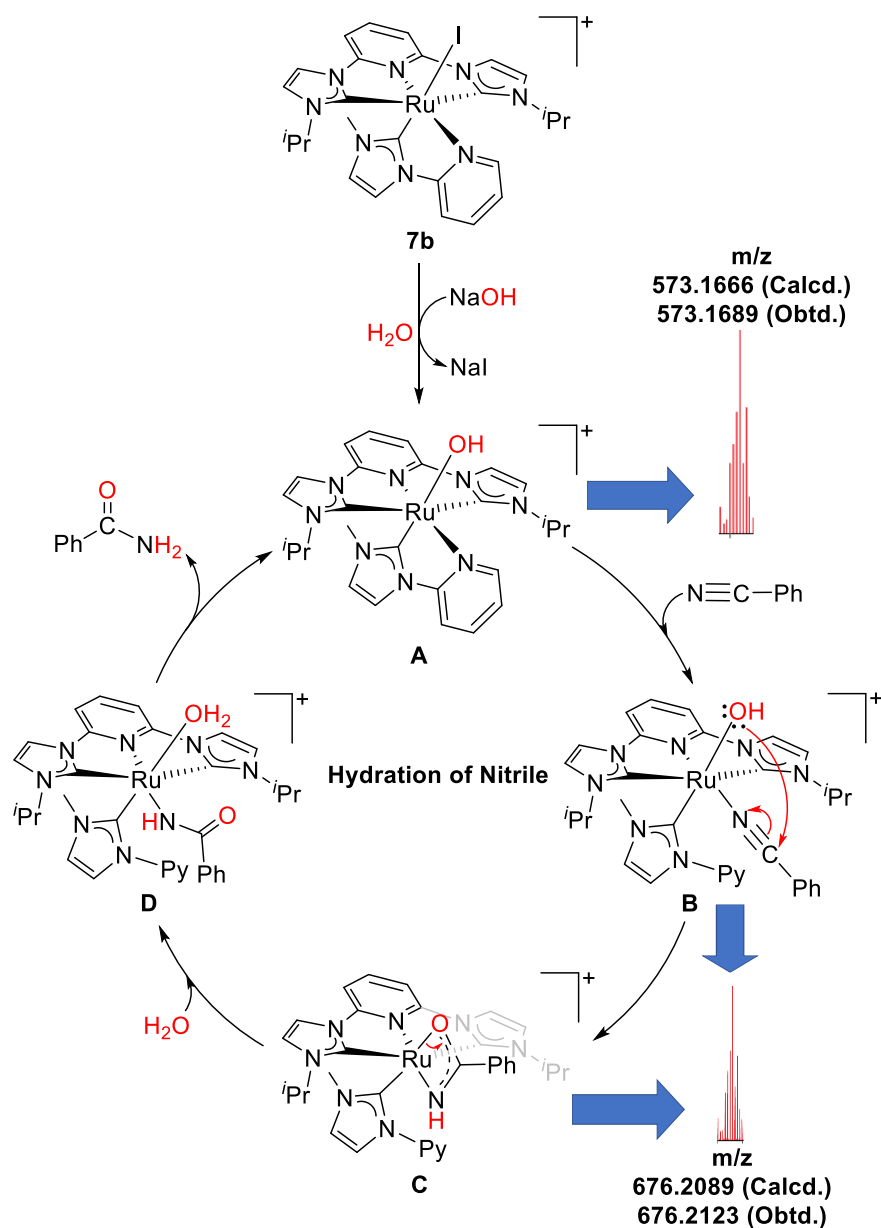
Figure 5.3. Plausible mechanism for the hydration of nitrile by complex **7b** with two key intermediates was identified through the LCMS analysis of the catalytic sample.

5.2.4. Recyclability experiment

The recovery of the homogeneous catalysts from the reaction mixture has several restrictions, despite their various advantages. Due to the good solubility of ruthenium catalysts in water, we cannot recover the catalyst from the reaction mixture and reuse it for further catalytic reactions. However, we recovered the catalysis product using crystallization and reused the remaining reaction mixture for a few more cycles of catalytic reactions. We employed 4-methylbenzonitrile (**Ic**) as a model substrate to get 4-methylbenzamide (**IIc**) under reaction conditions similar to those in Scheme **5.1**. The aqueous solution containing **7b** was reused five successive times, with a loss of catalytic activity after the second cycle (Figure **5.4**). After each catalytic cycle, the reaction mixture was cooled at 4 ˚C to get the crystals of the 4-methylbenzamide (**IIc**), and the aqueous solution containing **7b** was further reused in the next hydration reaction.
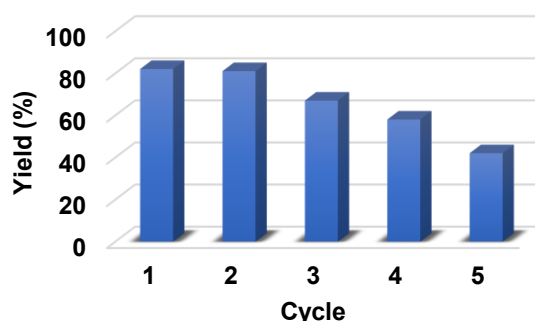
Figure 5.4. Recyclability experiment of catalyst **7b** for the hydration of 4-methylbenzonitrile (**Ic**) to 4-methylbenzamide (**IIc**). Reaction conditions were identical to those indicated in Scheme **5.1**.

5.3. Conclusion

All new Ru(II) complexes were investigated for the catalytic activity of the hydration of nitriles in an aqueous medium under mild reaction conditions. These Ru(II) complexes revealed higher reactivity with excellent selectivity in the hydration of nitriles. Particularly, complex

[Ru(CNC$^{i\text{-Pr}}$)(CN^{Me})I]PF$_6$ (**7b**) exhibited the best reactivity among all the complexes. The mechanistic investigation shed light on the catalytic pathway initiated by a [Ru-OH] species, where the pyridine bidentate ligand demonstrated hemilability, facilitating the binding of the nitrile substrate to the metal centre. This catalysis was reported in mild reaction conditions i.e., low catalyst loading, low base loading, lower temperature, and less reaction time in an aqueous medium. The broad applicability of these Ru(II) complexes as catalysts for nitrile hydration was demonstrated by the successful conversion of a wide variety of nitriles, including electron-releasing, electron-withdrawing, and heterocyclic nitriles, into the corresponding amides with high reactivity and good yields. The present study contributes to the advancement of nitrile hydration as an efficient, versatile, and sustainable approach for amide synthesis. Furthermore, the successful conversion of diverse nitriles highlights these catalyst's potential for synthesising valuable amide derivatives in various chemical and pharmaceutical applications.

5.4. Experimental Section

5.4.1. General Consideration

All reactions were carried out under open-air conditions. All the used cationic Ru(II) pincer catalysts were synthesized by our reported procedure, as already discussed in Chapter 4. Deuterated dimethyl sulphoxide (DMSO-d$_6$), and deuterated chloroform (CDCl$_3$) were purchased from EURISOtop or Sigma-Aldrich. NMR spectra were recorded on Bruker Avance NEO spectrometer operating at 500 MHz for ^{1}H and 126 MHz for ^{13}C NMR. NMR chemical shifts are reported in ppm and referenced to the solvent peaks for ^{1}H (CDCl$_3$ δ 7.26 and DMSO-d$_6$ δ 2.50 ppm) and ^{13}C (natural abundance of ^{13}C in CDCl$_3$ δ 77.16 and DMSO-d$_6$ δ 39.52 ppm). Multiplicities are given as s (singlet), d (doublet), t (triplet), and m (multiplet), and the coupling

constants *J* are given in hertz. The mass chromatograms were recorded on Bruker-Daltonics-MicroTOF-QII mass spectrometer in HPLC grade methanol. GC Samples were analysed in Shimadzu QP2010 Ultra, without an internal standard in HPLC grade methanol.

5.4.2. General procedure for catalyst optimization of the hydration of benzonitrile

In a Schlenk tube, benzonitrile (0.103 mL, 1 mmol), ruthenium catalysts (0.5-1 mol%), and different bases (10-20 mol%) were dissolved in H_2O (5 mL) under open-air conditions. The reaction mixture was quickly heated to reflux by lowering it into a preheated oil bath at different temperatures and times. The conversion of the benzamide product was determined by the relative peak area of the reactant and the product in GC without an internal standard.

5.4.3. General procedure for substrate scope for hydration of nitriles

In a Schlenk tube, nitriles (1 mmol), catalyst **7b** (0.008 g, 0.01 mmol), and NaOH (0.008 g, 0.2 mmol) were dissolved in H_2O (5 mL) under an open-air condition. The reaction mixture was heated at 60 ˚C for 6 h. After completion of the reaction, the reaction mixture was cooled at 4 ˚C to get the crystals of the amides in most cases. Some of them were purified by silica gel column chromatography using hexane and ethyl acetate as eluents. NMR data for the amide products matched with the reported values.

5.4.4. Experimental details for mass analysis of the hydration of benzonitrile

In a Schlenk tube, catalyst **7b** (0.008 g, 0.01 mmol) was added to a solution of benzonitrile (0.103 ml, 1 mmol) and NaOH (0.008 g, 0.2 mmol) in H_2O under open-air conditions. The resulting reaction

mixture was heated at 60 ˚C by lowering into a preheated oil bath, and then samples were taken at 1 h and 3 h for LCMS analysis.

5.4.5. Identification of catalytic reaction intermediate (A) $[Ru(CNC^{i-Pr})(CN^{Me})OH]^+$
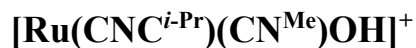
In an NMR tube, catalyst **7b** (0.025 g, 0.03 mmol) and KOH (0.004 g, 0.06 mmol) were added in dmso-d_6 under open-air conditions. The resulting reaction mixture was stirred and heated gently for 30 minutes, and then the ^{1}H NMR spectrum was recorded (Figure **5.7**). Further, LCMS analysis was done by adding catalyst **7b** (0.025 g, 0.03 mmol) and NaOH (0.003 g, 0.06 mmol) in H_2O in a Schlenk tube, and the resulting reaction mixture was heated at 60 ˚C for 3 h under open-air conditions (Figure **5.8**). HRMS for intermediate (A) $[C_{26}H_{30}N_8RuOH]^+$ Calculated - 573.1666, Found - 573.1629.

5.4.6. NMR data of products after hydration reaction

Benzamide (IIa): ^{1}H NMR (500 MHz, CDCl$_3$) δ 7.82 (d, J = 7.5 Hz, 2H), 7.52 (t, J = 7.5 Hz, 1H), 7.43 (t, J = 7.6 Hz, 2H), 6.29 (s, 2H, NH). ^{13}C NMR (126 MHz, CDCl$_3$) δ 169.83, 133.52, 132.10, 128.73, 127.46.

3-Methylbenzamide (IIb): ^{1}H NMR (500 MHz, CDCl$_3$) δ 7.59 (s, 1H), 7.53 (dd, J = 5.3, 3.4 Hz, 1H), 7.26 – 7.21 (m, 2H), 6.35 (s, 1H, NH), 6.33 (s, 1H, NH), 2.32 (s, 3H). ^{13}C NMR (126 MHz, CDCl$_3$) δ 170.17, 138.55, 133.50, 132.78, 128.55, 128.21, 124.42, 21.41.

4-Methylbenzamide (IIc): ^{1}H NMR (500 MHz, CDCl$_3$) δ 7.71 (d, J = 8.2 Hz, 2H), 7.24 (d, J = 8.0 Hz, 2H), 6.10 (s, 1H, NH), 5.97 (s, 1H, NH), 2.40 (s, 3H). ^{13}C NMR (126 MHz, CDCl$_3$) δ 169.60, 142.66, 130.63, 129.41, 127.51, 21.62.

3-Methoxybenzamide (IId): ^{1}H NMR (500 MHz, DMSO-d_6) δ 7.97 (s, 1H), 7.46 – 7.41 (m, 2H), 7.38 – 7.34 (m, 2H), 7.07 (dd, J = 8.1, 2.9

Hz, 1H), 3.79 (s, 3H). ^{13}C NMR (126 MHz, DMSO-d$_6$) δ 167.71, 159.17, 135.74, 129.37, 119.73, 117.11, 112.67, 55.25.

4-Methoxybenzamide (IIe): ^{1}H NMR (500 MHz, DMSO-d$_6$) δ 7.86 – 7.83 (m, 3H, 1NH), 7.17 (s, 1H, NH), 6.97 (d, *J* = 8.8 Hz, 2H), 3.79 (s, 3H). ^{13}C NMR (126 MHz, DMSO-d$_6$) δ 167.52, 161.63, 129.40, 126.52, 113.43, 55.35.

2-Aminobenzamide (IIf): ^{1}H NMR (500 MHz, DMSO-d$_6$) δ 7.71 (s, 1H, NH), 7.52 (d, *J* = 8.0 Hz, 1H), 7.12 (t, *J* = 7.6 Hz, 1H), 7.04 (s, 1H, NH), 6.67 (d, *J* = 8.2 Hz, 1H), 6.54 (s, 2H, NH$_2$^{Ar}), 6.47 (t, *J* = 7.4 Hz, 1H). ^{13}C NMR (126 MHz, DMSO-d$_6$) δ 171.35, 150.22, 131.94, 128.79, 116.45, 114.43, 113.72.

3-Aminobenzamide (IIg): ^{1}H NMR (500 MHz, DMSO-d$_6$) δ 7.71 (s, 1H, NH), 7.11 (s, 1H), 7.06 – 7.03 (m, 2H, 1NH), 6.97 (dt, *J* = 7.6, 1.3 Hz, 1H), 6.68 – 6.66 (m, 1H), 5.17 (s, 2H, NH$_2$^{Ar}). ^{13}C NMR (126 MHz, DMSO-d$_6$) δ 168.78, 148.60, 135.22, 128.58, 116.53, 114.71, 113.13.

4-Aminobenzamide (IIh): ^{1}H NMR (500 MHz, DMSO-d$_6$) δ 7.58 (d, *J* = 8.4 Hz, 2H), 7.51 (s, 1H, NH), 6.82 (s, 1H, NH), 6.52 (d, *J* = 8.2 Hz, 2H), 5.59 (s, 2H, NH$_2$^{Ar}). ^{13}C NMR (126 MHz, DMSO-d$_6$) δ 168.12, 151.70, 129.16, 120.96, 112.50.

4-Formylbenzamide (IIj): ^{1}H NMR (500 MHz, DMSO-d$_6$) δ 10.06 (s, 1H), 8.18 (s, 1H, NH), 8.04 (d, *J* = 7.9 Hz, 2H), 7.97 (d, *J* = 7.9 Hz, 2H), 7.59 (s, 1H, NH). ^{13}C NMR (126 MHz, DMSO-d$_6$) δ 193.07, 167.34, 139.40, 137.94, 129.50, 128.28.

Methyl 4-carbamoylbenzoate (IIk): ^{1}H NMR (500 MHz, DMSO-d$_6$) δ 8.15 (s, 1H, NH), 8.01 (d, *J* = 8.2 Hz, 2H), 7.97 (d, *J* = 8.3 Hz, 2H), 7.56 (s, 1H, NH), 3.87 (s, 3H). ^{13}C NMR (126 MHz, DMSO-d$_6$) δ 167.33, 165.92, 138.50, 131.96, 129.23, 127.96, 52.52.

2-Nitrobenzamide (IIm): ^{1}H NMR (500 MHz, DMSO-d$_6$) δ 8.14 (s, 1H, NH), 7.99 (dd, J = 8.1, 1.3 Hz, 1H), 7.76 (td, J = 7.5, 1.2 Hz, 1H), 7.68 – 7.62 (m, 3H, 1NH). ^{13}C NMR (126 MHz, DMSO-d$_6$) δ 167.24, 147.27, 133.39, 132.61, 130.67, 128.88, 123.99.

3-Nitrobenzamide (IIn): ^{1}H NMR (500 MHz, DMSO-d$_6$) δ 8.69 (s, 1H), 8.38 – 8.36 (m, 1H), 8.34 (s, 1H, NH), 8.30 (dt, J = 7.8, 1.4 Hz, 1H), 7.77 (t, J = 8.0 Hz, 1H), 7.71 (s, 1H, NH). ^{13}C NMR (126 MHz, DMSO-d$_6$) δ 165.78, 147.85, 135.81, 133.85, 130.12, 125.94, 122.27.

4-Nitrobenzamide (IIo): ^{1}H NMR (500 MHz, DMSO-d$_6$) δ 8.30 (d, J = 8.8 Hz, 2H), 8.27 (s, 1H, NH), 8.09 (d, J = 8.8 Hz, 2H), 7.72 (s, 1H, NH). ^{13}C NMR (126 MHz, DMSO-d$_6$) δ 166.27, 149.10, 140.02, 128.95, 123.50.

2-Chlorobenzamide (IIp): ^{1}H NMR (500 MHz, CDCl$_3$) δ 7.77 – 7.74 (m, 1H), 7.42 – 7.35 (m, 2H), 7.34 – 7.31 (m, 1H), 6.54 (s, 1H, NH), 6.41 (s, 1H, NH). ^{13}C NMR (126 MHz, CDCl$_3$) δ 168.54, 133.98, 131.90, 130.93, 130.67, 130.50, 127.25.

2-Bromobenzamide (IIq): ^{1}H NMR (500 MHz, DMSO-d$_6$) δ 7.88 (s, 1H, NH), 7.63 (d, J = 7.9 Hz, 1H), 7.57 (s, 1H, NH), 7.43 – 7.39 (m, 2H), 7.35 – 7.31 (m, 1H). ^{13}C NMR (126 MHz, DMSO-d$_6$) δ 169.26, 139.36, 132.81, 130.78, 128.65, 127.60, 118.69.

4-Chlorobenzamide (IIr): ^{1}H NMR (500 MHz, CDCl$_3$) δ 7.75 (d, J = 8.4 Hz, 2H), 7.43 (d, J = 8.3 Hz, 2H), 6.04 (s, 1H, NH), 5.82 (s, 1H, NH). ^{13}C NMR (126 MHz, CDCl$_3$) δ 168.33, 138.50, 131.82, 129.07, 128.94.

4-Bromobenzamide (IIs): ^{1}H NMR (500 MHz, CDCl$_3$) δ 7.68 (d, J = 8.5 Hz, 2H), 7.59 (d, J = 8.5 Hz, 2H), 6.01 (s, 1H, NH), 5.71 (s, 1H, NH). ^{13}C NMR (126 MHz, CDCl$_3$) δ 168.35, 132.27, 132.06, 129.11, 126.99.

4-Iodobenzamide (IIt): ^{1}H NMR (500 MHz, DMSO-d6) δ 8.03 (s, 1H, NH), 7.83 (d, J = 8.4 Hz, 2H), 7.64 (d, J = 8.5 Hz, 2H), 7.42 (s, 1H, NH). ^{13}C NMR (126 MHz, DMSO-d6) δ 167.27, 137.15, 133.74, 129.51, 98.94.

2-Naphthamide (IIu): ^{1}H NMR (500 MHz, DMSO-d6) δ 8.49 (s, 1H), 8.18 (s, 1H, NH), 8.01 – 7.95 (m, 4H), 7.61 – 7.55 (m, 2H), 7.49 (s, 1H, NH). ^{13}C NMR (126 MHz, DMSO-d6) δ 168.29, 134.33, 132.28, 131.68, 129.03, 127.97, 127.95, 127.79, 127.75, 126.85, 124.51.

Cinnamamide (IIv): ^{1}H NMR (500 MHz, DMSO-d6) δ 7.56 – 7.54 (m, 3H), 7.43 – 7.37 (m, 4H, 1NH), 7.11 (s, 1H, NH), 6.61 (d, J = 15.9 Hz, 1H). ^{13}C NMR (126 MHz, DMSO-d6) δ 166.79, 139.28, 134.91, 129.54, 128.99, 127.61, 122.33.

Nicotinamide (IIw): ^{1}H NMR (500 MHz, DMSO-d6) δ 9.02 (s, 1H), 8.69 (dd, J = 4.8, 1.7 Hz, 1H), 8.20 (dt, J = 7.9, 2.0 Hz, 1H), 8.16 (s, 1H, NH), 7.60 (s, 1H, NH), 7.49 (dd, J = 7.9, 4.8 Hz, 1H). ^{13}C NMR (126 MHz, DMSO-d6) δ 166.50, 151.93, 148.70, 135.19, 129.69, 123.45.

Isonicotinamide (IIx): ^{1}H NMR (500 MHz, DMSO-d6) δ 8.72 – 8.70 (m, 2H), 8.24 (s, 1H, NH), 7.77 – 7.75 (m, 2H), 7.72 (s, 1H, NH). ^{13}C NMR (126 MHz, DMSO-d6) δ 166.37, 150.25, 141.31, 121.44.

2-Thiophenecarboxamide (IIy): ^{1}H NMR (500 MHz, DMSO-d6) δ 7.96 (s, 1H, NH), 7.74 – 7.72 (m, 2H), 7.37 (s, 1H, NH), 7.12 (dd, J = 4.9, 3.7 Hz, 1H). ^{13}C NMR (126 MHz, DMSO-d6) δ 162.92, 140.32, 131.01, 128.69, 127.92.

Butyramide (IIz): ^{1}H NMR (500 MHz, DMSO-d6) δ 7.31 (s, 1H, NH), 6.69 (s, 1H, NH), 2.00 (t, J = 7.4 Hz, 2H), 1.47 (q, J = 7.4 Hz, 2H), 0.83 (t, J = 7.4 Hz, 3H). ^{13}C NMR (126 MHz, DMSO-d6) δ 174.64, 37.21, 18.65, 13.80.

5.4.7. Characterisation data for reaction intermediates
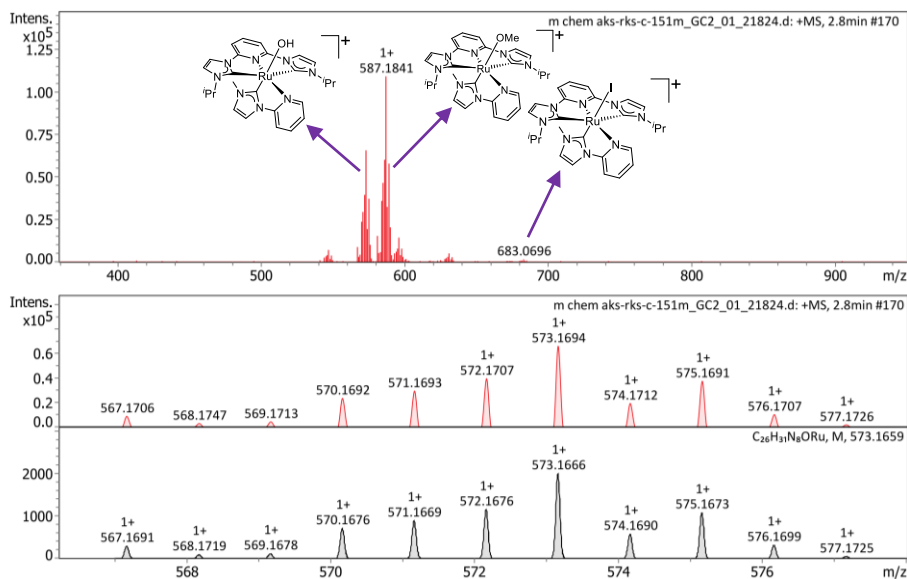
Figure 5.5. LCMS spectrogram of the catalytic reaction mixture after one hour. The Ru-OMe complex is generated in situ as the mass sample is prepared in methanol solvent.
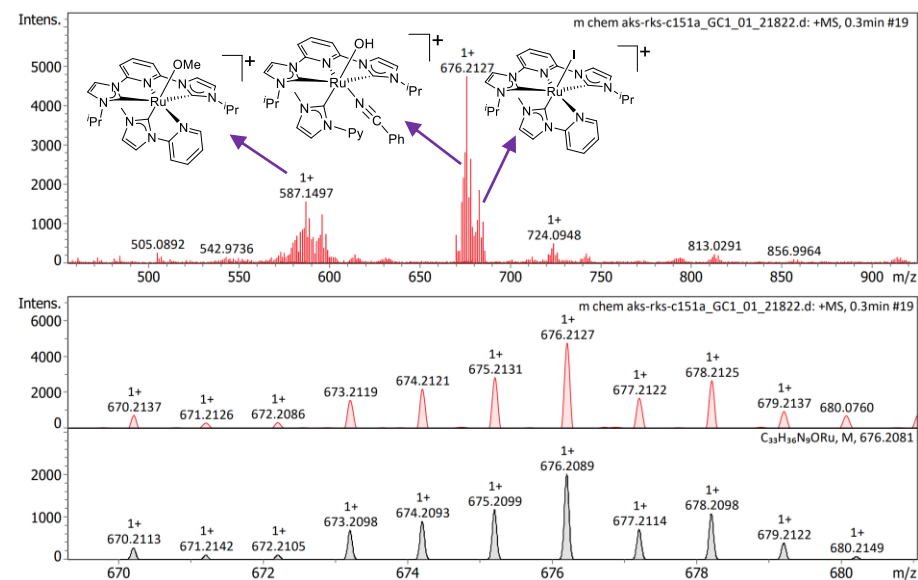
Figure 5.6. LCMS spectrogram of the catalytic reaction mixture after three hours. The Ru-OMe complex is generated in situ as the mass sample is prepared in methanol solvent.
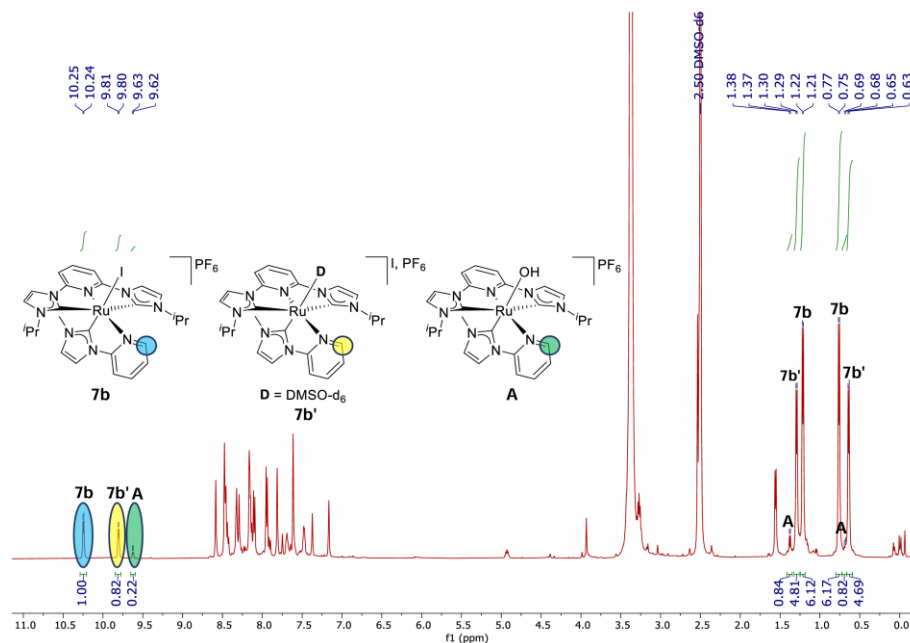
Figure 5.7. ^{1}H NMR spectrum of the reaction mixture in dmso-d$_6$ for identifying Ru-OH intermediate **A**.
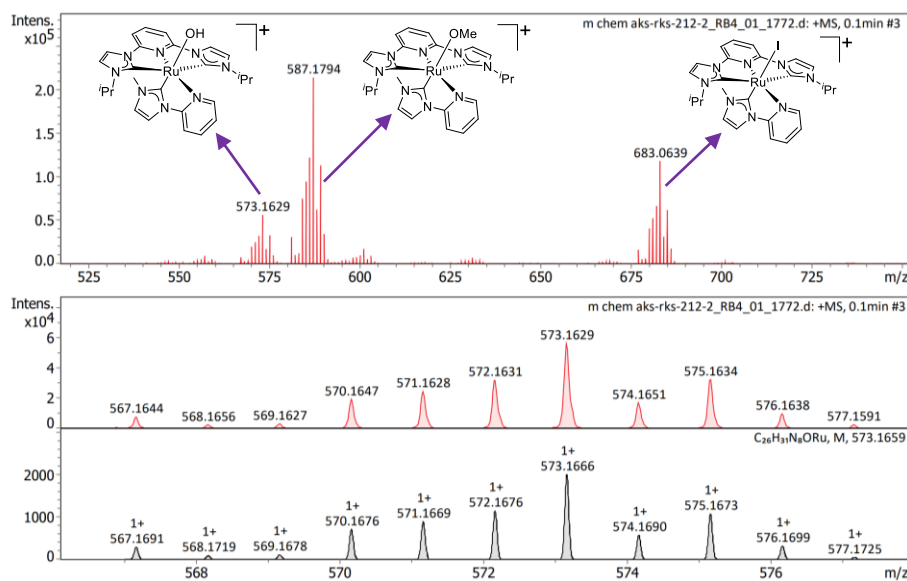
Figure 5.8. LCMS spectrogram of the Ru-OH intermediate **A**. The Ru-OMe complex is generated in situ as the mass sample is prepared in methanol solvent.

5.5. References

1. Peris E. (2018), Smart *N*-Heterocyclic Carbene Ligands in Catalysis, Chem. Rev., 118(19), 9988-10031 (DOI: 10.1021/acs.chemrev.6b00695).

2. Udvardy A., Joó F., Kathó Á. (2021), Synthesis and catalytic applications of Ru(II)-phosphaurotropine complexes with the use of simple water-soluble Ru(II)-precursors, Coord. Chem. Rev., 438, 213871 (DOI: 10.1016/j.ccr.2021.213871).

3. Ishizuka T., Sugimoto H., Itoh S., Kojima T. (2022), Recent progress in oxidation chemistry of high-valent ruthenium-oxo and osmium-oxo complexes and related species, Coord. Chem. Rev., 466, 214536 (DOI: 10.1016/j.ccr.2022.214536).

4. Jacobsen H., Correa A., Poater A., Costabile C., Cavallo L. (2009), Understanding the M(NHC) (NHC = *N*-heterocyclic carbene) bond, Coord. Chem. Rev., 253(5), 687-703 (DOI: 10.1016/j.ccr.2008.06.006).

5. Nareddy P., Jordan F., Szostak M. (2017), Recent Developments in Ruthenium-Catalyzed C–H Arylation: Array of Mechanistic Manifolds, ACS Catal., 7(9), 5721-5745 (DOI: 10.1021/acscatal.7b01645).

6. Filonenko G. A., Cosimi E., Lefort L., Conley M. P., Copéret C., Lutz M., Hensen E. J. M., Pidko E. A. (2014), Lutidine-Derived Ru-CNC Hydrogenation Pincer Catalysts with Versatile Coordination Properties, ACS Catal., 4(8), 2667-2671 (DOI: 10.1021/cs500720y).

7. Chang W., Gong X., Wang S., Xiao L.-P., Song G. (2017), Acceptorless dehydrogenation and dehydrogenative coupling of alcohols catalysed by protic NHC ruthenium complexes, Org. Biomol. Chem., 15(16), 3466-3471 (DOI: 10.1039/C7OB00542C).

8. Urbina-Blanco C. A., Leitgeb A., Slugovc C., Bantreil X., Clavier H., Slawin A. M. Z., Nolan S. P. (2011), Olefin Metathesis

Featuring Ruthenium Indenylidene Complexes with a Sterically Demanding NHC Ligand, Chem. Eur. J., 17(18), 5045-5053 (DOI: 10.1002/chem.201003082).

9. Boudreaux C. M., Liyanage N. P., Shirley H., Siek S., Gerlach D. L., Qu F., Delcamp J. H., Papish E. T. (2017), Ruthenium(II) complexes of pyridinol and *N*-heterocyclic carbene derived pincers as robust catalysts for selective carbon dioxide reduction, Chem. Commun., 53(81), 11217-11220 (DOI: 10.1039/C7CC05706G).

10. Zhao Q., Meng G., Nolan S. P., Szostak M. (2020), *N*-Heterocyclic Carbene Complexes in C–H Activation Reactions, Chem. Rev., 120(4), 1981-2048 (DOI: 10.1021/acs.chemrev.9b00634).

11. Hopkinson M. N., Richter C., Schedler M., Glorius F. (2014), An overview of *N*-heterocyclic carbenes, Nature, 510(7506), 485-496 (DOI: 10.1038/nature13384).

12. Younus H. A., Ahmad N., Su W., Verpoort F. (2014), Ruthenium pincer complexes: Ligand design and complex synthesis, Coord. Chem. Rev., 276, 112-152 (DOI: 10.1016/j.ccr.2014.06.016).

13. Malineni J., Keul H., Möller M. (2015), A green and sustainable phosphine-free NHC-ruthenium catalyst for selective oxidation of alcohols to carboxylic acids in water, Dalton Trans., 44(39), 17409-17414 (DOI: 10.1039/C5DT01358E).

14. Wu X.-J., Wang H.-J., Yang Z.-Q., Tang X.-S., Yuan Y., Su W., Chen C., Verpoort F. (2019), Efficient and phosphine-free bidentate *N*-heterocyclic carbene/ruthenium catalytic systems for the dehydrogenative amidation of alcohols and amines, Org. Chem. Front., 6(5), 563-570 (DOI: 10.1039/C8QO00902C).

15. Randl S., Gessler S., Wakamatsu H., Blechert S. (2001), Highly Selective Cross Metathesis with Acrylonitrile Using a Phosphine Free Ru-Complex, Synlett, 2001(3), 430-432 (DOI: 10.1055/s-2001-11393).

16. Day C. S., Fogg D. E. (2018), High-Yield Synthesis of a Long-Sought, Labile Ru-NHC Complex and Its Application to the Concise Synthesis of Second-Generation Olefin Metathesis Catalysts, Organometallics, 37(24), 4551-4555 (DOI: 10.1021/acs.organomet.8b00745).

17. Beletskaya I. P., Cheprakov A. V. (2000), The Heck Reaction as a Sharpening Stone of Palladium Catalysis, Chem. Rev., 100(8), 3009-3066 (DOI: 10.1021/cr9903048).

18. He Y.-M., Fan Q.-H. (2010), Phosphine-free chiral metal catalysts for highly effective asymmetric catalytic hydrogenation, Org. Biomol. Chem., 8(11), 2497-2504 (DOI: 10.1039/B925199P).

19. Saha R., Mukherjee A., Bhattacharya S. (2022), Development of a ruthenium–aquo complex for utilization in synthesis and catalysis for selective hydration of nitriles and alkynes, New J. Chem., 46(19), 9098-9110 (DOI: 10.1039/D1NJ04736A).

20. Dragutan V., Dragutan I., Delaude L., Demonceau A. (2007), NHC-Ru complexes-Friendly catalytic tools for manifold chemical transformations, Coord. Chem. Rev., 251(5), 765-794 (DOI: 10.1016/j.ccr.2006.09.002).

21. Colacino E., Martinez J., Lamaty F. (2007), Preparation of NHC-ruthenium complexes and their catalytic activity in metathesis reaction, Coord. Chem. Rev., 251(5), 726-764 (DOI: 10.1016/j.ccr.2006.07.017).

22. Daw P., Petakamsetty R., Sarbajna A., Laha S., Ramapanicker R., Bera J. K. (2014), A Highly Efficient Catalyst for Selective Oxidative Scission of Olefins to Aldehydes: Abnormal-NHC-Ru(II) Complex in Oxidation Chemistry, J. Am. Chem. Soc., 136(40), 13987-13990 (DOI: 10.1021/ja5075294).

23. Carey J. S., Laffan D., Thomson C., Williams M. T. (2006), Analysis of the reactions used for the preparation of drug candidate molecules, Org. Biomol. Chem., 4(12), 2337-2347 (DOI: 10.1039/B602413K).

24. Wang M.-X. (2015), Enantioselective Biotransformations of Nitriles in Organic Synthesis, Acc. Chem. Res., 48(3), 602-611 (DOI: 10.1021/ar500406s).

25. Pattabiraman V. R., Bode J. W. (2011), Rethinking amide bond synthesis, Nature, 480(7378), 471-479 (DOI: 10.1038/nature10702).

26. Ahmed T. J., Knapp S. M. M., Tyler D. R. (2011), Frontiers in catalytic nitrile hydration: Nitrile and cyanohydrin hydration catalyzed by homogeneous organometallic complexes, Coord. Chem. Rev., 255(7), 949-974 (DOI: 10.1016/j.ccr.2010.08.018).

27. Allen C. L., Williams J. M. J. (2011), Metal-catalysed approaches to amide bond formation, Chem. Soc. Rev., 40(7), 3405-3415 (DOI: 10.1039/C0CS00196A).

28. O'Connor C. (1970), Acidic and basic amide hydrolysis, Q. Rev. Chem. Soc., 24(4), 553-564 (DOI: 10.1039/QR9702400553).

29. Tu T., Wang Z., Liu Z., Feng X., Wang Q. (2012), Efficient and practical transition metal-free catalytic hydration of organonitriles to amides, Green Chem., 14(4), 921-924 (DOI: 10.1039/C2GC16637B).

30. Edward J. T., Meacock S. C. R. (1957), 383. Hydrolysis of amides and related compounds. Part I. Some benzamides in strong aqueous acid, J. Chem. Soc., 2000-2007 (DOI: 10.1039/JR9570002000).

31. García-Álvarez R., Díez J., Crochet P., Cadierno V. (2010), Arene-Ruthenium(II) Complexes Containing Amino-Phosphine Ligands as Catalysts for Nitrile Hydration Reactions, Organometallics, 29(17), 3955-3965 (DOI: 10.1021/om1006227).

32. Prejanò M., Alberto M. E., Russo N., Marino T. (2020), Hydration of Aromatic Nitriles Catalyzed by Mn-OH Complexes: A Rationalization from Quantum Chemical Investigations, Organometallics, 39(18), 3352-3361 (DOI: 10.1021/acs.organomet.0c00436).

33. Fan X.-N., Deng W., Liu Z.-J., Yao Z.-J. (2020), Half-Sandwich Iridium Complexes for the One-Pot Synthesis of Amides: Preparation, Structure, and Diverse Catalytic Activity, Inorg. Chem., 59(22), 16582-16590 (DOI: 10.1021/acs.inorgchem.0c02497).

34. Marcé P., Lynch J., Blacker A. J., Williams J. M. J. (2016), A mild hydration of nitriles catalysed by copper(II) acetate, Chem. Commun., 52(7), 1436-1438 (DOI: 10.1039/C5CC08714G).

35. Tomás-Mendivil E., Cadierno V., Menéndez M. I., López R. (2015), Unmasking the Action of Phosphinous Acid Ligands in Nitrile Hydration Reactions Catalyzed by Arene-Ruthenium(II) Complexes, Chem. Eur. J., 21(47), 16874-16886 (DOI: 10.1002/chem.201503076).

36. Lee W.-C., Frost B. J. (2012), Aqueous and biphasic nitrile hydration catalyzed by a recyclable Ru(II) complex under atmospheric conditions, Green Chem., 14(1), 62-66 (DOI: 10.1039/C1GC15950J).

37. Vyas K. M., Mandal P., Singh R., Mobin S. M., Mukhopadhyay S. (2020), Arene-ruthenium (II)-phosphine complexes: Green catalysts for hydration of nitriles under mild conditions, Inorg. Chem. Commun. 112, 107698 (DOI: 10.1016/j.inoche.2019.107698).

38. Ferrer Í., Rich J., Fontrodona X., Rodríguez M., Romero I. (2013), Ru(II) complexes containing dmso and pyrazolyl ligands as catalysts for nitrile hydration in environmentally friendly media, Dalton Trans., 42(37), 13461-13469 (DOI: 10.1039/C3DT51580J).

39. Chouhan K. K., Chowdhury D., Mukherjee A. (2023), Cyclotrimetaphosphate-assisted ruthenium catalyst for the hydration of nitriles and oxidation of primary amines to amides under aerobic conditions in water, Org. Biomol. Chem., 21(11), 2429-2439 (DOI: 10.1039/D3OB00062A).

40. González-Fernández R., Crochet P., Cadierno V. (2016), Ruthenium-Catalyzed Synthesis of β-Hydroxyamides from β-Ketonitriles in Water, Org. Lett., 18(23), 6164-6167 (DOI: 10.1021/acs.orglett.6b03172).

41. Cadierno V., Francos J., Gimeno J. (2008), Selective Ruthenium-Catalyzed Hydration of Nitriles to Amides in Pure Aqueous Medium Under Neutral Conditions, Chem. Eur. J., 14(22), 6601-6605 (DOI: 10.1002/chem.200800847).

42. García-Álvarez R., Zablocka M., Crochet P., Duhayon C., Majoral J.-P., Cadierno V. (2013), Thiazolyl-phosphine hydrochloride salts: effective auxiliary ligands for ruthenium-catalyzed nitrile hydration reactions and related amide bond forming processes in water, Green Chem., 15(9), 2447-2456 (DOI: 10.1039/C3GC41201F).

43. Lee W.-C., Sears J. M., Enow R. A., Eads K., Krogstad D. A., Frost B. J. (2013), Hemilabile β-Aminophosphine Ligands Derived from 1,3,5-Triaza-7-phosphaadamantane: Application in Aqueous Ruthenium Catalyzed Nitrile Hydration, Inorg. Chem., 52(4), 1737-1746 (DOI: 10.1021/ic301160x).

44. Sears J. M., Lee W.-C., Frost B. J. (2015), Water soluble diphosphine ligands based on 1,3,5-triaza-7-phosphaadamantane (PTA-PR$_2$): Synthesis, coordination chemistry, and ruthenium catalyzed nitrile hydration, Inorg. Chim. Acta, 431, 248-257 (DOI: 10.1016/j.ica.2015.03.033).

45. Tomás-Mendivil E., Suárez F. J., Díez J., Cadierno V. (2014), An efficient ruthenium(IV) catalyst for the selective hydration of nitriles to amides in water under mild conditions, Chem. Commun., 50(68), 9661-9664 (DOI: 10.1039/C4CC04058A).

46. Guo B., Vries J. G. de, Otten E. (2019), Hydration of nitriles using a metal-ligand cooperative ruthenium pincer catalyst, Chem. Sci., 10(45), 10647-10652 (DOI: 10.1039/C9SC04624K).

47. Yadav S., Gupta R. (2022), Hydration of Nitriles Catalyzed by Ruthenium Complexes: Role of Dihydrogen Bonding Interactions

in Promoting Base-Free Catalysis, Inorg. Chem., 61(39), 15463-15474 (DOI: 10.1021/acs.inorgchem.2c02058).

48. Tomás-Mendivil E., García-Álvarez R., Vidal C., Crochet P., Cadierno V. (2014), Exploring Rhodium(I) Complexes [RhCl(COD)(PR$_3$)] (COD = 1,5-Cyclooctadiene) as Catalysts for Nitrile Hydration Reactions in Water: The Aminophosphines Make the Difference, ACS Catal., 4(6), 1901-1910 (DOI: 10.1021/cs500241p).

49. Goto A., Endo K., Saito S. (2008), Rh[I]-Catalyzed Hydration of Organonitriles under Ambient Conditions, Angew. Chem. Int. Ed., 47(19), 3607-3609 (DOI: 10.1002/anie.200800366).

50. Fan X.-N., Deng W., Liu Z.-J., Yao Z.-J. (2020), Half-Sandwich Iridium Complexes for the One-Pot Synthesis of Amides: Preparation, Structure, and Diverse Catalytic Activity, Inorg. Chem., 59(22), 16582-16590 (DOI: 10.1021/acs.inorgchem.0c02497).

51. Buil M. L., Cadierno V., Esteruelas M. A., Gimeno J., Herrero J., Izquierdo S., Oñate E. (2012), Selective Hydration of Nitriles to Amides Promoted by an Os-NHC Catalyst: Formation and X-ray Characterization of κ^2-Amidate Intermediates, Organometallics, 31(19), 6861-6867 (DOI: 10.1021/om3006799).

52. Ramón R. S., Marion N., Nolan S. P. (2009), Gold Activation of Nitriles: Catalytic Hydration to Amides, Chem. Eur. J., 15(35), 8695-8697 (DOI: 10.1002/chem.200901231).

53. Xing X., Xu C., Chen B., Li C., Virgil S. C., Grubbs R. H. (2018), Highly Active Platinum Catalysts for Nitrile and Cyanohydrin Hydration: Catalyst Design and Ligand Screening via High-Throughput Techniques, J. Am. Chem. Soc., 140(50), 17782-17789 (DOI: 10.1021/jacs.8b11667).

54. Andrew R. E., González-Sebastián L., Chaplin A. B. (2016), NHC-based pincer ligands: carbenes with a bite, Dalton Trans., 45(4), 1299-1305 (DOI: 10.1039/C5DT04429D).

55. Gunanathan C., Milstein D. (2014), Bond Activation and Catalysis by Ruthenium Pincer Complexes, Chem. Rev., 114(24), 12024-12087 (DOI: 10.1021/cr5002782).

56. Niren N. M. (2006), Pharmacologic doses of nicotinamide in the treatment of inflammatory skin conditions: a review, Cutis, 77(1 Suppl), 11-16 (PMID: 16871774).

57. Rolfe H. M. (2014), A review of nicotinamide: treatment of skin diseases and potential side effects, J. Cosmet. Dermatol., 13(4), 324-328 (DOI: 10.1111/jocd.12119).

58. Ahmed T. J., Knapp S. M. M., Tyler D. R. (2011), Frontiers in catalytic nitrile hydration: Nitrile and cyanohydrin hydration catalyzed by homogeneous organometallic complexes, Coord. Chem. Rev., 255(7), 949-974 (DOI: 10.1016/j.ccr.2010.08.018).

59. Rong M. K., van Duin K., van Dijk T., de Pater J. J. M., Deelman B.-J., Nieger M., Ehler A. W., Slootweg J. C., Lammertsma K. (2017), Iminophosphanes: Synthesis, Rhodium Complexes, and Ruthenium(II)-Catalyzed Hydration of Nitriles, Organometallics, 36(5), 1079-1090 (DOI: 10.1021/acs.organomet.7b00057).

60. Czégéni C. E., De S., Udvardy A., Derzsi N. J., Papp G., Papp G., Joó F. (2020), Selective Hydration of Nitriles to Corresponding Amides in Air with Rh(I)-*N*-Heterocyclic Complex Catalysts, Catalysts, 10(1), 125 (DOI: 10.3390/catal10010125).

Chapter 6

Syntheses, Characterization, and Catalytic Activity of Dicationic Ru(II)-CNC Pincer Complexes with CH₃CN and PPh₃ Ligands

6.1. Introduction

NHCs have drawn significant consideration as a substitute for phosphines, becoming more privileged ligands than phosphines in organometallic, inorganic, and organic chemistry [1–5]. The *N*-heterocyclic pincer carbene ligands are exciting derivatives that can introduce a highly entropic chelate effect and provide a range of more stable complexes with exciting chemical properties [6–8]. From this point of view, chelation plays an essential role in the electronic properties of the metal, thus modifying the catalytic and photoelectronic properties [9–11]. NHC metal complexes have attracted attention over the past few decades due to their extensive investigation and applications in various organic transformations [12–17]. Ruthenium pincer complexes are one of the most effective catalysts for important organic transformations, possibly due to their stability and being readily available in different stable oxidation states and coordination geometries [18–20].

Polypyridine complexes of Ru(II) and other transition metals are extensively studied to synthesize non-fossil-based, environmentally friendly fuels and usable fuel precursors [21–25]. NHC and pyridine rings have also been mixed to construct bidentate, tridentate pincer, and tetradentate ligands, and their metal complexes are highly active for CO_2 reduction and water oxidation catalysis [26–29]. Metal complexes with NHC and pyridine ligands play an important role in

increasing the electron density at the metal centre and can show various redox states, which is considered an attractive possibility for various applications [18, 30, 31]. The substituents on the *N*-wing tip of NHC are employed to modify the steric environment around the metal centre is an essential structural feature of the complexes based on CNC pincer ligands.

Amides are very significant compounds in both chemical and biological systems [32]. It is commonly used in synthetic intermediates in pharmaceuticals, material science, polymer chemistry, and fine chemical production [33–35]. Previously, many synthetic methods were reported for the synthesis of amides [36]. Therefore, a major concern about developing a convenient method for nitrile hydration is the most desirable methodology in modern chemistry that developed atom-efficient catalytic procedures. Previously, many catalysts have been reported for the synthesis of amides that stop the overhydration of amides [37, 38]. Many transition metal catalysts have been reported for the hydration of nitriles, and these catalysts facilitated the direct nucleophilic addition of a water molecule to a nitrile bond, affording the formation of amides [39–43]. Additionally, many ruthenium complexes have been investigated as effective catalysts for the hydration of nitrile catalysts [33, 44, 45].

R = Me (**7a**), R = *i*Pr (**7b**), R = Cy (**7c**)

R = Me (**11a**), R = *i*Pr (**11b**), R = Cy (**11c**)

R = Me (**12a**), R = *i*Pr (**12b**), R = Cy (**12c**)
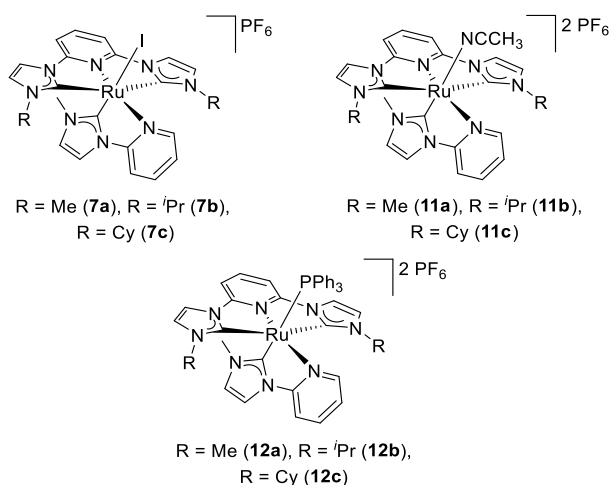
Figure 6.1. Cationic Ru(II)-CNC pincer complexes in this study.

Herein, we report the reactivity of Ru(II)-CNC pincer complexes [Ru(CNC^{Me})(CN^{Me})I]PF$_6$ (**7a**), [Ru(CNC$^{i\text{-}Pr}$)(CN^{Me})I]PF$_6$ (**7b**) and [Ru(CNC^{Cy})(CN^{Me})I]PF$_6$ (**7c**) with CH$_3$CN and PPh$_3$ ligands and afforded newly synthesized complexes i.e., [Ru(CNC^{Me})(CN^{Me})CH$_3$CN]2PF$_6$ (**11a**), [Ru(CNC$^{i\text{-}Pr}$)(CN^{Me})CH$_3$CN]2PF$_6$ (**11b**), [Ru(CNC^{Cy})(CN^{Me})CH$_3$CN]2PF$_6$ (**11c**), [Ru(CNC^{Me})(CN^{Me})PPh$_3$]2PF$_6$ (**12a**), [Ru(CNC$^{i\text{-}Pr}$)(CN^{Me})PPh$_3$]2PF$_6$ (**12b**) and [Ru(CNC^{Cy})(CN^{Me})PPh$_3$]2PF$_6$ (**12c**) (Figure **6.1**). Dicationic Ru(II)-NHC complexes with CH$_3$CN ligand were obtained upon heating at 40 ˚C, while their phosphine analogues were obtained at refluxed temperature in methanol solutions. Photophysical and electrochemical studies have been analyzed to rationalize their reactivities. The catalytic activity was investigated for nitrile hydration under mild reaction conditions to compare the dissociation of the sixth coordinated ligand. Furthermore, we have compared the catalytic activity of all the complexes with I$^-$, CH$_3$CN, and PPh$_3$ ligands and shows that complexes with I$^-$ are the most active catalyst than CH$_3$CN and the poor catalytic activity of PPh$_3$-based ligands.

6.2. Results and Discussion

6.2.1. Synthesis and characterization of dicationic Ru(II)-CNC pincer complexes

Complexes (**7a-c**) have been prepared according to the previously reported procedure as discussed in chapter two [Ru(CNC^{Me})(CN^{Me})I]PF$_6$ (**7a**), [Ru(CNC$^{i\text{-}Pr}$)(CN^{Me})I]PF$_6$ (**7b**) and [Ru(CNC^{Cy})(CN^{Me})I]PF$_6$ (**7c**). We have noticed that the Ru-I bond *trans* to carbene was labile and could easily be displaced by solvent molecules (CH$_3$CN) during recrystallization. To further explore these studies, we have treated the iodide complexes **7a-c** with CH$_3$CN and PPh$_3$ ligands and afforded new complexes through substitution reaction. Complexes (**11a-c**) have been prepared by using complexes

(**7a-c**) upon treatment with AgPF$_6$ in acetonitrile at 40 °C under an inert atmosphere afforded the desired complexes [Ru(CNC^{Me})(CN^{Me})CH$_3$CN]2PF$_6$ (**11a**), [Ru(CNC^{i-Pr})(CN^{Me})CH$_3$CN]2PF$_6$ (**11b**) and [Ru(CNC^{Cy})(CN^{Me})CH$_3$CN]2PF$_6$ (**11c**). However, ruthenium phosphine complexes (**12a-c**) were obtained upon refluxing the complexes (**7a-c**) in methanol with PPh$_3$ ligand, followed by ion exchange with the saturated solution of KPF$_6$ afforded complexes [Ru(CNC^{Me})(CN^{Me})PPh$_3$]2PF$_6$ (**12a**), [Ru(CNC^{i-Pr})(CN^{Me})PPh$_3$]2PF$_6$ (**12b**) and [Ru(CNC^{Cy})(CN^{Me})PPh$_3$]2PF$_6$ (**12c**) (Scheme **6.1**). All six complexes have been characterized by NMR and HRMS techniques. The single-crystal X-ray diffraction technique has determined the solid-state structure of complexes **11a**, **11c**, **12a**, and **12b**.
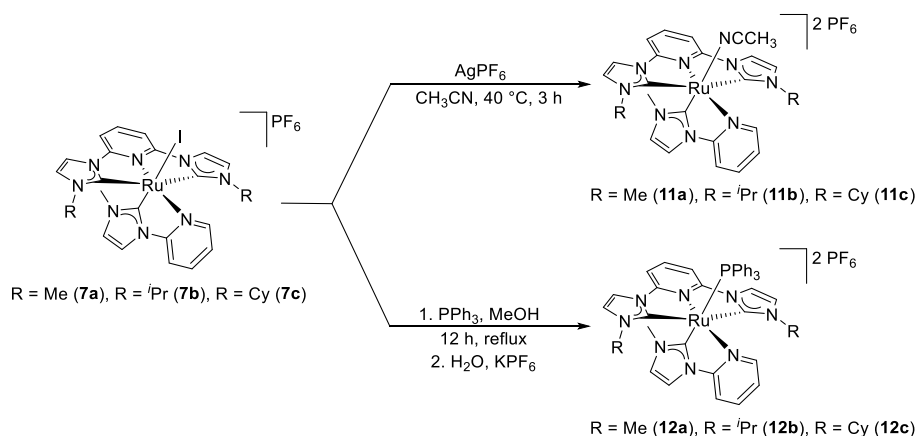
Scheme 6.1. Syntheses of dicationic Ru(II)-CNC pincer complexes.

The ^{1}H NMR spectrum of complex **11a** in dmso-d$_6$ shows that the acetonitrile was dissociated from the metal centre, and a dmso-d$_6$ coordinated species was generated with the free acetonitrile signal in the ^{1}H NMR spectrum (Figure **6.2**). The dissociation of acetonitrile is a clear indication of the *in-situ* generation of dmso-d$_6$ coordinated species **7a'**, similar to complex **7a**, while NMR was recorded in dmso-d$_6$ solvent. Further, the NMR spectrum of complex **11a** has been recorded in less nucleophilic, non-coordinating solvent acetone-d$_6$ to obtain the acetonitrile-coordinated signal in the ^{1}H NMR spectrum

(Figure **6.3**). Similarly, complexes **11b** and **11c** have dissociated acetonitrile signals in dmso-d$_6$ and coordinated signals in acetone-d$_6$.
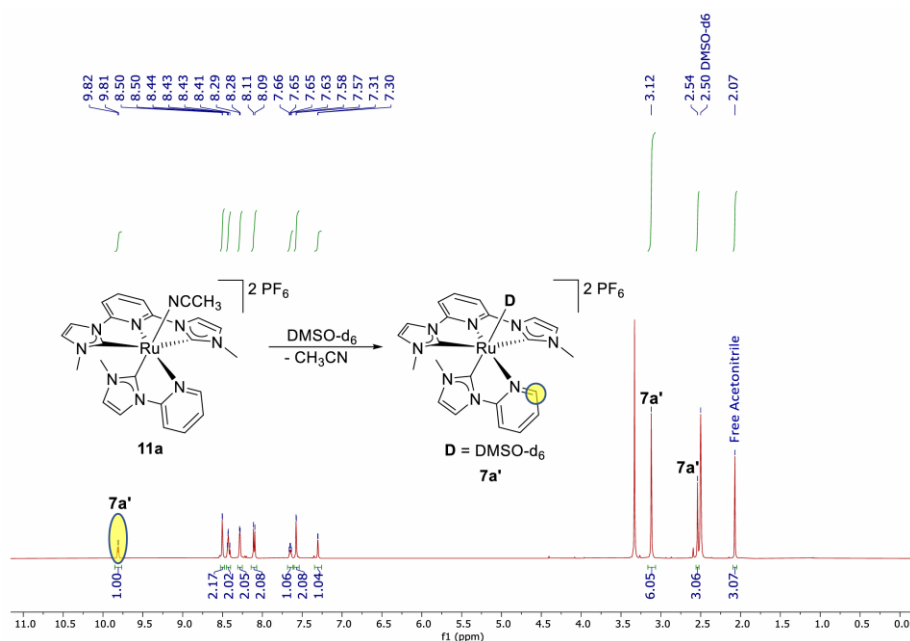
Figure 6.2. ^{1}H NMR spectrum of complex **11a** in dmso-d$_6$ supporting the *in-situ* generation of complex **7a'** with dissociated acetonitrile.
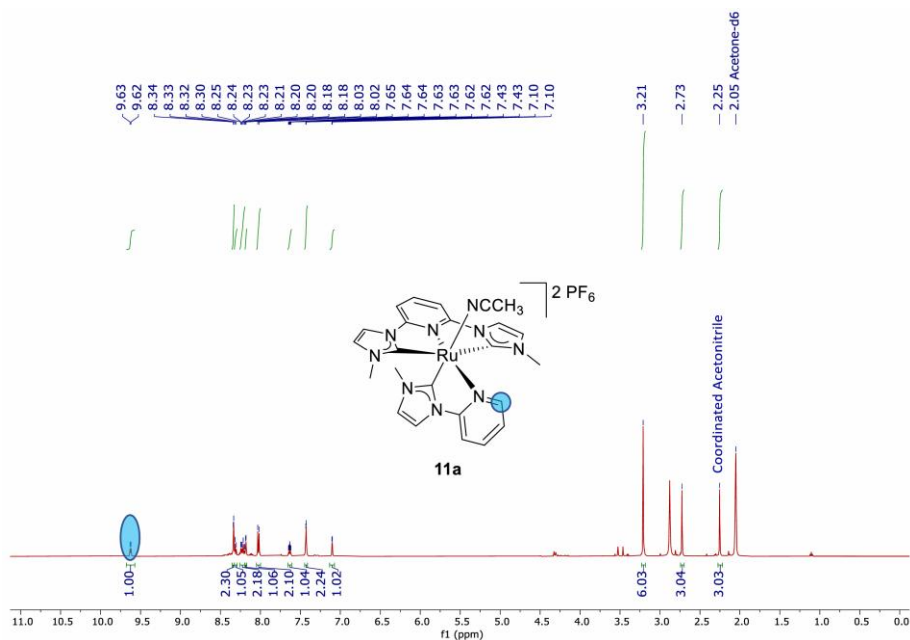
Figure 6.3. ^{1}H NMR spectrum of complex **11a** in acetone-d$_6$ with coordinated acetonitrile.

The ^{1}H NMR spectra of complexes **11a-c** show a doublet for the *ortho* proton of pyridine of the bidentate ligand at 9.63, 9.63, and 9.70 ppm in acetone-d$_6$, respectively, similar to the complexes **7a-c**. The methyl protons for the pincer and bidentate ligand of complex **11a** appear at 3.21 and 2.73 ppm, while the ruthenium coordinated acetonitrile peak appears at 2.25 ppm. In complex **11b**, the isopropyl group of the pincer ligand gives one multiplet at 3.51 – 3.43 ppm for the methine proton and two doublets for the methyl groups at 1.34 and 0.90 ppm and a singlet for the bidentate methyl proton at 2.74 ppm, and ruthenium coordinated acetonitrile exhibits at 2.28 ppm. In complex **11c**, the aliphatic protons of cyclohexyl for the methine proton appear as a multiplet at 2.89 – 2.80 ppm, the other peaks for cyclohexyl appear at their expected regions. The methyl protons of the bidentate ligand in complex **11c** appear at 2.73 ppm, and a signal at 2.25 ppm for ruthenium-coordinated acetonitrile. ^{13}C NMR spectrum of complexes **11a** and **11b**, the carbene carbon signals appear at 191.63 and 189.84 ppm for CNC and 189.41 and 189.60 ppm for CN ligand, respectively, while in complex **11c**, the carbene carbon signals appear at 189.92 and 189.85 ppm. ^{31}P NMR spectra of complexes **11a-c** show peaks as a septate at -144.27, -144.25, and -144.26 ppm for the PF$_6^-$ counterion. In ESI$^+$ HRMS spectra of complexes **11a-c**, the signal at *m/z* 270.5651, 298.5954 and 338.6266 corresponds to [**11a**-2PF$_6$]$^{2+}$, [**11b**-2PF$_6$]$^{2+}$ and [**11c**-2PF$_6$]$^{2+}$, while the other signals at *m/z* 250.0519, 278.0825 and 318.1143 corresponds to [**11a**-2PF$_6$-CH$_3$CN]$^{2+}$, [**11b**-2PF$_6$-CH$_3$CN]$^{2+}$ and [**11c**-2PF$_6$-CH$_3$CN]$^{2+}$ and an additional signal at *m/z* 259.0562, 287.0872 and 327.1185 corresponds to [**11a**-2PF$_6$-CH$_3$CN+H$_2$O]$^{2+}$, [**11b**-2PF$_6$-CH$_3$CN+H$_2$O]$^{2+}$ and [**11c**-2PF$_6$-CH$_3$CN+H$_2$O]$^{2+}$, respectively.

In ^{1}H NMR spectra of complexes **12a-c**, the *ortho* proton of pyridine of the bidentate ligand gives a doublet at 8.65, 8.71, and 8.75 ppm, respectively, similar to the complexes **7a-c**. In complex **12a**, the methyl protons appear at 2.96 and 2.31 ppm for pincer and bidentate

218

ligands. The isopropyl proton in complex **12b** gives one multiplet at 3.20 – 3.12 ppm for the methine proton, two doublets at 1.26 and 0.49 ppm for the methyl group and a singlet at 2.32 ppm for the bidentate methyl proton. In complex **12c,** the methine proton of cyclohexyl appears as a multiplet at 2.76 – 2.69 ppm, and the other aliphatic protons of cyclohexyl appear at their expected regions, while the methyl protons appear at 2.31 ppm for the bidentate ligand. In ^{13}C NMR spectra of complexes **12a**–**c**, the carbene signals have appeared at 189.74, 187.83, and 188.07 ppm for CNC and 185.46, 185.33, and 185.83 ppm for CN ligand, respectively.

Table 6.1. ^{13}C NMR Chemical Shifts of C_{NHC} in Complexes (**12a**–**c**).

Entry	Complex	C_{NHC} chemical shifts (ppm) with coupling constant (Hz)	
		cis	*trans*
1	**12a**	189.74, J = 11.4	185.46, J = 80.8
2	**12b**	187.83, J = 11.6	185.33, J = 80.7
3	**12c**	188.07, J = 11.3	185.83, J = 80.9

The coupling constants ($J_{P\text{-}Ru\text{-}C}$) have provided important information to assign and distinguish between *cis* and *trans*-carbene carbon to the PPh$_3$ ligand [46]. It is evident that the coupling constant between C and P atoms is remarkably high for *trans* position than *cis* (i.e., $J_{P(cis)\text{-}Ru\text{-}C}$ = 11.3–11.6 Hz, *cis* carbene carbon; $J_{P(trans)\text{-}Ru\text{-}C}$ = 80.7–80.9 Hz, *trans* carbene carbon)(Table **6.1**). Thus, complex giving coupling constant of ~11 Hz is referred to as *cis* where the carbene carbon is *cis* to PPh$_3$ with CNC ligand, similarly complex with high coupling constant value >80 Hz is *trans* showing carbene carbon is *trans* to PPh$_3$ with CN ligand [46]. The above discussion confirmed that the CNC carbene is *cis* to PPh$_3$ and CN carbene is *trans* to the PPh$_3$ ligand. ^{31}P NMR spectrum of complexes **12a-c** exhibited peaks at 36.77, 35.47, and 35.33 ppm for coordinated PPh$_3$ ligand and the peak at -144.20, -144.19, and -144.20 ppm for PF$_6^-$ counterion, respectively.

Complexes **12a-c** displayed the ESI$^+$ HRMS signal at *m/z* 381.0984, 409.1299, and 449.1608 corresponds to [**12a**-2PF$_6$]$^{2+}$, [**12b**-2PF$_6$]$^{2+}$ and [**12c**-2PF$_6$]$^{2+}$, respectively.

6.2.2. Description of the crystal structures

6.2.2.1. Molecular structure of complexes 11a and 11c

The molecular structure of complexes **11a** and **11c** have been confirmed by single crystal X-ray diffraction analysis, and their crystallographic parameters and final refinements for the complexes are given in Table **6.2**. Selected bond lengths and bond angles are given in Table **6.3**.

Figure 6.4. Single crystal X-ray structure of complex **11a**. All hydrogen atoms and two PF$_6^-$ counter-anions are omitted for clarity. Selected bond lengths (Å) and bond angles (∘): Ru1-C1, 2.061(7); Ru1-C2, 2.046(7); Ru1-C3, 1.970(7); Ru1-N1, 2.013(6); Ru1-N2, 2.083(7); Ru1-N3, 2.103(7); N1-Ru1-C1, 77.2(3); N2-Ru1-N3, 92.7(3); C3-Ru1-N2, 78.2(3); N1-Ru1-N2, 177.5(2); C1-Ru1-N2, 100.4(3); C3-Ru1-N3, 170.4(3); C3-Ru1-C1, 91.2(3); C2-Ru1-N2, 105.0(3); C2-Ru1-N3, 84.6(3); C2-Ru1-C1, 154.6(3).

Complexes **11a** and **11c** are crystallized in a monoclinic and triclinic system with I2/a and P-1 space groups with distorted octahedral geometry. Complexes **11a** and **11c** consist of two almost planar five-membered metallacycles of the CNC pincer ligand, one five-membered metallacycle of the CN ligand, and CH_3CN as the sixth coordinated ligand around the ruthenium centre (Figure **6.4** and **6.5**). The CNC pincer ligand occupies three meridional sites with C1-Ru1-C2 angles 154.6(3)° in **11a** and 153.6(6)° in **11c**, and their bite angles of C1-Ru1-N1 are 77.2(3)° in **11a** and 77.1(5)° in **11c**, while the bidentate CN ligand occupies two sites at the ruthenium centre, with bite angles of N2-Ru1-C3 are 78.2(3)° in **11a** and 77.4(5)° in **11c**, similar to our previously reported complexes [47]. The two pyridine units from CNC and CN ligands are *trans* to each other in both complexes. The bond length of Ru-NCCH$_3$ in complex **11a** is 2.103 Å, which is slightly larger than complex **11c** 2.025 Å and other reported acetonitrile complexes [26, 48]. The bond lengths of Ru-N of the pyridine group (~2.0 - 2.1 Å) and Ru–C(NHC) bond lengths (~1.8 - 2.1 Å) are similar to our previously reported metal complexes [47].
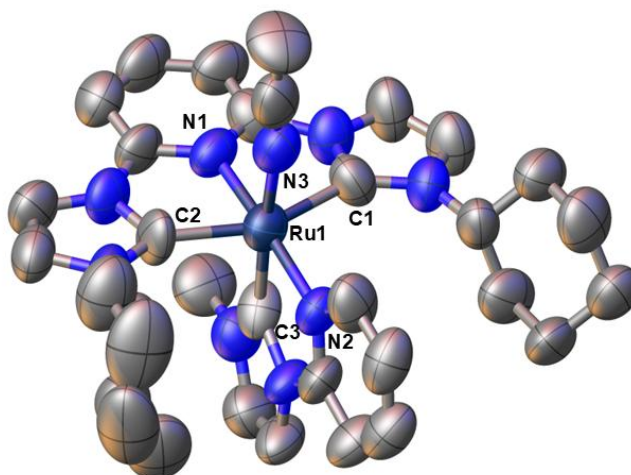
Figure 6.5. Single crystal X-ray structure of complex **11c**. All hydrogen atoms and two PF_6^- counter-anions are omitted for clarity. Selected bond lengths (Å) and bond angles (°): Ru1-C1, 2.058(14);

Ru1-C2, 2.022(11); Ru1-C3, 1.846(13); Ru1-N1, 2.024(11); Ru1-N2, 2.092(10); Ru1-N3, 2.025(17); N1-Ru1-C1, 77.1(5); N3-Ru1-N2, 94.3(5); C3-Ru1-N2, 77.4(5); N1-Ru1-N2, 174.6(5); C1-Ru1-N2, 102.8(5); C3-Ru1-N3, 171.6(5); C3-Ru1-C1, 93.2(6); C2-Ru1-N2, 103.6(5); C2-Ru1-N3, 89.2(6); C2-Ru1-C1, 153.6(6).

Table 6.2. Crystal data and structure refinement parameters of complexes **11a** and **11c**.

	11a	11c
Empirical formula	$C_{24}H_{25}F_{12}N_9P_2Ru$	$C_{34}H_{41}F_{12}N_9P_2Ru$
T/K	300	300
Crystal System	monoclinic	triclinic
Space Group	I2/a	P-1
a/Å	17.9622(11)	10.8823(6)
b/Å	11.5925(9)	11.1404(7)
c/Å	32.0737(18)	17.2730(11)
α/°	90	96.048(5)
β/°	90.338(5)	93.326(5)
γ/°	90	100.138(5)
V/Å³	6678.5(8)	2043.6(2)
Z	8	2
ρ$_{calc}$g/cm³	1.652	1.571
λ/Å (Mo/Cu-Kα)	0.71073	1.54184
Reflections Collected	20164	14737
Data/restr./param.	7974/0/437	7716/0/527
R (int)	0.0674	0.1635
Final R indices	$R_1 = 0.0863$,	$R_1 = 0.1618$,
[I>2σ(I)]	$wR_2 = 0.2298$	$wR_2 = 0.3874$
R indices (all data)	$R_1 = 0.1587$	$R_1 = 0.2153$,
	$wR_2 = 0.2852$	$wR_2 = 0.4549$
GOF on F2	0.959	1.222

Table 6.3. Selected bond lengths and bond angles of complexes **11a** and **11c**.

Complex	Bond lengths (Å)	Bond angles (°)
11a	Ru1-C1, 2.061(7) Ru1-C2, 2.046(7) Ru1-C3, 1.970(7) Ru1-N1, 2.013(6) Ru1-N2, 2.083(7) Ru1-N3, 2.103(7)	N1-Ru1-N2, 177.5(2) N1-Ru1-N3, 86.9(2) N1-Ru1-C1, 77.2(3) N1-Ru1-C2, 77.4(3) N2-Ru1-N3, 92.7(3) C1-Ru1-N2, 100.4(3) C1-Ru1-N3, 93.5(3) C3-Ru1-N1, 102.3(3) C3-Ru1-N2, 78.2(3) C3-Ru1-N3, 170.4(3) C3-Ru1-C1, 91.2(3) C3-Ru1-C2, 94.7(3) C2-Ru1-N2, 105.0(3) C2-Ru1-N3, 84.6(3) C2-Ru1-C1, 154.6(3)
11c	Ru1-C1, 2.058(14) Ru1-C2, 2.022(11) Ru1-C3, 1.846(13) Ru1-N1, 2.024(11) Ru1-N2, 2.092(10) Ru1-N3, 2.025(17)	N1-Ru1-N2, 174.6(5) N1-Ru1-N3, 91.1(5) N1-Ru1-C1, 77.1(5) C2-Ru1-N1, 76.5(5) N3-Ru1-N2, 94.3(5) C1-Ru1-N2, 102.8(5) N3-Ru1-C1, 90.1(6) C3-Ru1-N1, 97.2(5) C3-Ru1-N2, 77.4(5) C3-Ru1-N3, 171.6(5) C3-Ru1-C1, 93.2(6) C3-Ru1-C2, 91.2(6) C2-Ru1-N2, 103.6(5) C2-Ru1-N3, 89.2(6) C2-Ru1-C1, 153.6(6)

6.2.2.2. Molecular structure of complexes 12a and 12b

The molecular structures of **12a** and **12b** were determined using the single-crystal X-ray diffraction technique. Crystal data and structure refinement parameters of complexes **12a** and **12b** are given in Table **6.4**, while selected bond lengths and bond angles of complexes are in Table **6.5**. Complexes **12a** and **12b** crystallized in triclinic (P-1) and

monoclinic (P2$_1$/n) crystal systems, respectively. The structure of both the complexes **12a** and **12b** consists of two almost planar five-membered metallacycles of the CNC pincer ligand, one five-membered metallacycle of the CN ligand, and the PPh$_3$ ligand occupies the sixth coordination position around the ruthenium centre (Figure **6.6** and **6.7**). Pincer ligand occupies three meridional sites with C1-Ru1-C2 angles 154.73(17)° in **12a** and 154.18(13)° in **12b**, and their bite angles of C1-Ru1-N1 are 77.40(15)° in **12a** and 77.42(12)° in **12b**, while the bite angles of N2-Ru1-C3 are 76.93(14)° in **12a** and 76.88(11)° in **12b** which occupies two sites at the ruthenium centre, similar to our previously reported complexes [47]. The Ru-PPh$_3$ bond length is 2.4331 Å in **12a**, and 2.4328 Å in **12b**, which are *trans* to carbene and are larger than our previously reported complexes [49] and similar to the Grubbs [46] complex. The bond lengths of Ru-N of the pyridine group and Ru–C(NHC) (~2.0 - 2.1 Å) are similar to our previously reported metal complexes [47].
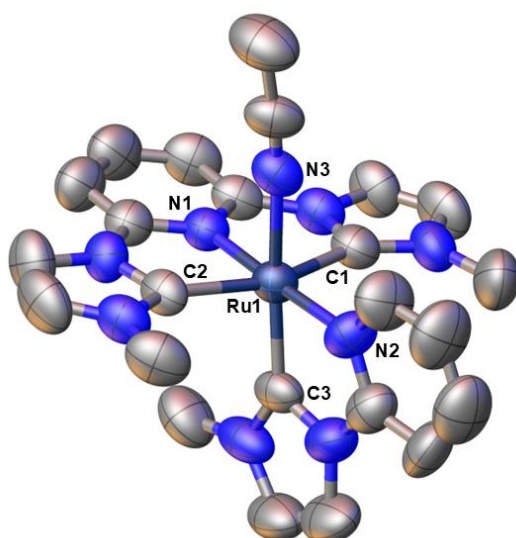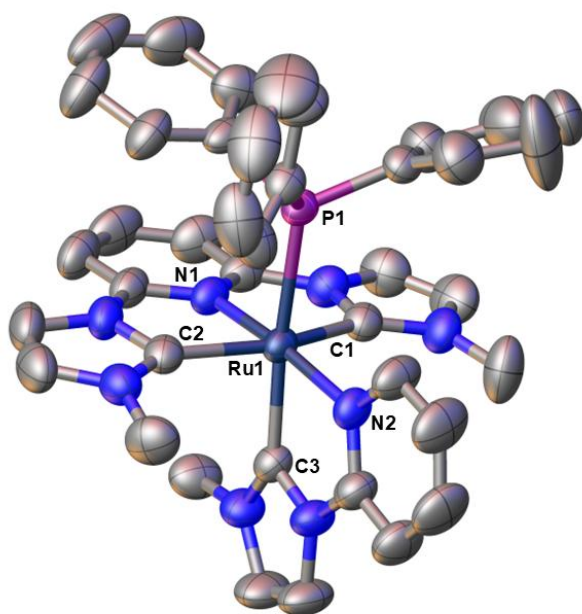

Figure 6.6. Single crystal X-ray structure of complex **12a**. All hydrogen atoms and two PF$_6^-$ counter-anions are omitted for clarity. Selected bond lengths (Å) and bond angles (°): Ru1-C1, 2.058(4); Ru1-

C2, 2.072(4); Ru1-C3, 2.039(4); Ru1-N1, 2.010(3); Ru1-N2, 2.120(3); Ru1-P1, 2.4331(10); N1-Ru1-P1, 88.12(9); N1-Ru1-C1, 77.40(15); N1-Ru1-N2, 174.08(12); N1-Ru1-C3, 97.15(14); N2-Ru1-P1, 97.79(10); C3-Ru1-N2, 76.93(14); C2-Ru1-P1, 92.78(11); C3-Ru1-P1, 174.46(11); C1-Ru1-C2, 154.73(17); C1-Ru1-N2, 102.22(15).
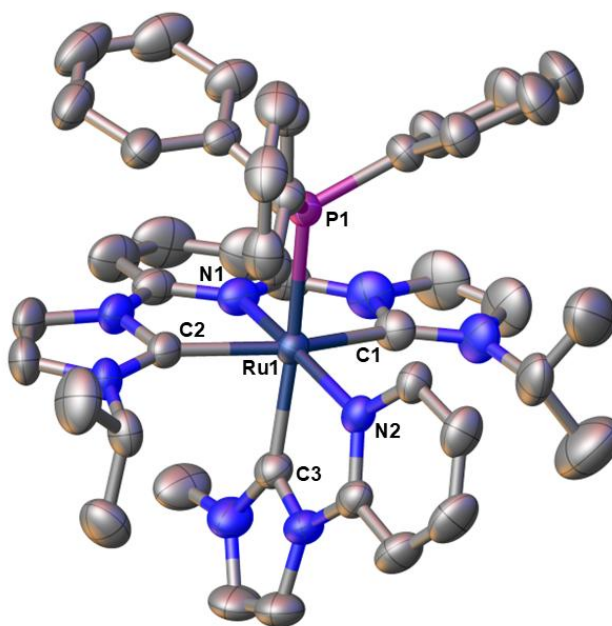
Figure 6.7. Single crystal X-ray structure of complex **12b**. All hydrogen atoms and two PF_6^- counter-anions are omitted for clarity. Selected bond lengths (Å) and bond angles (∘): Ru1-C1, 2.082(3); Ru1-C2, 2.086(3); Ru1-C3, 2.031(3); Ru1-N1, 2.018(3); Ru1-N2, 2.123(3); Ru1-P1, 2.4328(8); N1-Ru1-P1, 90.47(8); N1-Ru1-C1, 77.42(12); N1-Ru1-N2, 171.13(10); N1-Ru1-C3, 96.73(12); N2-Ru1-P1, 96.77(7); C3-Ru1-N2, 76.88(11); C2-Ru1-P1, 89.72(9); C3-Ru1-C2, 83.90(12); C3-Ru1-C1, 95.12(13); C3-Ru1-P1, 169.06(9); C1-Ru1-C2, 154.18(13); C1-Ru1-N2, 96.84(11); C2-Ru1-N2, 107.96(11).

Table 6.4. Crystal data and structure refinement parameters of complexes **12a** and **12b**.

	12a	12b
Empirical formula	$C_{40}H_{37}F_{12}N_8P_3Ru$	$C_{44}H_{45}F_{12}N_8P_3Ru$
T/K	300	300
Crystal System	triclinic	monoclinic
Space Group	P-1	$P2_1/n$
a/Å	10.1649(3)	14.9521(3)
b/Å	11.2079(4)	15.3079(3)
c/Å	20.4433(5)	20.7687(4)
α/°	86.120(3)	90
β/°	79.132(2)	91.415(2)
γ/°	85.538(3)	90
V/Å³	2277.0(12)	4752.20(16)
Z	2	4
ρ_{calc}g/cm³	1.534	1.548
λ/Å (Mo-Kα)	0.71073	0.71073
Reflections Collected	30659	20578
Data/restr./param.	11356/0/580	10197/0/619
R (int)	0.0380	0.0423
Final R indices [I>2σ(I)]	$R_1 = 0.0628$, wR$_2$ = 0.1876	$R_1 = 0.0473$, wR$_2$ = 0.1188
R indices (all data)	$R_1 = 0.0794$, wR$_2$ = 0.1997	$R_1 = 0.0646$, wR$_2$ = 0.1311
GOF on F2	1.061	1.061

Table 6.5. Selected bond lengths and bond angles of complexes **12a** and **12b**.

Complex	Bond lengths (Å)	Bond angles (°)
12a	Ru1-C1, 2.058(4) Ru1-C2, 2.072(4) Ru1-C3, 2.039(4) Ru1-N1, 2.010(3) Ru1-N2, 2.120(3) Ru1-P1, 2.4331(10)	N1-Ru1-P1, 88.12(9) N1-Ru1-N2, 174.08(12) N1-Ru1-C2, 77.65(15) N1-Ru1-C3, 97.15(14) N1-Ru1-C1, 77.40(15) N2-Ru1-P1, 97.79(10) C2-Ru1-P1, 92.78(11) C2-Ru1-N2, 102.19(15) C3-Ru1-P1, 174.46(11) C3-Ru1-N2, 76.93(14) C3-Ru1-C2, 90.02(15) C3-Ru1-C1, 89.16(15) C1-Ru1-P1, 90.34(11) C1-Ru1-N2, 102.22(15) C1-Ru1-C2, 154.73(17)
12b	Ru1-C1, 2.082(3) Ru1-C2, 2.086(3) Ru1-C3, 2.031(3) Ru1-N1, 2.018(3) Ru1-N2, 2.123(3) Ru1-P1, 2.4328(8)	N1-Ru1-P1, 90.47(8) N1-Ru1-N2, 171.13(10) N1-Ru1-C2, 77.08(12) N1-Ru1-C3, 96.73(12) N1-Ru1-C1, 77.42(12) N2-Ru1-P1, 96.77(7) C2-Ru1-P1, 89.72(9) C2-Ru1-N2, 107.96(11) C3-Ru1-P1, 169.06(9) C3-Ru1-N2, 76.88(11) C3-Ru1-C2, 83.90(12) C3-Ru1-C1, 95.12(13) C1-Ru1-P1, 94.48(10) C1-Ru1-N2, 96.84(11) C1-Ru1-C2, 154.18(13)

6.2.3. Spectroscopic properties

The UV-vis spectra of all the complexes (**7a**–**c** and **11a**–**12c**) corresponding to MLCT $d\pi$–π^* and intraligand π–π^* absorption spectra recorded in acetonitrile were shown in Figure **6.8**. The absorption wavelengths and extinction coefficients are displayed together with a tentative conclusion based on the λ values and extinction coefficients, as shown in Table **6.6**. Complexes (**7a**–**c**) show

more intense peaks of MLCT dπ−π* at 377–416 nm and less intense peaks of π−π* transition at 229–287 nm. A blue-shift λ_{max} 377–382 nm was observed from the MLCT due to the higher electron density of the NHC ligands. Similarly, a red shift was also observed in the absorption spectra at 416 nm for MLCT transition (Figure **6.8a**). In the case of complexes (**11a–c**), both types of absorption spectra, i.e., MLCT dπ−π* at 362–383 nm and intraligand π−π* transition at 229–286 nm are observed (Figure **6.8b**). The absorption spectra show a blue-shifted λ_{max} 362–383 nm as compared to complexes (**7a–c**). The MLCT dπ−π* peaks were also shifted at lower wavelengths due to the presence of a σ-donor and π-acceptor CH_3CN group in the complexes (**11a–c**). Upon comparing the absorption spectra of these complexes, it was found that a blue-shifted absorption spectrum was sighted at 377–382 nm for the NHC ligand of the complexes (**7a–c**). On the other hand, this peak shifted at a lower wavelength, i.e., a hypsochromic shift by replacing the anionic I⁻ ligand with the neutral CH_3CN in complexes (**11a–c**). It was reasoned that the σ- and π-donor ability of I⁻ reduces the energy difference between fully occupied d orbitals of the metal and empty π* orbitals of the ligands. In complexes (**12a–c**), both the type of absorption spectra, i.e., MLCT dπ−π* at 323–365 nm and intraligand π−π* transition at 226–285 nm, were found (Figure **6.8c**). The absorption spectra show a blue-shifted λ_{max} 323–365 nm in phosphine-bound complexes. The MLCT dπ−π* peaks were also shifted at lower wavelengths due to the presence of a strong σ-donor and π-acceptor PPh_3 group in the complexes (**12a–c**). Upon comparing the absorption spectra of these complexes, it was found that a blue-shifted absorption spectrum was sighted at 377–382 nm for the NHC ligand of the complexes (**7a–c**). On the other hand, this peak shifted at a lower wavelength, i.e., a hypsochromic shift by replacing the anionic I⁻ ligand with the neutral PPh_3 in complexes (**12a–c**). It was reasoned that the strong σ- and π-donor ability of I⁻ reduces the energy difference

228

between fully occupied d orbitals of the metal and empty π^* orbitals of the ligands.

Figure 6.8. Absorption spectra of Ru(II)-CNC pincer complexes; (**a**) complexes **7a–c**, (**b**) complexes **11a–c**, and (**c**) complexes **12a–c** recorded in acetonitrile at room temperature (10^{-5} M).

Table 6.6. UV−Vis spectroscopic absorptions in CH_3CN for cationic Ru(II)-CNC pincer Complexes.

Entry	Complex	Assignment	λ_{max}, nm (ε, $M^{-1}cm^{-1}$)
1	**7a**	$\pi \rightarrow \pi^*$	229 (77970), 272 (31460), 285 (24860)
		$d\pi \rightarrow \pi^*$	377 (20130), 416 (13180)
2	**7b**	$\pi \rightarrow \pi^*$	230 (51200), 274 (19550), 286 (15930)
		$d\pi \rightarrow \pi^*$	380 (12740), 416 (8250)
3	**7c**	$\pi \rightarrow \pi^*$	230 (57900), 274 (22780), 287 (19790)
		$d\pi \rightarrow \pi^*$	382 (13070), 416 (8600)
4	**11a**	$\pi \rightarrow \pi^*$	229 (57750), 271 (29280), 285 (21950)
		$d\pi \rightarrow \pi^*$	362 (20290), 383 (17220)
5	**11b**	$\pi \rightarrow \pi^*$	229 (67120), 271 (33610), 286 (26310)
		$d\pi \rightarrow \pi^*$	363 (22630), 382 (20070)

6	**11c**	$\pi \to \pi^*$	230 (50050), 272 (25910), 286 (20780)
		$d\pi \to \pi^*$	364 (16820), 382 (15800)
7	**12a**	$\pi \to \pi^*$	226 (60540), 274 (24540), 282 (18700)
		$d\pi \to \pi^*$	323 (8680), 363 (12880)
8	**12b**	$\pi \to \pi^*$	227 (64250), 274 (26070), 284 (19270)
		$d\pi \to \pi^*$	324 (9080), 364 (13250)
9	**12c**	$\pi \to \pi^*$	226 (62070), 275 (26050), 285 (19960)
		$d\pi \to \pi^*$	325 (9530), 365 (12160)

6.2.4. Electrochemical properties

To investigate the redox properties of complexes (**7a–c** and **11a–12c**), cyclic voltammetry (CV) and differential pulse voltammetry (DPV) spectra were recorded in acetonitrile solvent using 0.1M tetrabutylammonium hexafluorophosphate (TBAPF$_6$) as the supporting electrolyte.
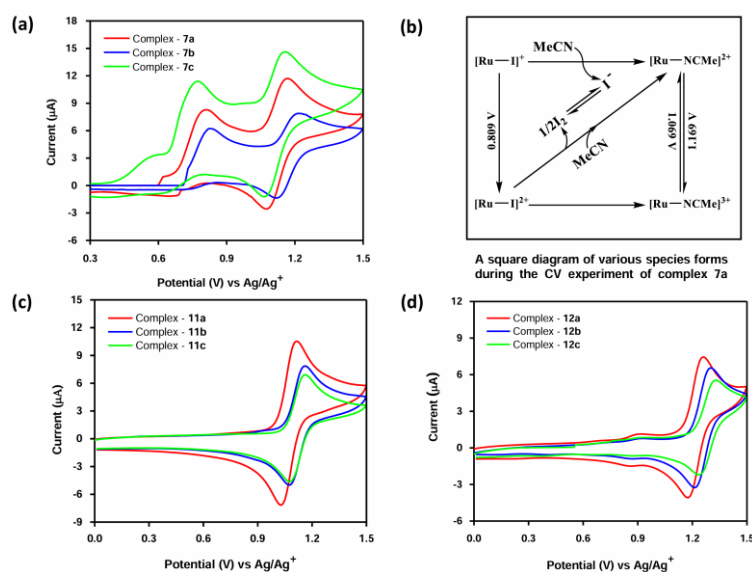
Figure 6.9. Cyclic voltammograms (CV) of Ru(II)-CNC pincer complexes; (**a**) complexes **7a–c**, (**b**) possible species formed during the CV experiment of complex **7a** and similarly for complexes **7b** and **7c**, (**c**) complexes **11a–c**, and (**d**) complexes **12a–c**, recorded in a 0.1 M solution of TBAPF$_6$ as supporting electrolyte in dry acetonitrile at 100mV/s scan rate versus SCE at 25 ˚C.

Complex (**7a–c**) having NHC and iodo ligands exhibits two oxidation potential peaks, the first irreversible and the second reversible at different heights within the accessible potential gaps. The first oxidation potential is due to the metal complexes (**7a–c**), where the iodo ligand is present, and the iodo ligand acts as an oxidant, and the ruthenium centre was oxidized with the removal of the iodide ligand, due to this reason oxidation potential at 0.629V, 0.729V, and 0.569V for **7a-c** is not reversible. The oxidation pattern of complexes (**7a–c**) shows an irreversible process at 0.809V, 0.829V, and 0.769V and other reversible processes at 1.119V, 1.155V, and 1.105V respectively (Figure **6.9a**). Upon comparing with the similar type of moiety with a pincer and bidentate ligand [Ru(tpy)(bpy)Cl]$^+$ shows a similar oxidation potential at 0.80V in acetonitrile [27]. The third oxidation potential peak is reversible, where acetonitrile was bound with the metal centre. In complexes **7a-c**, three oxidation potential peaks were observed during the CV experiment, and these species are shown in Figure **6.9b**. Complexes (**11a–c**) having NHC and acetonitrile ligands exhibit one redox peak in a cyclic voltammogram. The oxidation pattern of complexes (**11a–c**) shows a reversible process due to the Ru^{II}/Ru^{III} couple at 1.074V, 1.119V, and 1.119V, respectively (Figure **6.9c**). In cyclic voltammogram of complexes (**12a–c**) having NHC and phosphine ligands exhibit one oxidation potential peak. The oxidation pattern of complexes (**12a–c**) shows a reversible process due to the Ru^{II}/Ru^{III} couple at 1.229V, 1.259V, and 1.284V, respectively (Figure **6.9d**). Upon comparing with the similar type of moiety with a pincer and bidentate ligand [Ru(tpy)(bpy)Cl]$^+$ shows a less positive oxidation potential with monoelectronic reversible process attributed to the Ru^{II}/Ru^{III} couple at 0.80V in acetonitrile [27]. While comparing with the other reported metal complexes, it was shown that these complexes show almost similar positive couple for Ru^{II}/Ru^{III} in [Ru(by)$_3$]$^{2+}$ and [Ru(tpy)$_2$]$^{2+}$ (for both 1.28V in acetonitrile) [27] with comparing of complexes (**12a–c**). Complexes (**12a–c**) show high positive values because of the presence

of a strong σ-donor and π-acceptor triphenylphosphine group in the complexes **12a-c**. The lower Ru^{II}/Ru^{III} redox potential can be possible because of an electron-rich Ru(II) centre.

6.2.5. Justification of CV peaks

Complex (**7a–c**) having NHC and iodo ligands exhibits two oxidation potential peaks; the first is irreversible, and the second one is quasi-reversible when recorded in the experiments at 0.0 to 1.0 potential. The first oxidation potential is irreversible, and the second one is quasi-reversible for the metal complexes (**7a–c**), where the iodo ligand is present, the iodo ligand acted as an oxidant, and the metal centre was oxidized, and iodide was removed. For this reason, oxidation potential is not entirely reversible. The oxidation pattern of complexes (**7a–c**) shows a quasi-reversible process at 0.739V, 0.759V, and 0.769V respectively (Figure **6.10**). Upon comparing with the similar type of moiety with a pincer and bidentate ligand $[Ru(tpy)(bpy)Cl]^+$ shows a similar oxidation potential at 0.80V in acetonitrile [27]. The reason behind the recording of these experiments was that when the metal centre was oxidized, the experiments showed a quasi-reversible peak because a previously irreversible peak was observed when the experiment recorded at 1.5 oxidation potential. We concluded that when the experiment was recorded at 1.5 oxidation potential, all the complexes were bound with acetonitrile, so this complex showed irreversible peaks, and when recording the experiment at 1.0 potential, the acetonitrile was not bound with the metal centre and complexes showed quasi-reversible peaks. This hypothesis was confirmed when recording the UV-Vis data of the same samples; we get the pair of peaks confirmed that some complexes bound with iodide and some of them bound with acetonitrile, and similar results were obtained when refluxed the complexes in acetonitrile and pair of peaks obtained in UV-vis data in Figure **6.11**. The absorption wavelengths and extinction coefficients are shown in Table **6.7**.
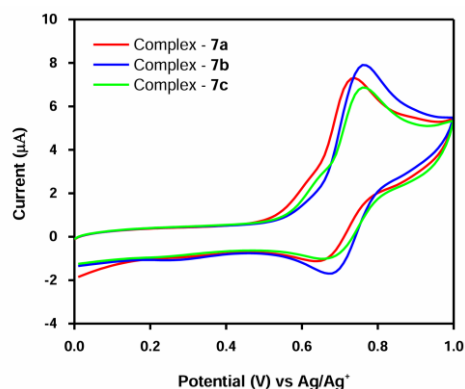
Figure 6.10. Cyclic voltammograms (CV) of complexes (**7a**–**c**) recorded in a 0.1 M solution of TBAPF$_6$ as supporting electrolyte in dry acetonitrile at 100mV/s scan rate versus SCE at 25 ˚C.

Table 6.7. UV−vis spectroscopic absorptions in CH$_3$CN after refluxing in acetonitrile (entries 1-3) and after oxidizing electrochemically (entries 4-6) for the complexes (**7a**–**c**).

Entry	Complex	Assignment	λ_{max}, nm (ε, M^{-1}cm^{-1})
1	**7a**	$\pi \rightarrow \pi^*$	229 (78570), 238 (74680), 270 (37030), 285 (29430)
		$d\pi \rightarrow \pi^*$	361 (22260), 382(19380), 416 (5600)
2	**7b**	$\pi \rightarrow \pi^*$	230 (78020), 237 (74100), 271 (34640), 285 (28600)
		$d\pi \rightarrow \pi^*$	363 (21160), 381 (19970), 415 (6430)
3	**7c**	$\pi \rightarrow \pi^*$	231 (92220), 237 (89820), 272 (42580), 285 (36150)
		$d\pi \rightarrow \pi^*$	365 (22590), 380 (21920), 414 (7480)
4	**7a**	$\pi \rightarrow \pi^*$	230 (39140), 237 (37580), 270 (18110), 285 (14350)
		$d\pi \rightarrow \pi^*$	363 (11130), 381 (10240), 418 (3250)
5	**7b**	$\pi \rightarrow \pi^*$	230 (36220), 237 (34030), 271 (15220), 285 (12490)
		$d\pi \rightarrow \pi^*$	365 (9130), 380 (9300), 416 (3620)
6	**7c**	$\pi \rightarrow \pi^*$	232 (50230), 239 (48120), 273 (21330), 285 (18910)
		$d\pi \rightarrow \pi^*$	369 (12270), 381 (12520), 415 (6150)

233
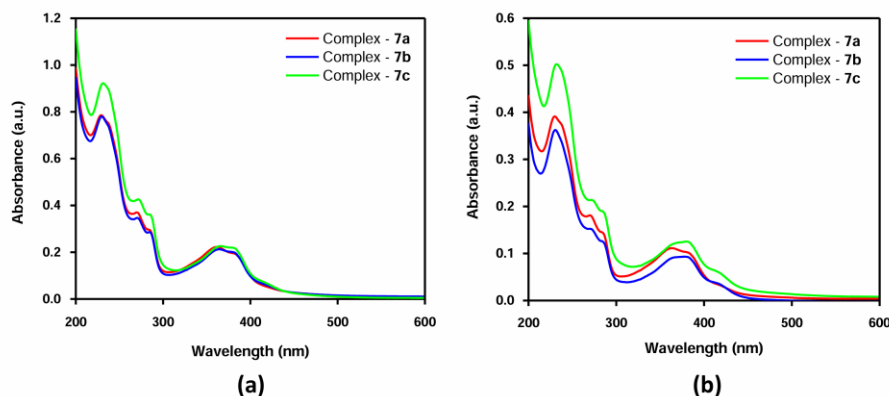
Figure 6.11. Absorption spectra of Ru(II)-CNC pincer complexes (**7a-c**) recorded in acetonitrile at room temperature (10^{-5} M). (**a**) After refluxing in acetonitrile (Table **6.7**, entries 1-3), and (**b**) after oxidizing electrochemically (Table **6.7**, entries 4-6) recorded their absorption spectra.

6.2.6. Catalytic application for hydration of benzonitrile

We have investigated the catalytic application for the hydration of nitriles using Ru(II) multiple carbene complexes, as discussed in Chapter 5. Continuing this study, we have investigated the catalytic reactivity for the hydration of benzonitrile with all the synthesized dicationic Ru(II)-CNC pincer complexes. As a model substrate, we used benzonitrile in an aqueous medium with catalytic amounts of base and ruthenium catalyst, and GCMS monitored the conversion. Using 1 mmol of benzonitrile with 1 mol% of catalyst **11b**, and a catalytic amount of NaOH (20 mol%) at 60 ˚C for 6 h afforded better catalytic reactivity than other newly synthesized catalysts, 88% conversion (Table **6.8**, entry **5**). Using similar reaction conditions for catalysts **11a** and **11c** shows good reactivity of 80% and 71% conversions (Table **6.8**, entries **4** and **6**). As previously discussed in Chapter 5, the catalyst **7a-c** with similar reaction conditions showed 87%, 99%, and 72% conversions (Table **6.8**, entries **1-3**). Further, investigated the catalytic reactivity of PPh$_3$ coordinated ruthenium complex with similar reaction conditions for catalysts **12a**, **12b**, and **12c** shows lower catalytic

reactivity as compared to acetonitrile and iodide coordinated complexes 33%, 43%, and 32% conversions (Table **6.8**, entries **7-9**). The reaction mechanism was similar to our previously reported one and involved a Ru-OH species to facilitate the hydration reaction [47].

Table 6.8. Catalytic evaluation for hydration of benzonitrile in an aqueous medium.
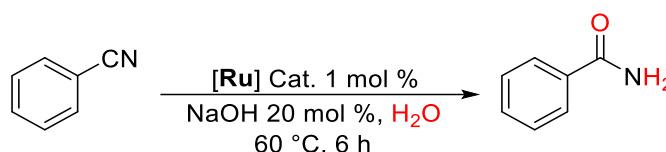
Entry[a]	Catalyst	Conversion[b] (%)	TON[c]/TOF[d] (h^{-1})
1.	**7a**	87(82)	87/14
2.	**7b**	99(93)	99/16
3.	**7c**	72(64)	72/12
4.	**11a**	80(75)	80/13
5.	**11b**	88(81)	88/15
6.	**11c**	71(66)	71/12
7.	**12a**	33(27)	33/6
8.	**12b**	43(36)	43/7
9.	**12c**	32(26)	32/5

[a]Reaction conditions: Benzonitrile (1 mmol), Catalyst (1 mol %), NaOH (20 mol%), H_2O (5 mL) under open-air conditions. [b]Conversion was determined by gas chromatography (GCMS) without an internal standard, and the isolated yield after the work-up is given in parentheses. [c]TON = [(Number of moles of substrate converted)/(Number of moles of catalyst)] at the end of the reaction. [d]TOF = [(TON)/hour].

6.2.7. DFT calculations for nitrile hydration

DFT calculations were performed to investigate the mechanism of the catalytic cycle. The computed reaction profile and the calculated Gibbs free energies (kcal/mol) are presented in Figure **6.12**. The initial step involves the dissociation of the sixth coordinated ligand to create a vacant site at the ruthenium centre for the model of species **A**. The active species **B** has lower energy than species **A**, is obtained upon

coordination of the hydroxide ligand. Three possibilities starting from the active species **B** are computed; **(i)** outer-sphere attack of nitrile to the coordinated Ru-OH, proceeding through the transition state **P1TS1**, **(ii)** generation of vacant site by rearrangement of hydroxyl group and simultaneous pyridyl-*N* dissociation, proceeding through the transition state **P2TS1**, and **(iii)** coordination of incoming nitrile by simultaneous pyridyl-*N* dissociation, proceeding through the transition state **P3TS1**. Among the transition states, the **P1TS1**, was found with the lowest energy barrier and, therefore, the remaining two paths were not pursued further. The iminolate intermediate **C** is obtained from **P1TS1**, which undergoes rearrangement via **P1TS2** to give the amido intermediate **D**. Protonolysis by a water molecule via intermediate **E**, transition state **P1TS3**, leads to the intermediate **F** having the hydrogen bonded final product. Release of the amide product from **F** regenerates the catalytically active species **B**.
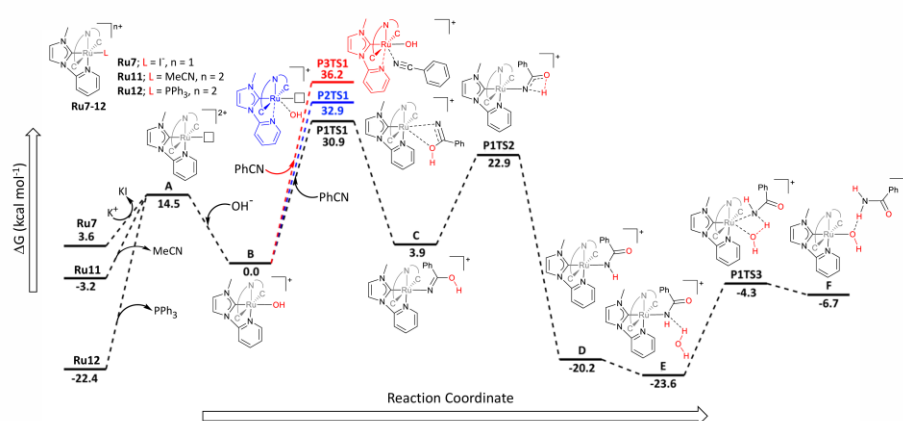
Figure 6.12. Relative Gibbs free energy profile for the Ru-catalysed nitrile hydration.

6.2.8. Mechanism for the hydration of nitrile

The mechanism of nitrile hydration catalyzed by transition metal complexes has been shown to follow several different routes, depending on the metal precursors, often involving a cooperative interaction between the ligand and water to facilitate nucleophilic

236

attack at the electrophilic centre of the nitrile [33, 41, 50–54]. Recently, Gupta and coworkers have described an interesting mechanism involving a Ru–H···H–OH dihydrogen-bonding interaction, which facilitates the nucleophilic attack of water on the coordinated nitrile [44]. Otten has also proposed a mechanism for nitrile hydration using a ruthenium pincer catalyst, emphasizing a metal–ligand cooperative effect within the catalytic cycle and the formation of a Ru–OH species during the catalysis [33]. Metal-hydroxy intermediates have also been observed in nitrile hydration with other transition metal complexes [51, 55].
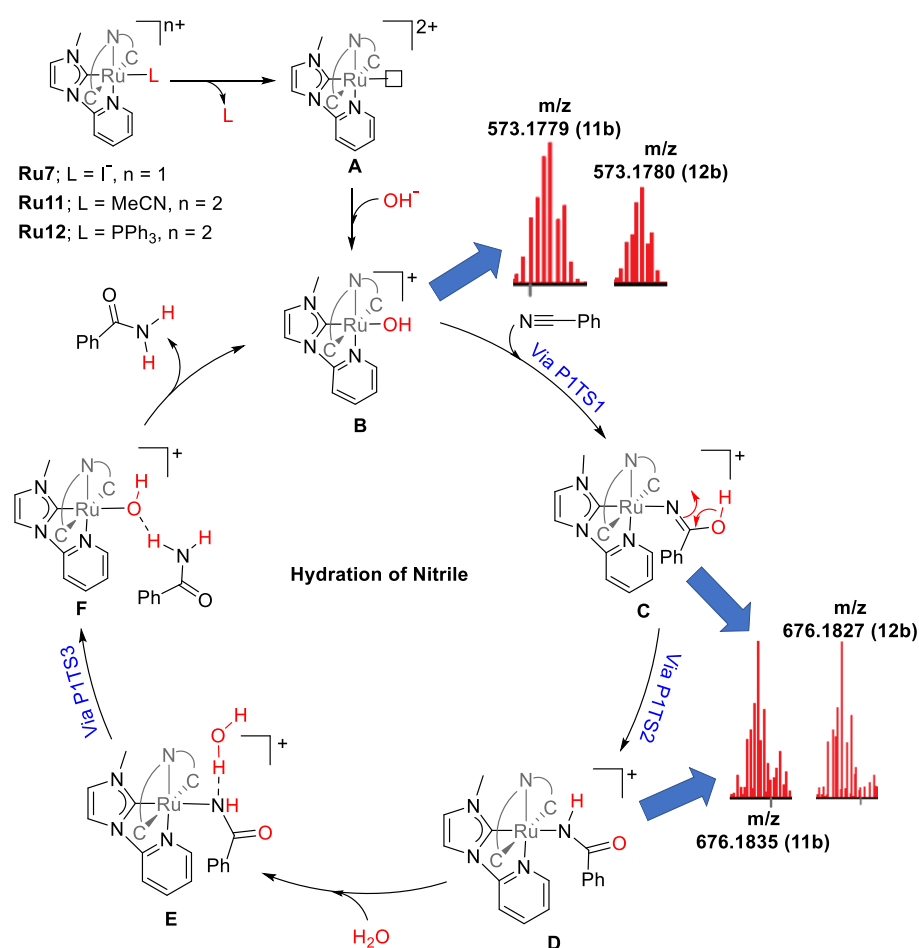
Figure 6.13. Plausible mechanism for the hydration of nitrile, supported by DFT and with two key intermediates, identified through the LCMS analysis of the catalytic sample.

237

Recently, we have reported a plausible reaction mechanism for nitrile hydration, including an active intermediate Ru-OH species [47]. Based on mechanistic investigations and DFT calculations, a revised catalytic cycle for nitrile hydration to amide catalyzed by complexes **Ru7-12** is shown in Figure **6.13**. We have analysed our catalytic samples with these new catalysts through mass spectrometry to get some insight into the reaction mechanism, revealing the formation of the same intermediate Ru-OH species **B**, identified in the mass analysis of catalytic samples at *m/z* 573.1779 with catalyst **11b** and 573.1780 with catalyst **12b**. The reaction starts with the active intermediate Ru-OH species **B**, generated from the precatalysts **Ru11-12** upon removal of the monodentate ligand and coordination of the hydroxide ion. The intermediate **C** is produced via the electrophilic attack of the incoming nitrile on the nucleophilic hydroxyl group through an outer-sphere pathway via the **P1TS1** transition state without dissociation of the pyridine unit of the bidentate ligand. Further, intermediate **D** was produced by the rearrangement of iminolate to amido via proton transfer through transition state **P1TS2**. The intermediate **D** has also been identified in LCMS at *m/z* 676.1835 with catalyst **11b** and 676.1827 with catalyst **12b**. Further, the metal-bound amido species in the intermediate **D** gets protonated with a H_2O molecule via intermediate **E** and transition state **P1TS3**, to give intermediate **F**. Release of the final amide product from intermediate **F** regenerates the active catalyst **B**.

6.3. Conclusion

In summary, syntheses, and characterization of novel dicationic Ru(II)-CNC pincer complexes [Ru(CNC^{Me})(CN^{Me})CH$_3$CN]2PF$_6$ (**11a**), [Ru(CNC$^{i\text{-}Pr}$)(CN^{Me})CH$_3$CN]2PF$_6$ (**11b**), [Ru(CNC^{Cy})(CN^{Me})CH$_3$CN]2PF$_6$ (**11c**), [Ru(CNC^{Me})(CN^{Me})PPh$_3$]2PF$_6$ (**12a**), [Ru(CNC$^{i\text{-}Pr}$)(CN^{Me})PPh$_3$]2PF$_6$ (**12b**) and [Ru(CNC^{Cy})(CN^{Me})PPh$_3$]2PF$_6$ (**12c**) was accomplished. All the new

complexes were fully characterized by multinuclear NMR and HRMS techniques, and complexes **11a**, **11c**, **12a**, and **12b** were characterized by single-crystal X-ray diffraction techniques. In the UV-vis spectra, the absorbance band was shifted towards the lower wavelength i.e., hypsochromic shift, when anionic I^- ligand was exchanged to neutral PPh_3 and CH_3CN ligands. The electrochemical studies of complexes (**7a–c** and **11a–12c**) show some reversible and irreversible peaks with different heights within the accessible potential gap. Upon comparison of the catalytic activity for the hydration of nitrile under mild reaction conditions for all the complexes with I^-, CH_3CN, and PPh_3 ligands, it was found that the complexes **7a-c** are more active catalysts than CH_3CN-based complexes **11a-c** and the poor catalytic activity of PPh_3 based complexes **12a-c**. Investigation of the catalytic activity of new complexes towards nitrile hydration reveals that the reaction proceeds through a common Ru-OH intermediate generated by removal of the I^-, CH_3CN or PPh_3 ligands. DFT investigations reveal a single-site catalysis through an outer-sphere electrophilic attack of nitrile on the Ru-bound hydroxyl group.

6.4. Experimental Section

6.4.1. General Considerations

All reactions and manipulations were carried out under an inert atmosphere using standard Schlenk techniques. Solvents were purchased from S. D. Fine-Chem Limited and distilled under an inert atmosphere. The synthesis of ruthenium complexes **7a-c** was based on the procedure previously reported, as discussed in Chapter 4. Deuterated acetone (Acetone-d_6), deuterated dimethyl sulphoxide (DMSO-d_6), and deuterated chloroform (CDCl$_3$) were purchased either from EURISOtop or Sigma-Aldrich. NMR spectra were recorded on Bruker Avance (III) spectrometer and Bruker Avance NEO spectrometer operating at 400 and 500 MHz for ^{1}H, 162 and 202 MHz

for ^{31}P, and 101 and 126 MHz for ^{13}C NMR. NMR chemical shifts are reported in ppm and referenced to the solvent peaks for ^{1}H (Acetone-d$_6$ δ 2.05, CDCl$_3$ δ 7.26 and DMSO-d$_6$ δ 2.50 ppm) and ^{13}C (natural abundance of ^{13}C in Acetone-d$_6$, δ 29.84 and δ 206.26, CDCl$_3$ δ 77.16 and DMSO-d$_6$ δ 39.52 ppm) NMR. ^{31}P NMR chemical shifts are referenced to an external 85% H$_3$PO$_4$ standard as 0 ppm. Multiplicities are given as s (singlet), d (doublet), t (triplet), and m (multiplet), and the coupling constants J are given in hertz. The mass chromatograms were recorded on Bruker-Daltonics-MicroTOF-QII mass spectrometer in HPLC grade methanol and acetonitrile. UV-visible absorption spectra were recorded on a PerkinElmer Lambda 35 instrument in acetonitrile. All cyclic voltammetry (CV) and differential pulse voltammetry (DPV) measurements were taken using a Palmsens4 electrochemical analyzer. All measurements were carried out in 0.1 M of TBAPF$_6$/acetonitrile (TBAPF$_6$ = Tetrabutylammonium hexafluorophosphate) at a scan rate of 100 mV/s. The working electrode was a glassy carbon electrode, and the counter electrode was a platinum wire. The reference electrode was Ag/AgCl in a saturated aqueous KCl solution. All E$_{1/2}$ values reported in this study were estimated from cyclic voltammetry as the average of the oxidative and reductive peak potentials (E$_{pa}$+E$_{pc}$)/2 at a scan rate of 100 mV/s. In differential pulse voltammetry (DPV) experiments, the maximum potential peak is directly taken. Elemental analysis was carried out on a Thermo Fischer Scientific Flash 2000 (formerly the Flash EA1112) is the CHNS-O elemental analyzer. GC Samples were analyzed in Shimadzu QP2010 Ultra without an internal standard in HPLC grade methanol.

6.4.2. General Procedure for Synthesis of metal complexes

A. An oven-dried Schlenk tube with a magnetic stirring bar was charged with metal complex (1 equiv.), $AgPF_6$ (1 equiv.) in acetonitrile (5 mL) was stirred, and the resulting mixture was heated at 40 ˚C under N_2 atmosphere for 3 h. On completion of the reaction, the reaction mixture was filtered, dried, dissolved in minimal acetonitrile, and then diethyl ether was added. A desired complex was precipitated out, filtered the precipitate, washed with Et_2O, and dried under vacuum.

B. An oven-dried Schlenk tube with a magnetic stirring bar was charged with metal complex (1 equiv.), PPh_3 (2 equiv.) in dry methanol (10 mL), the resulting mixture was refluxed under N_2 atmosphere for 12 h. On completion of the reaction, it was cooled to room temperature and an aqueous solution of KPF_6 (0.184 g, 1 mmol, 10 ml water) was added, then stirred for 2 min at room temperature. A desired complex was precipitated out, filtered the precipitate, washed with H_2O, and dried under vacuum.

6.4.2.1. Complex (7a) [Ru(CNC^Me)(CN^Me)I]PF₆

UV-vis absorption (MeCN, 21 °C): 229 nm (77970 cm^{-1} M^{-1}), 272 nm (31460 cm^{-1} M^{-1}), 285 nm (24860 cm^{-1} M^{-1}), 377 nm (20130 cm^{-1} M^{-1}), 416 nm (13180 cm^{-1} M^{-1}). Cyclic Voltammetry: (MeCN, 21 ˚C, 0 V = Ag/Ag$^+$): $E_{1/2}$ = 0.629V (irrev., I$^-$/I$_2$), 0.809V (irrev., [Ru]$^{+2/+3}$ for **7a**) and 1.119V (rev., [Ru]$^{+2/+3}$ for in situ generated **11a**).

6.4.2.2. Complex (7b) [Ru(CNC^{i-Pr})(CN^Me)I]PF₆

UV-vis absorption (MeCN, 21 °C): 230 nm (51200 cm^{-1} M^{-1}), 274 nm (19550 cm^{-1} M^{-1}), 286 nm (15930 cm^{-1} M^{-1}), 380 nm (12740 cm^{-1} M^{-1}), 416 nm (8250 cm^{-1} M^{-1}). Cyclic Voltammetry: (MeCN, 21 ˚C, 0 V = Ag/Ag$^+$): $E_{1/2}$ = 0.729V (irrev. I$^-$/I$_2$), 0.829V (irrev. [Ru]$^{+2/+3}$ for **7b**) and 1.155V (rev., [Ru]$^{+2/+3}$ for in situ generated **11b**).

6.4.2.3. Complex (7c) [Ru(CNC^{Cy})(CN^{Me})I]PF$_6$

UV-vis absorption (MeCN, 21 °C): 230 nm (57900 cm^{-1} M^{-1}), 274 nm (22780 cm^{-1} M^{-1}), 287 nm (19790 cm^{-1} M^{-1}), 382 nm (13070 cm^{-1} M^{-1}), 416 nm (8600 cm^{-1} M^{-1}). Cyclic Voltammetry: (MeCN, 21 ˚C, 0 V = Ag/Ag$^+$): E$_{1/2}$ = 0.569V (irrev. I$^-$/I$_2$), 0.769V (irrev. [Ru]$^{+2/+3}$ for **7c**) and 1.105V (rev., [Ru]$^{+2/+3}$ for in situ generated **11c**).

6.4.2.4. Synthesis of Complex (11a) [Ru(CNC^{Me})(CN^{Me})CH$_3$CN]2PF$_6$

This complex (**11a**) was prepared by general procedure **A**, from [Ru(CNC^{Me})(CN^{Me})I]PF$_6$ (0.050 g, 0.0648 mmol) and AgPF$_6$ (0.016 g, 0.0648 mmol) to give the desired complex as a yellow solid. Yield = 0.037 g (69%). ^{1}H NMR (500 MHz, DMSO-d$_6$) δ 9.81 (d, J = 5.8 Hz, 1H), 8.50 (d, J = 1.7 Hz, 2H), 8.44 – 8.41 (m, 2H), 8.28 (d, J = 4.0 Hz, 2H), 8.10 (d, J = 8.2 Hz, 2H), 7.66 – 7.63 (m, 1H), 7.58 (d, J = 1.7 Hz, 2H), 7.30 (d, J = 1.7 Hz, 1H), 3.12 (s, 6H), 2.54 (s, 3H), 2.07 (s, 3H). ^{13}C NMR (126 MHz, DMSO-d$_6$) δ 187.07, 183.36, 153.41, 152.51, 152.15, 141.57, 139.02, 125.99, 125.39, 122.50, 118.66, 118.08, 116.39, 112.71, 107.93, 35.83, 34.16, 1.15. ^{31}P NMR (202 MHz, DMSO-d$_6$) δ -144.20. ^{1}H NMR (500 MHz, Acetone-d$_6$) δ 9.63 (d, J = 5.7 Hz, 1H), 8.34 (d, J = 2.2 Hz, 2H), 8.31 (d, J = 8.2 Hz, 1H), 8.25 – 8.20 (m, 2H), 8.18 (d, J = 2.4 Hz, 1H), 8.02 (d, J = 8.2 Hz, 2H), 7.63 (t, J = 1.5 Hz, 1H), 7.43 (d, J = 2.2 Hz, 2H), 7.10 (d, J = 2.3 Hz, 1H), 3.21 (s, 6H), 2.73 (s, 3H), 2.25 (s, 3H). ^{13}C NMR (126 MHz, Acetone-d$_6$) δ 191.63, 189.41, 155.26, 153.25, 152.14, 141.12, 138.87, 126.59, 125.63, 125.56, 123.07, 118.39, 116.45, 112.94, 107.47, 36.50, 35.24, 3.42. ^{31}P NMR (202 MHz, Acetone-d$_6$) δ -144.27. HRMS for [M-2PF$_6$]$^{2+}$ [C$_{24}$H$_{25}$N$_9$Ru]$^{2+}$ in CH$_3$OH: calculated - 270.5636, found - 270.5651. Anal. Calcd. for [C$_{24}$H$_{25}$N$_9$Ru]2PF$_6$: C 34.71, H 3.03, N 15.18, found: C 34.99, H 2.89, N 14.94. UV-vis absorption (MeCN, 21 °C): 229 nm (57750 cm^{-1} M^{-1}), 271 nm (29280 cm^{-1} M^{-1}), 285 nm (21950 cm^{-1} M^{-1}), 362 nm (20290 cm^{-1} M^{-1}), 383 nm (17220 cm^{-1} M^{-1}).

Cyclic Voltammetry: (MeCN, 21 °C, 0 V = Ag/Ag$^+$): E$_{1/2}$(Ru$^{+2/+3}$) = 1.074 V (rev.).

6.4.2.5. Synthesis of Complex (11b) [Ru(CNC$^{i\text{-}Pr}$)(CN^{Me})CH$_3$CN]2PF$_6$

This complex (**11b**) was prepared by general procedure **A**, from [Ru(CNC$^{i\text{-}Pr}$)(CN^{Me})I]PF$_6$ (0.050 g, 0.0604 mmol) and AgPF$_6$ (0.015 g, 0.0604 mmol) to give the desired complex as a greenish-yellow solid. Yield = 0.036 g (67%). ^{1}H NMR (500 MHz, DMSO-d$_6$) δ 9.82 (d, J = 5.9 Hz, 1H), 8.59 (d, J = 2.1 Hz, 2H), 8.46 – 8.43 (m, 2H), 8.34 – 8.31 (m, 2H), 8.10 (d, J = 8.2 Hz, 2H), 7.81 (d, J = 2.2 Hz, 2H), 7.71 – 7.68 (m, 1H), 7.37 (d, J = 2.1 Hz, 1H), 3.46 – 3.40 (m, 2H), 2.54 (s, 3H), 2.07 (s, 3H), 1.30 (d, J = 6.8 Hz, 6H), 0.65 (d, J = 6.8 Hz, 6H). ^{13}C NMR (126 MHz, DMSO-d$_6$) δ 185.24, 183.56, 153.25, 152.80, 152.20, 141.75, 139.45, 126.66, 122.83, 120.25, 119.45, 118.08, 115.94, 112.36, 107.97, 52.00, 34.32, 22.82, 21.14, 1.14. ^{31}P NMR (202 MHz, DMSO-d$_6$) δ -144.20. ^{1}H NMR (500 MHz, Acetone-d$_6$) δ 9.63 (d, J = 5.7 Hz, 1H), 8.40 (d, J = 2.4 Hz, 2H), 8.35 – 8.32 (m, 1H), 8.29 – 8.27 (m, 1H), 8.24 (d, J = 7.5 Hz, 1H), 8.22 (d, J = 2.3 Hz, 1H), 8.04 (d, J = 8.2 Hz, 2H), 7.66 (t, J = 6.5 Hz, 1H), 7.62 (d, J = 2.3 Hz, 2H), 7.17 (d, J = 2.3 Hz, 1H), 3.51 – 3.43 (m, 2H), 2.74 (s, 3H), 2.28 (s, 3H), 1.34 (d, J = 6.8 Hz, 6H), 0.90 (d, J = 6.9 Hz, 6H). ^{13}C NMR (126 MHz, Acetone-d$_6$) δ 189.84, 189.60, 155.09, 153.34, 152.43, 141.29, 139.22, 126.71, 126.11, 123.17, 120.32, 119.08, 116.27, 112.81, 107.51, 53.11, 35.37, 23.00, 22.67, 3.37. ^{31}P NMR (202 MHz, Acetone-d$_6$) δ -144.25. HRMS for [M-2PF$_6$]$^{2+}$ [C$_{28}$H$_{33}$N$_9$Ru]$^{2+}$ in CH$_3$OH: calculated - 298.5949, found - 298.5954. Anal. Calcd. for [C$_{28}$H$_{33}$N$_9$Ru]2PF$_6$: C 37.93, H 3.75, N 14.22, found: C 37.67, H 3.48, N 13.89. UV-vis absorption (MeCN, 21 °C): 229 nm (67120 cm^{-1} M^{-1}), 271 nm (33610 cm^{-1} M^{-1}), 286 nm (26310 cm^{-1} M^{-1}), 363 nm (22630 cm^{-1} M^{-1}), 382 nm (20070 cm^{-1} M^{-1}). Cyclic Voltammetry: (MeCN, 21 °C, 0 V = Ag/Ag$^+$): E$_{1/2}$(Ru$^{+2/+3}$) = 1.119 V (rev.).

6.4.2.6. Synthesis of Complex (11c) [Ru(CNC^{Cy})(CN^{Me})CH$_3$CN]2PF$_6$

This complex (**11c**) was prepared by general procedure **A**, from [Ru(CNC^{Cy})(CN^{Me})I]PF$_6$ (0.050 g, 0.0550 mmol) and AgPF$_6$ (0.014 g, 0.0550 mmol) to give the desired complex as a light-yellow solid. Yield = 0.034 g (64%). ^{1}H NMR (500 MHz, DMSO-d$_6$) δ 9.88 (d, J = 5.8 Hz, 1H), 8.57 (d, J = 1.8 Hz, 2H), 8.49 (d, J = 1.7 Hz, 1H), 8.46 – 8.43 (m, 1H), 8.41 (d, J = 4.1 Hz, 2H), 8.10 (d, J = 8.2 Hz, 2H), 7.79 (d, J = 1.7 Hz, 3H), 7.37 (d, J = 1.6 Hz, 1H), 3.02 – 2.96 (m, 2H), 2.53 (s, 3H), 2.07 (s, 3H), 1.83 (d, J = 10.5 Hz, 2H), 1.74 – 1.65 (m, 4H), 1.47 (d, J = 12.5 Hz, 2H), 1.42 – 1.37 (m, 2H), 1.35 – 1.29 (m, 2H), 1.01 – 0.94 (m, 2H), 0.83 – 0.76 (m, 2H), 0.62 (d, J = 11.3 Hz, 2H), 0.22 – 0.15 (m, 2H). ^{13}C NMR (126 MHz, DMSO-d$_6$) δ 185.48, 183.83, 153.26, 153.05, 152.19, 141.79, 139.45, 126.70, 122.90, 120.74, 119.43, 118.07, 115.87, 112.59, 108.05, 59.55, 34.36, 33.40, 31.02, 25.06, 24.88, 24.02, 1.14. ^{31}P NMR (202 MHz, DMSO-d$_6$) δ - 144.20. ^{1}H NMR (500 MHz, Acetone-d$_6$) δ 9.70 (d, J = 5.8 Hz, 1H), 8.37 (d, J = 2.6 Hz, 2H), 8.37 – 8.35 (s, 2H), 8.33 (d, J = 7.9 Hz, 1H), 8.26 (d, J = 2.4 Hz, 1H), 8.03 (d, J = 8.2 Hz, 2H), 7.76 (td, J = 5.8, 2.9 Hz, 1H), 7.58 (d, J = 2.3 Hz, 2H), 7.17 (d, J = 2.3 Hz, 1H), 2.89 – 2.80 (m, 2H), 2.73 (s, 3H), 2.25 (s, 3H), 1.94 – 1.89 (m, 3H), 1.76 – 1.72 (m, 2H), 1.69 – 1.66 (m, 2H), 1.60 – 1.56 (m, 2H), 1.48 – 1.43 (m, 3H), 1.07 – 1.02 (m, 2H), 1.01 – 0.96 (m, 2H), 0.86 – 0.77 (m, 2H), 0.59 – 0.49 (m, 2H). ^{13}C NMR (126 MHz, Acetone-d$_6$) δ 189.92, 189.85, 155.02, 153.31, 152.56, 141.35, 139.11, 126.61, 126.14, 123.49, 120.83, 119.00, 116.12, 113.02, 107.54, 60.76, 35.40, 33.83, 33.48, 26.20, 26.16, 25.17, 3.36. ^{31}P NMR (202 MHz, Acetone-d$_6$) δ - 144.26. HRMS for [M-2PF$_6$]$^{2+}$ [C$_{34}$H$_{41}$N$_9$Ru]$^{2+}$ in CH$_3$OH: calculated - 338.6263, found - 338.6266. Anal. Calcd. for [C$_{34}$H$_{41}$N$_9$Ru]2PF$_6$: C 42.24, H 4.27, N 13.04, found: C 43.96, H 3.99, N 12.86. UV-vis absorption (MeCN, 21 °C): 230 nm (50050 cm^{-1} M^{-1}), 272 nm (25910 cm^{-1} M^{-1}), 286 nm (20780 cm^{-1} M^{-1}), 364 nm (16820 cm^{-1} M^{-1}), 382

nm (15800 cm^{-1} M^{-1}). Cyclic Voltammetry: (MeCN, 21 ˚C, 0 V = Ag/Ag$^+$): E$_{1/2}$(Ru$^{+2/+3}$) = 1.119 V (rev.).

6.4.2.7. Synthesis of Complex (12a) [Ru(CNC^{Me})(CN^{Me})PPh$_3$]2PF$_6$

This complex (**12a**) was prepared by general procedure **B**, from [Ru(CNC^{Me})(CN^{Me})I]PF$_6$ (0.100 g, 0.129 mmol) and PPh$_3$ (0.068 g, 0.259 mmol) to give the desired complex as a light-yellow solid. Yield = 0.110 g (81%). ^{1}H NMR (400 MHz, DMSO-d$_6$) δ 8.65 (d, J = 5.1 Hz, 1H), 8.47 – 8.46 (m, 1H), 8.37 (m, 2H), 8.32 (d, J = 8.1 Hz, 1H), 8.21 (t, J = 7.6 Hz, 1H), 7.97 (t, J = 8.0 Hz, 1H), 7.61 (d, J = 8.1 Hz, 2H), 7.52 (m, 2H), 7.48 – 7.44 (m, 3H), 7.35 – 7.32 (m, 7H), 7.27 – 7.24 (m, 1H), 6.92 – 6.87 (m, 6H), 2.96 (s, 6H), 2.31 (s, 3H). ^{13}C NMR (126 MHz, DMSO-d$_6$) δ 189.74 (d, J_{CP}= 11.4 Hz), 185.46 (d, J_{CP}= 80.8 Hz), 154.17 (d, J_{CP}= 7.3 Hz), 152.61, 151.95, 139.67, 139.36, 132.50 (d, J_{CP}= 10.7 Hz), 130.67, 130.45 (d, J_{CP}= 12.8 Hz), 128.88 (d, J_{CP}= 8.7 Hz), 126.04, 125.67, 122.16, 118.20, 116.37, 113.14, 106.73, 35.74, 34.27. ^{31}P NMR (202 MHz, DMSO-d$_6$) δ 36.77, -144.20. HRMS for [M-2PF$_6$]$^{2+}$ [C$_{40}$H$_{37}$N$_8$PRu]$^{2+}$ in CH$_3$CN: calculated - 381.0961, found - 381.0984. Anal. Calcd. for [C$_{40}$H$_{37}$N$_8$PRu]2PF$_6$: C 45.68, H 3.55, N 10.65, found: C 45.39, H 3.82, N 10.44. UV-vis absorption (MeCN, 21 °C): 226 nm (60540 cm^{-1} M^{-1}), 274 nm (24540 cm^{-1} M^{-1}), 282 nm (18700 cm^{-1} M^{-1}), 323 nm (8680 cm^{-1} M^{-1}), 363 nm (12880 cm^{-1} M^{-1}). Cyclic Voltammetry: (MeCN, 21 ˚C, 0 V = Ag/Ag$^+$): E$_{1/2}$(Ru$^{+2/+3}$) = 1.229V (rev.).

6.4.2.8. Synthesis of Complex (12b) [Ru(CNC^{i-Pr})(CN^{Me})PPh$_3$]2PF$_6$

This complex (**12b**) was prepared by general procedure **B**, from [Ru(CNC^{i-Pr})(CN^{Me})I]PF$_6$ (0.100 g, 0.120 mmol) and PPh$_3$ (0.063 g, 0.241 mmol) to give the desired complex as an off-green solid. Yield = 0.109 g (81%). ^{1}H NMR (500 MHz, DMSO-d$_6$) δ 8.71 (d, J = 5.7 Hz, 1H), 8.54 (d, J = 1.7 Hz, 1H), 8.46 (d, J = 1.8 Hz, 2H), 8.38 (d, J = 8.4 Hz, 1H), 8.28 (t, J = 7.7 Hz, 1H), 7.99 (t, J = 8.2 Hz, 1H), 7.78 (d, J =

2.0 Hz, 2H), 7.61 (d, J = 8.2 Hz, 2H), 7.46 – 7.41 (m, 4H), 7.34 – 7.28 (m, 7H), 7.18 – 7.13 (m, 1H), 6.91 – 6.87 (m, 5H), 3.20 – 3.12 (m, 2H), 2.32 (s, 3H), 1.26 (d, J = 6.7 Hz, 6H), 0.49 (d, J = 6.5 Hz, 6H). ^{13}C NMR (126 MHz, DMSO-d_6) δ 187.83 (d, J_{CP} = 11.6 Hz), 185.33 (d, J_{CP}= 80.7 Hz), 154.79 (d, J_{CP} = 7.2 Hz), 152.64, 151.73, 139.87, 139.81, 132.42 (d, J_{CP}= 10.5 Hz), 131.10, 130.82, 130.42, 128.88 (d, J_{CP} = 8.8 Hz), 122.33, 120.61, 119.01, 116.34, 112.81, 106.75, 51.71, 34.41, 23.37, 20.46. ^{31}P NMR (202 MHz, DMSO-d_6) δ 35.47, -144.19. HRMS for $[M-2PF_6]^{2+}$ $[C_{44}H_{45}N_8PRu]^{2+}$ in CH_3CN: calculated - 409.1274, found - 409.1299. Anal. Calcd. for $[C_{44}H_{45}N_8PRu]2PF_6$: C 47.70, H 4.09, N 10.11, found: C 47.46, H 3.94, N 10.17. UV-vis absorption (MeCN, 21 °C): 227 nm (64250 cm^{-1} M^{-1}), 274 nm (26070 cm^{-1} M^{-1}), 284 nm (19270 cm^{-1} M^{-1}), 324 nm (9080 cm^{-1} M^{-1}), 364 nm (13250 cm^{-1} M^{-1}). Cyclic Voltammetry: (MeCN, 21 ˚C, 0 V = Ag/Ag$^+$): $E_{1/2}$(Ru$^{+2/+3}$) = 1.259V (rev.).

6.4.2.9. Synthesis of Complex (12c) [Ru(CNC^{Cy})(CN^{Me})PPh$_3$]2PF$_6$

This complex (**12c**) was prepared by general procedure **B**, from [Ru(CNC^{Cy})(CN^{Me})I]PF$_6$(0.100 g, 0.110 mmol) and PPh$_3$ (0.058 g, 0.220 mmol) to give the desired complex as an off-yellow solid. Yield = 0.104 g (79%). ^{1}H NMR (500 MHz, DMSO-d_6) δ 8.75 (d, J = 5.5 Hz, 1H), 8.61 (d, J = 2.2 Hz, 1H), 8.53 (d, J= 8.3 Hz, 1H), 8.42 (d, J = 2.3 Hz, 2H), 8.36 (t, J = 7.6 Hz, 1H), 8.01 (t, J = 8.1 Hz, 1H), 7.75 (m, 1H), 7.62 (d, J = 8.2 Hz, 2H), 7.45 (t, J = 7.3 Hz, 3H), 7.42 – 7.38 (m, 3H), 7.32 (d, J = 7.3 Hz, 1H), 7.29 – 7.25 (m, 5H), 7.18 – 7.14 (m, 1H), 6.91 – 6.86 (m, 5H), 2.76 – 2.69 (m, 2H), 2.31 (s, 3H), 1.79 – 1.75 (m, 4H), 1.68 – 1.65 (m, 2H), 1.51 (d, J = 12.0 Hz, 2H), 1.43 (d, J = 12.3 Hz, 2H), 1.27 – 1.20 (m, 2H), 1.05 – 0.97 (m, 2H), 0.68 – 0.60 (m, 2H), 0.42 – 0.35 (m, 2H), 0.24 (d, J = 10.8 Hz, 2H). ^{13}CNMR (126 MHz, DMSO-d_6) δ 188.07 (d, J_{CP} = 11.3 Hz), 185.83 (d, J_{CP} = 80.9 Hz), 155.17 (d, J_{CP} = 7.3 Hz), 152.57, 151.74, 139.92, 139.64, 132.39 (d, J_{CP} = 10.4 Hz), 131.03, 130.72 (d, J_{CP}= 8.2 Hz), 130.51, 128.80 (d, J_{CP} = 8.9 Hz), 122.32, 121.20, 118.98, 115.97, 113.11, 106.88, 59.65,

34.46, 34.08, 30.35, 25.17, 25.10, 24.01. ^{31}P NMR (202 MHz, DMSO-d_6) δ 35.33, -144.20. HRMS for [M-2PF$_6$]$^{2+}$ [C$_{50}$H$_{53}$N$_8$PRu]$^{2+}$ in CH$_3$CN: calculated - 449.1588, found - 449.1608. Anal. Calcd. for [C$_{50}$H$_{53}$N$_8$PRu]2PF$_6$: C 50.55, H 4.50, N 9.43, found: C 50.68, H 4.34, N 9.19. UV-vis absorption (MeCN, 21 °C): 226 nm (62070 cm^{-1} M^{-1}), 275 nm (26050 cm^{-1} M^{-1}), 285 nm (19960 cm^{-1} M^{-1}), 325 nm (9530 cm^{-1} M^{-1}), 365 nm (12160 cm^{-1} M^{-1}). Cyclic Voltammetry: (MeCN, 21 ˚C, 0 V = Ag/Ag$^+$): E$_{1/2}$(Ru$^{+2/+3}$) = 1.284V (rev.).

6.4.3. X-ray data collection and structure refinement

Single crystal X-ray data were recorded at room temperature on a Rigaku Oxford diffractometer with graphite-monochromated Mo Kα radiation (λ = 0.71073 Å) for complexes **11a**, **12a**, and **12b** and a Cu Kα radiation (λ = 1.54184 Å) for complex **11c**. The data collection was evaluated with the help of CrysAlisPro CCD software. Using Olex2 [56], the structure was solved with the SHELXT [57] structure solution program using Intrinsic Phasing and refined with the SHELXL [58] refinement package using least squares minimization. The final refinement included atomic positions for all the atoms, anisotropic thermal parameters for all the non-hydrogen atoms, and isotropic thermal parameters for all the hydrogen atoms. Structural parameters and final refinements for complexes **11a** and **11c** are given in Table **6.2**, while complexes **12a** and **12b** are given in Table **6.4**. Selected bond lengths and bond angles for all the complexes are given in Tables **6.3** and **6.5**.

6.4.4. Computational details

DFT calculations were performed using the ORCA 6.0.1 program package developed by Neese and co-workers [59–61]. The geometry optimizations were carried out using the r2Scan-3c composite functional, which is shown to produce excellent geometries for transition metal complexes [62]. Solvation effects in water were included using SMD solvation model during all calculations [63]. Stationary points were confirmed to have either no imaginary frequency (all reactants and intermediates) or only one imaginary frequency along the reaction coordinates (for all transition states) by performing analytical frequency calculations at the same level of the DFT method. For final energies, single point calculations including solvation effects were performed using range separated hybrid meta-GGA functional ωB97M-V [64] developed by Martin Head-Gorden and coworkers, which includes VV10 non-local correlation. Larger basis sets def2-QZVP with def2-ECP on Ru, and def2-TZVP on all other atoms with def2-ECP on I were used for final single point energy calculations. The energies obtained from single point calculations were converted to Gibbs free energies using the total corrections obtained for the thermochemical calculations following the frequency calculations at the r2Scan-3c level and the solvation energies. To account for the entropy penalty during the change in number of components during a chemical change, the MHP scheme proposed by Martin, Hay, and Pratt was applied, which has also been used in several systems to produce reasonable results [65]. According to this method, a correction of (n-m) $\times$ 4.3 kcal/mol is imposed whenever a reaction component changes from m components to n components. Gibbs free energies, ΔG, are reported in Kcal/mol.

6.4.5. General procedure for hydration of benzonitrile

In a Schlenk tube, Benzonitrile (1 mmol), catalyst (0.01 mmol), and NaOH (0.008 g, 0.2 mmol) were dissolved in H_2O (5 mL) under an open-air condition. The reaction mixture was heated at 60 $^\circ$C for 6 h. The conversion of the benzamide product was determined by the relative peak area of the reactant and product in GC without an internal standard. The product was purified by silica gel column chromatography using hexane and ethyl acetate as eluents. NMR data of the benzamide product matched with the reported values. Benzamide: ^{1}H NMR (500 MHz, CDCl$_3$) δ 7.82 (d, J = 7.6 Hz, 2H), 7.53 (t, J = 7.4 Hz, 1H), 7.44 (t, J = 7.6 Hz, 2H), 6.16 (s, 2H, NH). ^{13}C NMR (126 MHz, CDCl$_3$) δ 169.70, 133.51, 132.13, 128.76, 127.47.

6.4.6. Experimental details for mass analysis of the hydration of benzonitrile

In a Schlenk tube, catalyst (0.0087 g **11b** or 0.011 g **12b**, 0.01 mmol) was added to a solution of benzonitrile (0.103 ml, 1 mmol) and NaOH (0.008 g, 0.2 mmol) in H_2O under open-air conditions. The resulting reaction mixture was heated at 60 $^\circ$C by lowering it into a preheated oil bath, and then samples were taken for LCMS analysis.

6.4.7. Characterization data of metal complexes
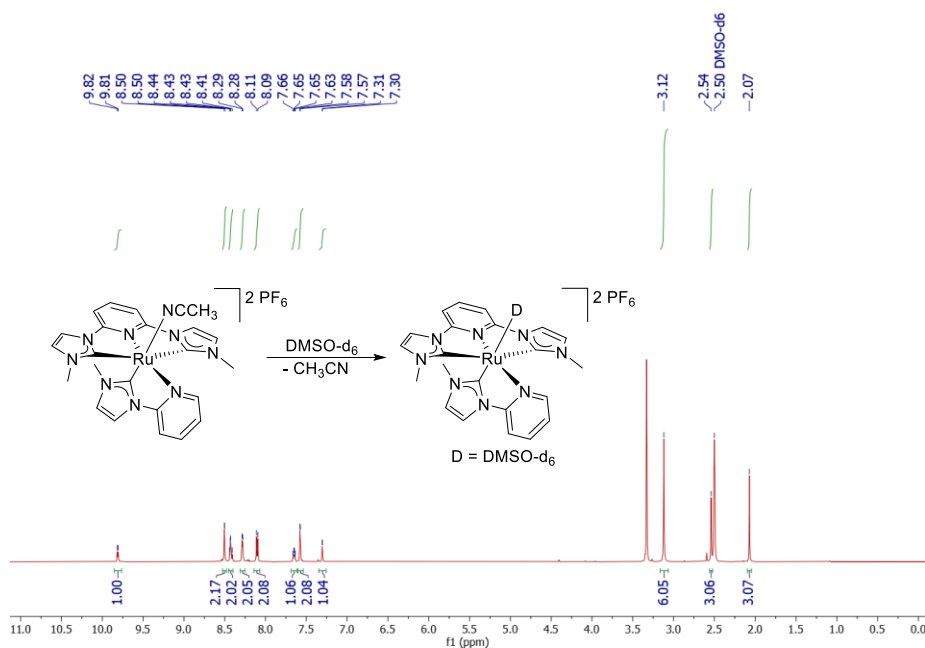
Figure 6.14. ^{1}H NMR spectrum of complex **11a** in dmso-d$_6$ with dissociated acetonitrile.
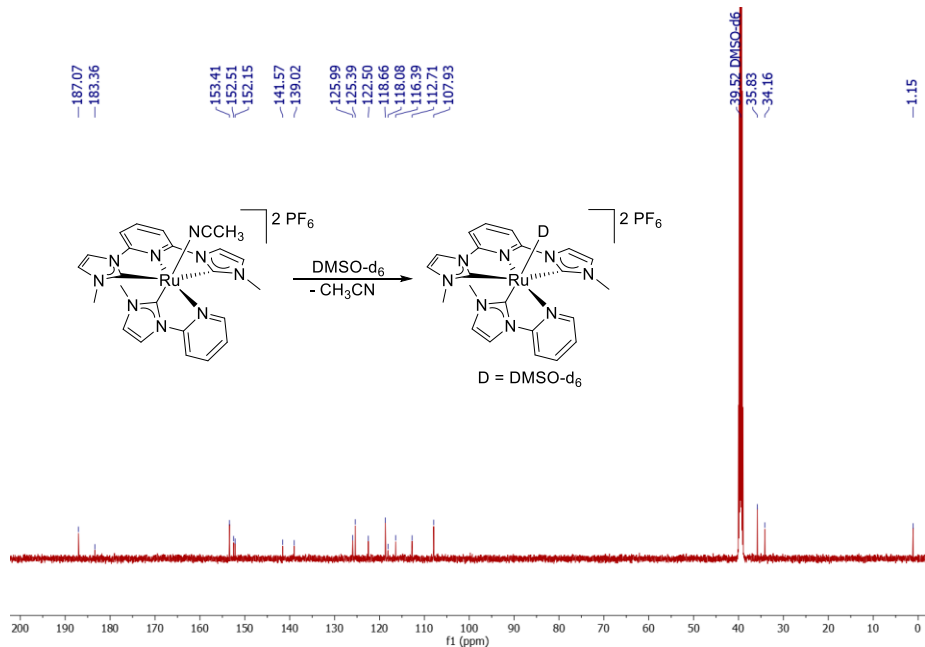
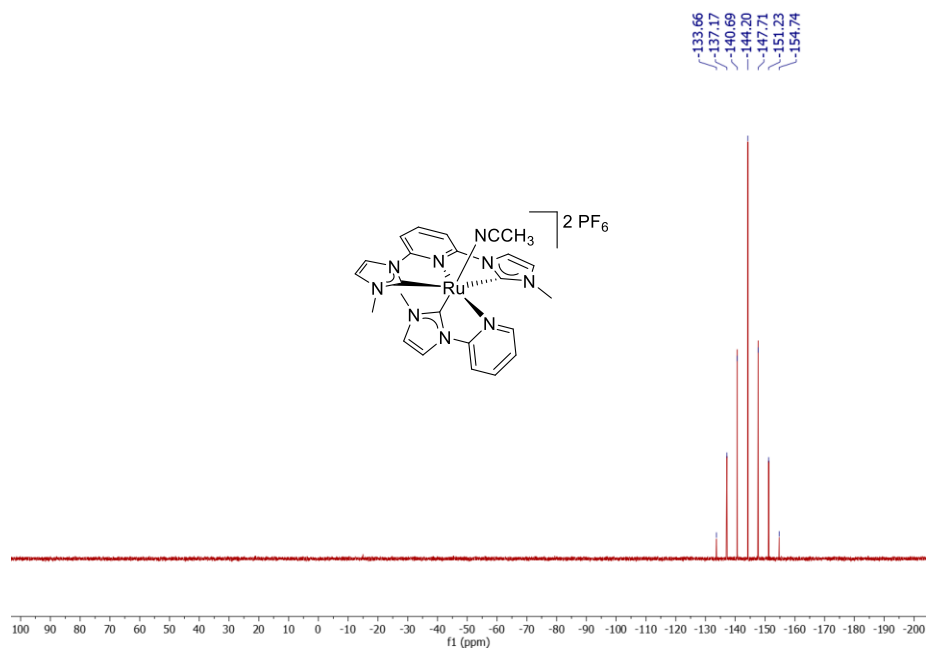**Figure 6.15.** ^{13}C NMR spectrum of complex **11a** in dmso-d$_6$ with dissociated acetonitrile.

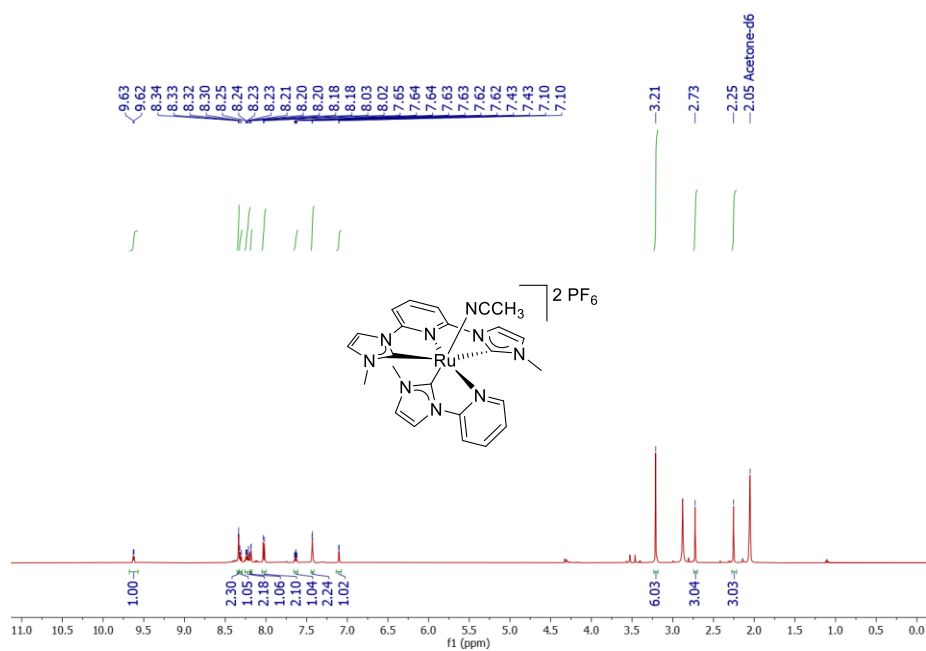**Figure 6.16.** ^{31}P NMR spectrum of complex **11a** in dmso-d$_6$.

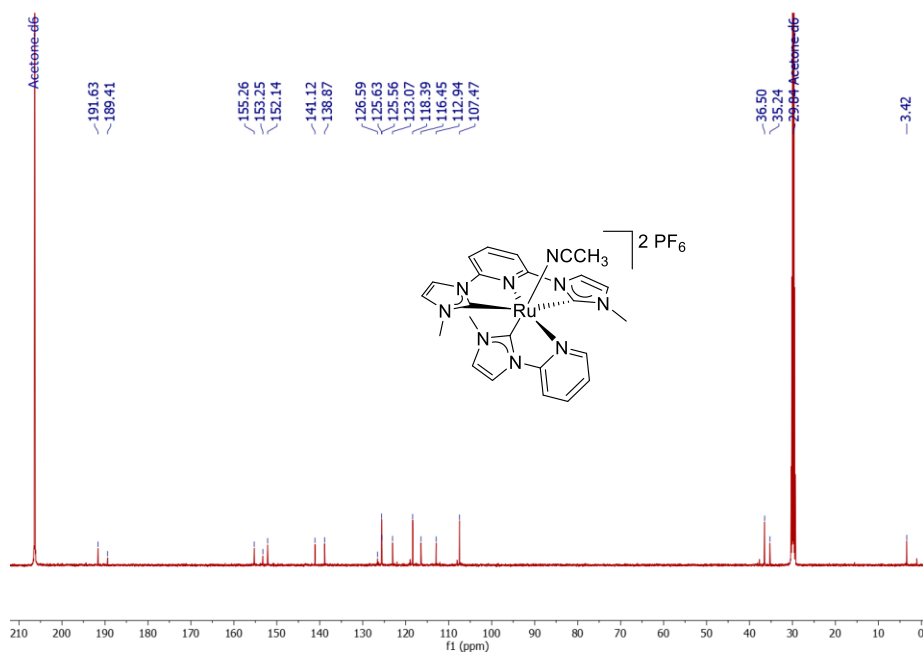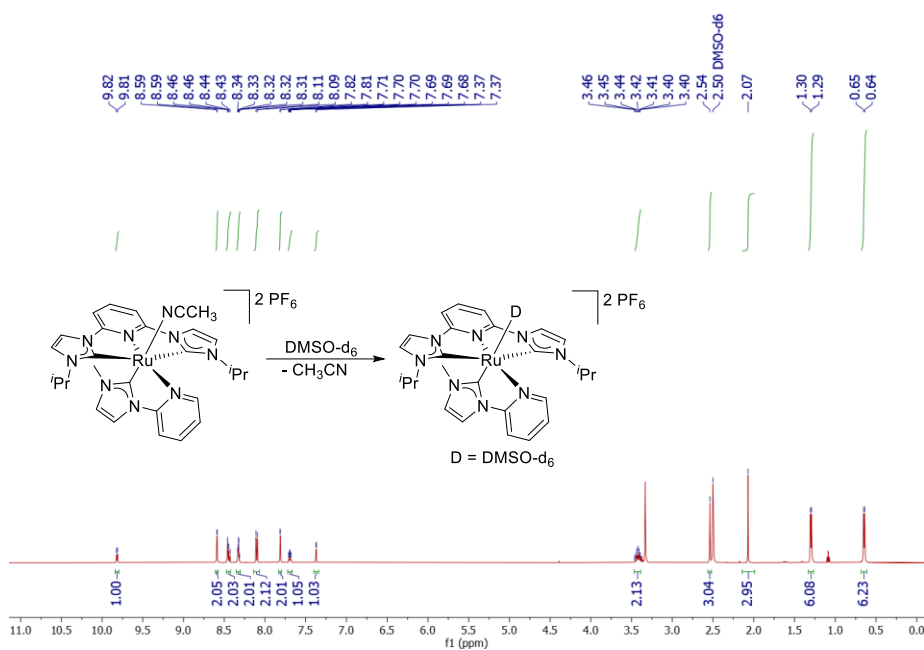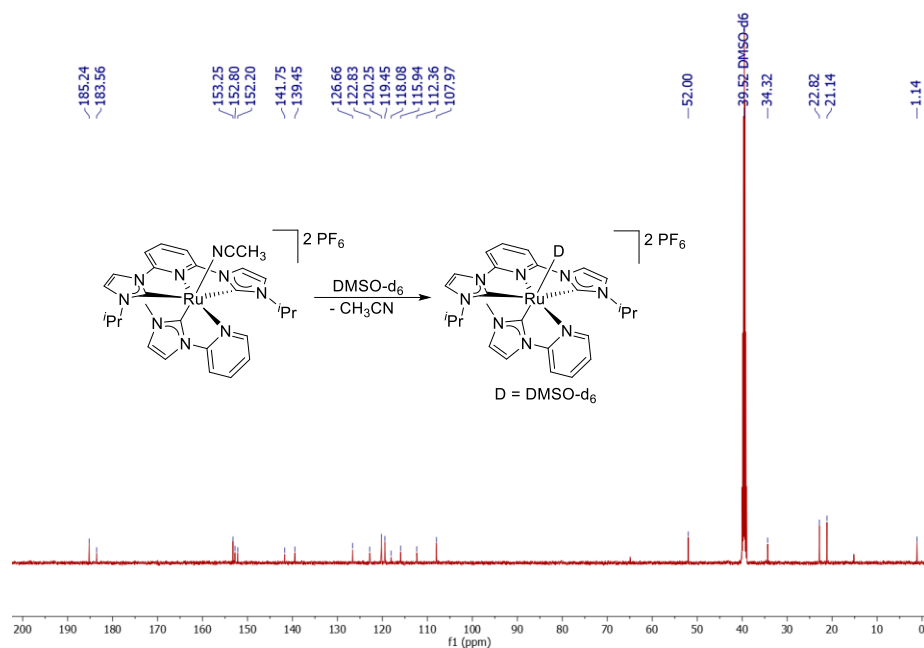**Figure 6.17.** ^{1}H NMR spectrum of complex **11a** in acetone-d$_6$ with coordinated acetonitrile.

Figure 6.18. ^{13}C NMR spectrum of complex **11a** in acetone-d$_6$ with coordinated acetonitrile.
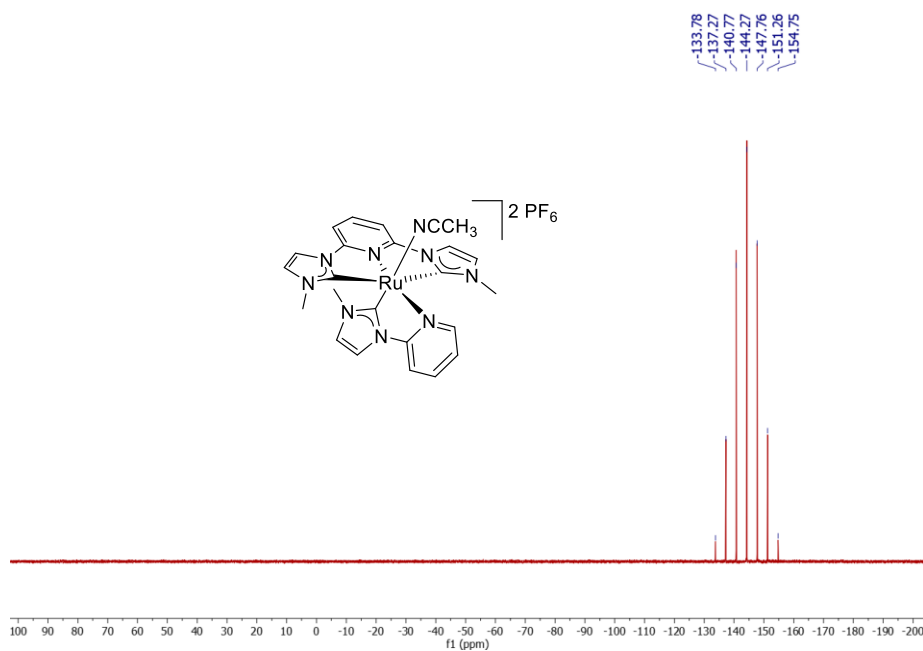
Figure 6.19. ^{31}P NMR spectrum of complex **11a** in acetone-d$_6$.
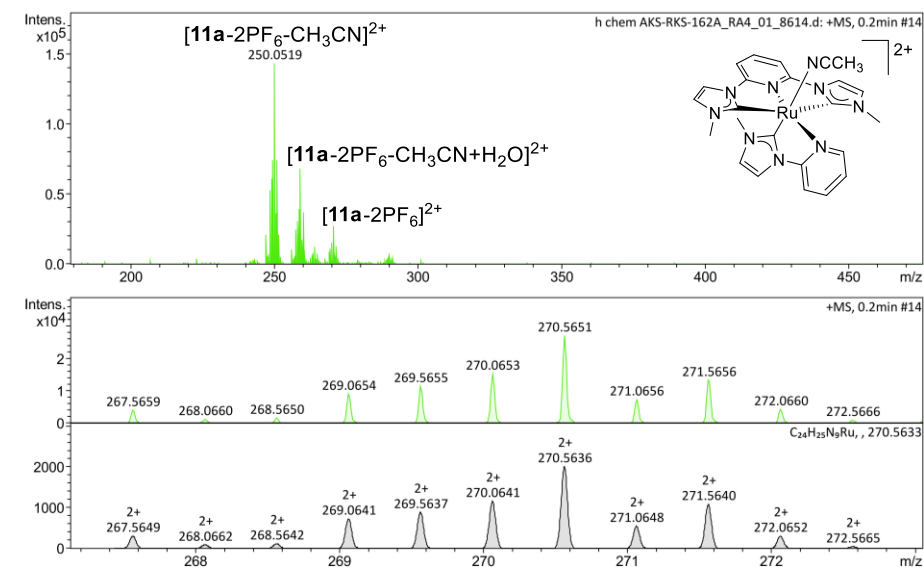
Figure 6.20. HRMS spectrogram of complex **11a** in methanol.

Figure 6.21. ^{1}H NMR spectrum of complex **11b** in dmso-d$_6$ with dissociated acetonitrile.

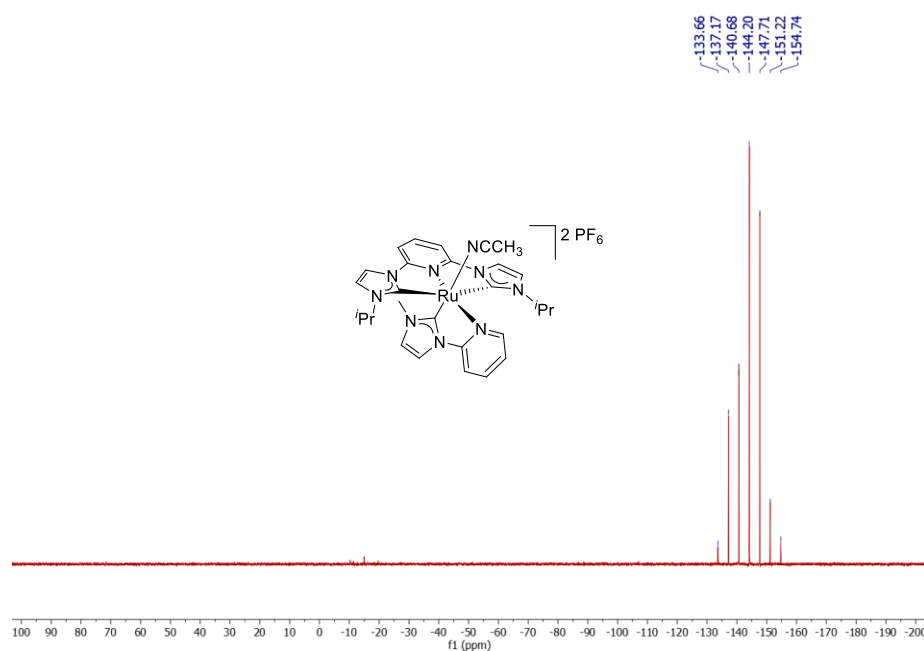**Figure 6.22.** ¹³C NMR spectrum of complex **11b** in dmso-d₆ with dissociated acetonitrile.

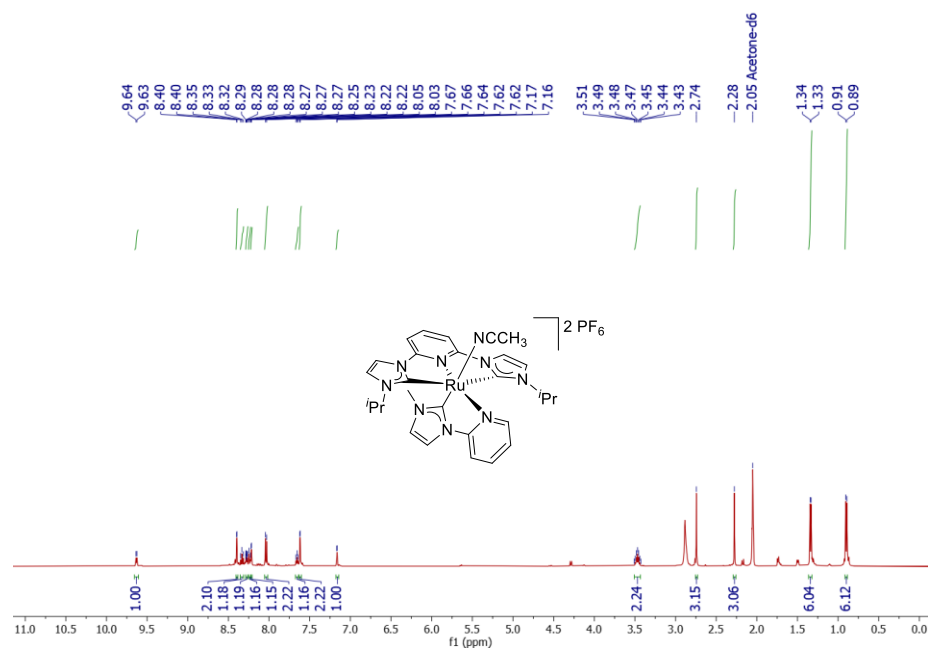**Figure 6.23.** ³¹P NMR spectrum of complex **11b** in dmso-d₆.

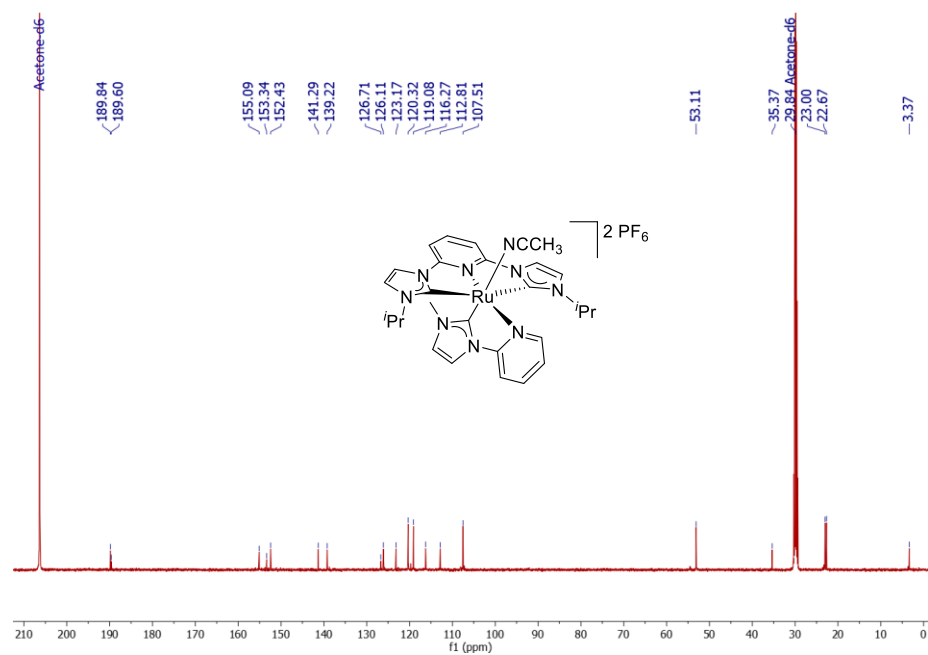**Figure 6.24.** ^{1}H NMR spectrum of complex **11b** in acetone-d$_6$ with coordinated acetonitrile.

Figure 6.25. ^{13}C NMR spectrum of complex **11b** in acetone-d$_6$ with coordinated acetonitrile.
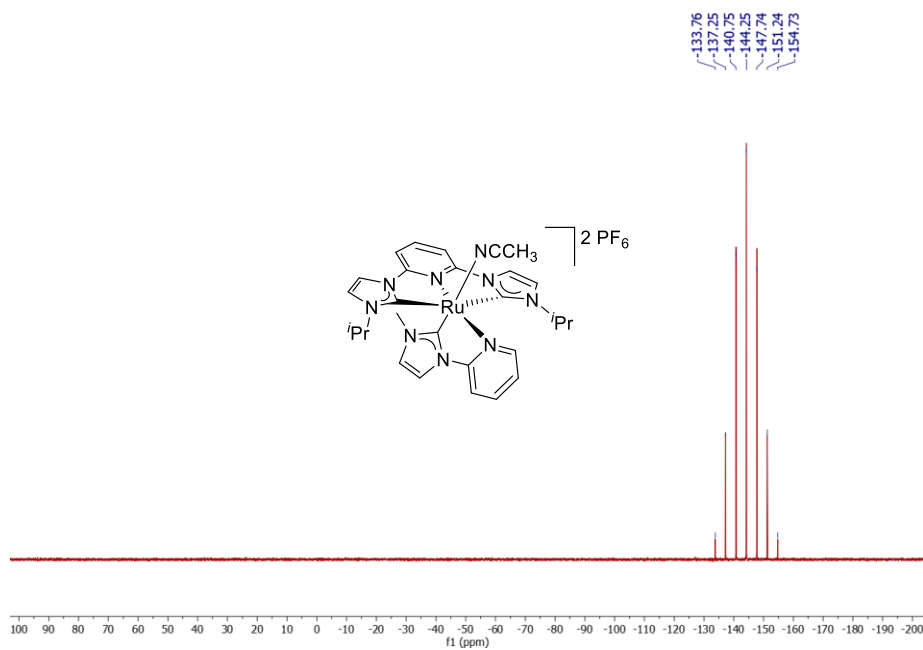
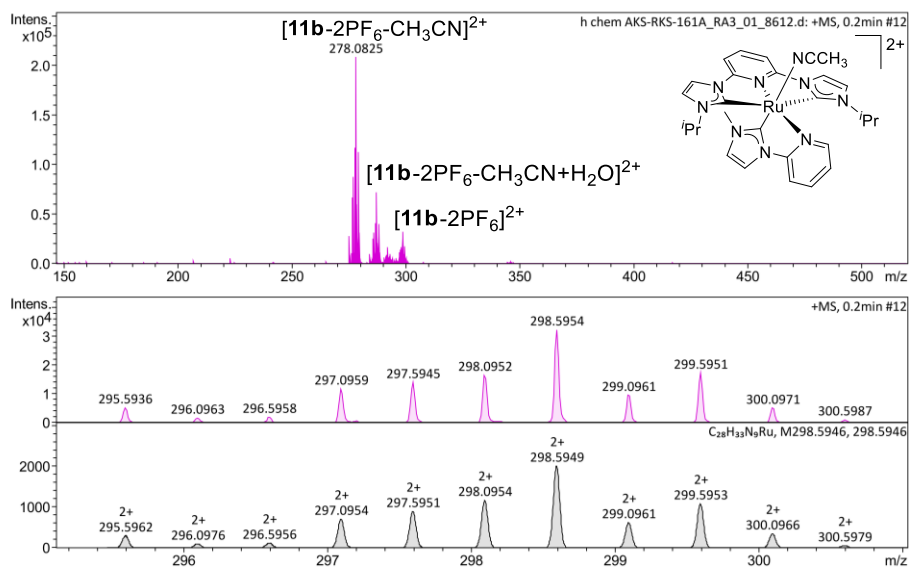**Figure 6.26.** ^{31}P NMR spectrum of complex **11b** in acetone-d_6.

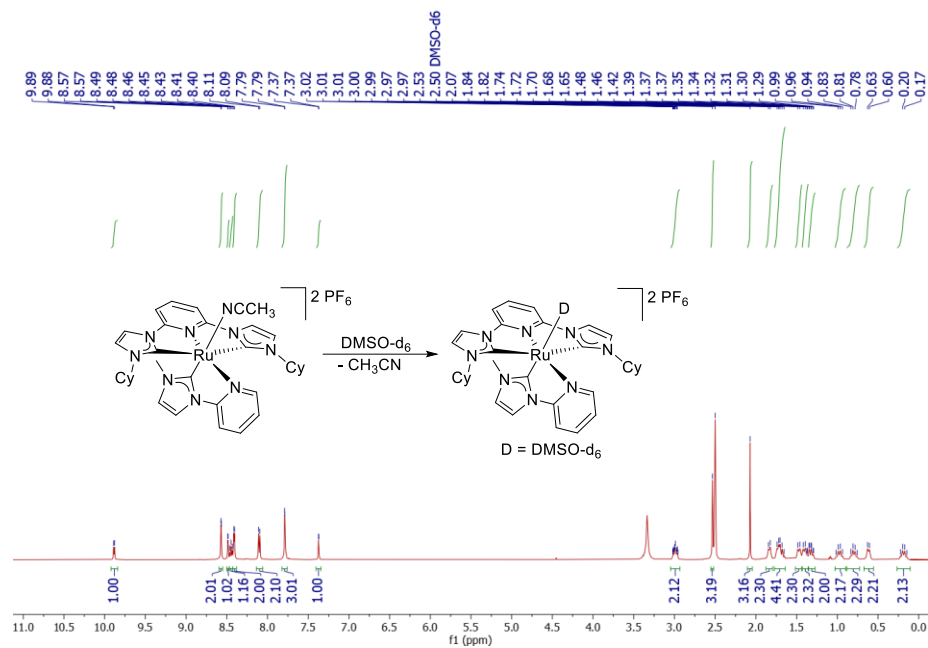

Figure 6.27. HRMS spectrogram of complex **11b** in methanol.

Figure 6.28. ^{1}H NMR spectrum of complex **11c** in dmso-d$_6$ with dissociated acetonitrile.
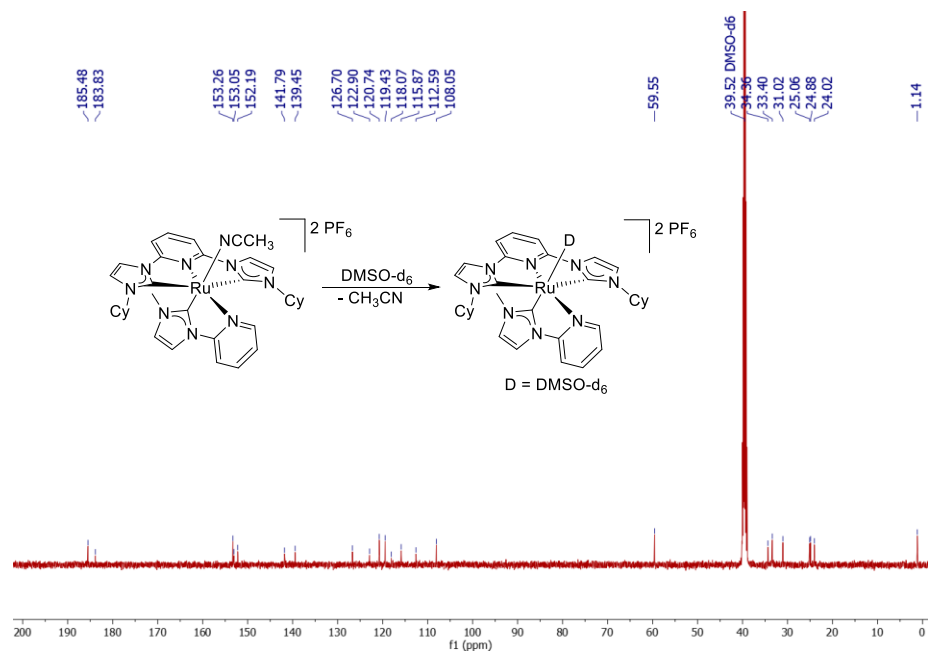

Figure 6.29. ^{13}C NMR spectrum of complex **11c** in dmso-d$_6$ with dissociated acetonitrile.
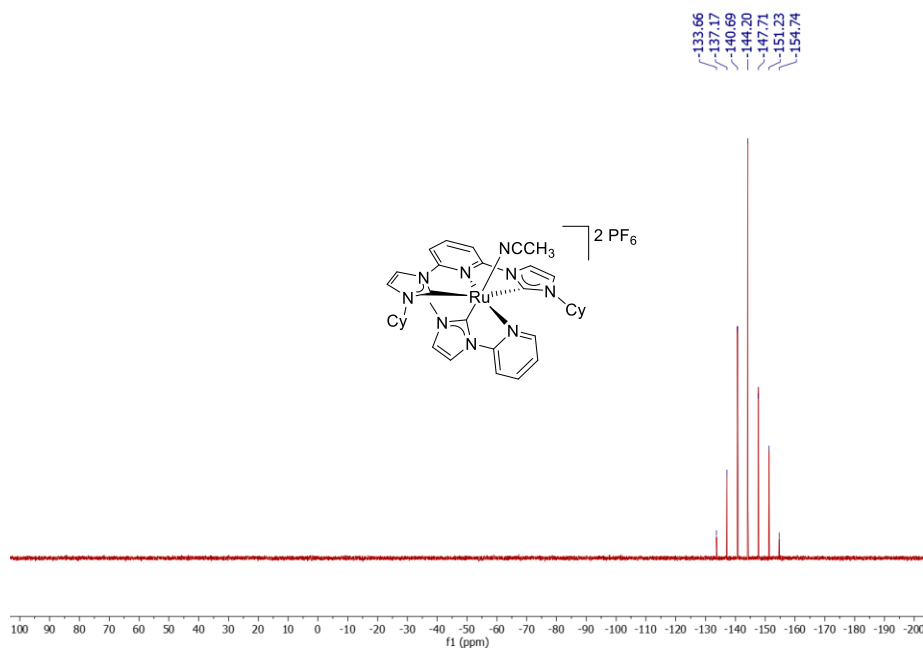
Figure 6.30. ^{31}P NMR spectrum of complex **11c** in dmso-d$_6$.
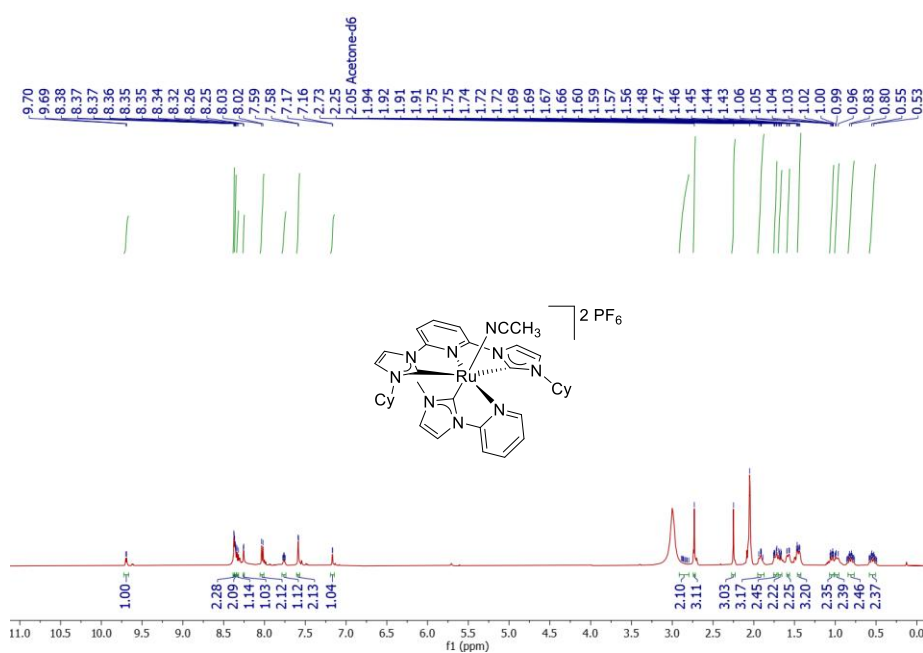

Figure 6.31. ^{1}H NMR spectrum of complex **11c** in acetone-d$_6$ with coordinated acetonitrile.
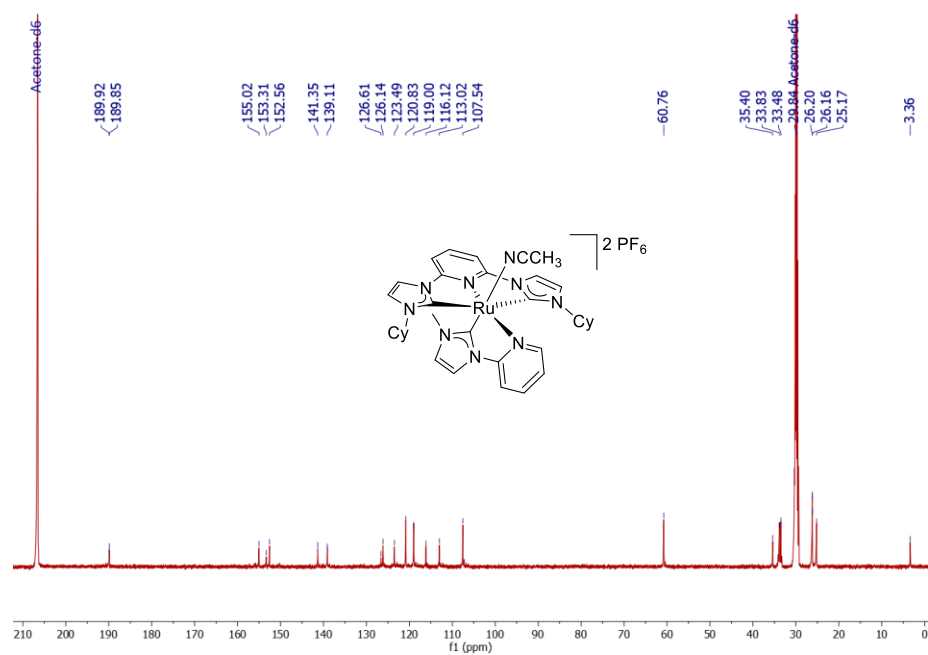
Figure 6.32. ¹³C NMR spectrum of complex **11c** in acetone-d₆ with coordinated acetonitrile.
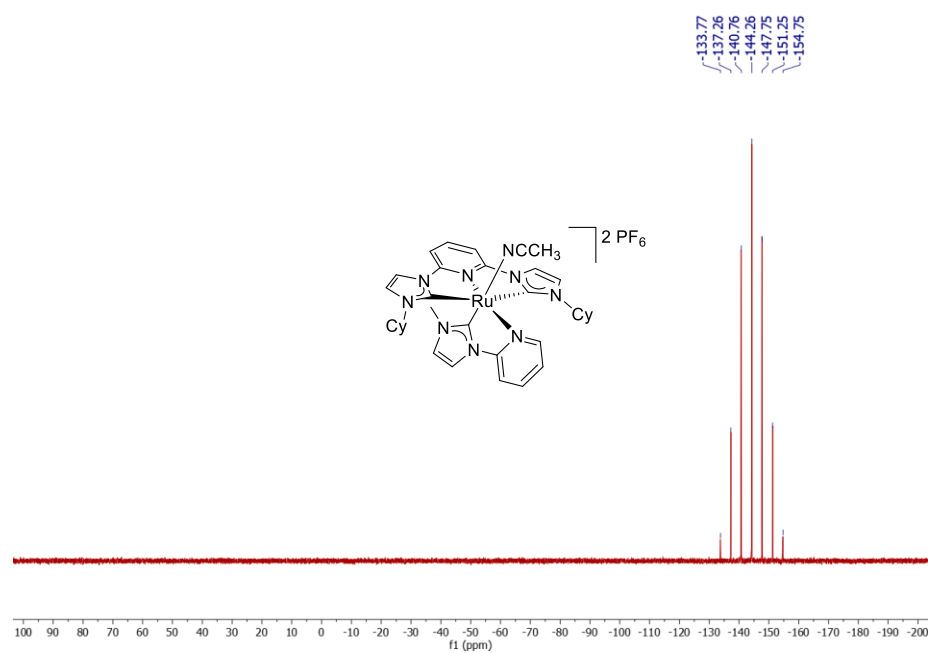
Figure 6.33. ³¹P NMR spectrum of complex **11c** in acetone-d₆.
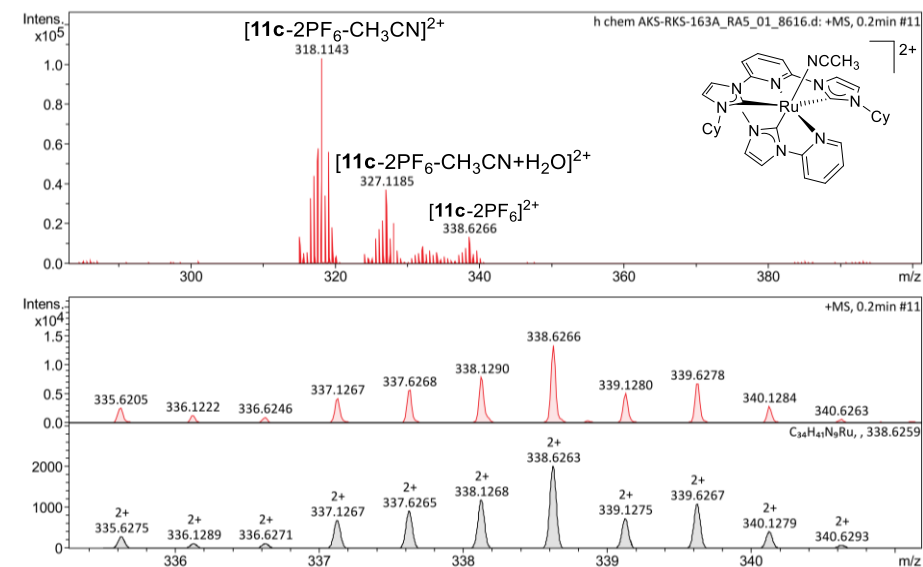
Figure 6.34. HRMS spectrogram of complex **11c** in methanol.
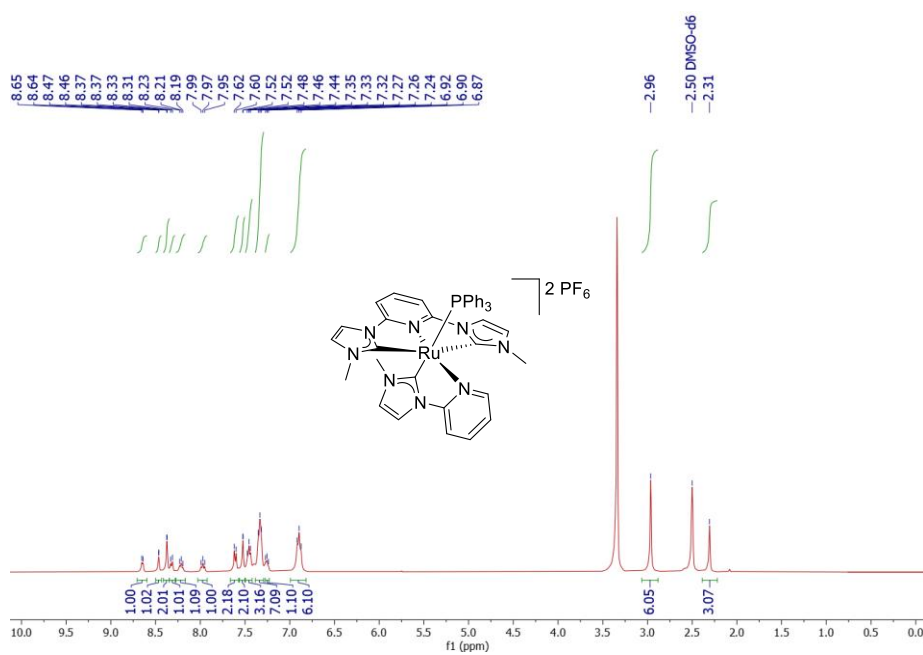
Figure 6.35. ^{1}H NMR spectrum of complex **12a** in dmso-d$_6$.
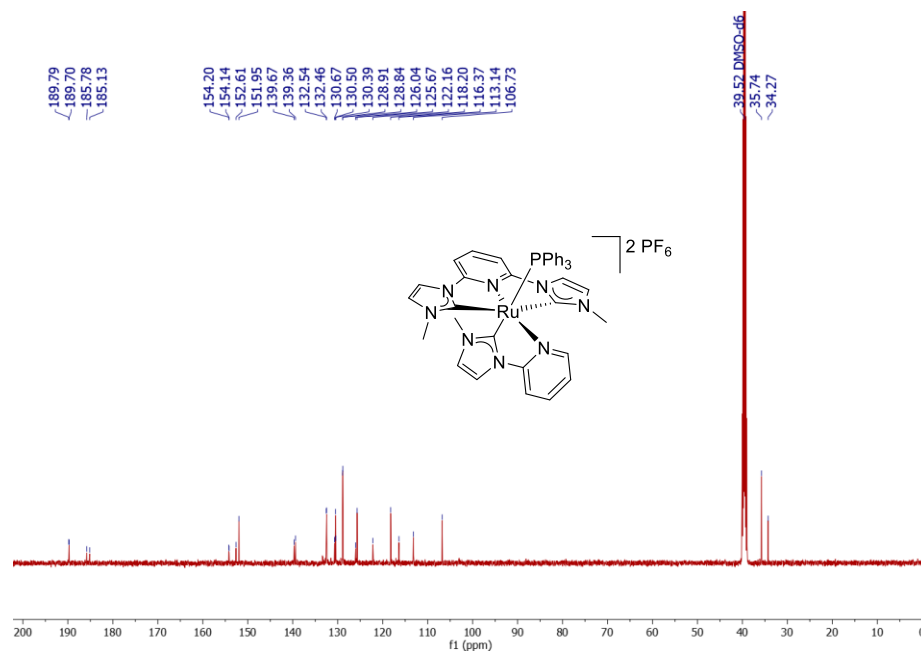
Figure 6.36. ^{13}C NMR spectrum of complex **12a** in dmso-d$_6$.
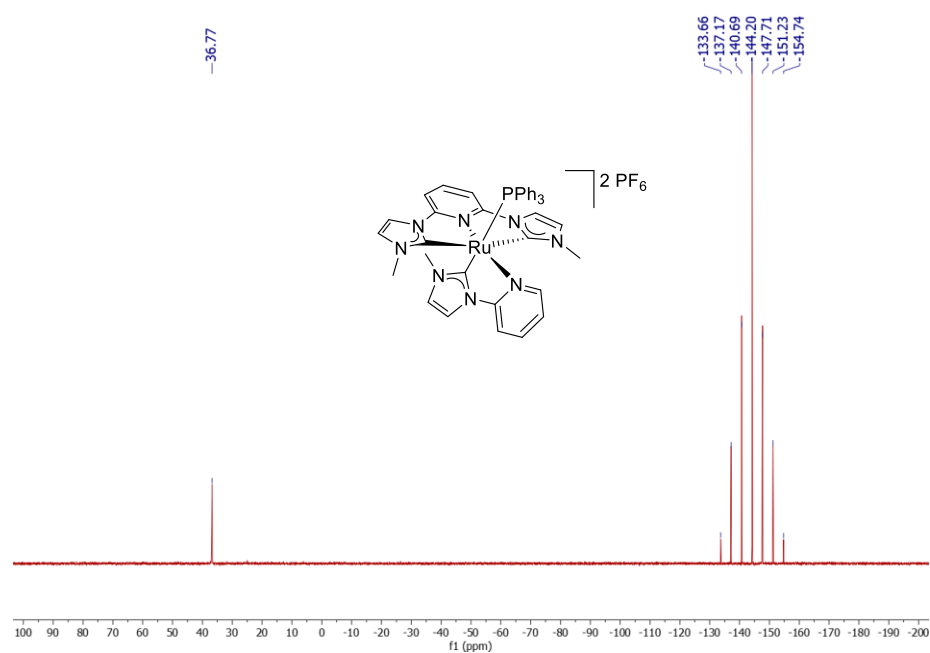
Figure 6.37. ^{31}P NMR spectrum of complex **12a** in dmso-d$_6$.
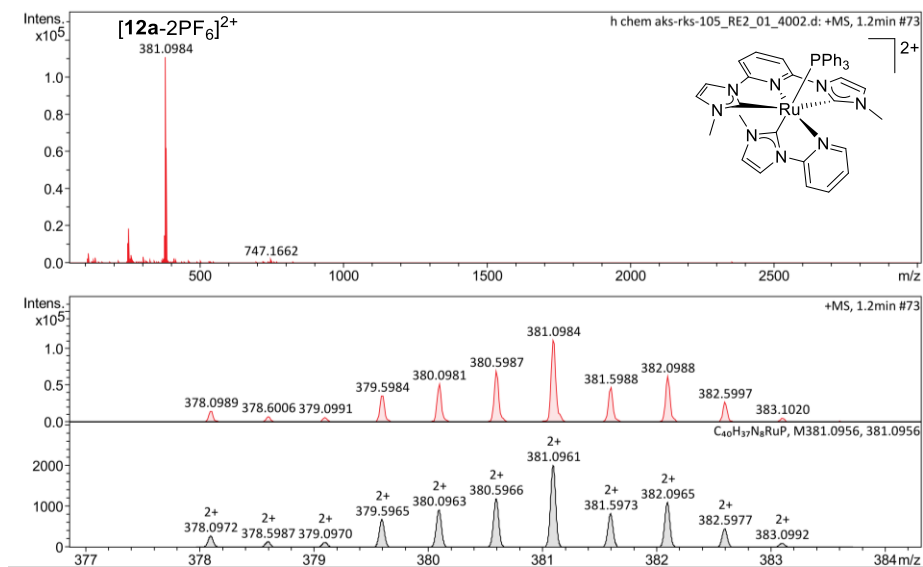
Figure 6.38. HRMS spectrogram of complex **12a** in acetonitrile.
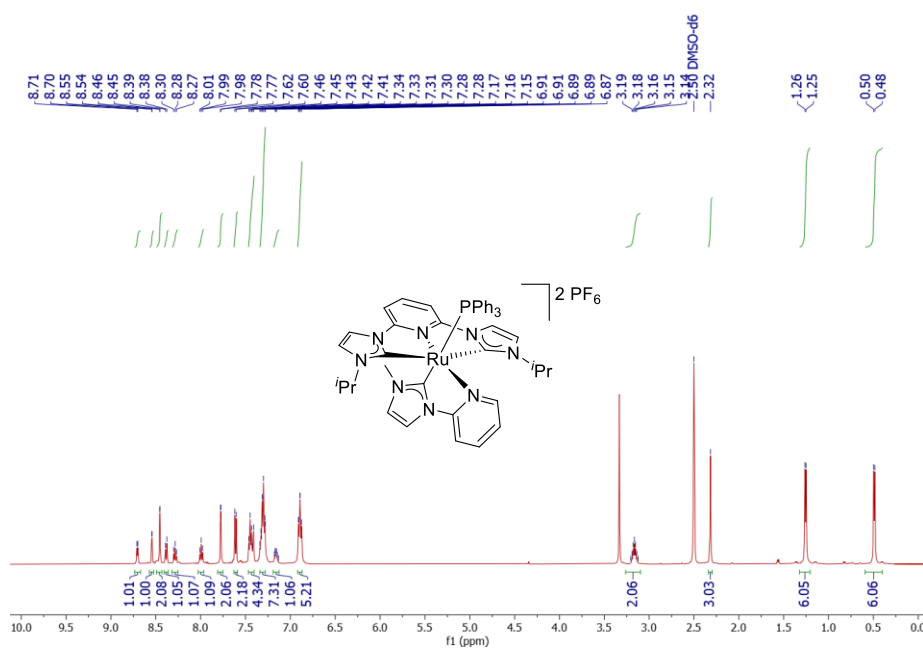
Figure 6.39. ^{1}H NMR spectrum of complex **12b** in dmso-d_6.
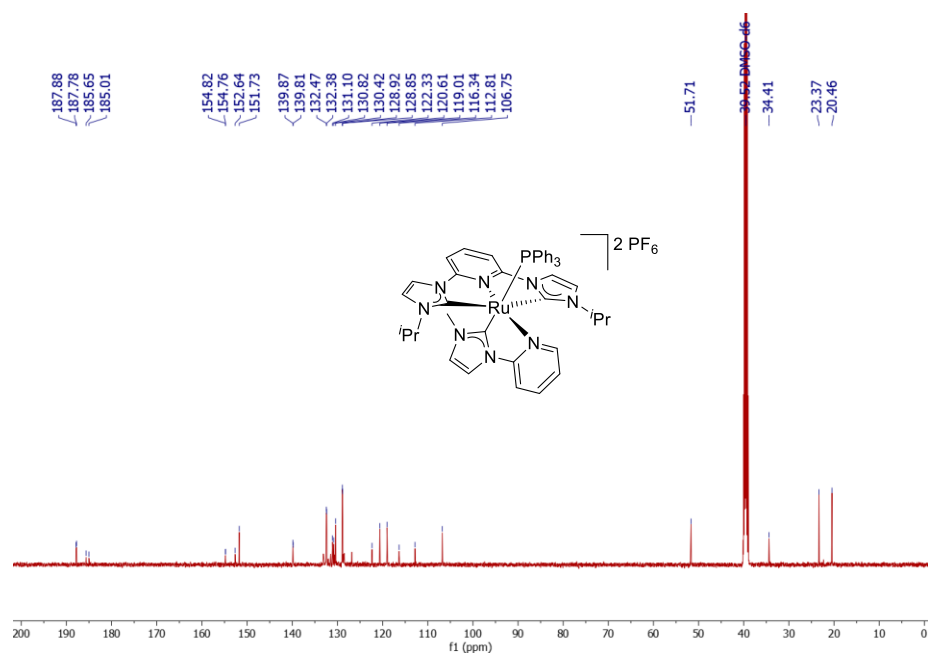
Figure 6.40. ^{13}C NMR spectrum of complex **12b** in dmso-d$_6$.
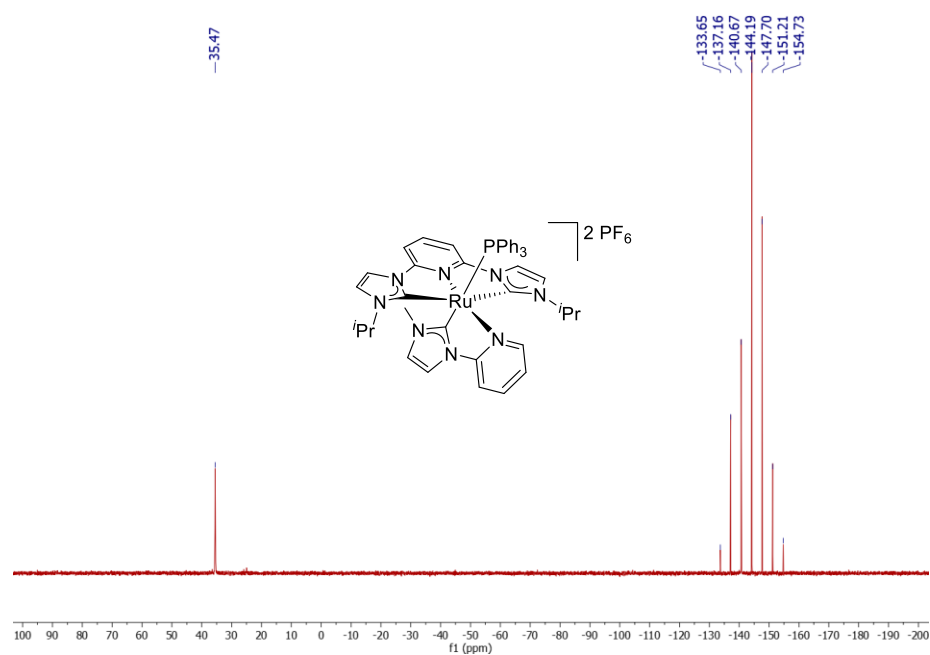
Figure 6.41. ^{31}P NMR spectrum of complex **12b** in dmso-d$_6$.
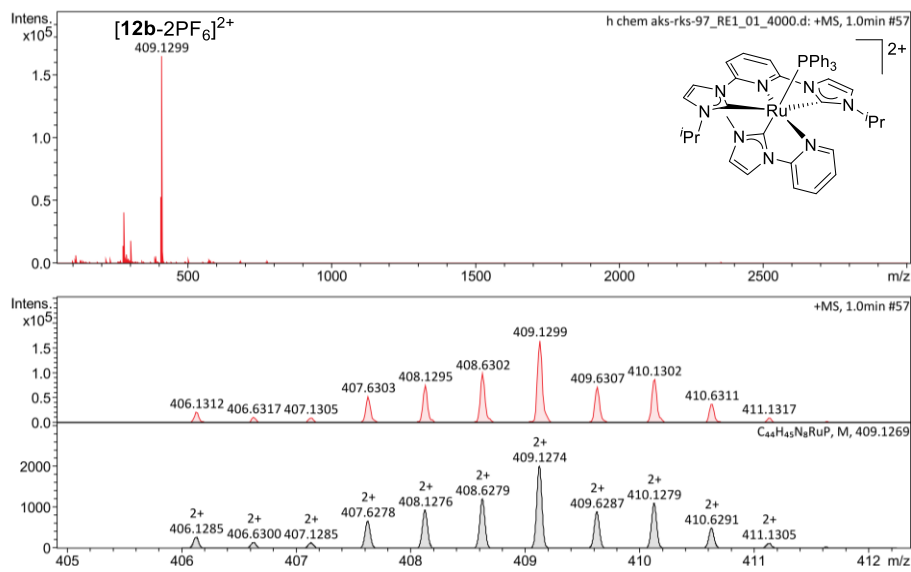
Figure 6.42. HRMS spectrogram of complex **12b** in acetonitrile.
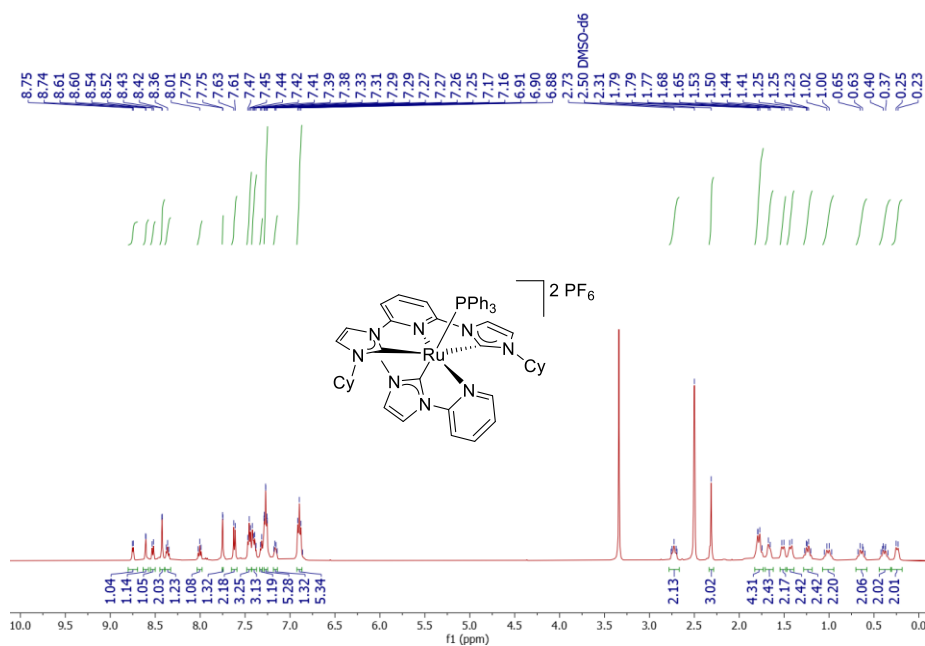
Figure 6.43. ^{1}H NMR spectrum of complex **12c** in dmso-d$_6$.
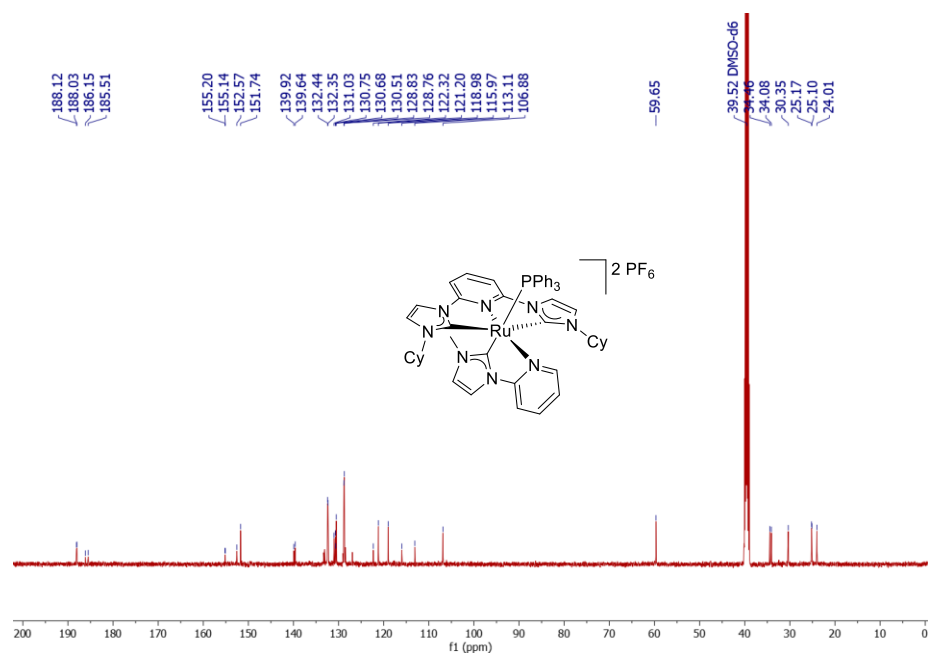
Figure 6.44. ^{13}C NMR spectrum of complex **12c** in dmso-d[6].
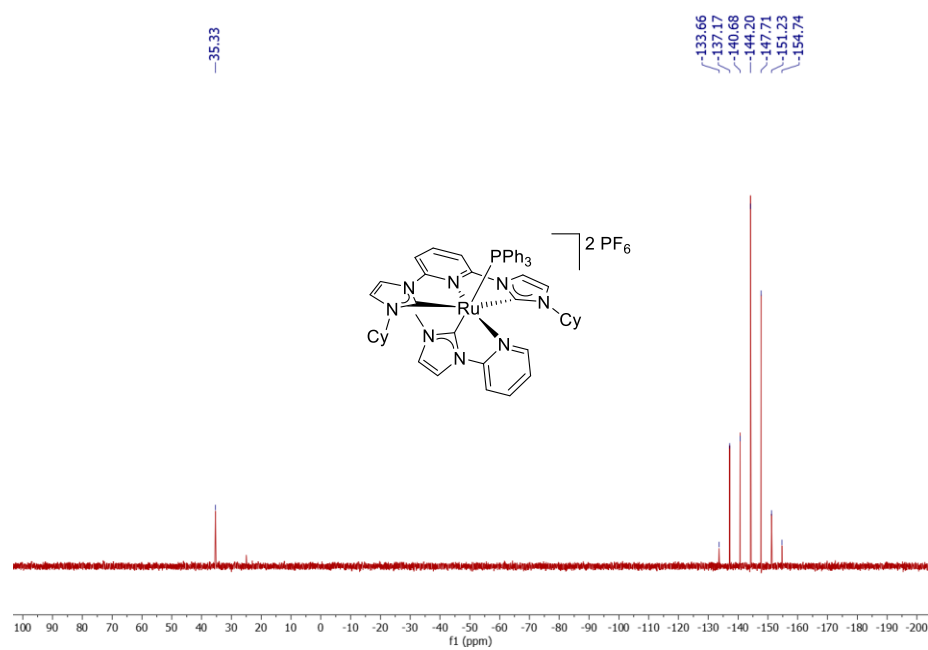
Figure 6.45. ^{31}P NMR spectrum of complex **12c** in dmso-d[6].
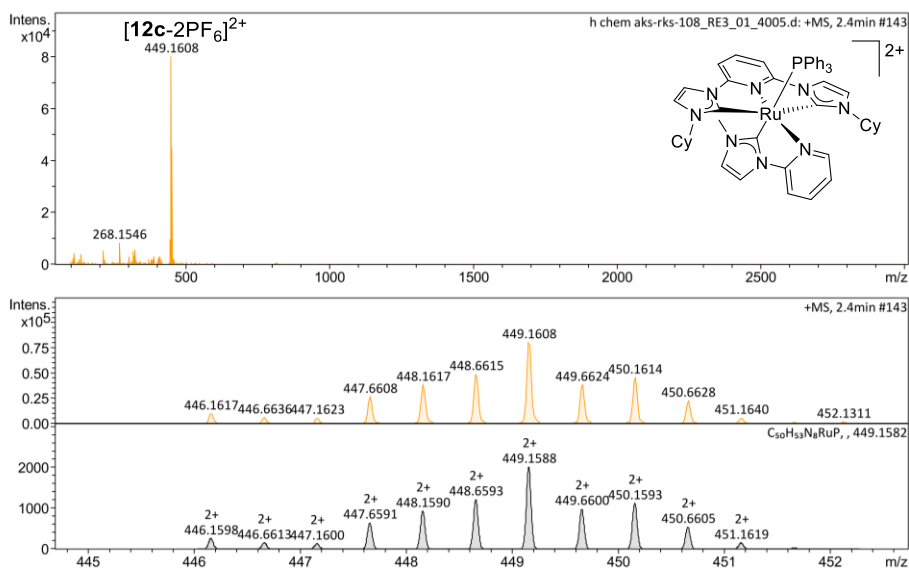
Figure 6.46. HRMS spectrogram of complex **12c** in acetonitrile.
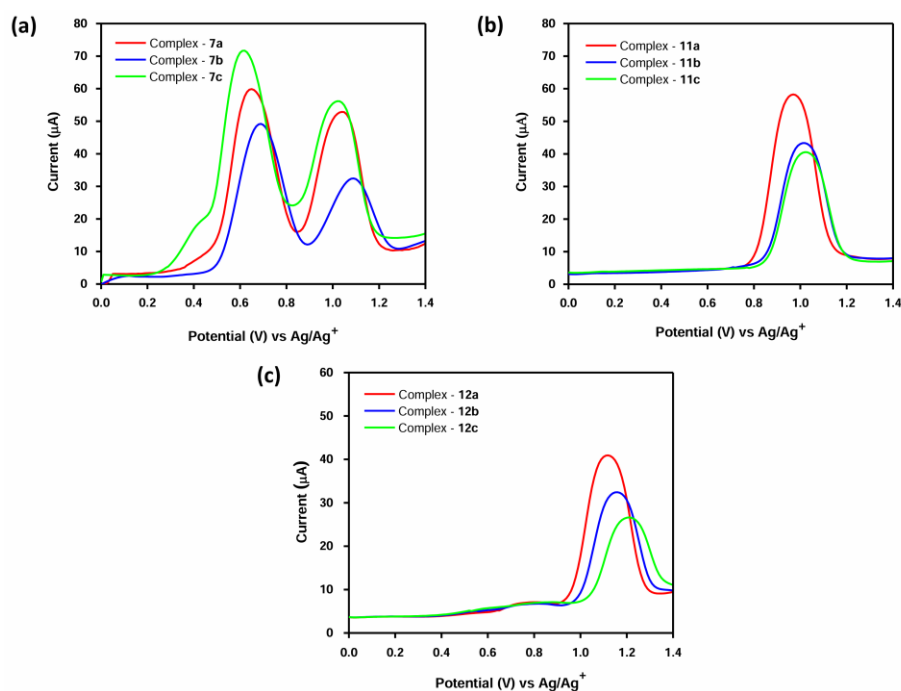
Figure 6.47. Differential Pulse Voltammograms (DPV) of Ru(II)-CNC pincer complexes; (**a**) complexes **7a**–**c**, (**b**) complexes **11a**–**c**, and (**c**) complexes **12a**–**c** was recorded in a 0.1 M solution of TBAPF$_6$ as supporting electrolyte in dry acetonitrile at 100mV/s scan rate versus SCE at 25 ˚C.
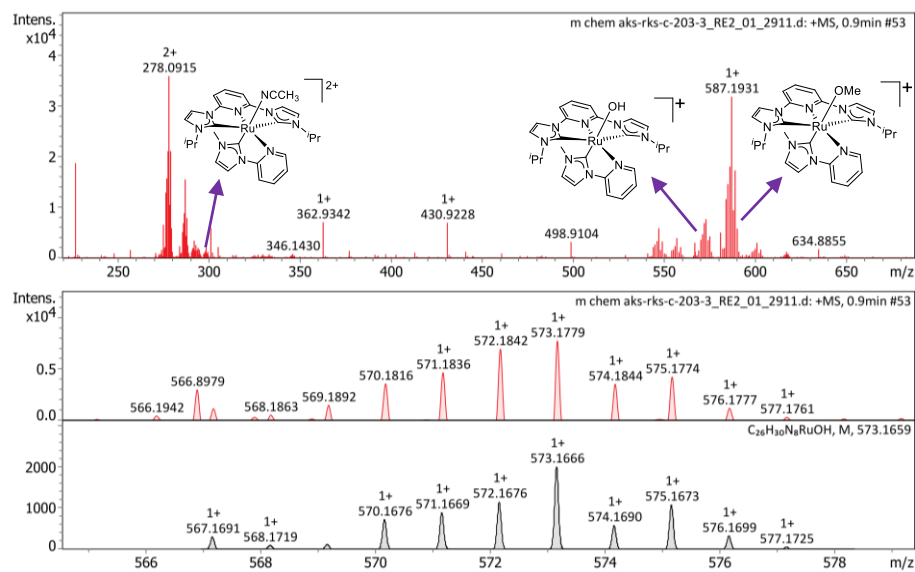
Figure 6.48. LCMS spectrogram of the catalytic reaction mixture for Ru-OH intermediate **B** with catalyst **11b**.
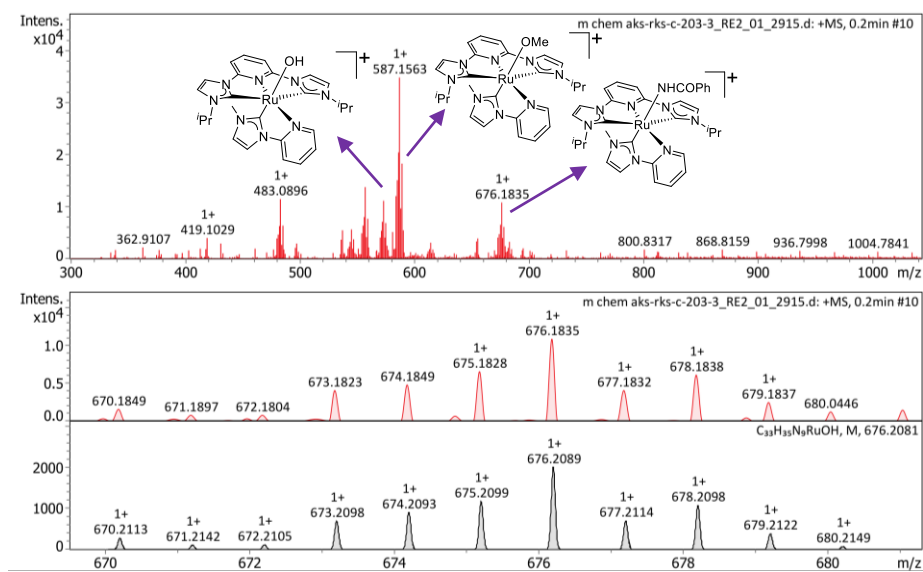
Figure 6.49. LCMS spectrogram of the catalytic reaction mixture for intermediates **C** and **D** with catalyst **11b**.
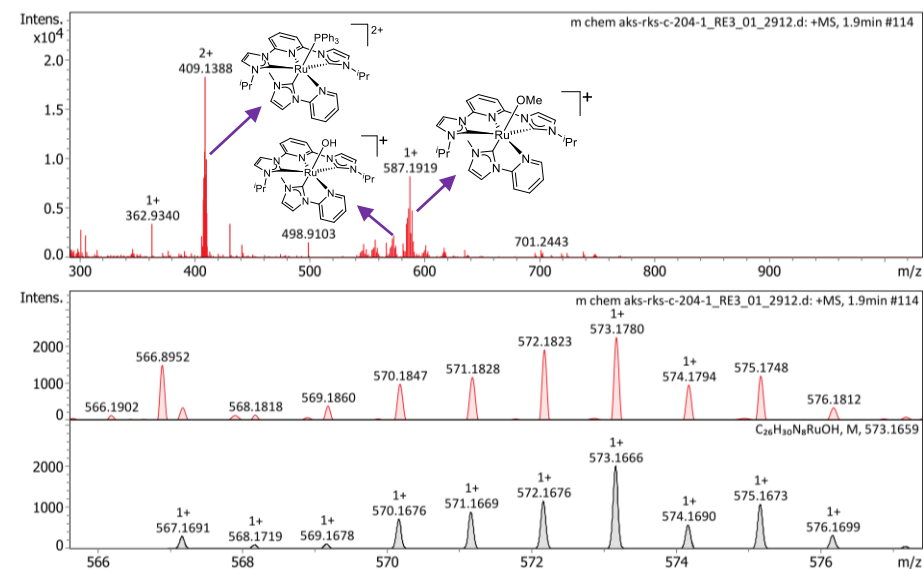
Figure 6.50. LCMS spectrogram of the catalytic reaction mixture for Ru-OH intermediate **B** with catalyst **12b**.
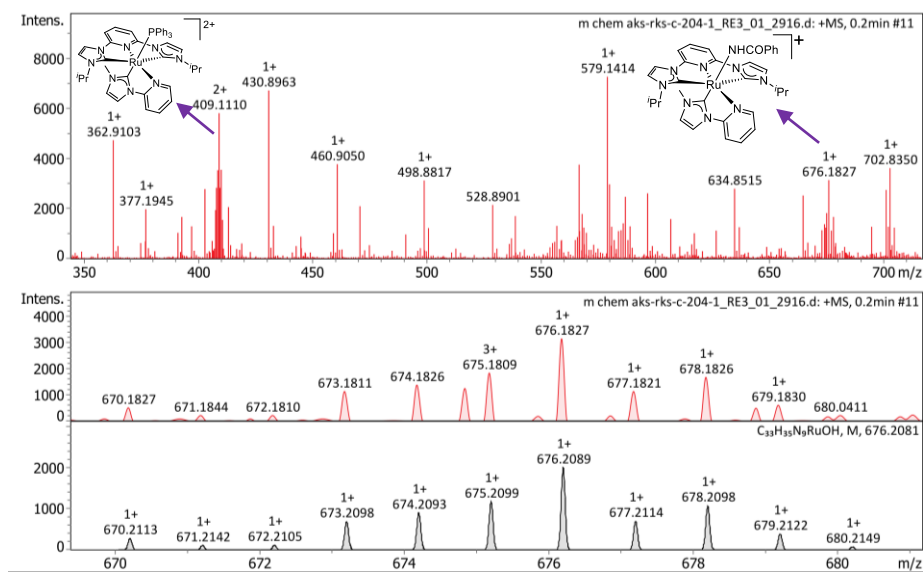
Figure 6.51. LCMS spectrogram of the catalytic reaction mixture for intermediates **C** and **D** with catalyst **12b**.

6.5. References

1. Hahn F. E., Jahnke M. C. (2008), Heterocyclic Carbenes: Synthesis and Coordination Chemistry, Angew. Chem. Int. Ed., 47(17), 3122-3172 (DOI: 10.1002/anie.200703883).

2. Tonner R., Heydenrych G., Frenking G. (2007), Bonding Analysis of *N*-Heterocyclic Carbene Tautomers and Phosphine Ligands in Transition-Metal Complexes: A Theoretical Study, Chem. Asian J., 2(12), 1555-1567 (DOI: 10.1002/asia.200700235).

3. Díez-González S., Marion N., Nolan S. P. (2009), *N*-Heterocyclic Carbenes in Late Transition Metal Catalysis, Chem. Rev., 109(8), 3612-3676 (DOI: 10.1021/cr900074m).

4. Jacobsen H., Correa A., Poater A., Costabile C., Cavallo L. (2009), Understanding the M(NHC) (NHC = *N*-heterocyclic carbene) bond, Coord. Chem. Rev., 253(5), 687-703 (DOI: 10.1016/j.ccr.2008.06.006).

5. Singh R. K., Khan T. K., Misra S., Singh A. K. (2021), CAACs as efficient ancillary ligands for the synthesis of robust catalysts, J. Organomet. Chem., 956, 122133 (DOI: 10.1016/j.jorganchem.2021.122133).

6. Peris E., Crabtree R. H. (2018), Key factors in pincer ligand design, Chem. Soc. Rev., 47(6), 1959-1968 (DOI: 10.1039/C7CS00693D).

7. Arikawa Y., Nakamura T., Higashi T., Horiuchi S., Sakuda E., Umakoshi K. (2017), Reactivity of a Methoxido–Ruthenium Complex Bearing a Pincer-Type Bis(carbene) Ligand toward Thiocyanate, Carbon Disulfide, and Isothiocyanate, Eur. J. Inorg. Chem., 2017(5), 881-884 (DOI: 10.1002/ejic.201601324).

8. Andrew R. E., González-Sebastián L., Chaplin A. B. (2016), NHC-based pincer ligands: carbenes with a bite, Dalton Trans., 45(4), 1299-1305 (DOI: 10.1039/C5DT04429D).

9. de Frémont P., Marion N., Nolan S. P. (2009), Carbenes: Synthesis, properties, and organometallic chemistry, Coord. Chem. Rev., 253(7), 862-892 (DOI: 10.1016/j.ccr.2008.05.018).

10. Fantasia S., Petersen J. L., Jacobsen H., Cavallo L., Nolan S. P. (2007), Electronic Properties of *N*-Heterocyclic Carbene (NHC) Ligands: Synthetic, Structural, and Spectroscopic Studies of (NHC)Platinum(II) Complexes, Organometallics, 26(24), 5880-5889 (DOI: 10.1021/om700857j).

11. Son S. U., Park K. H., Lee Y.-S., Kim B. Y., Choi C. H., Lah M. S., Jang Y. H., Jang D.-J., Chung Y. K. (2004), Synthesis of Ru(II) Complexes of *N*-Heterocyclic Carbenes and Their Promising Photoluminescence Properties in Water, Inorg. Chem., 43(22), 6896-6898 (DOI: 10.1021/ic049514f).

12. Filonenko G. A., Cosimi E., Lefort L., Conley M. P., Copéret C., Lutz M., Hensen E. J. M., Pidko E. A. (2014), Lutidine-Derived Ru-CNC Hydrogenation Pincer Catalysts with Versatile Coordination Properties, ACS Catal., 4(8), 2667-2671 (DOI: 10.1021/cs500720y).

13. Chang W., Gong X., Wang S., Xiao L.-P., Song G. (2017), Acceptorless dehydrogenation and dehydrogenative coupling of alcohols catalysed by protic NHC ruthenium complexes, Org. Biomol. Chem., 15(16), 3466-3471 (DOI: 10.1039/C7OB00542C).

14. Urbina-Blanco C. A., Leitgeb A., Slugovc C., Bantreil X., Clavier H., Slawin A. M. Z., Nolan S. P. (2011), Olefin Metathesis Featuring Ruthenium Indenylidene Complexes with a Sterically Demanding NHC Ligand, Chem. Eur. J., 17(18), 5045-5053 (DOI: 10.1002/chem.201003082).

15. Puerta-Oteo R., Munarriz J., Polo V., Jiménez M. V., Pérez-Torrente J. J. (2020), Carboxylate-Assisted β-(Z) Stereoselective Hydrosilylation of Terminal Alkynes Catalyzed by a Zwitterionic Bis-NHC Rhodium(III) Complex, ACS Catal., 10(13), 7367-7380 (DOI: 10.1021/acscatal.0c01582).

16. Xu Q., Duan W.-L., Lei Z.-Y., Zhu Z.-B., Shi M. (2005), A novel *cis*-chelated Pd(II)-NHC complex for catalyzing Suzuki and Heck-type cross-coupling reactions, Tetrahedron, 61(47), 11225-11229 (DOI: 10.1016/j.tet.2005.09.010).

17. Brewster T. P., Blakemore J. D., Schley N. D., Incarvito C. D., Hazari N., Brudvig G. W., Crabtree R. H. (2011), An Iridium(IV) Species, [Cp*Ir(NHC)Cl]$^+$, Related to a Water-Oxidation Catalyst, Organometallics, 30(5), 965-973 (DOI: 10.1021/om101016s).

18. Gunanathan C., Milstein D. (2014), Bond Activation and Catalysis by Ruthenium Pincer Complexes, Chem. Rev., 114(24), 12024-12087 (DOI: 10.1021/cr5002782).

19. Fogler E., Balaraman E., Ben-David Y., Leitus G., Shimon L. J. W., Milstein D. (2011), New CNN-Type Ruthenium Pincer NHC Complexes, Mild, Efficient Catalytic Hydrogenation of Esters, Organometallics, 30(14), 3826-3833 (DOI: 10.1021/om200367j).

20. Mejuto C., García-Eleno M. A., Guisado-Barrios G., Spasyuk D., Gusev D., Peris E. (2015), Ruthenium complexes with an *N*-heterocyclic carbene NNC-pincer ligand: preparation and catalytic properties, Org. Chem. Front., 2(8), 936-941 (DOI: 10.1039/C5QO00137D).

21. Ishida H., Tanaka K., Tanaka T. (1987), Electrochemical CO_2 reduction catalyzed by ruthenium complexes [Ru(bpy)$_2$(CO)$_2$]$^{2+}$ and [Ru(bpy)$_2$(CO)Cl]$^+$. Effect of pH on the formation of CO and HCOO$^-$, Organometallics, 6(1), 181-186 (DOI: 10.1021/om00144a033).

22. Ishida H., Terada T., Tanaka K., Tanaka T. (1990), Photochemical carbon dioxide reduction catalyzed by bis(2,2'-bipyridine)dicarbonylruthenium(2+) using triethanolamine and 1-benzyl-1,4-dihydronicotinamide as an electron donor, Inorg. Chem., 29(5), 905-911 (DOI: 10.1021/ic00330a004).

23. Suzuki T. M., Tanaka H., Morikawa T., Iwaki M., Sato S., Saeki S., Inoue M., Kajino T., Motohiro T. (2011), Direct assembly synthesis of metal complex-semiconductor hybrid photocatalysts anchored by phosphonate for highly efficient CO_2 reduction, Chem. Commun., 47(30), 8673-8675 (DOI: 10.1039/C1CC12491A).

24. Tamaki Y., Morimoto T., Koike K., Ishitani O. (2012), Photocatalytic CO_2 reduction with high turnover frequency and selectivity of formic acid formation using Ru(II) multinuclear complexes, Proc. Natl. Acad. Sci., 109(39), 15673-15678 (DOI: 10.1073/pnas.1118336109).

25. Kärkäs M. D., Verho O., Johnston E. V., Åkermark B. (2014), Artificial Photosynthesis: Molecular Systems for Catalytic Water Oxidation, Chem. Rev., 114(24), 11863-12001 (DOI: 10.1021/cr400572f).

26. Boudreaux C. M., Liyanage N. P., Shirley H., Siek S., Gerlach D. L., Qu F., Delcamp J. H., Papish E. T. (2017), Ruthenium(II) complexes of pyridinol and *N*-heterocyclic carbene derived pincers as robust catalysts for selective carbon dioxide reduction, Chem. Commun., 53(81), 11217-11220 (DOI: 10.1039/C7CC05706G).

27. Tseng H.-W., Zong R., Muckerman J. T., Thummel R. (2008), Mononuclear Ruthenium(II) Complexes That Catalyze Water Oxidation, Inorg. Chem., 47(24), 11763-11773 (DOI: 10.1021/ic8014817).

28. Arikawa Y., Nakamura T., Ogushi S., Eguchi K., Umakoshi K. (2015), Fixation of atmospheric carbon dioxide by ruthenium complexes bearing an NHC-based pincer ligand: formation of a methylcarbonato complex and its methylation, Dalton Trans., 44(12), 5303-5305 (DOI: 10.1039/C5DT00476D).

29. Concepcion J. J., Jurss J. W., Norris M. R., Chen Z., Templeton J. L., Meyer T. J. (2010), Catalytic Water Oxidation by Single-Site Ruthenium Catalysts, Inorg. Chem., 49(4), 1277-1279 (DOI: 10.1021/ic901437e).

30. Díez-González S., Marion N., Nolan S. P. (2009), *N*-Heterocyclic Carbenes in Late Transition Metal Catalysis, Chem. Rev., 109(8), 3612-3676 (DOI: 10.1021/cr900074m).

31. Kuwata S., Hahn F. E. (2018), Complexes Bearing Protic *N*-Heterocyclic Carbene Ligands, Chem. Rev., 118(19), 9642-9677 (DOI: 10.1021/acs.chemrev.8b00176).

32. Carey J. S., Laffan D., Thomson C., Williams M. T. (2006), Analysis of the reactions used for the preparation of drug candidate molecules, Org. Biomol. Chem., 4(12), 2337-2347 (DOI: 10.1039/B602413K).

33. Guo B., Vries J. G. de, Otten E. (2019), Hydration of nitriles using a metal-ligand cooperative ruthenium pincer catalyst, Chem. Sci., 10(45), 10647-10652 (DOI: 10.1039/C9SC04624K).

34. Wang M.-X. (2015), Enantioselective Biotransformations of Nitriles in Organic Synthesis, Acc. Chem. Res., 48(3), 602-611 (DOI: 10.1021/ar500406s).

35. Pattabiraman V. R., Bode J. W. (2011), Rethinking amide bond synthesis, Nature, 480(7378), 471-479 (DOI: 10.1038/nature10702).

36. de Figueiredo R. M., Suppo J.-S., Campagne J.-M. (2016), Nonclassical Routes for Amide Bond Formation, Chem. Rev., 116(19), 12029-12122 (DOI: 10.1021/acs.chemrev.6b00237).

37. O'Connor C. (1970), Acidic and basic amide hydrolysis, Q. Rev. Chem. Soc., 24(4), 553-564 (DOI: 10.1039/QR9702400553).

38. Tu T., Wang Z., Liu Z., Feng X., Wang Q. (2012), Efficient and practical transition metal-free catalytic hydration of organonitriles to amides, Green Chem., 14(4), 921-924 (DOI: 10.1039/C2GC16637B).

39. Kukushkin V. Yu., Pombeiro A. J. L. (2002), Additions to Metal-Activated Organonitriles, Chem. Rev., 102(5), 1771-1802 (DOI: 10.1021/cr0103266).

40. Kukushkin V. Yu., Pombeiro A. J. L. (2005), Metal-mediated and metal-catalyzed hydrolysis of nitriles, Inorg. Chim. Acta, 358(1), 1-21 (DOI: 10.1016/j.ica.2004.04.029).

41. Ahmed T. J., Knapp S. M. M., Tyler D. R. (2011), Frontiers in catalytic nitrile hydration: Nitrile and cyanohydrin hydration catalyzed by homogeneous organometallic complexes, Coord. Chem. Rev., 255(7), 949-974 (DOI: 10.1016/j.ccr.2010.08.018).

42. Gao P., Szostak M. (2023), Hydration reactions catalyzed by transition metal-NHC (NHC = *N*-heterocyclic carbene) complexes, Coord. Chem. Rev., 485, 215110 (DOI: 10.1016/j.ccr.2023.215110).

43. García-Álvarez R., Zablocka M., Crochet P., Duhayon C., Majoral J.-P., Cadierno V. (2013), Thiazolyl-phosphine hydrochloride salts: effective auxiliary ligands for ruthenium-catalyzed nitrile hydration reactions and related amide bond forming processes in water, Green Chem., 15(9), 2447-2456 (DOI: 10.1039/C3GC41201F).

44. Yadav S., Gupta R. (2022), Hydration of Nitriles Catalyzed by Ruthenium Complexes: Role of Dihydrogen Bonding Interactions in Promoting Base-Free Catalysis, Inorg. Chem., 61(39), 15463-15474 (DOI: 10.1021/acs.inorgchem.2c02058).

45. Tomás-Mendivil E., Suárez F. J., Díez J., Cadierno V. (2014), An efficient ruthenium(IV) catalyst for the selective hydration of nitriles to amides in water under mild conditions, Chem. Commun., 50(68), 9661-9664 (DOI: 10.1039/C4CC04058A).

46. Trnka T. M., Morgan J. P., Sanford M. S., Wilhelm T. E., Scholl M., Choi T.-L., Ding S., Day M. W., Grubbs R. H. (2003), Synthesis and Activity of Ruthenium Alkylidene Complexes Coordinated with Phosphine and *N*-Heterocyclic Carbene

Ligands, J. Am. Chem. Soc., 125(9), 2546-2558 (DOI: 10.1021/ja021146w).

47. Singh R. K., Yadav D., Singh A. K. (2023), Cationic ruthenium(II)-CNC pincer complexes as phosphine-free catalysts for nitrile hydration to amides in aqueous medium, Mol. Catal., 549, 113523 (DOI: 10.1016/j.mcat.2023.113523).

48. Hunt L. A., Das S., Lamb R. W., Nugegoda D., Curiac C., Figgins M. T., Lambert E. C., Qu F., Hammer N. I., Delcamp J. H., Webster C. E., Papish E. T. (2023), Ruthenium (II) Complexes of CNC Pincers and Bipyridine in the Photocatalytic CO_2 Reduction Reaction to CO Using Visible Light: Catalysis, Kinetics, and Computational Insights, ACS Catal., 13(9), 5986-5999 (DOI: 10.1021/acscatal.2c05459).

49. Yadav D., Misra S., Kumar D., Singh S., Singh A. K. (2021), Cationic ruthenium(II)-NHC pincer complexes: Synthesis, characterisation and catalytic activity for transfer hydrogenation of ketones, Appl. Organomet. Chem., 35(8), e6287 (DOI: 10.1002/aoc.6287).

50. Rong M. K., van Duin K., van Dijk T., de Pater J. J. M., Deelman B.-J., Nieger M., Ehlers A. W., Slootweg J. C., Lammertsma K. (2017), Iminophosphanes: Synthesis, Rhodium Complexes, and Ruthenium(II)-Catalyzed Hydration of Nitriles, Organometallics, 36(5), 1079-1090 (DOI: 10.1021/acs.organomet.7b00057).

51. Czégéni C. E., De S., Udvardy A., Derzsi N. J., Papp G., Papp G., Joó F. (2020), Selective Hydration of Nitriles to Corresponding Amides in Air with Rh(I)-*N*-Heterocyclic Complex Catalysts, Catalysts, 10(1), 125 (DOI: 10.3390/catal10010125).

52. Ramón R. S., Marion N., Nolan S. P. (2009), Gold Activation of Nitriles: Catalytic Hydration to Amides, Chem. Eur. J., 15(35), 8695-8697 (DOI: 10.1002/chem.200901231).

53. García-Álvarez R., Francos J., Tomás-Mendivil E., Crochet P., Cadiernoet V. (2014), Metal-catalyzed nitrile hydration reactions: The specific contribution of ruthenium, J. Organomet. Chem. 771, 93-104 (DOI: 10.1016/j.jorganchem.2013.11.042).

54. Lau C. P., Ng S. M., Jia G., Lin Z. (2007), Some ruthenium hydride, dihydrogen, and dihydrogen-bonded complexes in catalytic reactions, Coord. Chem. Rev., 251, 2223-2237 (DOI: 10.1016/j.ccr.2006.12.001).

55. Buil M. L., Cadierno V., Esteruelas M. A., Gimeno J., Herrero J., Isquierdo S., Oñate E. (2012), Selective Hydration of Nitriles to Amides Promoted by an Os–NHC Catalyst: Formation and X-ray Characterization of κ2-Amidate Intermediates, Organometallics, 31, 6861-6867(DOI: 10.1021/om3006799).

56. Dolomanov O. V., Bourhis L. J., Gildea R. J., Howard J. a. K., Puschmann H. (2009), OLEX2: a complete structure solution, refinement and analysis program, J. Appl. Cryst., 42(2), 339-341 (DOI: 10.1107/S0021889808042726).

57. Sheldrick G. M. (2015), SHELXT - Integrated space-group and crystal-structure determination, Acta Cryst. Sect. A: Found. Adv., 71(1), 3-8 (DOI: 10.1107/S2053273314026370).

58. Sheldrick G. M. (2015), Crystal structure refinement with SHELXL, Acta Cryst. Sect. C: Struct. Chem., 71(1), 3-8 (DOI: 10.1107/S2053229614024218).

59. Neese F. (2012), The ORCA program system, WIREs Comput. Mol. Sci., 2(1), 73-78 (DOI: 10.1002/wcms.81).

60. Neese F., Wennmohs F., Becker U., Riplinger C. (2020), The ORCA quantum chemistry program package, J. Chem. Phys., 152(22), 224108 (DOI: 10.1063/5.0004608).

61. Neese F. (2022), Software update: The ORCA program system-Version 5.0, WIREs Comput. Mol. Sci., 12(5), e1606 (DOI: 10.1002/wcms.1606).

62. Grimme S., Hansen A., Ehlert S., Mewes J.-M. (2021), r2SCAN-3c: A "Swiss army knife" composite electronic-structure method, J. Chem. Phys., 154, 064103 (DOI: 10.1063/5.0040021).

63. Marenich A. V., Cramer C. J., Truhlar D. G. (2009), Universal Solvation Model Based on Solute Electron Density and on a Continuum Model of the Solvent Defined by the Bulk Dielectric Constant and Atomic Surface Tensions, J. Phys. Chem. B, 113(18), 6378-6396 (DOI: 10.1021/jp810292n).

64. Mardirossian N., Head-Gordon M. (2016), ωB97M-V: A combinatorially optimized, range-separated hybrid, meta-GGA density functional with VV10 nonlocal correlation, J. Chem. Phys., 144(21), 214110 (DOI: 10.1063/1.4952647).

65. Martin R. L., Hay P. J., Pratt L. R. (1998), Hydrolysis of Ferric Ion in Water and Conformational Equilibrium, J. Phys. Chem. A, 102(20), 3565-3573 (DOI: 10.1021/jp980229p).

Chapter 7
Conclusion and Future Scope

7.1. Conclusion

In summary, my thesis has primarily focused on the syntheses, characterization, and catalytic activities of cationic Ru(II)-CNC pincer complexes. These complexes are effectively studied in various catalytic reactions with excellent selectivity for products.

Chapter 1 briefly described the pincer ligand system with different types of donor ligands and their coordination geometries. In particular, it introduces NHC ligands and their linkage mode with metal centres. Further, the transition metal complexes with pincer ligand backbone and ruthenium complexes with NHC-based pincer ligands were discussed. The application of transition metal complexes, particularly ruthenium-based complexes is discussed in catalysis.

Chapter 2 discusses the syntheses and characterization of Ru(II)-CNC pincer complexes with bulky N-cyclohexyl wingtips. The catalytic reactivity was investigated for the transfer hydrogenation of cyclohexanone and acceptorless dehydrogenation of benzyl alcohol. Catalyst $[Ru(CNC^{Cy})(CO)(PPh_3)Cl]PF_6$ (**1c**) shows better reactivity as compared to its PPh$_3$ and DMSO analogues. A plausible reaction mechanism was described for TH and AAD reactions. A reactive hydride intermediate was involved to facilitate these catalytic reactions.

Chapter 3 described the catalyst optimization for ADC reaction with N-methyl, N-isopropyl, and N-cyclohexyl complexes with different ancillary ligands (CO, COD, DMSO, and PPh$_3$). Catalyst $[Ru(CNC^{iPr})(PPh_3)_2Cl]PF_6$ (**3b**) shows excellent reactivity for ADC catalysis among all the catalysts. A reversal in catalytic activity was

observed in the ADC reaction, which can be explained in terms of the *trans*-effect. Complexes containing PPh$_3$ and DMSO ligands performed better reactivity than complexes containing CO and COD ligands. The ADC of various amines, including benzylic, heterocyclic, cyclic, and acyclic aliphatic amines, was investigated using benzyl alcohol to directly form C–N bonds under optimized reaction conditions. The aldehyde group has traditionally been employed as a directing group for C–H activation, this work presents the first report of *ortho*-C–H activation facilitating nucleophilic attack on the aldehyde group. Additionally, the substrate scope for the dehydrogenative coupling of benzyl alcohol with a wide range of amines was examined, which led to the synthesis of imines and amines, including some biologically important imines.

Chapter 4 described the syntheses and characterization of Ru(II) pincer complexes with multiple NHC carbene donor ligands. Discussion about the two sets of NMR peaks and their crystal structures, i.e., *cis* and *trans*. Further, justification through the NMR data with the help of less nucleophilic, non-coordinating solvent acetone-d$_6$ and discusses the *in situ* generated Ru-DMSO complex. After this justification, confirmation of the formation of only *trans* complexes.

Chapter 5 discusses the catalyst optimization in different reaction conditions for the hydration of nitriles. Notably, complex [Ru(CNC$^{i\text{-}Pr}$)(CN^{Me})I]PF$_6$ (**7b**) exhibited excellent catalytic reactivity among all the complexes. These catalysts are highly applicable for the hydration of nitriles, including aromatic, aliphatic, and heterocyclic nitriles. A plausible reaction mechanism was described for nitrile hydration, including a reactive intermediate, i.e., Ru-OH species; the bidentate pyridine ligand demonstrated hemilability and facilitated the binding of the nitrile substrate to the ruthenium centre. The catalyst recyclability experiment was performed for this transformation, and the catalyst was recovered up to five successive times.

Chapter 6 describes the syntheses, characterization, and catalytic activity of dicationic Ru(II)-CNC pincer complexes with CH_3CN and PPh_3 ligands and discusses their photophysical and electrochemical properties. A brief discussion concerning the electronic effect of the following ligands I^-, CH_3CN, and PPh_3, from UV-Visible spectra.

7.2. Future Scope

This thesis highlights the essential strategies for synthesizing CNC carbene complexes and studies their reactivity. The employment of these catalysts in different organic transformations shows better reactivity, and studying their photophysical and electrochemical properties afforded conclusive results. These catalysts will be explored for small molecule activation, H_2O oxidation, carbon dioxide reduction, and various organic transformations. Developing more selective catalysts is a crucial step in synthetic chemistry because it allows for specific organic transformations with minimal side-product formation. Selective catalysts can lead to higher yields of the desired product, making chemical processes more sustainable and cost-effective. Consequently, the synthesis of novel and selective catalysts for various organic reactions remains a highly desirable goal. Although numerous catalysts have been extensively developed in recent years, there is still limited information regarding the impact of co-ligands on catalyst selectivity. Conducting systematic studies to develop more selective catalysts for various reactions has the potential to revolutionize the field. Despite rapid advancements, the development of a robust catalytic system utilizing pincer NHCs for a wide range of catalytic processes is still a critical priority for the scientific community. Additionally, the exploration of air-stable and low-cost metal homogeneous catalysts for selective organic transformations under optimal reaction conditions still needs to be explored.